



# CENTER FOR INFRASTRUCTURE ENGINEERING STUDIES

## **ARCHING EFFECT IN MASONRY WALLS REINFORCED WITH FIBER REINFORCED POLYMER (FRP) MATERIALS**

by

**Nestore Galati**

**Gustavo Tumialan**

**Antonio Nanni**

University of Missouri-Rolla

**CIES  
03-33**

## Disclaimer

The contents of this report reflect the views of the author(s), who are responsible for the facts and the accuracy of information presented herein. This document is disseminated under the sponsorship of the Center for Infrastructure Engineering Studies (CIES), University of Missouri -Rolla, in the interest of information exchange. CIES assumes no liability for the contents or use thereof.

The mission of CIES is to provide leadership in research and education for solving society's problems affecting the nation's infrastructure systems. CIES is the primary conduit for communication among those on the UMR campus interested in infrastructure studies and provides coordination for collaborative efforts. CIES activities include interdisciplinary research and development with projects tailored to address needs of federal agencies, state agencies, and private industry as well as technology transfer and continuing/distance education to the engineering community and industry.

Center for Infrastructure Engineering Studies (CIES)  
University of Missouri-Rolla  
223 Engineering Research Lab  
1870 Miner Circle  
Rolla, MO 65409-0710  
Tel: (573) 341-6223; fax -6215  
E-mail: [cies@umr.edu](mailto:cies@umr.edu)  
[www.cies.umr.edu](http://www.cies.umr.edu)

**ARCHING EFFECT IN MASONRY WALLS  
REINFORCED WITH FIBER REINFORCED POLYMER  
(FRP) MATERIALS**

by

**NESTORE GALATI  
GUSTAVO TUMIALAN  
ANTONIO NANNI**

DEPARTMENT OF ENGINEERING MECHANICS

UNIVERSITY OF MISSOURI-ROLLA

Report No. CIES 03-42

CENTER FOR INFRASTRUCTURE ENGINEERING STUDIES

UNIVERSITY OF MISSOURI - ROLLA

## ABSTRACT

It is generally accepted by the designer of masonry structures that some arching action takes place in walls subjected to transverse lateral loading and that this action is often sufficient to give generous strength and rigidity to panels that might otherwise be unstable. In order for this arching action to take place it is necessary for the masonry panels to be restrained at the supports.

In this thesis the strengthening of masonry walls with FRP laminates encountering arching effect was studied. An experimental program was carried out in order to study the influence of the boundary conditions on the effectiveness of the strengthening technique. The parameters investigated were material properties (i.e. type of masonry support), amount of reinforcement and slenderness ratio.

An analytical model was developed in order to predict the out-of-plane capacity of masonry walls reinforced with FRP and restrained against rigid supports. It can be stated that there is a very good agreement between the analytical model and the experimental results. The analytical model was also used to predict the ultimate load of URM walls strengthened with composites and tested to failure at a decommissioned building in St. Louis, Missouri. Again, the model showed to produce a very good accuracy with experimental results.

## TABLE OF CONTENTS

	Page
ABSTRACT .....	ii
LIST OF ILLUSTRATIONS .....	vi
LIST OF TABLES .....	viii
INTRODUCTION .....	1
<b>PAPERS</b>	
1. FIELD ASSESSMENT OF URM WALLS STRENGTHENED WITH FRP LAMINATES .....	7
ABSTRACT .....	7
INTRODUCTION .....	8
EXPERIMENTAL STUDY .....	10
Test Specimens .....	10
Material Characterization .....	11
Field Test Setup .....	13
Mechanism of Failure .....	14
Test Results.....	15
ANALYTICAL STUDY .....	17
Analytical Derivations .....	18
Validation of the Analytical Model .....	22
CONCLUSIONS .....	23
ACKNOWLEDGEMENTS .....	24
REFERENCES .....	25
NOTATION.....	27

2. INFLUENCE OF ARCHING MECHANISM IN MASONRY WALLS STRENGTHENED WITH FRP LAMINATES .....	43
Abstract.....	43
Introduction.....	44
Experimental Program.....	45
Test Setup .....	47
Test Results.....	48
Results Discussion.....	49
Analytical Study .....	53
Conclusions .....	56
Acknowledgements.....	56
References.....	57
3. ARCHING EFFECT IN MASONRY WALLS REINFORCED WITH FIBER REINFORCED POLYMER (FRP) MATERIALS .....	59
Abstract.....	59
INTRODUCTION .....	60
RESEARCH SIGNIFICANCE.....	62
EXPERIMENTAL PROGRAM.....	62
Test Matrix.....	62
Materials .....	63
Test Setup .....	64
TEST RESULTS .....	66
Modes of Failure .....	66
Discussion of Results .....	68

ANALYTICAL STUDY .....	70
Analytical Derivations .....	71
Validation of the Analytical Model .....	74
SUMMARY AND CONCLUSIONS .....	76
ACKNOWLEDGEMENTS .....	77
NOTATION.....	77
REFERENCES .....	79
CONCLUSIONS .....	96
APPENDICES	
A. TEST SETUP AND MODES OF FAILURE .....	99
B. DIAGRAMS .....	110
C. OUT-OF-PLANE RELATED PAPERS .....	143
VITA .....	200

## LIST OF ILLUSTRATIONS

Figure	Page
1. Out-of-Plane Mechanism of Failure .....	3
 PAPER 1	
1. Vertical Cross Section of Typical Wall .....	32
2. Test Setup .....	33
3. Views of Test Setup .....	34
4. Out-of-Plane Mechanism of Failure .....	35
5. Mode of Failure .....	36
6. Behavior Comparison of Walls UP, UM, SP and SM.....	37
7. Strain Comparison for Walls SP and SM.....	38
8. Rotations in Upper and Lower Regions .....	39
9. Height vs. Deflection Curves .....	40
10. Upper Part of Analyzed Wall .....	41
11. Comparison of Experimental and Analytical Results .....	42
 PAPER 2	
1. Test Specimens and Strain Gage Locations .....	47
2. Test Setup Scheme .....	48
3. Failure of the Specimens .....	50
4. Load vs. Mid-height Deflection .....	51
5. In-Plane Load vs. Out-of-Plane Load.....	52
6. In-Plane/Out-of-Plane Load Ratio as a Function of FRP Width.....	52
7. Comparison between Simply Supported and End-Restrained Walls .....	54

8. Out-of-Plane Mechanism of Failure .....	55
--	----

### PAPER 3

1. Test Setup Scheme .....	86
2. Calibration Curve of the System .....	87
3. Test Specimens And Strain Gage Locations .....	88
4. Out-of-Plane Mechanism of Failure .....	89
5. Modes of Failure.....	90
6. Load vs. Deflection of URM Walls Strengthened with FRP Laminates.....	91
7. Out-of-Plane Load versus In-Plane Load of URM Walls Strengthened with FRP Laminates .....	92
8. In-Plane/Out-of-Plane Load Ratio as a Function of FRP Width.....	93
9. Comparison between Simply Supported and End-Restrained Walls .....	94
10. Half Part of Analyzed Wall .....	95

**LIST OF TABLES**

Table	Page
<b>PAPER 1</b>	
1. Properties of Constituents Materials .....	29
2. Engineering Properties of Masonry.....	30
3. Results of Unstrengthened and Strengthened Walls .....	31
<b>PAPER 2</b>	
1. Test Matrix .....	46
2. Test Results .....	51
3. Comparison between Theoretical and Analytical Out-of-Plane Loads.....	55
<b>PAPER 3</b>	
1. Test Matrix .....	81
2. Properties of FRP Constituent Materials .....	82
3. Compressive Strength of Masonry Walls .....	83
4. Test Results .....	84
5. Comparison between Theoretical and Analytical Load Capacities.....	85

## INTRODUCTION

The work presented herein focuses on problems related to the upgrade to out-of-plane loads of Unreinforced Masonry Walls (URM walls) and, in particular, on infill walls. The study of the mechanics of infill walls reinforced with Fiber Reinforced Polymers (FRP), and particularly crack pattern and mode of failure made possible to develop an analytical model able to predict their out-of-plane behavior with very good accuracy. The proposed analytical model can be easily modified to take different load conditions into consideration and it can be implemented in the form of design guidelines.

Masonry constitutes approximately 70% of the existing building inventory in USA. 70% of people in the world live in or use masonry buildings. 30% of those people live in seismic regions. Failure of URM walls is one of the main causes of material damages and loss of human life during a seismic event. Composite materials have shown a great potential for the strengthening of masonry structures in the forms of externally bonded fiber reinforced polymer (FRP) laminates or Near Surface Mounted (NSM) FRP bars. Researches (Ehsani et al., 1999, Hamilton et al. 1999, Tumialan et al., 2002) have proven that the use of FRP can notably increase the flexural capacity of unreinforced masonry (URM) walls. However, this assertion is true in the case of walls that can be treated as simply supported (i.e. walls exhibiting large slenderness ratios).

The resistance of URM walls to out-of-plane loads can be substantially increased by utilizing the large in-plane compressive forces that can be induced when the wall is butted up against rigid supports. It has been shown experimentally (L.R. Baker, 1978; A.W. Hendry, 1981) that, under certain conditions, masonry walls can withstand much

higher loads than are predicted on the basis of conventional bending analysis. This can be explained by arching behavior.

Due to arching, the increase of capacity in walls strengthened with FRP laminates may be considerably less than expected. Experimental works (Tumialan et al. 2001) have shown that the resultant force between the out-of-plane load and the induced membrane force could cause the crushing of the masonry units at the boundary regions. In this case, the application of the FRP did not exhibit the same effectiveness as in the case of walls having simply supported conditions.

The most common mode of failure in walls in which arching mechanism occurs is crushing of masonry at the boundary regions. This kind of failure is due to the resultant force from shear and the in-plane forces at the supports. In fact, flexural cracking occurs at the supports due to negative moments followed by cracking at mid-height due to positive moments, as a result, a three-hinged arch is formed. When the deflection increases due to out-of-plane bending, the wall is restrained against the supports, in this case the upper and lower beams. This action induces an in-plane compressive force ( $F_V$  in Figure 1), which accompanied by the shear force ( $F_H$  in Figure 1) in the support creates a resultant force that causes the crushing of the masonry at the supports ( $F_R$  in Figure 1). If the slenderness ratio is very small (i.e. less than 10), in the case of hollow blocks, splitting of the masonry at the supports can occur.

The basic idea for the work was to evaluate the opportunities offered by using FRP materials for strengthening infill walls to out-of-plane loads, in order to finally compile design and construction guidelines on their seismic retrofitting and upgrade with composite materials.

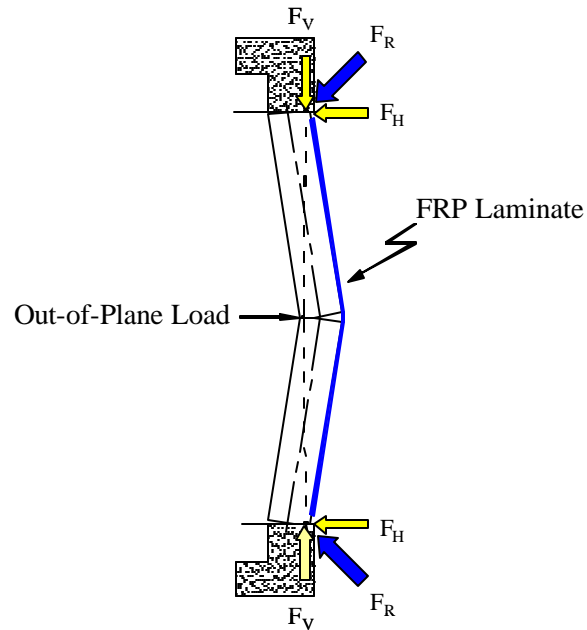


**Figure 1 Out-of-Plane Mechanism of Failure**

This work presents the experimental results of masonry specimens confined by two rigid supports, simulating upper and lower floor beams, subjected to out-of-plane loading. Experimental results show that the contribution of FRP to the wall capacity is less than in the case of simply supported conditions. An analytical method is presented for determining the capacity of masonry walls strengthened with FRP laminates considering the arching mechanism. The method analyzes infill walls that span between two rigid supports. The method shows good agreement with the experimental results and allows for appropriate design.

The present work has been developed through three papers.

The first paper is titled “FIELD ASSESSMENT OF URM WALLS STRENGTHENED WITH FRP LAMINATES”. It presents the results of an experimental investigation on URM walls strengthened with composites and tested to failure at a decommissioned building in St. Louis, Missouri. In this context, this experimental

program offered a unique opportunity for performing field experimentation on URM walls strengthened FRP laminates showing that shear-compression led to controlling the failure of either the upper or lower boundary masonry units. An analytical model is presented for determining the transverse load, mid-height deflection, and rotations at the supports that both unreinforced and externally strengthened infill walls can resist. The limitation of the present analytical model was to assume that materials behave linearly elastic up to failure. This assumption is certainly true for the FRP material but it is not for the masonry material. Apart from this limitation, the model shows very good agreement with the experimental results. The contribution of this author in the first paper was only on the analysis.

The second paper is titled “INFLUENCE OF ARCHING MECHANISM IN MASONRY WALLS STRENGTHENED WITH FRP LAMINATES”. It presents the experimental results of a group of ten walls having a slenderness ratio equal to 12, confined by two rigid supports. The experimental results are then compared with the analytical values obtained by using the analytical model presented in the first paper. A good agreement between analytical and experimental work can be stated. However, the analytical model presents the same limitations described before.

The third paper is titled “ARCHING EFFECT IN MASONRY WALLS REINFORCED WITH FIBER REINFORCED POLYMER (FRP) MATERIALS”. This paper presents the experimental results of a group of twenty-four walls having three different slenderness ratios: 8, 12 and 19. Twenty walls were tested confining the two ends between two rigid supports and the last four were tested under simply supported conditions. The analytical model presented in the first paper has been modified in order

to take into consideration the non-linearity of the masonry material. A very good agreement between analytical and experimental results can be stated. The maximum deviation between analytical and experimental results was 31% and was due to the fact that the arching mechanism was not completely developed due to set-up difficulties.

The connections between the three papers are now clear. The unique possibility to test infill walls in a decommissioned building in St. Louis made possible to individuate a mode of failure that is not generally considered in the design. Through the study of crack pattern and mode of failure, an analytical model was developed to interpret the experimental results. In the second paper, the analytical model developed has been used to predict the out-of-plane behavior of masonry walls built between two rigid supports and tested in laboratory conditions. For this part of the research, only slenderness ratios equal to 12 were considered. The analytical model showed a good agreement with the experimental results. However, the limitation due to material non-linearity was a big concern in the application of the initial analytical model. Therefore, the analytical model was modified to take material non-linearity into consideration and it was used to design a new laboratory investigation in which different slenderness ratios were considered. The third paper describes the last version of the analytical model and the complete experimental program.

The raw data are presented in Appendixes A and B. In particular, Appendix A is related to the testing: it describes the test setup and the typical modes of failure. Appendix B shows the data generated by the experimental investigations. For each specimen the curves load versus mid-span deflection, in-plane versus out-of-plane loads and strains versus out-of-plane load are presented.

This and other work on reinforcement to out-of-plane loads was conducted during this research period. In particular, Appendix C presents a list of speeches made by the author on this topic and reports three papers related to the out-of plane strengthening using FRP material in which the author was involved. The first paper is titled: "STRENGTHENING OF URM WALLS SUBJECT TO OUT-OF-PLANE LOADS". It presents provisional design guidelines for the strengthening of URM walls using FRP laminates. Simply supported boundary conditions were considered. The contribution of the author in this work was in the development of the analytical model and in design guidelines. This paper has been accepted for publication by the ACI Structural Journal. The second paper is titled: "STRENGTHENING OF MASONRY WITH NEAR SURFACE MOUNTED FRP BARS". It has been published in the proceeding of the ICCI 2002 conference, San Francisco, California, June 2002. The third paper is titled: "FLEXURAL STRENGTHENING OF UNREINFORCED MASONRY WITH FRP BARS". It has been published in the proceeding of the COMPOSITES 2002 Convention and Trade Show Composites Fabricators Association September 25-27, 2002 Atlanta, Georgia USA. The second and the third papers deal with the strengthening to out-of-plane load of UMR walls using NSM FRP rods. This emerging technology has shown to be very promising for the strengthening of masonry structures. The contribution of this author in these two papers was on the experimental side (design and realization of the experiments), and on the analytical derivations.

**FIELD ASSESSMENT OF URM WALLS  
STRENGTHENED WITH FRP LAMINATES**

**By J. Gustavo Tumialan<sup>1</sup>, Associate Member, ASCE, Nestore Galati<sup>2</sup>, and Antonio  
Nanni<sup>3</sup>, Fellow, ASCE**

**ABSTRACT:** Unreinforced masonry (URM) walls strengthened with composites were tested to failure at a decommissioned building in St. Louis, Missouri. The walls were subjected to out-of-plane loading. Previous work on URM as well as reinforced masonry walls strengthened with FRP laminates has shown remarkable increases in capacity and ductility. However, most of this research work has been conducted in the laboratory, where, it is a difficult to reproduce real field conditions. In this context, this experimental program offered a unique opportunity for performing field experimentation on URM walls strengthened FRP laminates showing that shear-compression led to controlling the failure of either the upper or lower boundary masonry units. An analytical model that provides good agreement with the experimental results is also presented. The model computes the applied concentrated out-of-plane load, mid-height deflection, and rotations at the supports. The analytical model can be easily modified to take into account distributed loads acting on the wall.

---

<sup>1</sup> Research Engineer, Center for Infrastructure Engineering Studies, University of Missouri-Rolla, Rolla, MO 65409

<sup>2</sup> Research Engineer, Center for Infrastructure Engineering Studies, University of Missouri-Rolla, Rolla, MO 65409

<sup>3</sup> V&M Jones Professor of Civil Engineering, University of Missouri-Rolla, Rolla, MO 65409

**KEYWORDS:** Arching Mechanism, Fiber Reinforced Polymer (FRP) Laminates, Field Testing, Masonry Strengthening, Out-of-Plane Loading, Unreinforced Masonry (URM) Walls

## **INTRODUCTION**

Structural weakness or overloading, dynamic vibrations, settlement, and in-plane and out-of-plane deformations can cause failure of masonry structures. Unreinforced masonry (URM) buildings represent a large portion of the buildings around the world. Many of the existing buildings in the United States are URM buildings and under extreme events, have features that could threaten lives including unbraced parapets, inadequate connections to the roof, and the brittle nature of the URM elements themselves. Organizations such as The Masonry Society (TMS) and the Federal Emergency Management Agency (FEMA) have identified that failure of URM walls result in most of the material damage and loss of human life.

URM walls are commonly used as interior partitions or exterior walls bound by steel or concrete frames forming the building envelope. Depending on design considerations, these walls can resist lateral and/or gravity loads. Due to weak anchorage to adjacent concrete members, or to absence of anchorage, URM walls may crack, tear and collapse under the combined effects of out-of-plane and in-plane loads generated by seismic forces.

Fiber Reinforced Polymer (FRP) composites provide solutions for the strengthening of URM walls subjected to in-plane and out-of-plane overstresses caused by high wind pressures or earthquake loads. Even though most of the research on FRP

composites has focused on reinforced concrete (RC), available literature on masonry shows that each potential failure causes of URM walls can be prevented or lessened by using FRP composites.

Relatively stiff frames may restrain the movement of a wall when subjected to out-of-plane loading. As a consequence, in-plane compressive forces are built, which produce a load resisting mechanism, referred as to arching action, that improves the initial flexural behavior of the wall. At the ultimate state, due to the compressive stresses generated by this mechanism at the upper and lower zones of the wall, the masonry units along the edges may fracture. Therefore, the influence of arching mechanisms in the behavior of retrofitted walls needs to be taken into account to fully realize the effectiveness of strengthening strategies.

The Old City Hospital complex in St. Louis, Missouri was decommissioned and scheduled for demolition. Before the demolition took place, one of the buildings, the Malcolm Bliss Hospital, was used as a research test bed. The building structural system consisted of a five-story reinforced concrete-frame addition built in 1964. The building envelope was made of URM walls, which were tested under out-of-plane loading during this program. Previous works on URM walls strengthened with FRP laminates subject to out-of-plane loads have shown remarkable increases in capacity and ductility (Ehsani et al. 1999; Hamilton et al. 1999; Velazquez et al. 2000). However, most of this research has been conducted in the laboratory, where the boundary conditions are not representative of those found in the field. In this context, the tests performed at the Malcolm Bliss Hospital offered the opportunity for field validation of URM walls strengthened with FRP materials.

## **EXPERIMENTAL STUDY**

### **Test Specimens**

The experimental program carried out at the Malcolm Bliss Hospital included the testing of walls under out-of-plane and in-plane loading (Tumialan et al. 2001). This paper describes the test results of four full-scale URM walls subject to out-of-plane loading. The walls were constructed with clay units forming two wythes spaced at 1.90 cm. (0.75 in.). The wythes were joined by header units placed at each fourth course, and at each fourth unit within that course. The nominal dimensions of these walls were 2.44 by 2.44 m (8 by 8 ft); their overall thickness, including the two wythes and plaster was 33 cm. (13 in.). The outer wythe, corresponding to the veneer wall, was built using cored clay units with width of 10 cm. (4 in.), height of 5.6 cm. (2.25 in.), and length of 20 cm. (8 in.), and with three cores of 3.75 cm. (1.5 in.) diameter. The inner wythe or backup wall was constructed using two kinds of clay units. Tiles and bricks were laid in alternated courses. The actual dimensions of the tile units were 18.75 cm. (7.5 in.) wide by 18.75 cm. (7.5 in.) high by 30 cm. (12 in.) long. The brick units were solid, their dimensions were 10.6 cm. (4.25 in.) wide, 5.6 cm. (2.25 in.) high and 21.25 cm. (8.5 in.) long. The walls were finished with 25 mm (1 in.) thick cementitious plaster. The URM walls, classified as infill, belonged to a masonry typology commonly used during a time frame from late 1940's through the early 1960's. A section view of a typical wall is shown in Figure 1. The upper and lower boundaries for these walls were RC beams, cast integrally with the floor system.

Two URM walls, Wall UP and Wall UM, were selected as control specimens. In Wall UP the plaster was left in place; whereas, in Wall UM the plaster was removed.

Walls SP and SM, again with and without plaster, respectively, were strengthened with three vertically-oriented 500 mm (20 in.) wide Glass FRP (GFRP) strips spaced at 800 mm. (32 in.), center to center. The purpose of testing this group of walls was to observe the difference in behavior in walls strengthened with FRP attached to plaster and to masonry under out-of-plane loading.

### **Material Characterization**

One inherent difficulty when conducting a testing program in-situ is to characterize the materials. Samples obtained from similar walls in the building were collected. These samples included bricks, tiles, and mortar. Due to the brittle characteristic of the clay tiles, it was not possible to recover masonry assemblages from the backup wall for determining the compressive strength of masonry,  $f'_m$ . Instead, using some reclaimed units, an indirect method for the estimation of  $f'_m$  was used. The reclaimed clay units showed a unit strength,  $f_u$ , equal to 3.30 MPa (478 psi). Equation 1 presents the relationships used to estimate  $f'_m$  of structural clay tiles as a function of  $f_u$  (Bennet et al.1997). The value of  $f'_m$  was estimated as 2.02 MPa (293 psi).

$$f'_m = 1.06 (f_u)^{0.54} \text{ (MPa)} \quad (1)$$

In addition, compressive strengths of prisms built with clay tiles found in research investigations conducted prior to 1964, the date of the construction of the Malcolm Bliss Hospital, range from 1.60 MPa (232 psi) to 2.70 MPa (392 psi) (Bennett et al. 1997). Thereby, based on the result found using equation 1 and historical data, it was decided to adopt a  $f'_m$  value equal to 2.02 MPa (293 psi) for the analytical modeling of the wall.

Also, a value of 0.0015 for maximum strain associated to this  $f'_m$  was considered based on a previous investigation (Bennett et al. 1997).

In the case of the outer wall, some assemblages consisting of two courses of bricks were obtained for laboratory testing. The compressive strength of these assemblages was 9.67 MPa (1403 psi). The compressive strength of the mortar was 5.61 MPa (814 psi). It is important to mention that the latter value was not obtained from standard tests, but from cylinder-shaped mortar sample obtained from material entrapped in the cores of the brick veneer. Using the average compressive strength, the mortar can be classified as Type N according to ASTM C270.

GFRP sheets were used in this research study to strengthen in-situ masonry walls. The FRP system consisted of three basic components, namely: putty, impregnating resin and fiber sheets. The combination of these three materials forms the FRP laminate. Tensile tests were performed on GFRP laminates to determine their engineering properties. No independent tests were conducted to determine the properties of putty and impregnating resin; thus, the values provided by the manufacturer are presented. The properties of the constituent materials are illustrated in Table 1.

The GFRP sheets were applied to the wall surface by manual lay-up, for their installation a procedure recommended by the manufacturer was followed. Putty was used to level the surface of the wall. This task was carried out by a qualified contractor. Conventionally, when strengthening RC members, a coat of primer is applied to the surface of the member. However, since masonry possesses a high absorption rate, it was decided to use the impregnating resin as primer due to its higher viscosity.

## Field Test Setup

The masonry walls were tested under two out-of-plane loads, distributed by two 300×300×12.5 mm (12×12×½-in) steel plates to the external face of the wall. The loads were generated by means of a hydraulic jack activated by a manual pump. The force created by this jack reacted against a 1.50 m. (5 ft) steel girder, hereafter called Beam A, and a 3.35 m. (11 ft) steel girder, hereafter referred as to Beam B. When loading, two reacting forces were created on Beam A. These forces were transmitted to the masonry wall using two high-strength steel rods, which through steel plates pulled the wall from its exterior face. On the reaction side, the force generated by the hydraulic jack reacted against Beam B, which transmitted the load to the upper and lower floor system. Additional details of the test setup are presented elsewhere (Tumialan, 2001). A sketch of the test setup is shown in Figure 2.

Beam A was supported by a wooden panel resting on concrete blocks (see Figure 3a). Thin greased plates were placed between Beam A and the panel to reduce the friction restraint and provide smooth action. Beam B was erected into place using an electric hoist located at the roof level (see Figure 3b). The hoist was restrained by a steel frame located on the roof of the building. In this manner Beam B could be raised or lowered, depending on which wall was being tested.

The test setup was designed to load the walls with two concentrated loads, and measure deflections, strains and rotations due to these loads. The test conditions were those of walls away from corners, since both vertical edges were free. The load was applied in cycles of loading and unloading. The data obtained from a load cell, Linear Variable Differential Transducers (LVDTs), strain gages, and inclinometers were

collected by a data acquisition system at a frequency of 1 Hz. The LVDTs were placed along the wall height, in the centerline, to record out-of-plane deflections. One LVDT was placed at the wall mid-height, two were placed at the height quarters, and two were located near the boundaries. Also, an LVDT was placed on the upper RC beam to monitor any movement due to the loading. Strain gages were placed on the FRP laminates at mid-height, and quarter height of the wall. Inclometers were used to record rotations in the upper and lower borders.

### **Mechanism of Failure**

The failure of the URM walls was caused by the fracture of the tile units placed on the upper or bottom-most courses due to arching action. The fracture of these tiles is caused by angular distortion due to out-of-plane rotation, and mainly by a force generated by a shear-compression combination effect in the support area. Flexural cracking occurs at the supports followed by cracking at mid-height, as a result a three-hinged arch is formed. When the deflection increases due to out-of-plane bending the wall is restrained against the supports, in this case the upper and lower RC beams. This action induces an in-plane compressive force ( $F_V$  in Figure 4), which accompanied by the shear force ( $F_H$  in Figure 4), creates a resultant force ( $F_R$  in Figure 4) that causes the fracture of the tile. Typically, the crushing occurs in the mortar joint; however, due to tile characteristics, the failure in these walls was associated with the tiles. Once the out-of-plane peak load was reached, the load decreased abruptly. It has been reported that for slenderness ratios ( $h/t$ ) larger than 30, the effect of arching action is negligible (Angel et al., 1994). For the present study  $h/t$  was approximately equal to 8.

At the final stage, Wall UM exhibited fractured tiles in the support regions. In Walls UP and SP, where plaster was present, once the fracture of the tiles initiated, the layer of plaster began to delaminate from the masonry surface (see Figure 5a). In the case of Wall SP, since the FRP reinforcement adhered to the plaster surface was not efficiently engaging the flexural cracks, the wall capacity was not increased. In contrast when the externally bonded FRP strips were attached directly to the masonry, the failure was delayed because the FRP laminates were able to engage the flexural cracks running through the bed joints. Consequently, the wall capacity was improved but the mechanism of failure did not change (See Figure 5b).

### **Test Results**

Figure 6 compares the behavior of the four walls tested. Control Wall UP had a bi-linear behavior in the ascending region. This wall with plaster showed a capacity 25% larger than that found in control Wall UM, without plaster. In addition, the initial flexural stiffness in Wall UM up to cracking, which occurred at 55 kN (12.4 kips), was approximately 2.4 times smaller than in Wall UP. This difference can be attributed to an increment in the overall moment of inertia of the wall due to the plaster thickness. However, after initial cracking of Wall UP, Walls UM and UP appear to exhibit the same stiffness. Also, by comparing Wall UP with the strengthened Walls SP and SM, a difference in flexural stiffness after initial cracking was observed. In this case the increase in stiffness due to the presence of FRP reinforcement was about 1.8 times. The latter ones, Wall SP and SM, exhibited similar flexural stiffness up to failure. On the curves relative to Wall UP and Wall SP in Figure 6, it is observed that FRP laminates are

not fully utilized when they are attached to the plaster surface, since no increment in capacity was registered. When the FRP was attached directly on the masonry surface, an increment of 40% in capacity was observed by comparing Wall SM to the control Wall UM.

The aforementioned increment in capacity observed in Wall SM when compared to Wall SP is attributed to a better engagement of the FRP laminates to the surface when the out-of-plane bending increases. This can be corroborated from Figure 7; thus, up to a load of 90 kN (20 kips) the strains developed at mid-height in the FRP laminates attached to Wall SM doubled those of Wall SP. Only a partial load vs. strain history is presented because strain gauges stopped working around 5000  $\mu\text{s}$  due to an imperfection with the data acquisition system. The walls experienced more rotation in the zone where the crushing occurred. The rotations produced angular distortion, which is critical in a masonry unit composed of thin shells such as is the case of the clay tiles. The angular distortion along with a shear-compression combination effect caused the failure of the wall end units. Figure 8 illustrates the out-of-plane load vs. rotation in the boundary regions. From these diagrams the rotation values corresponding to the peak load, recorded by the inclinometers where the initial crushing was observed were  $0.12^\circ$  (bottom),  $0.18^\circ$  (top),  $0.22^\circ$  (bottom), and  $0.35^\circ$  (top) for Walls UP, UM, SP, and SM, respectively. Figure 9 presents the deflection profile for different load levels. The deformed shape was obtained from the LVDT recordings at mid-height, quarters and support regions. For comparison purposes with the inclinometer readings, the rotation values were also attained by computing the slope at the support regions at peak loads. The corresponding values at the bottom region were  $0.21^\circ$ ,  $0.19^\circ$ ,  $0.20^\circ$ , and  $0.29^\circ$  for

Walls UP, UM, SP, and SM, respectively. Thus, the values recorded by the inclinometers show good correlation with the slope values based on deflection measurements. The unstrengthened walls (Walls UP and UM) and one strengthened wall (Wall SP) exhibited similar rotation values. This is further evidence of the lack of contribution of the FRP reinforcement in Wall SP. In the case of Wall SM, the presence of FRP applied directly to the masonry surface allowed for larger deflections and larger rotations by engaging the flexural cracks in the bed joints.

### **ANALYTICAL STUDY**

An analytical model is presented for determining the transverse load, mid-height deflection, and rotations at the supports that both unreinforced and externally strengthened infill walls can resist. In the present analytical formulation, the presence of plaster is not included in the model because the experimental studies demonstrated that the strengthening of masonry without removal of plaster may not be desirable. The wall is idealized as a strip of variable width, which is subjected to a concentrated load applied normal to the plane of the wall. This model can be extended to distributed loads. The model takes into account the clamping forces in the supports, originated by arching action, which lead to increasing the out-of-plane resistance of URM walls. Previous researchers (Fricke, 1992, Angel et al., 1994) have found this resistance to be many times greater than the resistance predicted by conventional theories that do not consider post-cracking mechanisms.

To formulate the analytical model, it is assumed that materials behave linearly elastic up to failure. For the case of masonry, previous research has demonstrated that

consideration of a triangular stress distribution is adequate for arching mechanisms (Angel et al., 1994). It is also assumed that the wall is only cracked at mid-height, and that the two resulting segments can rotate as rigid bodies about the supports as illustrated in Figure 4.

### Analytical Derivations

Analyzing the top segment of the masonry wall shown in Figure 4, the free-body shown in Figure 10 can be derived. From the equilibrium of forces in the vertical direction, the following relationship can be drawn:

$$C_2 = C_1 + T_f \cos \mathbf{q} \quad (2)$$

where  $C_1$  and  $C_2$  are the clamping forces at top and mid-height of the wall, respectively,  $t_f$  is the force in the FRP laminate and  $\mathbf{q}$  is the rotation of the wall.

Considering a triangular stress distribution, the clamping forces by wall strip width,  $w_m$ , acting on the restrained ends of the wall can be calculated as:

$$C_1 = \frac{1}{2} w_m b_1 f_{m1} = \frac{1}{2} w_m b_1 E_{m1} \mathbf{e}_{m1} \quad (3a)$$

$$C_2 = \frac{1}{2} w_m b_2 f_{m2} = \frac{1}{2} w_m b_2 E_{m2} \mathbf{e}_{m2} \quad (3b)$$

The tensile force developed by the FRP laminate is:

$$T_f = A_f f_f = A_f E_f \mathbf{e}_f \quad (3c)$$

Replacing equations 3a, 3b and 3c in equation 2, the following relationship is obtained:

$$\frac{1}{2} w_m b_2 E_{m2} \mathbf{e}_{m2} = \frac{1}{2} w_m b_1 E_{m1} \mathbf{e}_{m1} + A_f E_f \mathbf{e}_f \cos \mathbf{q} \quad (4a)$$

This equation is valid only if the masonry properties are the same in the inner and outer wall. For a two-wythe wall some modifications need to be included to account for the material difference in the outer and inner walls. Brick headers provided adequate shear transfer between wythes. Thus, for simplicity, it is assumed that the two wythes are in contact. Then, equation 4a can be expressed as:

$$\frac{1}{2} w_m b_2 E_{m2} \mathbf{e}_{m2} = \frac{1}{2} w_m b_1 E_{m1} \mathbf{e}_{m1} + A_f E_f \mathbf{e}_f \cos \mathbf{q}, \text{ for } b_2 \leq t_o \quad (4b)$$

$$\frac{1}{2} w_m b_2 E_{m2} \mathbf{e}_{m2} - \frac{1}{2} w_m (E_{m2} - E_{m1}) \frac{(b_2 - t_o)^2}{b_2} \mathbf{e}_{m2} = \frac{1}{2} w_m b_1 E_{m1} \mathbf{e}_{m1} + A_f E_f \mathbf{e}_f \cos \mathbf{q} \quad (4c)$$

for  $b_2 > t_o$

where,  $t_o$  is the thickness of the outer wall. The first part of equation 4c represents the compression force  $C_2$  in the masonry at the mid-height of the wall when  $b_2 > t_o$ . In this case  $C_2$  can be expressed as:

$$C_2 = \frac{1}{2} w_m b_2 E_{m2} \mathbf{e}_{m2} - \frac{1}{2} w_m (b_2 - t_o) E_{m2} \mathbf{e}_{m2}^* + \frac{1}{2} w_m (b_2 - b_0) E_{m1} \mathbf{e}_{m2}^* \quad (4d)$$

where  $\mathbf{e}_{m2}^*$  represents the strain in the masonry in the separation line between the inner and the outer walls. The value of  $\mathbf{e}_{m2}^*$  can be found from triangles similarity and is given by:

$$\mathbf{e}_{m2}^* = \mathbf{e}_{m2} \frac{b_2 - t_o}{b_2} \quad (4e)$$

The first term in equation 4c is then obtained by substituting equations 4d in 4d. Taking moments about the point of application of the resulting force in masonry (point “o” in Figure 10), the following relationship is obtained:

$$\frac{Ph}{4} = A_f E_f \mathbf{e}_f a_f + \frac{w_m b_f E_{m1} \mathbf{e}_{m1}}{2 \cos \mathbf{q}} a_c \quad (5)$$

From Figure 10a, the following set of relationships can be derived based on geometrical considerations:

$$a_f = (t - b_2) \cos \mathbf{q} + \frac{2}{3} \frac{b_2}{\cos \mathbf{q}} \quad (6a)$$

$$a_c = b_f - \left( \frac{h}{2} - \mathbf{D}_1 \right) \sin \mathbf{q} - \frac{1}{3} \frac{b_1}{\cos \mathbf{q}} \quad (6b)$$

$$\cos \mathbf{q} = \frac{b_1}{\sqrt{\mathbf{D}_1^2 + b_1^2}} \quad (6c)$$

$$\sin \mathbf{q} = \frac{\mathbf{D}_1}{\sqrt{\mathbf{D}_1^2 + b_1^2}} \quad (6d)$$

In addition, from Figure 10b the following relationships can be determined:

$$\mathbf{d}_1 + \mathbf{d}_2 = \frac{h}{2} \left( \frac{1}{\cos \mathbf{q}} - 1 \right) \quad (7a)$$

$$\mathbf{d}_1 = \left( \frac{t}{2} - b_1 \right) \tan \mathbf{q} \quad (7b)$$

$$\mathbf{d}_2 = \left( \frac{t}{2} - b_2 \right) \tan \mathbf{q} \quad (7c)$$

Replacing equations 7b, 7c in equation 7a:

$$t - b_1 - b_2 = \frac{h}{2} \cdot \frac{1 - \cos \mathbf{q}}{\sin \mathbf{q}} \quad (8)$$

It is assumed that the compressive strains at the outermost fibers of the wall segment vary linearly along the half of the wall. Thereby, the strain at the restrained region is maximum, whereas, at the mid-span they are relieved due to the crack opening (Angel et al., 1994). The total shortening of the interior and exterior fibers ( $\mathbf{D}_1$  and  $\mathbf{D}_2$ ,

respectively), over the length of half strip, is that found by integrating these strains along the half length:

$$\mathbf{D} = \int_0^{h/2} \mathbf{e}(x) dx = \int_0^{h/2} \left( \frac{\mathbf{e}_{max}}{h/2} \right) x dx = \frac{1}{4} \mathbf{e}_{max} h \quad (9a)$$

Then  $\mathbf{D}_1$  and  $\mathbf{D}_2$  can be expressed as:

$$\mathbf{D}_1 = \frac{1}{4} \mathbf{e}_{m1} h \quad (9b)$$

$$\mathbf{D}_2 = \frac{1}{4} \mathbf{e}_{m2} h \quad (9c)$$

From similarity of triangles in Figure 10b, a relationship between the bearing widths and the shortening lengths can be obtained:

$$\frac{b_2}{b_1} = \frac{\mathbf{D}_2}{\mathbf{D}_1} \quad (10)$$

Combining equations 9b, 9c and 10, the following relationship is obtained:

$$\frac{b_2}{b_1} = \frac{\mathbf{e}_{m2}}{\mathbf{e}_{m1}} \quad (11)$$

Assuming that the deformation of the FRP occurs in an unbonded length,  $l_b$ , the strain in the FRP  $\mathbf{e}_f$  can be estimated using the equation:

$$\mathbf{e}_f = \frac{\mathbf{D}_f \cos \mathbf{q}}{l_b} = \frac{\frac{t-b_2}{b_2} \mathbf{D}_2}{l_b} = \frac{\frac{t-b_2}{b_1} \mathbf{D}_1}{l_b} \quad (12)$$

where  $\mathbf{D}_f$  is the elongation of the FRP laminate.

In addition, the mid-height deflection  $\mathbf{D}_o$  and the rotation  $\mathbf{q}$  can be calculated as:

$$\mathbf{D}_o = \left( \frac{h}{2} - \mathbf{D}_1 \right) \sin \mathbf{q} = \left( \frac{h}{2} - \mathbf{D}_1 \right) \frac{\mathbf{D}_1}{\sqrt{\mathbf{D}_1^2 + b_1^2}} \quad (13a)$$

$$\mathbf{q} = \sin^{-1} \left( \frac{\mathbf{D}_1}{\sqrt{\mathbf{D}_1^2 + b_1^2}} \right) \quad (13b)$$

### Validation of the Analytical Model

The out-of-plane loads causing the failure of the two-wythe unstrengthened wall (Wall UM) and FRP strengthened wall (Wall SM) are estimated. The geometrical properties have been previously described. The engineering properties of masonry are summarized in Table 2. Wall SM was strengthened with three 500 mm. (20 in.) wide GFRP strips spaced at 800 mm. (32 in.). Thus, the GFRP area for an 800 mm. (32 in.) wide vertical wall strip was 179 mm<sup>2</sup> (0.278 in<sup>2</sup>).

Considering the failure of the wall occurs in the boundary regions, and solving the equations 4a or 4b, 5, 8, 9 and 11, for the unstrengthened wall, and equations 4a or 4b, 5, 8, 9, 11 and 12 for the strengthened wall, it is possible to calculate the unknowns  $b_1$ ,  $b_2$ ,  $e_{m2}$ ,  $e_f$  and the out-of-plane force  $P$  at failure. Then, using these values of  $\mathbf{D}_1$  and  $b_1$  in equations 13a and 13b, the deflection  $\mathbf{D}_o$  and the rotation,  $\mathbf{q}$ , of the wall can be calculated. Table 3 summarizes these results and provides a comparison between theoretical and experimental values.

In order to compute the out-of-plane load in the strengthened wall, it is required to know the debonded length,  $l_b$  (see equation 12). To date there is no scientific evidence on the determination of this parameter. For the calculations carried out to determine  $P$  it was assumed that  $l_b$  was equal to 37.5 mm (1.5 in.) This assumption was based on experimental observations which suggested that the debonded length measured from the crack at mid-height extended approximately that distance in both directions perpendicular

to the crack. With the assumed  $l_b$ , the analytical strain in the FRP,  $e_f$ , equals 10500  $\mu$  strain at ultimate. The strain recording in the test stopped at 5000  $\mu$  strain. However, the trend indicates that an experimental strain in the FRP may have reached about 10000  $\mu$  strain; from which can be concluded that the assumption of  $l_b$  equal to 37.5 mm (1.5 in.) was reasonable.

In general, the results indicate a good agreement between the analytical and experimental values. As evidence of the validity of this process, the ascending part of the experimental out-of-plane load vs. mid-height deflection curves for Walls UM and SM, and the peak values obtained by the analytical model are plotted in Figure 11. Additional data validated by this analytical model is shown elsewhere (Galati et al., 2002).

## CONCLUSIONS

The unique opportunity of testing URM walls with and without strengthening and strengthened walls at the Malcolm Bliss Hospital, led to the following conclusions:

- A mechanism of failure that is not commonly observed in tests performed in the laboratory on walls strengthened with FRP was identified. Walls exhibited an arching mechanism where crushing at the supports controlled the wall behavior. This mechanism of failure must be considered in the quantification of upgraded wall capacities to avoid overestimating the wall response.
- The wall where the FRP laminates were applied directly to the masonry surface, exhibited a better performance than its counterpart, strengthened without the removal of plaster. The increase in capacity was about 17 % compared to the wall with plaster

(unstrengthened and strengthened), and 40 % compared to the control wall without plaster.

- In order to fully realize the benefits of the use of FRP composites, consideration must be given to detailing. For the test walls investigated herein, grouting of tile units at the support regions could have induced a different and preferable failure mode.

An analytical model to determine the peak load and deflection of both unreinforced and strengthened walls was developed:

- The model based on rigid body and material linearity shows good agreement with experimental results.
- The analytical model can be easily modified to take into account distributed loads acting on the wall, and incorporated in design provisions.

## **ACKNOWLEDGEMENTS**

This research study was sponsored by the National Science Foundation Industry/University Cooperative Research Center on Repair of Buildings and Bridges (RB<sup>2</sup>C) at the University of Missouri – Rolla. The authors would like to thank Raghu Annaiah, Pei-Chang Huang, Matthew Mettemeyer, and Steven Schiebel for their assistance in the conduction of the tests.

**REFERENCES**

- Angel, R., Abrams, D. P., Shapiro, D., Uzarski, J., and Webster, M. (1994). "Behavior of Reinforced Concrete Frames with Masonry Infills." *Struct. Res. Ser. 589, Department of Civ. Engrg.*, University of Illinois at Urbana-Champaign, IL.
- Benett, R. M., Boyd, K. A., and Flanagan, R. D. (1997). "Compressive Properties of Structural Clay Tile Prisms." *J. Struct. Engrg.*, ASCE, 123(7), 920-926.
- Ehsani, M. R., Saadatmanesh, H., and Velazquez-Dimas, J. I. (1999). "Behavior of Retrofitted URM Walls Under Simulated Earthquake Loading." *J. of Comp. for Const.*, ASCE, 3(8), 134-142.
- Galati N., Tumialan J.G, La Tegola A., and Nanni A., "Influence of Arching Mechanism in Masonry Walls Strengthened with FRP Laminates," ICCI 2002, San Francisco, CA, June 10-12, 2002, 10 pp. CD-ROM.
- Fricke, K. E., Jones, W. D., and Huff, T. E. (1992). "In situ lateral Load Testing of Unreinforced Masonry Hollow Clay Tile Wall." *6th Can. Masonry Symp.*, Saskatchewan, Canada, 519-530.
- Hamilton, H.R. III, Holberg A., Caspersen, J., and Dolan, C. W. (1999). "Strengthening Concrete Masonry with Fiber Reinforced Polymers." *4th Int. Symp. on Fiber Reinf. Polymer (FRP) for Reinf. Conc. Struct.*, Baltimore, MD, 1103-1115.
- Masonry Standards Joint Committee. (1999). "Building Code Requirements for Masonry Structures." *ACI-530-99/ASCE 5-99/TMS 402-99*, Detroit, MI, New York, NY, and Boulder, CO.

Masonry Standards Joint Committee. (2001). "Building Code Requirements for Masonry Structures – Working Draft." *ACI-530-99/ASCE 599/TMS 402-99*, Detroit, MI, New York, NY, and Boulder, CO.

Velazquez-Dimas, J. I, Ehsani, M. R., and Saadatmanesh, H. (2000). "Out-of-Plane Behavior of Brick Masonry Walls Strengthened with Fiber Composites." *Struct. J.*, *ACI*, 97(5), 377-387.

Tumialan J. G. (2001). "Strengthening of Masonry Structures with FRP Composites." *Doctoral Dissertation*, University of Missouri-Rolla, Rolla, MO.

**NOTATION**

$A_f$  = area of FRP

$a_c$  = arm distance between clamping forces

$a_f$  = arm distance between force in FRP and clamping force at mid-height

$b_1, b_2$  = bearing width at top and mid-height, respectively

$C_1, C_2$  = clamping forces at top and mid-height, respectively

$E_{m1}, E_{m2}$  = modulus of elasticity at top and mid-height, respectively

$E_f$  = modulus of elasticity of FRP

$F_H$  = shear force

$F_R$  = resultant force

$F_V$  = in-plane compressive force

$f_f$  = tensile stress in FRP

$f'_m$  = compressive strength of masonry

$f_{m1}, f_{m2}$  = compressive stress at top and mid-height, respectively

$f_u$  = compressive strength of clay tile unit

$h$  = height of the wall

$h/t$  = slenderness ratio

$l_b$  = unbonded length

$P$  = out-of-plane load per strip

$P_{total}$  = total out of plane load

$T_f$  = force in the FRP laminate

$t$  = overall thickness of the wall

$t_o$  = thickness of the outer wall

$w_m$  = wall strip width

$\Delta_o$  = wall deflection

$D_1, D_2$  = total shortening of interior and exterior masonry fiber in compression,  
respectively

$d_1, d_2$  = crack opening at top and mid-height, respectively, at the wall axis

$e_f$  = tensile strain in FRP

$e_{m2}^*$  = strain in the masonry in the separation line between the inner and the outer walls

$e_{m1}, e_{m2}$  = compressive strain at top and mid-height, respectively

$q$  = rotation of the wall

**Table 1. Properties of Constituents Materials**

<b>Material</b>	<b>Tensile Strength</b>	<b>Modulus of Elasticity</b>	<b>Strain at Rupture</b>	<b>Thickness</b>	<b>Poisson's Ratio</b>
	<b>MPa (ksi)</b>	<b>GPa (ksi)</b>	<b>%</b>	<b>mm (in)</b>	<b>s Ratio</b>
<b>(1)</b>	<b>(2)</b>	<b>(3)</b>	<b>(4)</b>	<b>(5)</b>	<b>(6)</b>
Putty <sup>(1)</sup>	15.2 (2.2)	1.79 (260)	7.0	NA	0.48
Impregnating Resin <sup>(1)</sup>	55.2 (8.0)	3.03 (440)	3.5	NA	0.40
E-Glass	1690 (245)	92.86 (13460)	1.82	0.36 (0.014)	NA

<sup>(1)</sup> Values provided by the manufacturer

**Table 2. Engineering Properties of Masonry**

<b>Material Property</b>	<b>Inner Wythe</b>	<b>Outer Wythe</b>
<b>(1)</b>	<b>(2)</b>	<b>(3)</b>
Compressive Strength, MPa (psi)	$f'_{m1} = 2.02$ (293)	$f'_{m2} = 9.7$ (1400)
Maximum Strain, mm/mm	$e'_{m1} = 0.0015$	$e'_{m2} = 0.0035$ <sup>(2)</sup>
Modulus of Elasticity, GPa (ksi)	$E_{m1} = 2.86$ (415) <sup>(1)</sup>	$E_{m2} = 6.75$ (980) <sup>(2)</sup>

<sup>(1)</sup>  $E_m = 0.68 f'_m + 1.5$  (GPa) (Bennet et al., 1997)

<sup>(2)</sup> Based on Masonry Standards Joint Committee (MSJC, 1999 and 2001):  $E_m = 700 f'_m$  (psi) and  $e'_m = 0.0035$  for clay

**Table 3. Results of Unstrengthened and Strengthened Walls**

	<b>Parameters</b>	<b>Unstrengthened Wall</b>	<b>Strengthened Wall</b>
	<b>(1)</b>	<b>(2)</b>	<b>(3)</b>
Geometry	$w_m$ , mm (in)	300 (12)	800 (32)
	Strips	8	3
	$A_f$ , mm <sup>2</sup> (in <sup>2</sup> )	0	179 (0.278)
Intermediate Results	$b_1$ , mm (in)	232 (9.1)	155 (61)
	$b_2$ , mm (in)	70 (2.75)	70 (2.75)
	$D_1$ , mm (in)	0.92 (3.6x10 <sup>-2</sup> )	0.92 (3.6x10 <sup>-2</sup> )
	$P$ , kN (kips)	14.4 (3.25)	52.6 (11.82)
Analytical Results	$P_{total}$ , kN (kips)	115.2 (25.9)	157.8 (35.5)
	$D_o$ mm (in)	4.7 (0.19)	7.2 (0.28)
	$q$ (°)	0.22	0.34
Experimental Results	$P_{total}$ , kN (kips)	106.9 (24.0)	151.6 (34.1)
	$D_o$ mm (in)	4.3 (0.17)	6.1 (0.24)
	$q$ (°)	0.18	0.35



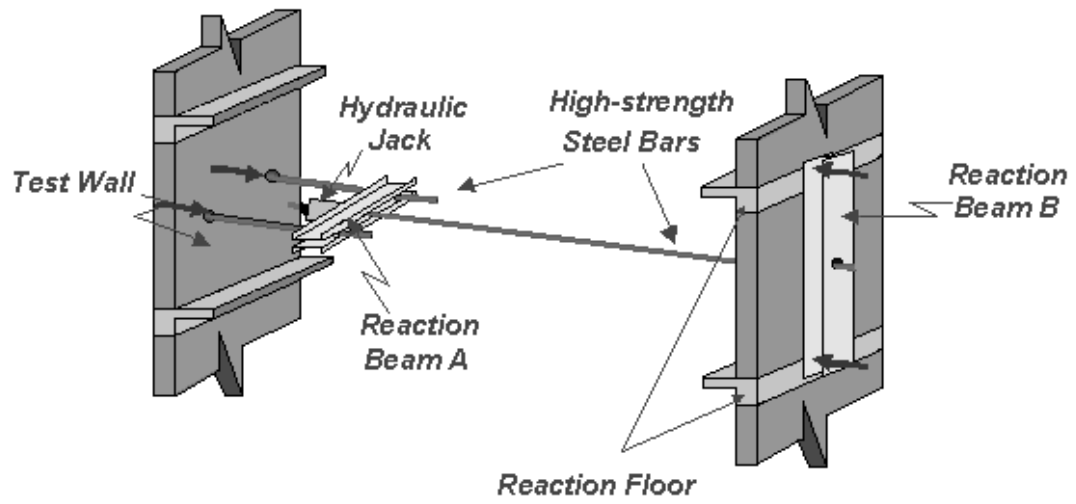
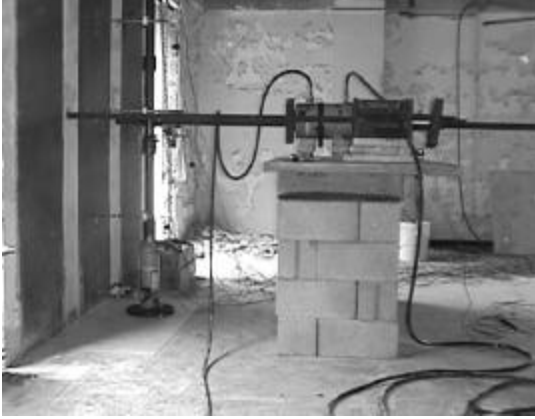


**Figure 2. Test Setup**



(a) Beam A and Hydraulic Jack



(b) Beam B

**Figure 3. Views of Test Setup**

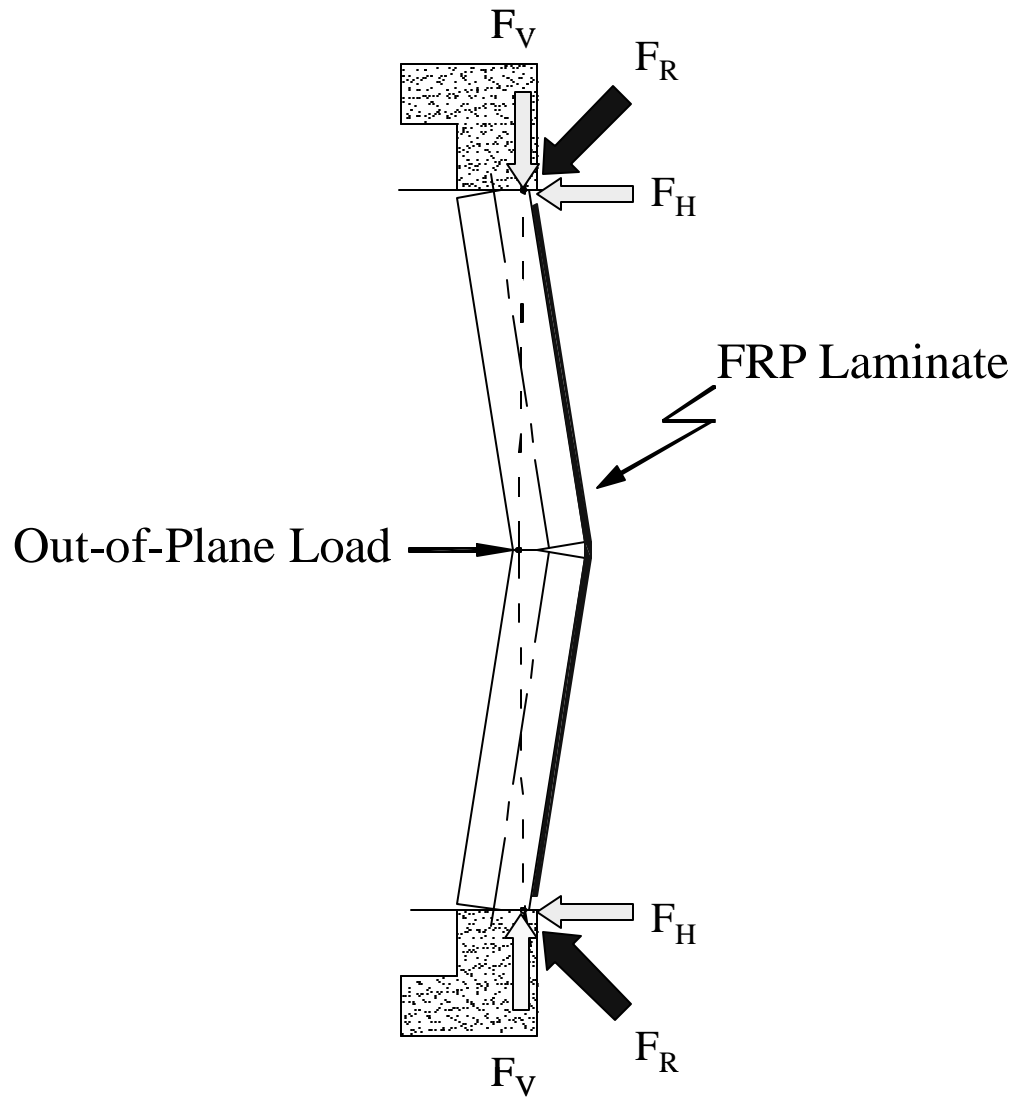


**Figure 4. Out-of-Plane Mechanism of Failure**



(a) Plaster Delamination (Wall SP)



(b) Fracture of Tile (Wall SM)

**Figure 5. Mode of Failure**

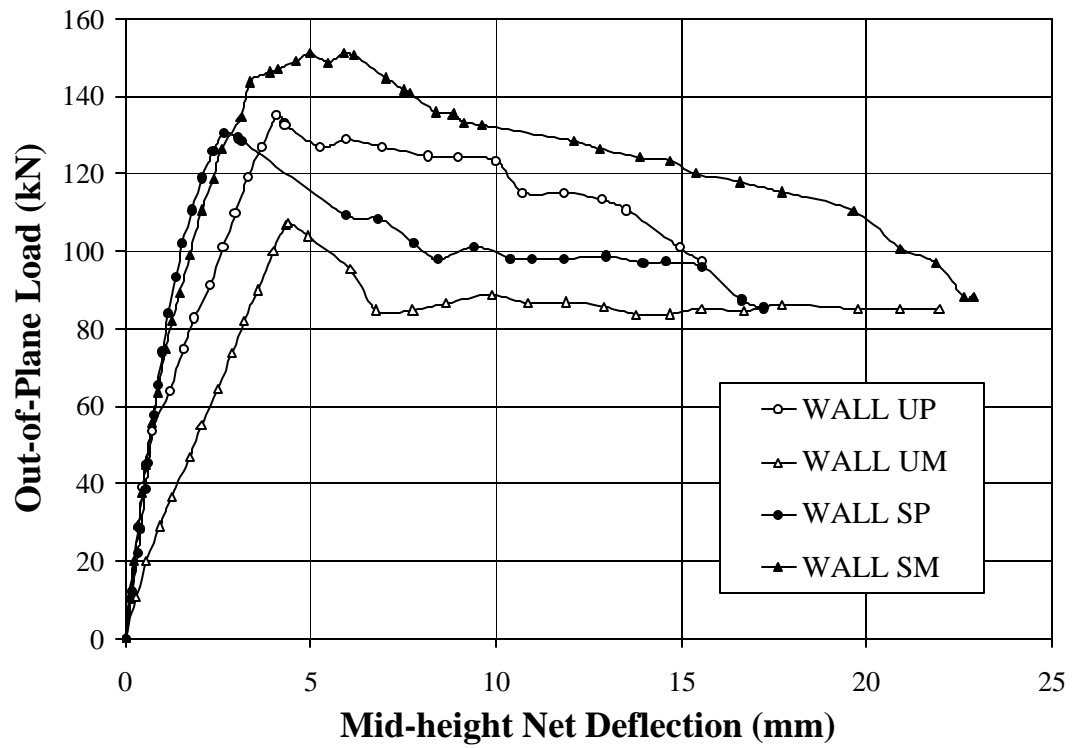


Figure 6. Behavior Comparison of Walls UP, UM, SP and SM

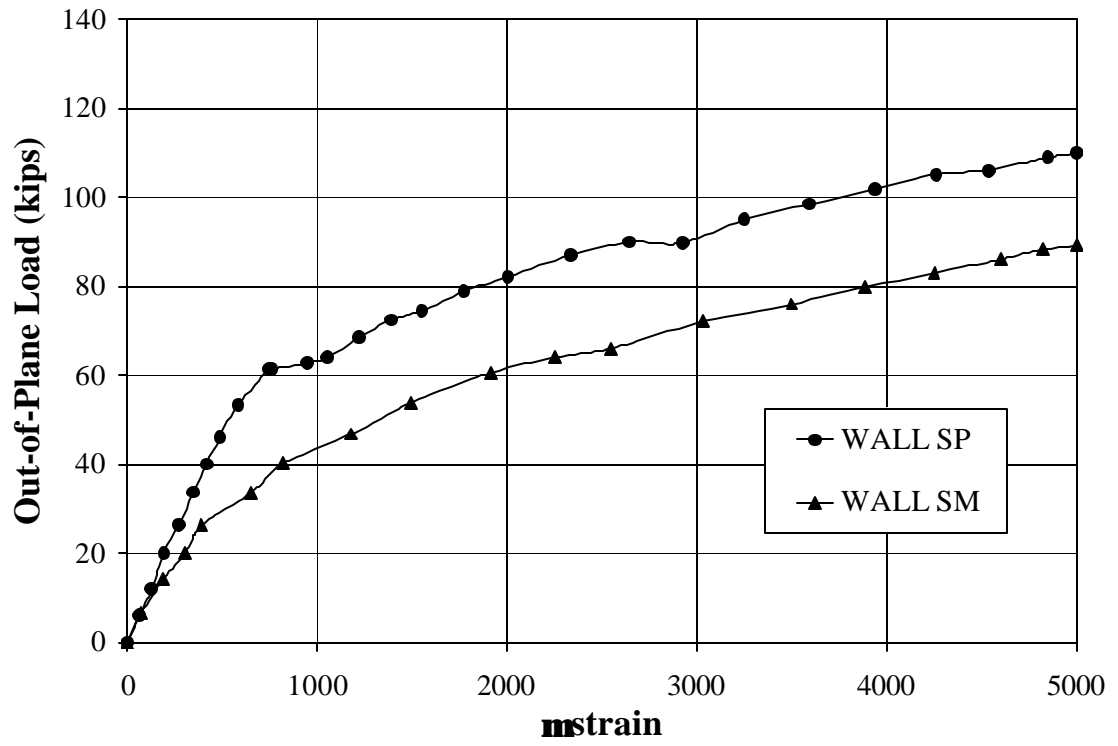
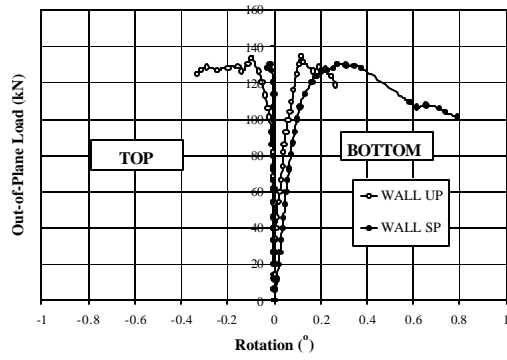
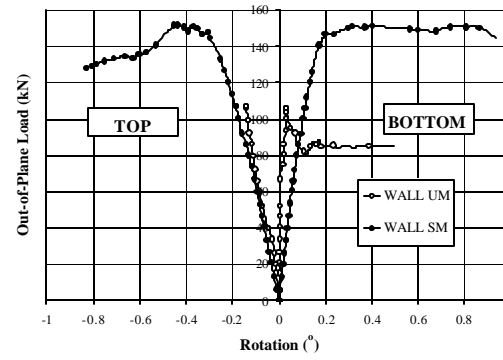


Figure 7. Strain Comparison for Walls SP and SM

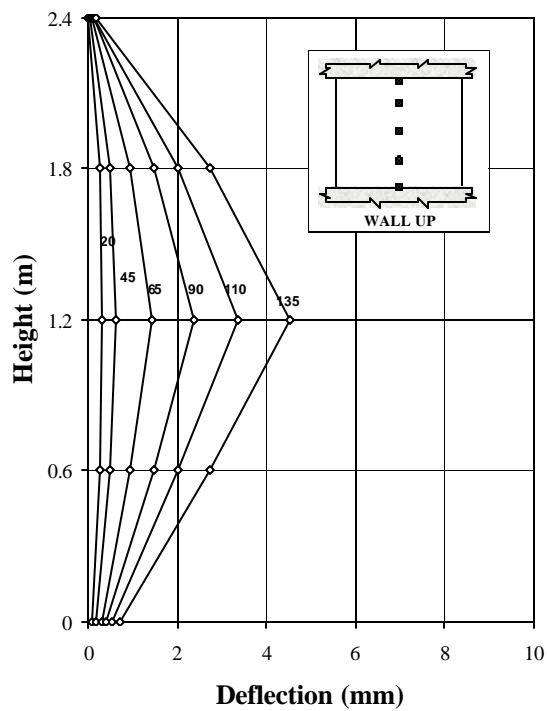


(a) Wall UP and Wall SP

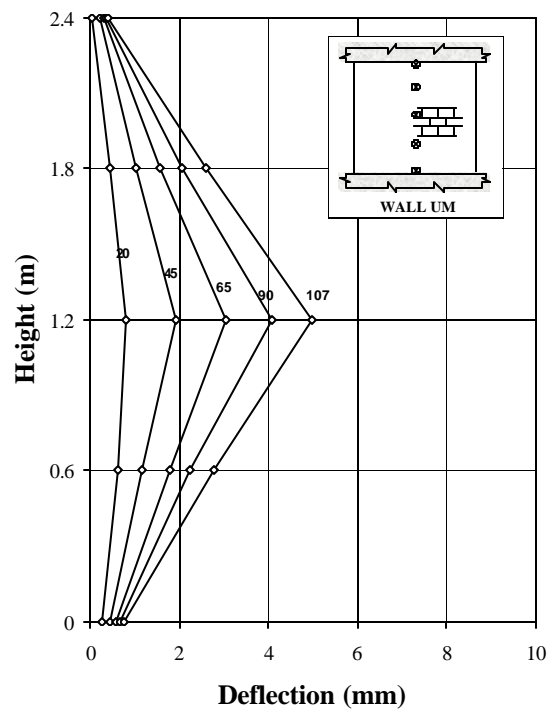


(b) Wall UM and Wall SM

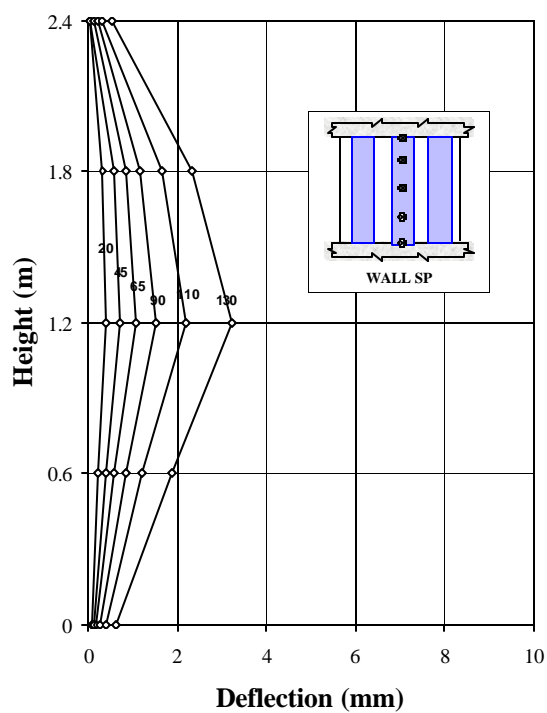
**Figure 8. Rotations in Upper and Lower Regions**



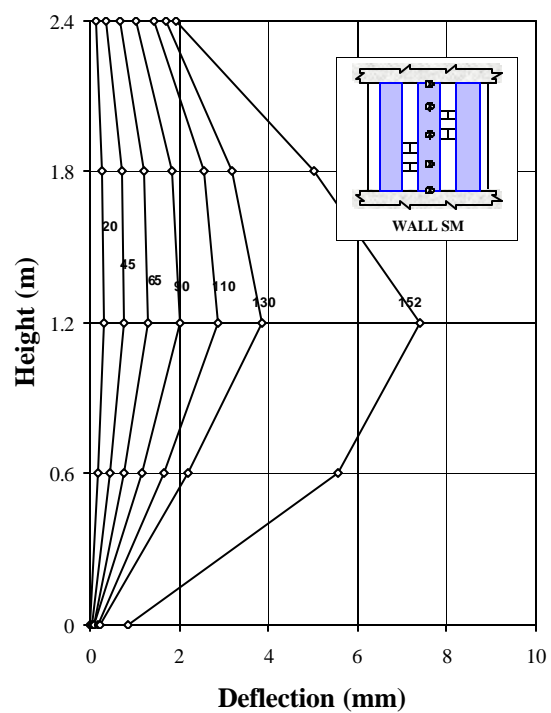
(a) Wall UP



(b) Wall UM

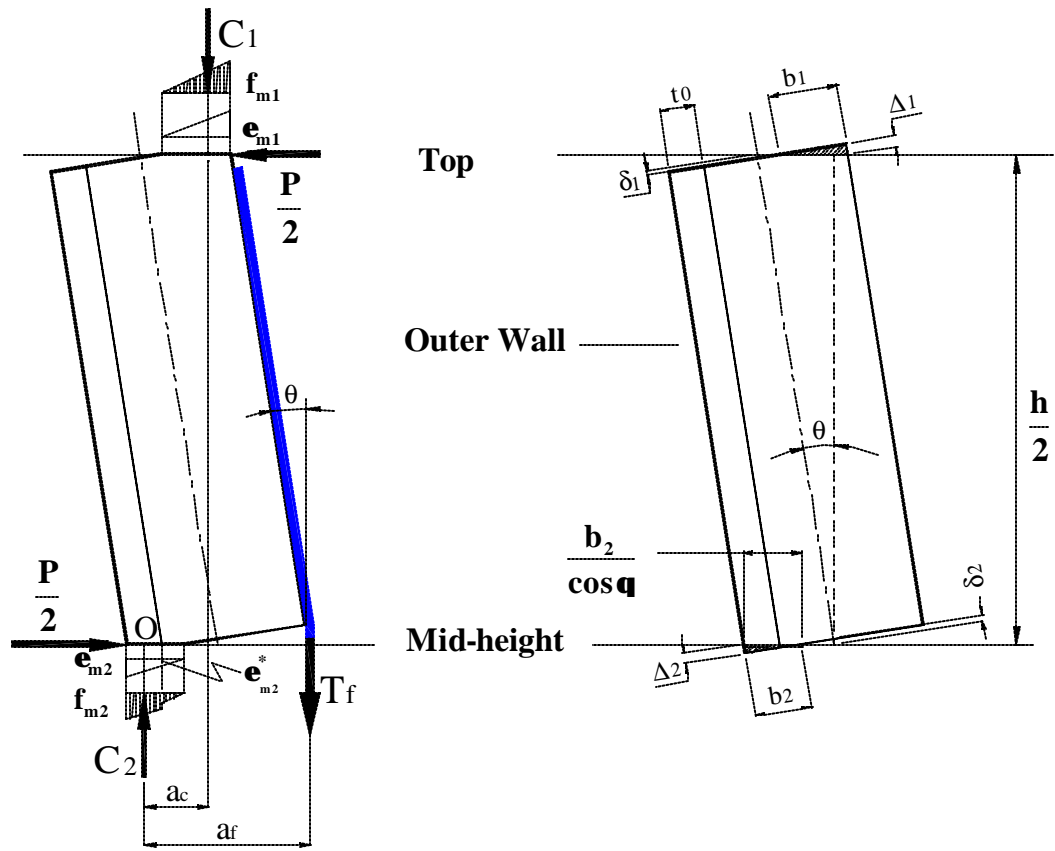


(a) Wall SP



(a) Wall SM

Figure 9. Height vs. Deflection Curves



(a) Free-body Diagram

(b) Geometrical Considerations

Figure 10. Upper Part of Analyzed Wall

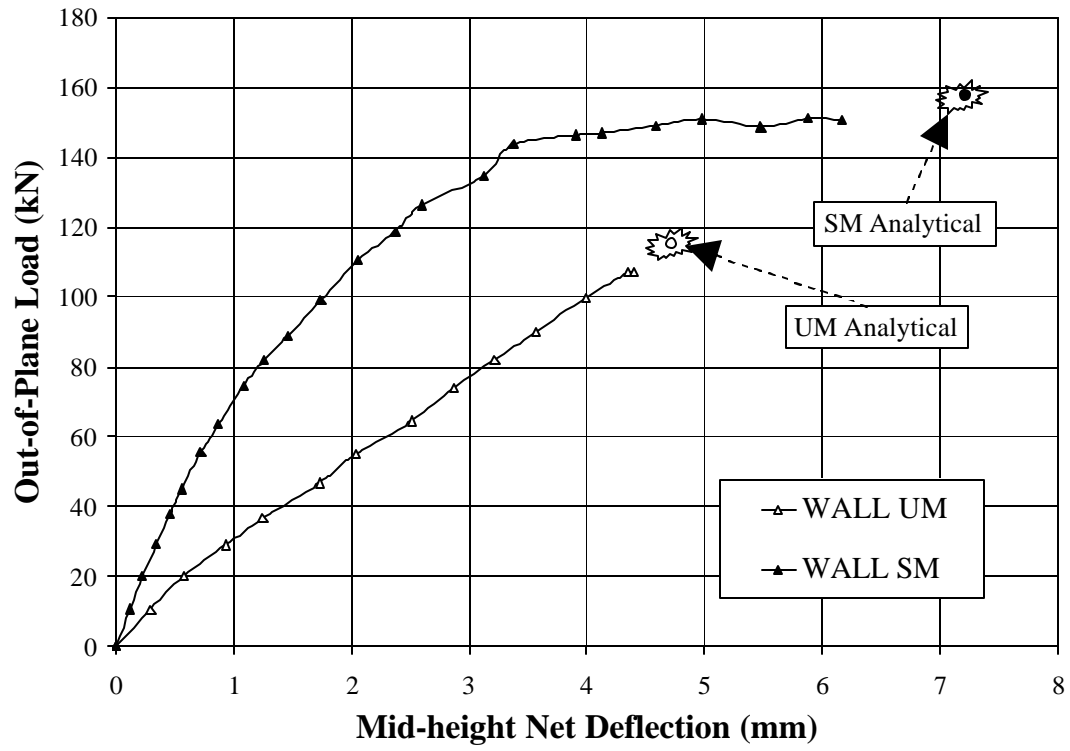


Figure 11. Comparison of Experimental and Analytical Results

# **INFLUENCE OF ARCHING MECHANISM IN MASONRY WALLS STRENGTHENED WITH FRP LAMINATES**

*Nestore Galati, University of Missouri–Rolla, Rolla MO*

*J. Gustavo Tumialan, University of Missouri–Rolla, Rolla MO*

*Antonio Nanni, University of Missouri–Rolla, Rolla MO*

*Antonio La Tegola, University of Lecce, Italy*

## **Abstract**

Fiber reinforced polymer (FRP) laminates have been proven to notably increase the flexural capacity of unreinforced masonry (URM) walls. This assertion is true in the case of walls that can be treated as simply supported (i.e. walls exhibiting large slenderness ratios). For walls with low slenderness ratios and that are built between rigid supports, when the out-of-plane deflection increases, the wall is restrained from free rotation at its ends. This action induces an in-plane compressive force, which, depending on the degree of support fixity, can increase several times the wall capacity. This mechanism is known as arching. Due to arching, the increase of capacity in walls strengthened with FRP laminates may be considerably less than expected. This paper presents the experimental results of masonry specimens confined by two rigid supports, simulating upper and lower floor beams, subjected to out-of-plane loading. Experimental results show that the contribution of FRP to the wall capacity is less than in the case of simply supported conditions. An analytical method is used for determining the capacity of masonry walls strengthened with FRP laminates considering the arching mechanism. The method analyzes infill walls that span between two rigid supports. The method shows good agreement with the experimental results and allows for appropriate design.

## Introduction

Masonry walls may be subjected to out-of-plane loads caused by high wind pressures or earthquakes. Externally bonded fiber reinforced polymer (FRP) laminates or near-surface-mounted (NSM) FRP bars have been successfully used to increase the flexural capacity of masonry members subject to out-of-plane loads (Ehsani et al., 1999, Hamilton et al. 1999, Tumialan et al., 2002).

The load-resisting mechanisms for FRP strengthened unreinforced masonry (URM) walls depend on the tensile strength of masonry, in-plane compressive strength, boundary conditions, slenderness ratio (height/thickness), and material and bond properties of the FRP. When a wall is built between supports that restrain the outward movement, membrane compressive forces in the plane of the wall, accompanied by shear forces at the supports are induced as the wall bends.

The in-plane compression forces can delay cracking. After cracking, a so-called arching action can be observed. Due to this action, the capacity of the wall can be much larger than that computed assuming simply supported conditions. Analysis has shown that the induced forces can increase the cracking load by a factor of about 2.5 if the end supports are completely rigid (L.R. Baker, 1978; A.W. Hendry, 1981). Experimental works (Tumialan et al. 2001) have shown that the resultant force between the out-of-plane load and the induced membrane force could cause the crushing of the masonry units at the boundary regions. In this case, the application of the FRP did not exhibit the same effectiveness as in the case of walls having simply supported conditions. This paper presents the experimental results of a group of ten walls having a slenderness ratio equal

to 12, confined by two rigid supports. A comparison between the experimental and analytical values of out-of-plane capacity is also presented.

### **Experimental Program**

As shown in Table 1, ten specimens were built in order to investigate the FRP effectiveness in walls exhibiting arching action. Five specimens were built with concrete blocks. The remaining five were built with clay masonry bricks. The nominal dimensions of these walls were 1.22 m (48 in.) by 0.61 m (24 in.); their overall thickness was 95 mm ( $3 \frac{3}{4}$  in.) for clay specimens and 92 mm ( $3 \frac{5}{8}$  in.) for concrete specimens, (Figure1). To study modes of failure, different amounts of glass FRP (GFRP) reinforcement were applied to the wall surface and expressed as a function of the balanced reinforced ratio,  $\rho_b$ . The balanced condition occurs when the compressive failure of the masonry is reached at the same time that the FRP laminate fails in tension. Two different surface preparation methods (with or without putty filler) were used. The surface preparation of all the masonry specimens built with clay units included the use of putty.

This was because the clay brick wall surfaces exhibited more unevenness than those with concrete blocks. The two series of walls were coded: CLx and COx. The first two characters in the code represent the type of masonry used, “CO” for concrete masonry and “CL” for clay masonry. The last character is a number that indicates the width of the GFRP strip in inches (one strip per specimen). Thus, CL3 is a clay masonry wall, strengthened with a GFRP laminate having a width of 75 mm (5in.). The specimens CL0 and CO0 are the control walls for clay and concrete masonry units respectively. In

every case, the length of the FRP strips was 1170 mm (46 in.); in this manner the laminate would not touch the roller supports used for testing.

For each specimen, a GFRP laminate was installed only on one side of the wall along the longitudinal axis. For the installation, the manual lay-up technique was followed.

Five strain gages (uniformly distributed and in correspondence of the bed joints where crushing is expected) were applied on the GFRP laminate (Figure 1) to monitor the tensile strain distribution along the laminate during the test.

Table 1. Test Matrix

<b>Specimen</b>	<b>Masonry Type</b>	<b>Thickness mm (in)</b>	<b>GFRP width mm (in)</b>	<b><math>r_b</math> (%)</b>	<b>h/t ratio</b>
CL0	Clay	95 (3 $\frac{3}{4}$ )	-	-	12.8
CL3	Clay	95 (3 $\frac{3}{4}$ )	76.2 (3)	43	12.8
CL5	Clay	95 (3 $\frac{3}{4}$ )	127.0 (5)	72	12.8
CL7	Clay	95 (3 $\frac{3}{4}$ )	177.8 (7)	100	12.8
CL9	Clay	95 (3 $\frac{3}{4}$ )	228.6 (9)	130	12.8
CO0	Concrete	92 (3 $\frac{5}{8}$ )	-	-	13.2
CO3	Concrete	92 (3 $\frac{5}{8}$ )	76.2 (3)	100	13.2
CO5	Concrete	92 (3 $\frac{5}{8}$ )	127.0 (5)	167	13.2
CO7	Concrete	92 (3 $\frac{5}{8}$ )	177.8 (7)	233	13.2
CO9	Concrete	92 (3 $\frac{5}{8}$ )	228.6 (9)	300	13.2

Note:  $\rho_b$  = balanced condition; h=height of the wall; t=thickness of the wall

Tests were performed to characterize the engineering properties of the materials used in this investigation. The average compressive strengths of concrete and clay masonry obtained from testing of prisms (ASTM C1314) were 10.5 MPa (1520 psi) and 17.1 MPa (2480 psi), respectively. Standard mortar specimens were tested according to ASTM C109. An average value of 7.6 MPa (1100 psi) at an age of 28 days was found; therefore, the mortar can be classified as Type N.

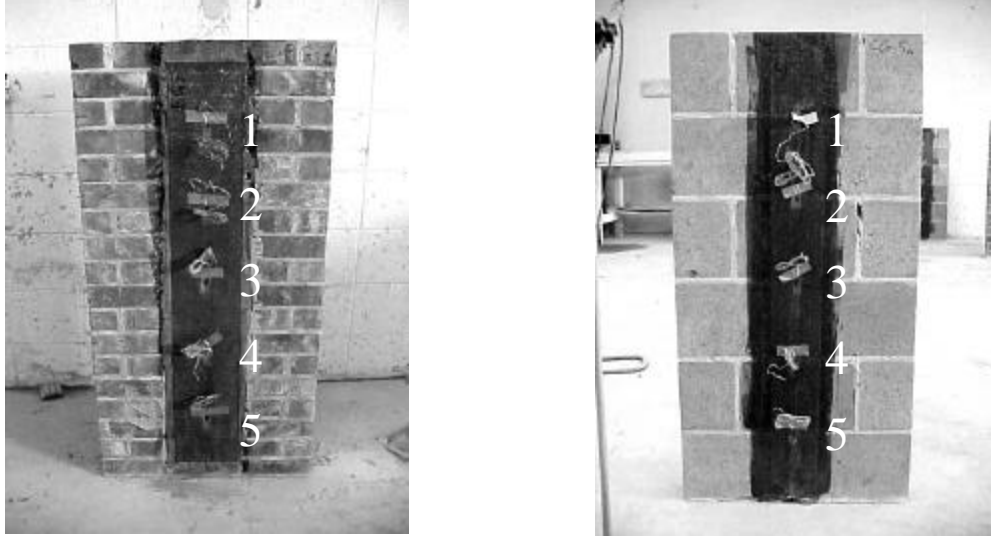


Figure 1. Test Specimens and Strain Gage Locations

Tensile tests were performed on FRP laminates to determine their engineering properties. The test results showed that the tensile strength of GFRP was 1690 MPa (245 ksi) and the modulus of elasticity was 92.9 GPa (13.46 msi).

### Test Setup

To reproduce the real boundary conditions when the wall is restrained inside a reinforced concrete (RC) frame, and to separate the two reaction forces (shear and in-plane load at the support), four reinforced concrete members were used. The bottom members provided the vertical reaction (See Figure 2). The top member resisted the horizontal load, created by the arching effect of the wall. High strength steel rods were used to connect these members to the steel test frame.

The masonry walls were tested under four-points bending. Loads were applied by 50.8 x 609.6 x 12.7 mm (2 x 24 x ½ in.) steel plates to the external face of the wall (figure 2). Their distance was 101.6 mm (4 in.) from the midspan. The loads were generated by means of a 12 ton hydraulic jack reacting against a steel frame. Linear Variable Displacement Transducers (LVDTs) were positioned in the middle of the walls

to measure the midspan deflection during the tests. Two load cells were used to record the in-plane (load cell 2) and the out-of-plane (load cell 1) loads. A horizontal load of 2.9 kN/m (200 lb/ft) was applied before testing to hold the walls in place. This load was selected in accordance with the Masonry Joint Standards Committee (MSJC, 1999) recommendations, which specify that level of load as the limit between non-loadbearing and loadbearing walls.

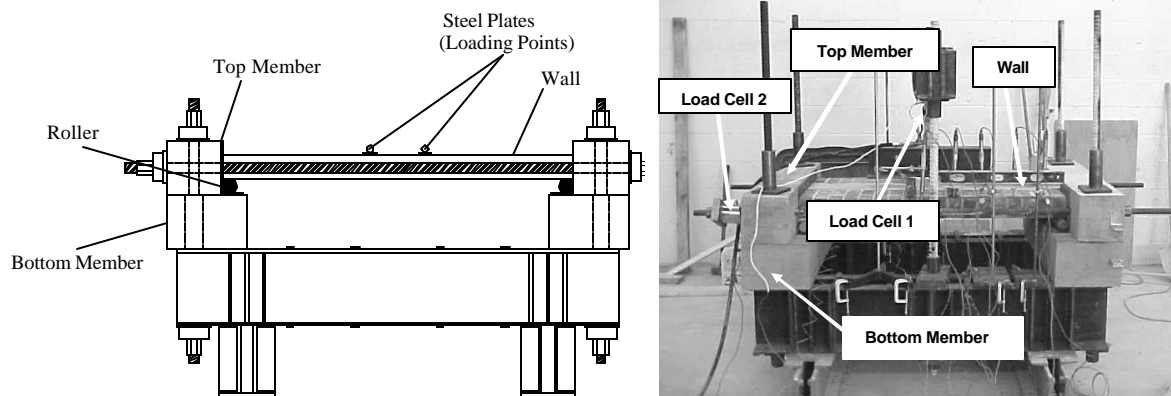


Figure 2. Test Setup Scheme

## Test Results

Three different modes of failure were observed:

- **Flexural Failure:** after developing flexural cracks primarily located at the mortar joints, a wall failed by either rupture of the FRP laminate or masonry crushing depending on the reinforcement ratio,  $\rho$ , and arching effect.
- **Crushing of the masonry at the supports:** this is the most common mode of failure in walls in which arching mechanism occurs. This kind of failure is due to the resultant force from shear and the in-plane forces at the supports.

- **Shear Failure:** cracking started with a development of fine vertical cracks at the maximum bending region. Only flexural-shear failure was observed. The sliding shear was not observed because of the in-plane force at the supports.

In the control specimens and in specimens CL3, CL5, CO3 and CO5 crushing of the masonry units at the boundary regions was observed. For specimens CL7, CO7, CL9 and CO9 failure occurred due to the shear. Figure 3 shows a series of pictures illustrating the various modes of failure.

Tests results in terms of ultimate load and maximum midspan deflection are summarized in Table 2. For the midspan deflection, the average value of the two LVDTs was used unless noted.

## **Results Discussion**

Figure 4 illustrates the out-of-plane load versus the mid-height deflection obtained for all specimens. For the clay masonry specimens (Figure 4a), a remarkable increment of flexural capacity compared to the control wall can be observed for all reinforced specimens. This increment may be overly optimistic because the arching mechanism was not completely developed in the control specimen due to set-up difficulties. It can be observed from Figure 4a that the different amounts of reinforcement do not dramatically influence the ultimate load. Higher reinforcement can only increase the stiffness and reduce deflection. By increasing the amount of reinforcement a drop in ductility was observed.

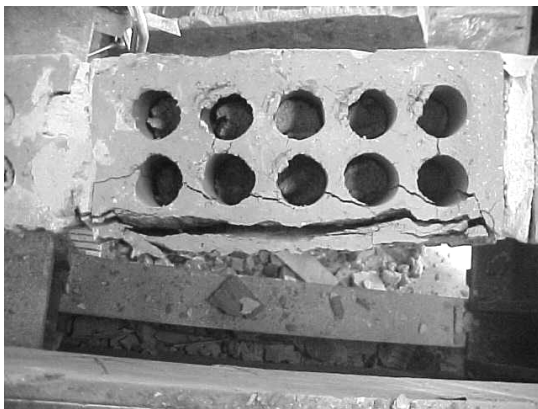
The results obtained in the case of the concrete blocks were similar to the ones obtained in the case of the clay bricks (see Figure 4b) even though the performance of the control specimen was closer to that of the reinforced ones.



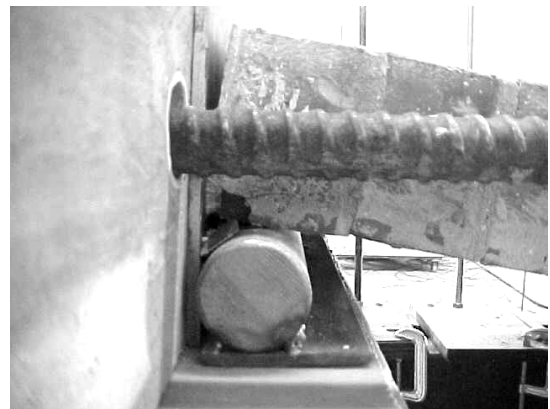
(a) Fiber Rupture (CL3)



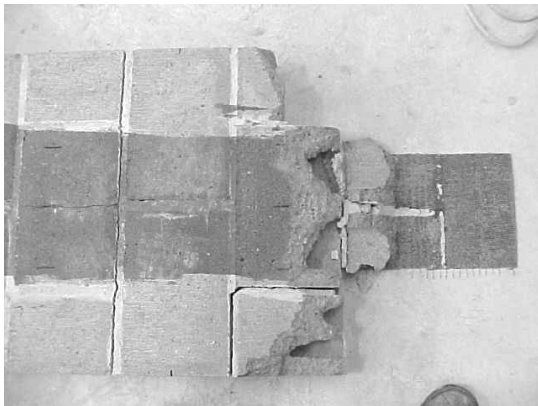
(b) Crushing of Units at Midspan (CO0)



(c) Crushing of Units at Support (CL5)



(d) Crushing of Units at Support (CL5)



(e) Shear Failure (CO9)



(f) Shear Failure (CL9)

Figure 3. Failure of the Specimens

Table 2. Test Results

Specimen	Out-of-Plane Load (kN)	In-Plane Load (kN)	Midspan Deflection [mm]	Mode of Failure
CL0	21.3	57.8	30.1 <sup>(*)</sup>	Crushing of Masonry Units
CL3	52.2	115.6	31.7	Fiber Rupture
CL5	45.6	101.4	28.9 <sup>(*)</sup>	Crushing of Masonry Units
CL7	54.9	97.9	24.1	Masonry Shear
CL9	53.1	80.9	18.1	Masonry Shear
CO0	22.4	83.6	31.1 <sup>(*)</sup>	Crushing of Masonry Units
CO3	29.0	82.7	26.5	Crushing of Masonry Units
CO5	27.1	58.7	18.1	Crushing of Masonry Units
CO7	33.1	58.7	20.7	Masonry Shear
CO9	34.7	38.3	21.6	Masonry Shear

Note: 1 mm = 0.03937 in.; 1 kN = 0.2248 kips <sup>(\*)</sup>:one LVDT

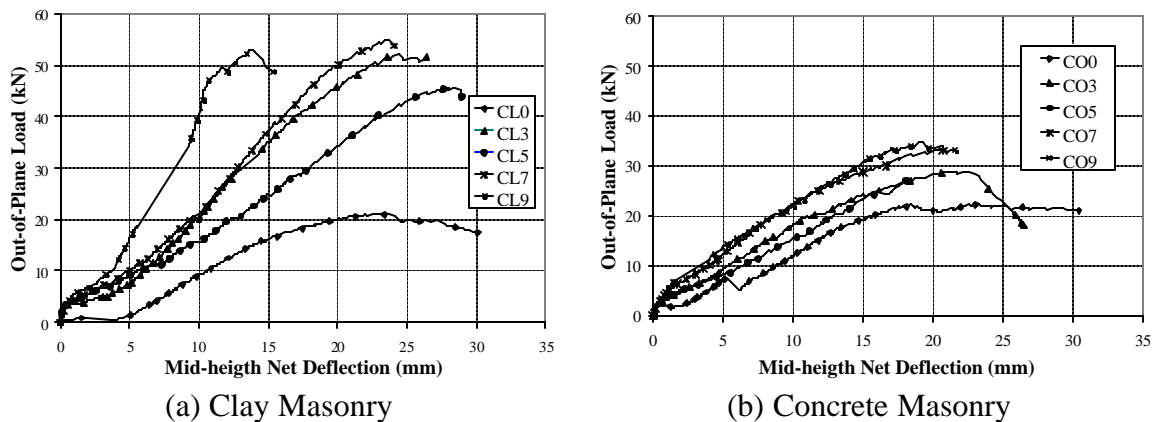
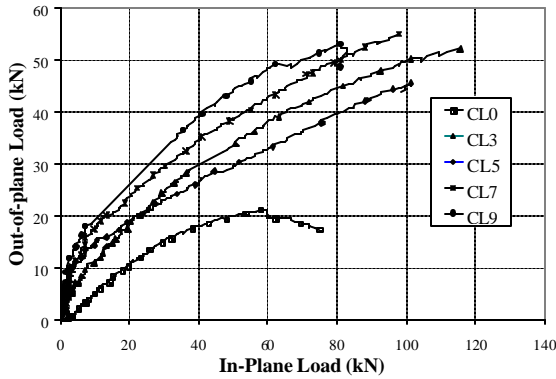
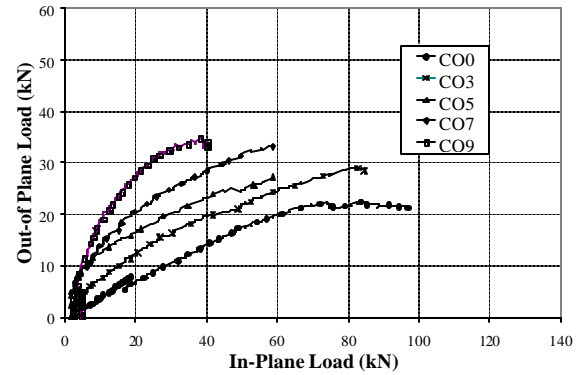


Figure 4. Load vs. Mid-height Deflection

By analyzing the experimental data, it is observed that when the first crack appeared in the walls, the in-plane restraining force suddenly increased. This can be referred to as the arching action. By plotting the out-of-plane load versus the in-plane load, it can be observed that the in-plane load remains practically constant until the first crack appears in the specimens (see Figure 5) and then grows almost linearly.



(a) Clay Masonry

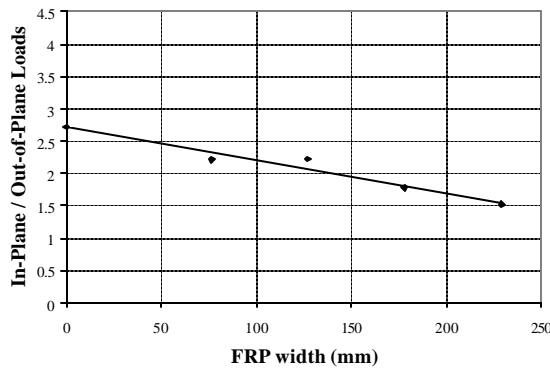


(b) Concrete Masonry

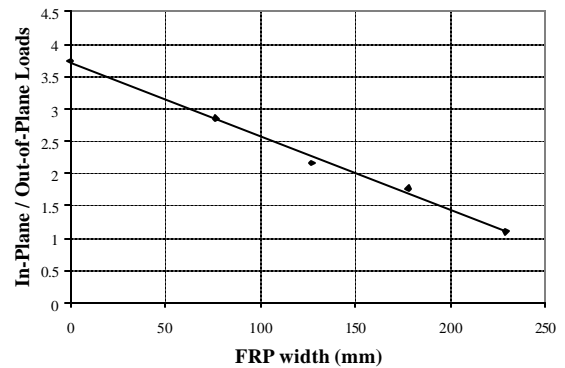
Figure 5. In-Plane Load vs. Out-of-Plane Load

By increasing the amount of FRP, due to the reduction of the displacement, the in-plane load decreased. The same trend can be observed by analyzing the maximum in-plane/out-of-plane load ratio as a function of the FRP width (Figure 6). The test results show a consistent pattern. The in-plane/out-of-plane load ratio decreases linearly when the FRP amount increases.

Figure 7 illustrates a comparison between the load-deflection curves obtained in the case of simply supported walls (Tumialan et al., 2002) and walls with the end restrained. A significant influence of the boundary conditions in the wall behavior is observed.



(a) Clay Masonry



(b) Concrete Masonry

Figure 6. In-Plane/Out-of-Plane Load Ratio as a Function of FRP Width

If the wall behaves as a simply supported element (i.e. large slenderness ratio or upper end is not restrained), the FRP reinforcement is very effective since the wall is in pure flexure and the crack openings are bridged by the reinforcement. In the case of the simply-supported specimens, the URM wall collapsed when the vertical load was about 3.1 kN (0.7 kips). Figure 7 shows that the increase in the ultimate load for walls strengthened with 75 mm (3 in.) and 125 mm (5 in.) wide GFRP laminates were about 175 and 325%, respectively. If the wall is restrained (i.e. arching mechanism is observed) the same effectiveness of the FRP reinforcement is not observed because crushing of the masonry units at the boundary regions controls the wall behavior. In this case, the increase in the out-of-plane capacity for strengthened specimens with 75 mm (3 in.) and 125 mm (5 in.) wide GFRP laminates was about 25%.

### **Analytical Study**

The experimental results have been compared with the analytical result obtained using a model developed by the same authors (Tumialan et al., 2001). Using this model it is possible to determine the out-of-plane and in-plane loads, mid-height deflection, and rotations at the supports that both unreinforced and externally strengthened walls can resist. In the present analytical formulation, the wall is idealized as a unit strip subjected to a concentrated load applied normal to its plane. This model can be extended to distributed loads. The model takes into account the clamping forces in the supports, originated by arching action, which leads to increasing the out-of-plane resistance. Previous researchers (Fricke, 1992, Angel et al., 1994) have found this resistance to be many times greater than the one predicted by conventional theories that do not consider post-cracking mechanisms.

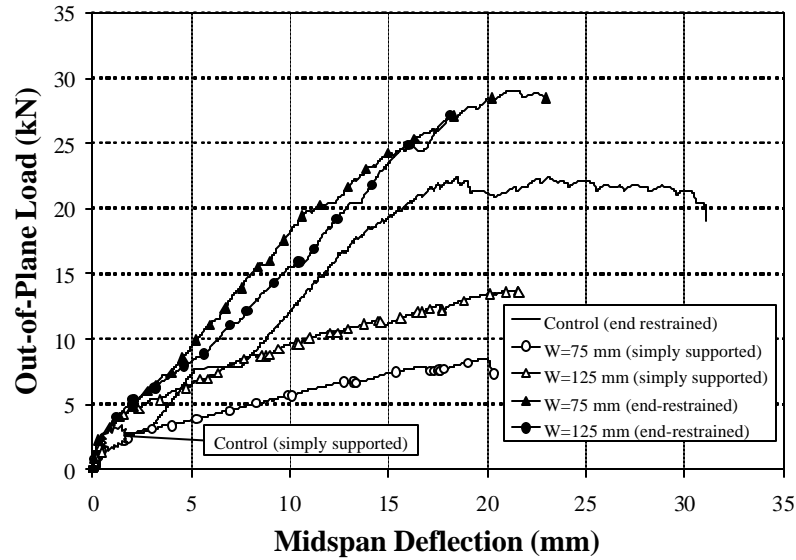


Figure 7. Comparison between Simply Supported and End-Restrained Walls

To formulate the analytical model, it is assumed that constituent materials are linearly elastic up to failure. For the case of masonry, a previous research study has demonstrated that consideration of a triangular stress distribution is adequate for arching mechanisms (Angel et al., 1994). It is also assumed that the wall is only cracked at mid-height, and that the two resulting segments can rotate as rigid bodies about the supports as illustrated in Figure 8. As a limit state, crushing of masonry at the boundary regions or flexural failure (i.e. rupture of fiber or crushing of masonry) is considered.

The forces  $F_V$  and  $F_H$  represent the in-plane reaction and the shear force at the support respectively. The resultant force from  $F_V$  and  $F_H$  causes, in many cases, the crushing of the masonry units at the support. The aforementioned analytical model fits very well with the experimental results (Table 3).

The discrepancy between the analytical and the experimental results for the CL0 specimen was caused by problems occurred during the test. The model indicates that the

predicted load for specimen CL3 was the limit between crushing of masonry at the supports and rupture of FRP. The latter was attained experimentally.

Table 3. Comparison between Theoretical and Analytical Out-of-Plane Loads

Specimen	FRP width (mm)	Experimental Load (kN)	Predicted Load (kN)	Percentage of Error (%)
CL0	0	21.3	44.1	107
CL3	75	52.2	51.0 <sup>(1)</sup>	2
CL5	125	45.6	54.8	20
CL7	175	55.0	58.1 <sup>(2)</sup>	5
CL9	225	53.1	61.0 <sup>(2)</sup>	15
CO0	0	22.4	24.0	7
CO3	75	29.0	29.4	1
CO5	125	27.1	32.0	18
CO7	175	33.1	34.5 <sup>(2)</sup>	4
CO9	225	34.7	36.5 <sup>(2)</sup>	5

Note: 1 mm = 0.03937 in.; 1 kN = 0.2248 kips

<sup>(1)</sup> Specimen failed by FRP rupture

<sup>(2)</sup> Specimens failed by shear

Shear failure was registered for specimens CL7, CL9, CO7, and CO9. The comparison between the experimental and predicted loads for these specimens suggests that crushing of the masonry units at the boundary regions was close to occur.

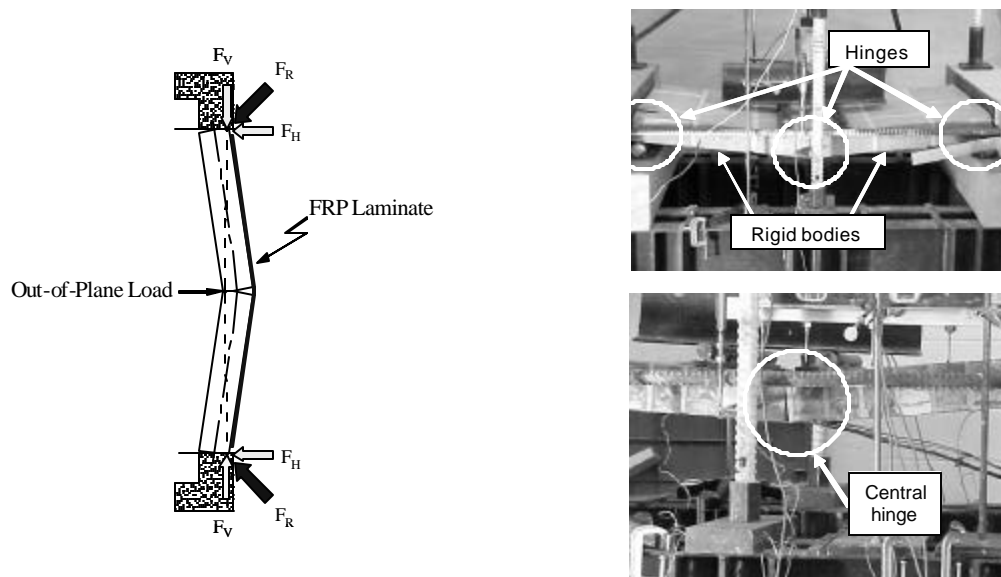


Figure 8. Out-of-Plane Mechanism of Failure

## **Conclusions**

The following conclusions can be drawn from this experimental program:

- A mechanism of failure that is not commonly considered for the analysis of FRP strengthened walls was studied. End-restrained walls exhibited an arching mechanism where crushing at the supports controlled the wall behavior. This mechanism of failure must be considered in the quantification of upgraded wall capacities to avoid overestimating the wall response.
- The analytical model used to determine the peak load and deflection of both unreinforced and strengthened walls shows good agreement with experimental results and can be easily modified to take into account distributed loads acting on the wall, and incorporated in design provisions.

## **Acknowledgements**

The support of the National Science Foundation Industry/University Cooperative Research Center at the University of Missouri–Rolla and Rolla Technical Institute (RTI) are acknowledged. The authors would also like to thank Marco Casareto, Alessandro Oliveri, and Alessandro Romelli, UMR Visiting Scholars from the University of Genoa, Italy, for their assistance.

## References

1. Angel, R., Abrams, D. P., Shapiro, D., Uzarski, J., and Webster, M. (1994). "Behavior of Reinforced Concrete Frames with Masonry Infills." Struct. Res. Ser. 589, Department of Civ. Engrg., University of Illinois at Urbana-Champaign, IL.
2. Baker L. R., (1978) " Precracking Behavior of Laterally Loaded Brickwork Panels with In-Plane Restrains," in Proceedings of the British Ceramic Society, No. 27, pp. 129 -146.
3. Ehsani, M. R., Saadatmanesh, H., and Velazquez-Dimas, J. I. (1999). "Behavior of Retrofitted URM Walls Under Simulated Earthquake Loading." J. of Comp. for Const., ASCE, 3(8), 134-142.
4. Hamilton, H.R. III, Holberg, A., Caspersen, J., and Dolan, C. W. (1999). "Strengthening Concrete Masonry with Fiber Reinforced Polymers." 4th Int. Symp. on Fiber Reinf. Polymer (FRP) for Reinf. Conc. Struct., Baltimore, MD, 1103-1115.
5. Hendry A. W., (1981). "Structural Brickwork", pp. 128 and 141, The Macmillan Press Ltd., Landon.
6. Masonry Standards Joint Committee. (1999). "Building Code Requirements for Masonry Structures." ACI-530-99/ASCE 5-99/TMS 402-99, Detroit, MI, New York, NY, and Boulder, CO.
7. Tumialan J. G. (2001). "Strengthening of Masonry Structures with FRP Composites." Doctoral Dissertation, University of Missouri-Rolla, Rolla, MO.
8. Tumialan, J. G., Galati, N., and Nanni, A., (2002). "Field Assessment Of URM Walls Strengthened With FRP Laminates", submitted to the Journal of Structural Engineering.

9. Tumialan, J. G., Galati, N., Namboorimadathil, S. M., and Nanni, A., (2002). "Strengthening of Masonry with FRP Bars" ICCI 2002, San Francisco, CA, June 10-12, 2002.
10. Tumialan J.G., Morbin A., Micelli F. and Nanni A., (2002). "Flexural Strengthening of URM Walls with FRP Laminates," ICCI 2002, San Francisco, CA, June 10-12, 2002.

## **ARCHING EFFECT IN MASONRY WALLS REINFORCED WITH FIBER REINFORCED POLYMER (FRP) MATERIALS**

Nestore Galati, J. Gustavo Tumialan and Antonio Nanni

**Abstract:** Fiber reinforced polymer (FRP) laminates have been proven to notably increase the flexural capacity of unreinforced masonry (URM) walls. This assertion is true in the case of walls that can be treated as simply supported (i.e. walls exhibiting large slenderness ratios). For walls with low slenderness ratios and that are built between rigid supports, when the out-of-plane deflection increases, the wall is restrained from free rotation at its ends. This action induces an in-plane compressive force, which, depending on the degree of support fixity, can increase several times the wall capacity. This mechanism is known as arching. Due to arching, the increase of capacity in walls strengthened with FRP laminates may be considerably less than expected. This paper presents the experimental results of masonry specimens confined by two rigid supports, simulating upper and lower floor beams, subjected to out-of-plane loading. Experimental results show that the contribution of FRP to the wall capacity is less than in the case of simply supported conditions. An analytical method is presented for determining the capacity of masonry walls strengthened with FRP laminates considering the arching mechanism. The method analyzes infill walls that span between two rigid supports. The method shows good agreement with the experimental results and allows for appropriate design.

**Keywords:** FRP Laminates, Flexural Strengthening, Masonry Strengthening, Out-of-Plane Failure, Unreinforced Masonry (URM)

**Nestore Galati** is a Graduate Research Assistant at CIES at UMR where he is pursuing a M.Sc. degree in Engineering Mechanics. He is also Doctoral student in Civil Engineering at the University of Lecce, Italy, where he received his B. Sc. in Civil Engineering. His research interests include repair of masonry and reinforced concrete structures.

**J. Gustavo Tumialan** is a Research Engineer at the Center for Infrastructure Engineering Studies (CIES) at the University of Missouri-Rolla (UMR), where he received his M.Sc. and Ph.D. degrees in Civil Engineering. He received his B.Sc. from the Pontificia Universidad Catolica del Peru (PUCP). His research interests include rehabilitation of masonry and reinforced concrete structures.

**Antonio Nanni**, FACI, is the V&M Jones Professor of Civil Engineering and Director of CIES at UMR. He is interested in construction materials, their structural performance, and field application. He is an active member of several ACI technical committees.

## **INTRODUCTION**

Masonry walls may be subjected to out-of-plane loads caused by high wind pressures or earthquakes. Externally bonded fiber reinforced polymer (FRP) laminates or near-surface-mounted (NSM) FRP bars have been successfully used to increase the flexural capacity of masonry members subject to out-of-plane loads (Ehsani et al., 1999, Hamilton et al. 1999, Tumialan et al., 2002).

The load-resisting mechanisms for FRP strengthened unreinforced masonry (URM) walls depend on the tensile strength of masonry, in-plane compressive strength, boundary conditions, slenderness ratio (height/thickness), and material and bond properties of the FRP. When a wall is built between supports that restrain the outward

movement, membrane compressive forces in the plane of the wall, accompanied by shear forces at the supports are induced as the wall bends.

The in-plane compression forces can delay cracking. After cracking, a so-called arching action can be observed. Due to this action, the capacity of the wall can be much larger than that computed assuming simply supported conditions. Analysis has shown that the induced forces can increase the cracking load by a factor of about 2.5 if the end supports are completely rigid (L.R. Baker, 1978; A.W. Hendry, 1981). Studies (Ref.) have shown that the induced membrane load is a function of the slenderness ratio ( $h/t$ ): the membrane load decreases by increasing the slenderness ratio.

Experimental works (Tumialan et al. 2001) have shown that the resultant force between the out-of-plane load and the induced membrane force could cause the crushing of the masonry units at the boundary regions. In this case, the application of the FRP did not exhibit the same effectiveness as in the case of walls having simply supported conditions.

This paper presents the experimental results of a group of twenty-four walls having three different slenderness ratios: 8, 12 and 19. Twenty walls were tested confining the two ends between two rigid supports and the last four were tested under simply supported conditions. The slenderness ratio for the wall tested under simply supported conditions was 12. An analytical model was developed to interpret the experimental observation. The experimental results were compared with the analytical values obtained with the analytical model.

## **RESEARCH SIGNIFICANCE**

To observe their improved performance and the mode of failure, URM specimens consisting of concrete and clay masonry panels were strengthened with different amounts of externally bonded FRP laminates to be tested under out-of-plane loads. Two different boundary conditions were considered: simply supported and fixed-fixed. Based on experimental evidence generated by this investigation, an analytical model has been developed to predict the structural behavior of URM panels strengthened with external bonded FRP laminates.

## **EXPERIMENTAL PROGRAM**

### **Test Matrix**

As shown in Table 1, twenty-four specimens were built in order to investigate the FRP effectiveness in walls exhibiting arching action. Fourteen walls were built with concrete blocks and the remaining 10 with clay bricks. Their nominal dimensions were 600 mm (24 in.) wide by 1200 mm (48 in.) high. The nominal wall thickness was about 95 mm (3.75 in.) All the specimens, except the control ones, were strengthened using GFRP laminates. The surface preparation of all the masonry specimens built with clay units included the use of putty. This was because the clay brick wall surfaces exhibited more unevenness than those of the concrete blocks. To study modes of failure, different amounts of glass FRP (GFRP) reinforcement were applied to the wall surface and expressed as a function of the balanced reinforced ratio. The balanced condition occurs when the compressive failure of the masonry is reached at the same time that the FRP laminate fails in tension.

All the masonry panels were strengthened with a single FRP strip placed along the longitudinal axis. The strip widths ranged from 75 mm (3 in.) to 228.6 mm (9 in.) on the tension side. Four different series of walls were tested: S8, S12, S19 and S $\infty$ . The difference between the different series is the slenderness ratio, defined as the ratio between the height and the thickness of the wall. For example, S8 means that the slenderness ratio for that series was equal to 8. The only difference is for the series S $\infty$  for which the real slenderness ratio was 12 but the walls were tested under simply supported conditions. Studies (Angel et al., 1994) showed that a masonry wall behaves as simply supported if the slenderness ratio is greater than 20. Therefore, testing a wall under simply supported conditions will simulate a wall with a slenderness ratio greater than 20.

The second part of the code is CLx or COx. The first two characters in the code represents the type of masonry used, "CO" for concrete masonry and "CL" for clay masonry. The last character is a number that indicates the width of the GFRP strip in inches (one strip per specimen). Thus, S12-CL5 is a clay masonry wall, strengthened with a GFRP laminate having a width of 127mm (5in.) and a slenderness ratio equal to 12. In each case, the length of the FRP strips was 1170 mm (46 in.), in this manner the laminate would not touch the roller supports used for testing.

## **Materials**

Tests were performed to characterize the engineering properties of the materials used in this investigation. The average compressive strengths of concrete and clay masonry obtained from the testing of prisms (ASTM C1314) is presented in Table 2.

Standard mortar specimens were tested according to ASTM C109. An average value of 7.6 MPa (1100 psi) at an age of 28 days was found; therefore, the mortar can be classified as Type N.

Tensile tests were performed on FRP laminates to determine their engineering properties, which are related to fiber content and not to composite area. The FRP coupons had a width of 38.1 mm (1.5 in.) and gage length of 152.4 mm (10 in.). The fiber thickness was 0.35 mm (0.014 in.). In order to provide appropriate anchorage during testing, rectangular GFRP tabs were used at both ends of each coupon to diffuse the clamping stresses. The tabs were made of two GFRP layers and were glued using the same resin used for the manual lay-up. Their dimensions were 51.0 mm (2 in.) by 38.1 mm (1.5 in.). Details of coupon fabrication and testing procedure are shown elsewhere (Yang X, 2001). The test results showed that the tensile strength of GFRP was equal to 1690 MPa (245 ksi) and the modulus of elasticity was 92.9 GPa (13460 ksi). Table 3 presents the properties of the FRP constituent materials.

### **Test Setup**

To reproduce the real boundary conditions when the wall is restrained inside a reinforced concrete (RC) frame, and to separate the two reaction forces (shear and in-plane load at the support), four reinforced concrete members were used. The bottom members provided the vertical reaction (See Figure 1). The top member resisted the membrane In-Plane load, created by the arching effect of the wall. High strength steel rods were used to connect these members to the steel test frame. Due to this connection between the two concrete members and the steel frame, part of the horizontal reaction cannot be measured by the load cell 2. Therefore, a calibration of the system was

necessary. This task was accomplished by measuring the ratio between a known applied load in the longitudinal direction and the measured one by load cell 2. Figure 2 shows the calibration curve. It can be stated that the ratio between the applied load and the measured load is 2.58; therefore the actual membrane force is 2.58 times the one read by load cell 2.

The masonry walls were tested under four-points bending. Loads were applied by 50.8 x 609.6 x 12.7 mm (2 x 24 x ½ in.) steel plates to the external face of the wall (figure 1). Their distance was 101.6 mm (4 in.) from the midspan. The loads were generated by means of a 12 ton hydraulic jack reacting against a steel frame. A total of six Linear Variable Displacement Transducers (LVDTs) were used to register deflections. Two LVDTs were placed at midspan, in both sides of the specimen; two were located at the fourths of the masonry panels. The remaining two were located at the supports to register settlements.

Five strain gauges were placed on the FRP laminates for all the reinforced specimens. One strain gauge was placed at midspan, two strain gauges were placed at 200 mm (8 in.) and two at 400 mm (16 in.) from each wall end. This relative distance between strain gages was changed for some of the specimens in order to make sure to have the strain gages in correspondence on the bed joints (see Figure 3). In fact, bed joints are the points where it is more likely for the failure to occur.

Two load cells were used to record the in-plane (load cell 2) and the out-of-plane (load cell 1) loads. A horizontal load of 2.9 kN/m (200 lb/ft) was applied before testing to hold the walls in place. This load was selected in accordance with the Masonry Joint

Standards Committee (MSJC, 1999) recommendations, which specify that level of load as the limit between non-loadbearing and loadbearing walls.

In the case of the series  $S_{\infty}$  the two top concrete members were removed and the walls were tested under simply supported boundaries conditions.

## **TEST RESULTS**

### **Modes of Failure**

The walls exhibited four different modes of failure: (1) Debonding of the FRP reinforcement from the masonry substrate, (2) Flexural Failure (i.e. crushing of the masonry in compression or rupture of the FRP in tension), (3) Shear failure of the masonry at the supports, and (4) Crushing of the masonry at the the boundary regions.

***FRP Debonding:*** due to shear transfer mechanisms at the interface masonry/FRP laminate, debonding of the laminate from the masonry substrate may occur before flexural failure. Debonding starts from flexural cracks at the maximum bending moment region and develops towards the supports. Since the tensile strength of masonry is lower than that of the epoxy resins, the failure line is in the masonry. In the case of concrete masonry walls, part of the concrete block faceshell remained attached to the FRP laminate.

***Flexural Failure:*** after developing flexural cracks primarily located at the mortar joints, a wall failed by either rupture of the FRP laminate or masonry crushing. FRP rupture occurred midspan. The compression failure was manifested by crushing of mortar joints.

***Shear Failure:*** cracking started with the development of fine vertical cracks at the maximum bending region. Thereafter two kinds of shear failure were observed:

flexural-shear and sliding shear. The former was oriented at approximately  $45^\circ$ , and the latter occurred along a bed joint causing sliding of the wall at that location, typically, at the first mortar joint in walls heavily strengthened. In the flexural-shear mode, shear forces transmitted over the crack caused a differential displacement in the shear plane, which resulted in FRP debonding. Sliding shear was not observed in the walls restrained at the ends, due to the fact that the in-plane force generated by arching delayed the formation of this mode of failure.

***Crushing of the masonry at the boundary regions:*** this is the most common mode of failure in walls in which arching mechanism occurs. This kind of failure is due to the resultant force from shear and the in-plane forces at the supports. In fact, flexural cracking occurs at the supports due to negative moments followed by cracking at mid-height due to positive moments, as a result a three-hinged arch is formed. When the deflection increases due to out-of-plane bending, the wall is restrained against the supports, in this case the upper and lower beams. This action induces an in-plane compressive force ( $F_V$  in figure 4), which accompanied by the shear force ( $F_H$  in figure 4) in the support creates a resultant force that causes the crushing of the masonry at the supports ( $F_R$  in figure 4). If the slenderness ratio is very small (i.e. less than 10), in the case of hollow blocks, splitting of the masonry at the supports can occur.

Figure 5 shows a series of pictures illustrating the various modes of failure. Test results in terms of ultimate load and maximum midspan deflection are summarized in Table 4. For the midspan deflection, the average value of the two LVDTs was used unless noted.

It can be stated that all the specimens with a slenderness ratio equal to 8 (series S8), failed by splitting of masonry at the supports. This mode of failure was essentially due to the high membrane force generated by the arching action. A comparison between the ultimate loads for the series S8 shows that the reinforcement was not effective because the entire load was carried by the compressed trusses generated by the arching action.

### **Discussion of Results**

Figure 6 illustrates the out-of-plane load versus the mid-height deflection obtained for all specimens. It can be stated that for the series S8, the effectiveness of the FRP reinforcement can be considered negligible. There is no improvement in the performance of the walls due to the very high arching action. Specimens S8-CO3 and S8-CO5 had a lower capacity than the control one. This behavior can be explained with the fact that the arching mechanism was not completely developed due to set-up difficulties.

In the case of series S12, the maximum increment in the ultimate load was 36% for both CL and CO series. This result shows that, due to the arching action, different amounts of reinforcement do not dramatically influence the ultimate load.

The maximum increment in the ultimate load for series S19 was equal to 70%. By comparing this result with the ones obtained for the previous series, it can be observed that the slenderness ratio has a key role in the behavior of the walls. By increasing the slenderness ratio of the specimens, an improvement in the effectiveness of the reinforcement can be obtained due to a reduction of the arching action.

Figure 6(e) illustrates the load vs. deflection curves for the series S $\infty$ . It is observed that the strength and stiffness of the FRP strengthened walls increased

dramatically when comparing them to a URM specimen. Following the recommendations of the Masonry Standards Joint Committee, the nominal moment for the URM concrete specimens was estimated as 3.1 kN. By comparing them to the experimental results of the FRP strengthened walls, it can be observed that depending on the amount of FRP, increments ranging from 2 to 7 times the nominal masonry capacity were achieved. Since there is a significant amount of variability attributed to labor and materials in masonry construction, this range of values should be taken simply as a reference. The test results showed a clear and consistent pattern. Up to cracking, the walls behaved almost in a linear fashion. Initial cracking occurred at the interface of mortar and masonry for concrete masonry and in the mortar joint itself for clay masonry.

Initial cracking was delayed due to the presence of FRP reinforcement. Following this, cracking at the adjacent joint occurred until almost every joint in the high moment bending area was cracked. After cracking, the flexural stiffness is a function of the amount of FRP; thus, a degradation of stiffness that is larger in walls with a high amount of FRP reinforcement was observed. In this phase of the test, the cracks widen until the failure occurred.

By analyzing the experimental data, it is observed that when the first crack appeared in the walls, the in-plane restraining force suddenly increased. This can be referred to as the arching action. By plotting the out-of-plane load versus the in-plane load, it can be observed that the in-plane load remains practically constant until the first crack appears in the specimens (see Figure 7) and then grows almost linearly.

By increasing the amount of FRP, due to the reduction of the displacement, the in-plane load decreased. The same trend can be observed by analyzing the maximum in-

plane/out-of-plane load ratio as a function of the FRP width (Figure 8). The test results show a consistent pattern. The in-plane/out-of-plane load ratio decreases linearly when the FRP amount increases.

Figure 9 illustrates a comparison between the load-deflection curves obtained in the case of simply supported walls ( $S_{\infty}$ -CO3 and  $S_{\infty}$ -CO5), and walls with the end restrained (S12-CO3 and S12-CO5). A significant influence of the boundary conditions in the wall behavior is observed. If the wall behaves as a simply supported element (i.e. large slenderness ratio or upper end is not restrained), the FRP reinforcement is very effective since the wall is in pure flexure and the crack openings are bridged by the reinforcement. In the case of the simply-supported specimens, the URM wall collapsed when the vertical load was about 3.1 kN. Figure 7 shows that the increase in the ultimate load for walls strengthened with 75 mm (3 in.) and 125 mm (5 in.) wide GFRP laminates were about 175 and 325%, respectively. If the wall is restrained (i.e. arching mechanism is observed) the same effectiveness of the FRP reinforcement is not observed because crushing of the masonry units at the boundary regions controls the wall behavior. In this case, the increase in the out-of-plane capacity for strengthened specimens with 75 mm (3 in.) and 125 mm (5 in.) wide GFRP laminates was about 25%.

## **ANALYTICAL STUDY**

An analytical model is presented for determining the out-of-plane capacity, membrane force corresponding to the ultimate transverse load, mid-height deflection, and rotations at the supports that both unreinforced and externally strengthened infill walls can resist. The wall is idealized as a strip of variable width, which is subjected to a concentrated load applied normal to the plane of the wall. This model can be extended to

distributed loads. The model takes into account the clamping forces in the supports, originated by arching action, which lead to increasing the out-of-plane resistance of URM walls. Previous researchers (Fricke, 1992, Angel et al., 1994) have found this resistance to be many times greater than the resistance predicted by conventional theories that do not consider post-cracking mechanisms.

To formulate the analytical model, it is assumed a parabolic distribution of stresses for the compressed masonry.

The stress block parameters associated with such parabolic distribution are given as:

$$\gamma\beta_1 = \left( \frac{\epsilon_m}{\epsilon'_m} \right) - \frac{1}{3} \left( \frac{\epsilon_m}{\epsilon'_m} \right)^2 \quad (1a)$$

$$\gamma\beta_1 \left( 1 - \frac{1}{2} \beta_1 \right) = \frac{2}{3} \left( \frac{\epsilon_m}{\epsilon'_m} \right) - \frac{1}{4} \left( \frac{\epsilon_m}{\epsilon'_m} \right)^2 \quad (1b)$$

According to MSJC, the maximum usable strain  $\epsilon_{mu}$  was considered to be 0.0035 mm/mm (in./in.) for clay masonry, and 0.0025 mm/mm (in./in.) for concrete masonry.

The tensile strength of masonry was neglected.

The FRP reinforcement has been assumed linear elastic up to failure. It is also assumed that the wall is only cracked at mid-height, and that the two resulting segments can rotate as rigid bodies about the supports as illustrated in Figure 4.

### **Analytical Derivations**

Analyzing the top segment of the masonry wall shown in Figure 10(a), the free-body shown in Figure 10(b) can be derived. From the equilibrium of forces in the vertical direction, the following relationship can be drawn:

$$C_2 = C_1 + T_f \quad (2)$$

where  $C_1$  and  $C_2$  are the clamping forces at top and mid-height of the wall, respectively,  $t_f$  is the force in the FRP laminate and  $\theta$  is the rotation of the wall.

Considering the stress block distribution, the clamping forces by wall strip width,  $w_m$ , acting on the restrained ends of the wall can be calculated as:

$$C_1 = \frac{\mathbf{g}_1 \mathbf{b}_{11} w_m b_1 f'_m}{\cos \mathbf{q}} \quad (3a)$$

$$C_2 = \frac{\mathbf{g}_2 \mathbf{b}_{12} w_m b_2 f'_m}{\cos \mathbf{q}} \quad (3b)$$

Where the additional subscripts 1 and 2 for  $\gamma$  and  $\beta_1$  has been used to single out the corresponding section.

The tensile force developed by the FRP laminate is:

$$T_f = A_f f_f = A_f E_f \mathbf{e}_f \quad (3c)$$

Replacing equations 3a, 3b and 3c in equation 2, the following relationship is obtained:

$$\mathbf{g}_2 \mathbf{b}_{12} w_m b_2 f'_m = \mathbf{g}_1 \mathbf{b}_{11} w_m b_1 f'_m + A_f E_f \mathbf{e}_f \cos \mathbf{q} \quad (4)$$

Taking moments about the point of application of the resulting force in masonry (point “o” in Figure 10), the following relationship is obtained:

$$\frac{Ph}{4} = A_f E_f \mathbf{e}_f a_f + \frac{\mathbf{g}_1 \mathbf{b}_{11} w_m b_1 f'_m}{\cos \mathbf{q}} a_c \quad (5)$$

From Figure 10(a), the following set of relationships can be derived based on geometrical considerations:

$$a_f = (t - b_2) \cos \mathbf{q} + \frac{2}{3} \frac{b_2}{\cos \mathbf{q}} \quad (6a)$$

$$a_c = b_f - \left( \frac{h}{2} - D_1 \right) \sin \mathbf{q} - \frac{l}{3} \frac{b_1}{\cos \mathbf{q}} \quad (6b)$$

$$\cos \mathbf{q} = \frac{b_1}{\sqrt{D_1^2 + b_1^2}} \quad (6c)$$

$$\sin \mathbf{q} = \frac{D_1}{\sqrt{D_1^2 + b_1^2}} \quad (6d)$$

In addition, from Figure 10(b) the following relationships can be determined:

$$d_1 + d_2 = \frac{h}{2} \left( \frac{l}{\cos \mathbf{q}} - l \right) \quad (7a)$$

$$d_1 = \left( \frac{t}{2} - b_1 \right) \tan \mathbf{q} \quad (7b)$$

$$d_2 = \left( \frac{t}{2} - b_2 \right) \tan \mathbf{q} \quad (7c)$$

Replacing equations 7b, 7c in equation 7a:

$$t - b_1 - b_2 = \frac{h}{2} \cdot \frac{l - \cos \mathbf{q}}{\sin \mathbf{q}} \quad (8)$$

It is assumed that the compressive strains at the outermost fibers of the wall segment vary linearly along the half of the wall. Thereby, the strain at the restrained region is maximum, whereas, at the mid-span they are relieved due to the crack opening (Angel et al., 1994). The total shortening of the interior and exterior fibers ( $D_1$  and  $D_2$ , respectively), over the length of half strip, is that found by integrating these strains along the half length:

$$D = \int_0^{h/2} \mathbf{e}(x) dx = \int_0^{h/2} \left( \frac{\mathbf{e}_{max}}{h/2} \right) x dx = \frac{l}{4} \mathbf{e}_{max} h \quad (9a)$$

Then  $\Delta_1$  and  $\Delta_2$  can be expressed as:

$$D_1 = \frac{l}{4} \mathbf{e}_{m1} h \quad (9b)$$

$$\mathbf{D}_2 = \frac{1}{4} \mathbf{e}_{m2} h \quad (9c)$$

From similarity of triangles in Figure 10(b), a relationship between the bearing widths and the shortening lengths can be obtained:

$$\frac{b_2}{b_1} = \frac{\mathbf{D}_2}{\mathbf{D}_1} \quad (10)$$

Combining equations 9b, 9c and 10, the following relationship is obtained:

$$\frac{b_2}{b_1} = \frac{\mathbf{e}_{m2}}{\mathbf{e}_{m1}} \quad (11)$$

Assuming that the deformation of the FRP occurs in an unbonded length,  $l_b$ , the strain in the FRP  $\Delta_f$  can be estimated using the equation:

$$\mathbf{e}_f = \frac{\mathbf{D}_f \cos \mathbf{q}}{l_b} = \frac{\frac{t-b_2}{b_2} \mathbf{D}_2}{l_b} = \frac{\frac{t-b_2}{b_1} \mathbf{D}_1}{l_b} \quad (12)$$

where  $\mathbf{D}_f$  is the elongation of the FRP laminate.

In addition, the mid-height deflection  $\mathbf{D}_o$  and the rotation  $\theta$  can be calculated as:

$$\mathbf{D}_o = \left( \frac{h}{2} - \mathbf{D}_1 \right) \sin \mathbf{q} = \left( \frac{h}{2} - \mathbf{D}_1 \right) \frac{\mathbf{D}_1}{\sqrt{\mathbf{D}_1^2 + b_1^2}} \quad (13a)$$

$$\mathbf{q} = \sin^{-1} \left( \frac{\mathbf{D}_1}{\sqrt{\mathbf{D}_1^2 + b_1^2}} \right) \quad (13b)$$

### Validation of the Analytical Model

The out-of-plane loads causing the failure of the wall (Wall UM) and FRP strengthened wall (Wall SM) are estimated. The geometrical properties and the material properties have been previously described (table 1, 2 and 3).

Considering the failure of the wall occurs in the boundary regions, and solving the equations 1, 2, 4, 5, 8, 9 and 11, for the unstrengthened wall, and equations 1, 2, 4, 5, 8, 9, 11 and 12 for the strengthened wall, it is possible to calculate the unknowns  $\gamma_1$ ,  $\gamma_2$ ,  $\beta_1$ ,  $\beta_2$ ,  $\epsilon_{m1}$ ,  $\epsilon_{m2}$ ,  $\epsilon_f$  and the out-of-plane force  $P$  at failure. Then, using these values of  $\Delta_1$  and  $b_1$  in equations 13a and 13b, the deflection  $\Delta_o$  and the rotation,  $\theta$  of the wall can be calculated.

In order to compute the out-of-plane load in the strengthened wall, it is required to know the debonded length,  $l_b$  (see equation 12). To date, there is no scientific evidence on the determination of this parameter. For the calculations carried out to determine  $P$  it was assumed that  $l_b$  was equal to 37.5 mm (1.5 in.) This assumption was based on experimental observations which suggested that the debonded length measured from the crack at mid-height extended approximately that distance in both directions perpendicular to the crack. With the assumed  $l_b$ , the analytical strain in the FRP,  $\epsilon_f$ , equals 10500  $\mu$  strain at ultimate. The strain recording reached about 10000  $\mu$  strain; from which can be concluded that the assumption of  $l_b$  equal to 37.5 mm (1.5 in.) was reasonable.

Table 5 summarizes the results obtained in terms of out-of-plane load. It can be observed that the analytical model fits very well the experimental results. As mentioned before, there were difficulties due to the test setup for series S8; this explains the deviation between experimental and theoretical results obtained for this series.

## SUMMARY AND CONCLUSIONS

The following conclusions can be drawn from this experimental program:

- A mechanism of failure that is not commonly considered for the analysis of FRP strengthened walls was studied. End-restrained walls exhibited an arching mechanism where crushing at the supports controlled the wall behavior. This mechanism of failure must be considered in the quantification of upgraded wall capacities to avoid overestimating the wall response.
- The test results allowed identifying four basic modes of failure. Two, shear failure and crushing of the masonry at the boundaries regions, related to the parent material (i.e. masonry); and two, associated with the reinforcing material, debonding and flexural failure (i.e. rupture of FRP or crushing of the masonry). For large amounts of reinforcement, shear failure was observed to be the controlling mode. For other reinforcement ratios, either FRP rupture or debonding or crushing of the masonry at the supports was observed, being the latter the most common.

An analytical model to determine the peak load and deflection of both unreinforced and strengthened walls was developed:

- The analytical model developed to determine the peak load and deflection of both unreinforced and strengthened walls shows good agreement with experimental results.
- The analytical model can be easily modified to take into account distributed loads acting on the wall, and incorporated in design provisions.

## ACKNOWLEDGEMENTS

The authors would like to acknowledge the support of the National Science Foundation Industry/University Cooperative Research Center at the University of Missouri–Rolla. The authors would also like to thank Marco Casareto, Alessandro Oliveri, and Alessandro Romelli, UMR Visiting Scholars from the University of Genoa, Italy, for their assistance.

## NOTATION

$A_f$	= area of FRP
$a_c$	= arm distance between clamping forces
$a_f$	= arm distance between force in FRP and clamping force at mid-height
$b_1, b_2$	= bearing width at top and mid-height, respectively
$C_1, C_2$	= clamping forces at top and mid-height, respectively
$E_f$	= Modulus of elasticity of FRP
$F_H$	= shear force
$F_R$	= resultant force
$F_V$	= in-plane compressive force
$f_f$	= tensile stress in FRP
$f'_m$	= compressive strength of masonry
$h$	= height of the wall
$h/t$	= slenderness ratio
$l_b$	= unbonded length
$P$	= out-of-plane load per strip

- $T_f$  = force in the FRP laminate
- $t$  = thickness of the wall
- $w_m$  = wall strip width
- $\beta_1$  = ratio of the depth of the equivalent rectangular stress block to the depth of the neutral axis
- $\Delta_o$  = wall deflection
- $D_1, D_2$  = total shortening of interior and exterior masonry fiber in compression, respectively
- $d_1, d_2$  = crack opening at top and mid-height, respectively, at the wall axis
- $e_f$  = tensile strain in FRP
- $e_{m1}, e_{m2}$  = compressive strain at top and mid-height, respectively
- $\gamma$  = multiplier on  $f'_m$  to determine the intensity of an equivalent block stress for masonry
- $q$  = rotation of the wall

**REFERENCES**

- Angel, R., Abrams, D. P., Shapiro, D., Uzarski, J., and Webster, M. (1994). "Behavior of Reinforced Concrete Frames with Masonry Infills." *Struct. Res. Ser. 589*, Department of Civ. Engrg., University of Illinois at Urbana-Champaign, IL.
- Benett, R. M., Boyd, K. A., and Flanagan, R. D. (1997). "Compressive Properties of Structural Clay Tile Prisms." *J. Struct. Engrg.*, ASCE, 123(7), 920-926.
- Ehsani, M. R., Saadatmanesh, H., and Velazquez-Dimas, J. I. (1999). "Behavior of Retrofitted URM Walls Under Simulated Earthquake Loading." *J. of Comp. for Const.*, ASCE, 3(8), 134-142.
- Galati N., Tumialan J.G, La Tegola A., and Nanni A., "Influence of Arching Mechanism in Masonry Walls Strengthened with FRP Laminates," ICCI 2002, San Francisco, CA, June 10-12, 2002, 10 pp. CD-ROM.
- Fricke, K. E., Jones, W. D., and Huff, T. E. (1992). "In situ lateral Load Testing of Unreinforced Masonry Hollow Clay Tile Wall." *6th Can. Masonry Symp.*, Saskatchewan, Canada, 519-530.
- Hamilton, H.R. III, Holberg, A., Caspersen, J., and Dolan, C. W. (1999). "Strengthening Concrete Masonry with Fiber Reinforced Polymers." *4th Int. Symp. on Fiber Reinf. Polymer (FRP) for Reinf. Conc. Struct.*, Baltimore, MD, 1103-1115.
- Masonry Standards Joint Committee. (1999). "Building Code Requirements for Masonry Structures." *ACI-530-99/ASCE 5-99/TMS 402-99*, Detroit, MI, New York, NY, and Boulder, CO.

- Masonry Standards Joint Committee. (2001). "Building Code Requirements for Masonry Structures – Working Draft." *ACI-530-99/ASCE 599/TMS 402-99*, Detroit, MI, New York, NY, and Boulder, CO.
- Velazquez-Dimas, J. I, Ehsani, M. R., and Saadatmanesh, H. (2000). "Out-of-Plane Behavior of Brick Masonry Walls Strengthened with Fiber Composites." *Struct. J.*, *ACI*, 97(5), 377-387.
- Tumialan J. G. (2001). "Strengthening of Masonry Structures with FRP Composites." *Doctoral Dissertation*, University of Missouri-Rolla, Rolla, MO.
- Tumialan, J. G., Galati, N., and Nanni, A., (2002). "Field Assessment Of URM Walls Strengthened With FRP Laminates", accepted for publication by the Journal of Structural Engineering.
- Tumialan, J. G., Galati, N., Namboorimadathil, S. M., and Nanni, A., (2002). "Strengthening of Masonry with FRP Bars" ICCI 2002, San Francisco, CA, June 10-12, 2002.

**Table 1. Test Matrix**

Specimen	Masonry Type	Thickness mm (in)	GFRP width mm (in)	$\rho_b$ (%)	h/t ratio
S8-CO0	Concrete	143 (5 $\frac{5}{8}$ )	-	-	8.5
S8-CO3	Concrete	143 (5 $\frac{5}{8}$ )	76.2 (3)	67	8.5
S8-CO5	Concrete	143 (5 $\frac{5}{8}$ )	127.0 (5)	111	8.5
S8-CO7	Concrete	143 (5 $\frac{5}{8}$ )	177.8 (7)	155	8.5
S8-CO9	Concrete	143 (5 $\frac{5}{8}$ )	228.6 (9)	200	8.5
S12-CL0	Clay	95 (3 $\frac{3}{4}$ )	-	-	12.8
S12-CL3	Clay	95 (3 $\frac{3}{4}$ )	76.2 (3)	43	12.8
S12-CL5	Clay	95 (3 $\frac{3}{4}$ )	127.0 (5)	72	12.8
S12-CL7	Clay	95 (3 $\frac{3}{4}$ )	177.8 (7)	100	12.8
S12-CL9	Clay	95 (3 $\frac{3}{4}$ )	228.6 (9)	130	12.8
S12-CO0	Concrete	92 (3 $\frac{5}{8}$ )	-	-	13.2
S12-CO3	Concrete	92 (3 $\frac{5}{8}$ )	76.2 (3)	100	13.2
S12-CO5	Concrete	92 (3 $\frac{5}{8}$ )	127.0 (5)	167	13.2
S12-CO7	Concrete	92 (3 $\frac{5}{8}$ )	177.8 (7)	233	13.2
S12-CO9	Concrete	92 (3 $\frac{5}{8}$ )	228.6 (9)	300	13.2
S19-CL0	Clay	64 (2 $\frac{1}{2}$ )	-	-	19.2
S19-CL3	Clay	64 (2 $\frac{1}{2}$ )	76.2 (3)	160	19.2
S19-CL5	Clay	64 (2 $\frac{1}{2}$ )	127.0 (5)	267	19.2
S19-CL7	Clay	64 (2 $\frac{1}{2}$ )	177.8 (7)	373	19.2
S19-CL9	Clay	64 (2 $\frac{1}{2}$ )	228.6 (9)	480	19.2
S $\infty$ -CO3	Concrete	92 (3 $\frac{5}{8}$ )	76.2 (3)	100	n.a.
S $\infty$ -CO5	Concrete	92 (3 $\frac{5}{8}$ )	127.0 (5)	167	n.a.
S $\infty$ -CO7	Concrete	92 (3 $\frac{5}{8}$ )	177.8 (7)	233	n.a.
S $\infty$ -CO9	Concrete	92 (3 $\frac{5}{8}$ )	228.6 (9)	300	n.a.

Note:  $\rho_b$  = balanced condition; h=height of the wall; t=thickness of the wall

**Table 2. Properties of FRP Constituent Materials**

Material	Tensile Strength MPa (ksi)	Modulus of Elasticity GPa (ksi)	Strain at Rupture %	Thickness mm (in)	Poisson's Ratio
Primer <sup>(1)</sup>	17.2 (2.5)	0.7 (104)	40	NA	0.48
Putty <sup>(1)</sup>	15.2 (2.2)	1.8 (260)	7.0	NA	0.48
Impregnating Resin <sup>(1)</sup>	55.2 (8.0)	3.0 (440)	3.5	NA	0.40
E-Glass	1690 (245)	92.9 (13460)	1.82	0.36 (0.014)	NA

<sup>(1)</sup> Values provided by the manufacturer

**Table 3. Compressive Strength of Masonry Walls**

Dimensions of Masonry Units mm (in.)	Type of Masonry	Compressive Strength MPa (ksi)
100 x 200 x 400 (3 5/8" x 7 7/8" x 15 3/4")	Concrete	10.5 (1.5)
150 x 200 x 400 (5 5/8" x 7 7/8" x 15 3/4")	Concrete	11.4 (1.6)
100 x 200 x 65 (3 3/4" x 2 1/2" x 7 7/8")	Clay	17.1 (2.5)
100 x 200 x 400 (2 1/2" x 2 1/2" x 9 1/2")	Clay	17.5 (2.5)

**Table 4. Test Results**

Specimen	Out-of-Plane Load (kN)	In-Plane Load (kN)	Midspan Deflection [mm]	Mode of Failure
S8-CO0	59.9	213.5	10.6	Splitting
S8-CO3	48.3	172.1	6.7	Splitting
S8-CO5	43.5	84.9	8.2	Splitting
S8-CO7	42.8	80.3	5.1	Splitting
S8-CO9	55.5	185.9	7.2	Splitting
S12-CL0	21.3	149.1	30.1 <sup>(*)</sup>	Crushing of Masonry Units
S12-CL3	52.2	298.2	31.7	Fiber Rupture
S12-CL5	45.6	261.6	28.9 <sup>(*)</sup>	Crushing of Masonry Units
S12-CL7	54.9	252.6	24.1	Masonry Shear <sup>(1)</sup>
S12-CL9	53.1	208.7	18.1	Masonry Shear <sup>(1)</sup>
S12-CO0	22.4	215.7	31.1 <sup>(*)</sup>	Crushing of Masonry Units
S12-CO3	29.0	213.4	26.5	Crushing of Masonry Units
S12-CO5	27.1	151.5	18.1	Crushing of Masonry Units
S12-CO7	33.1	151.4	20.7	Masonry Shear <sup>(1)</sup>
S12-CO9	34.7	98.8	21.6	Masonry Shear <sup>(1)</sup>
S19-CL0	7.8	52.6	17.9	Crushing of Masonry Units
S19-CL3	11.6	55.1	22.3	Debonding
S19-CL5	19.8	73.5	25.5	Debonding
S19-CL7	21.9	73.3	22.1	Masonry Shear <sup>(1)</sup>
S19-CL9	26.3	60.8	25.4	Masonry Shear <sup>(1)</sup>
S∞-CO3	7.3	-	20.2	Debonding
S∞-CO5	14.0	-	21.4	Debonding
S∞-CO7	15.4	-	19.2	Debonding
S∞-CO9	21.9	-	18.6	Masonry Shear <sup>(1)</sup>

Note: 1 mm = 0.03937 in.; 1 KN = 0.2248 kips <sup>(\*)</sup>:one LVDT

**Legend:** S: Masonry Shear <sup>(1)</sup> Flexural-Shear  
<sup>(2)</sup> Sliding Shear

**Table 5. Comparison between Theoretical and Analytical Load Capacities**

Specimen	Experimental Out-of-Plane Capacity (kN)	Theoretical Out-of-Plane Capacity (kN)	Percentage of Error (%)
S8-CO0	59.9	57.55	4.1
S8-CO3	48.3	58.94	18.1
S8-CO5	43.5	60.49	28.1
S8-CO7	42.8	62.27	31.3
S8-CO9	75.5	64.05	17.9
S12-CL0	35.0	44.1	20.6
S12-CL3	52.2	51.0 <sup>(1)</sup>	-2.4
S12-CL5	45.6	54.8	16.8
S12-CL7	54.9	58.1 <sup>(2)</sup>	5.5
S12-CL9	53.1	61.0 <sup>(2)</sup>	12.9
S12-CO0	22.4	24.0	6.7
S12-CO3	29.0	31.6	8.2
S12-CO5	27.1	33.5	19.1
S12-CO7	33.1	34.5 <sup>(2)</sup>	4.1
S12-CO9	34.7	36.5 <sup>(2)</sup>	4.9
S19-CL0	7.8	7.4	-5.4
S19-CL3	11.6	11.3	-2.7
S19-CL5	19.8	19.4	-2.1
S19-CL7	21.9	22.1	0.9
S19-CL9	26.3	27.3 <sup>(2)</sup>	3.7

Note: 1 mm = 0.03937 in.; 1 KN = 0.2248 kips <sup>(\*)</sup>:one LVDT

**Legend:**

<sup>(1)</sup> Specimen failed by FRP rupture

<sup>(2)</sup> Specimens failed by shear

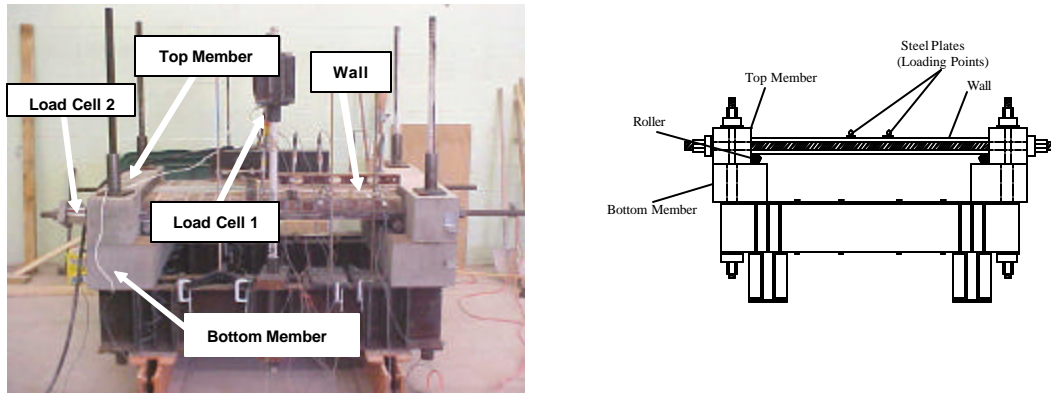


**Figure 1. Test Setup Scheme**

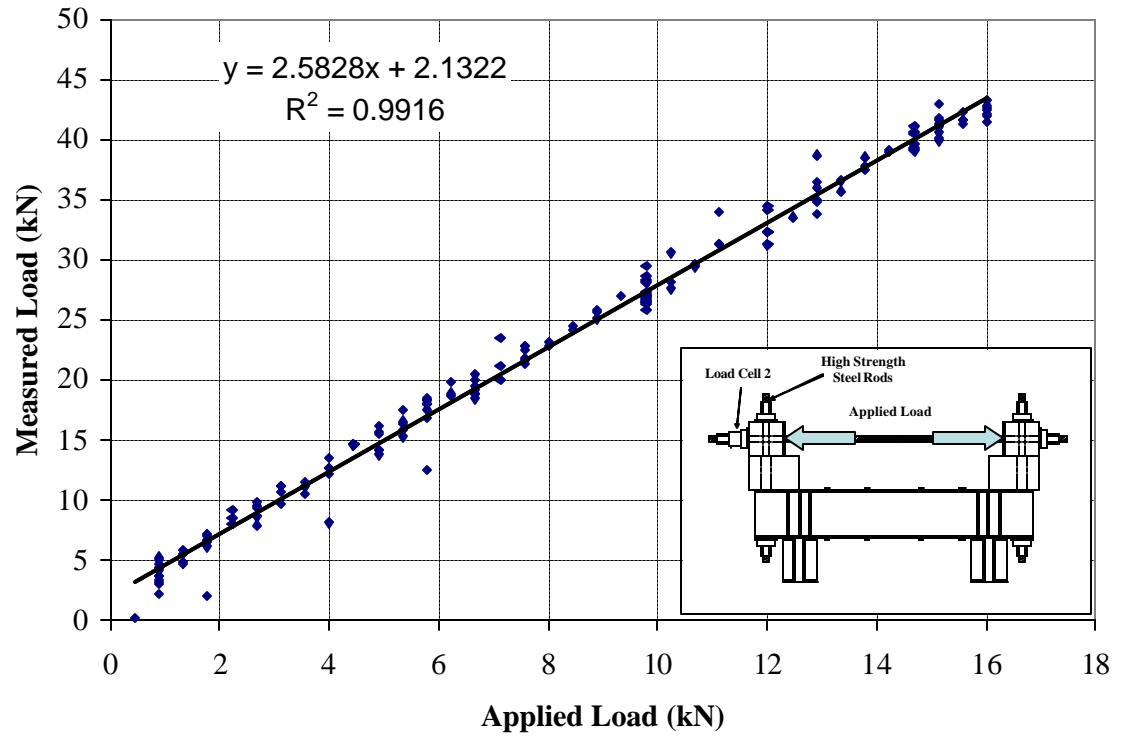
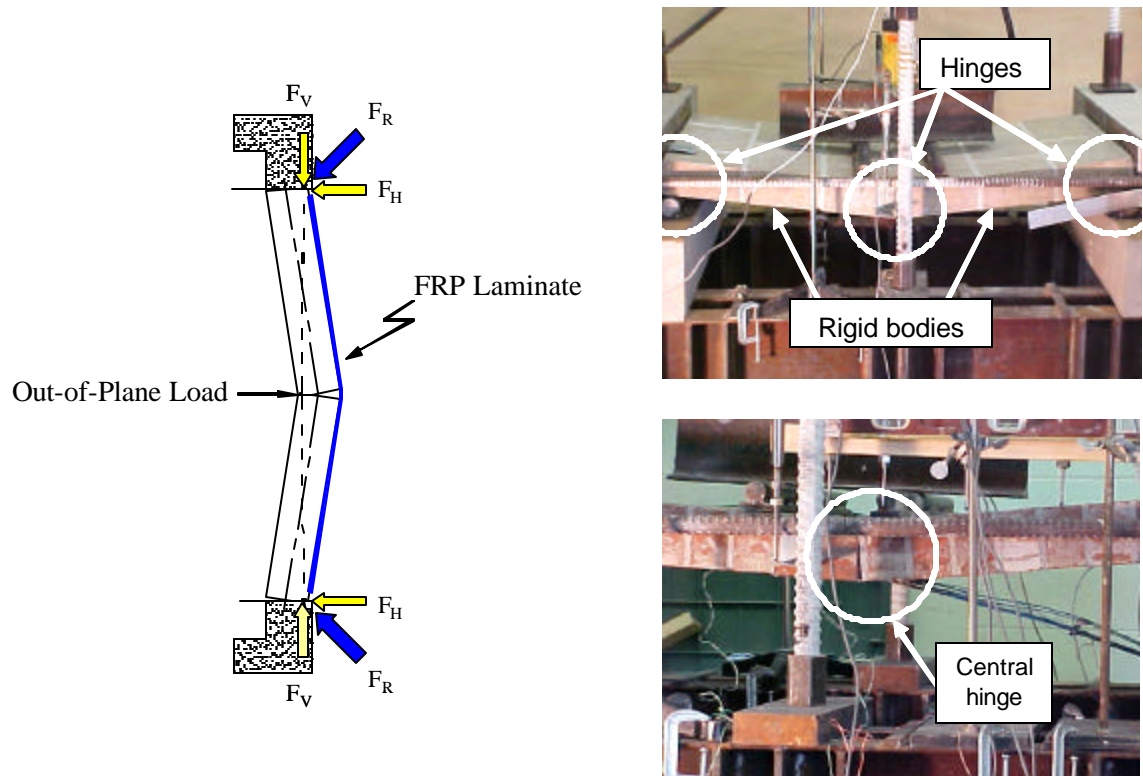


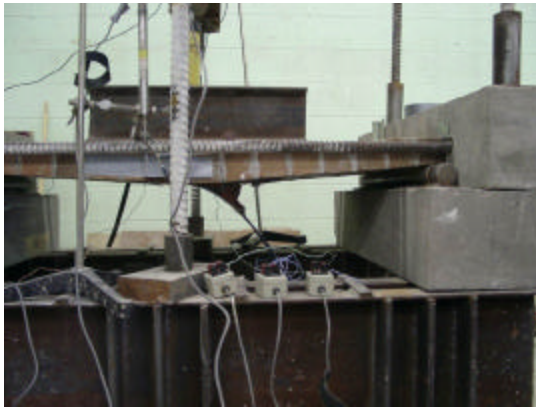
Figure 2. Calibration Curve of the System



**Figure 3. Test Specimens And Strain Gage Locations**



**Figure 4. Out-of-Plane Mechanism of Failure**



(a) FRP Debonding (S19-CL3)



(b) FRP rupture (S12-CL3)



(c) Crushing of Units at Midspan (S12-CO0)



(d) Crushing of Units at Support (S12-CL5)

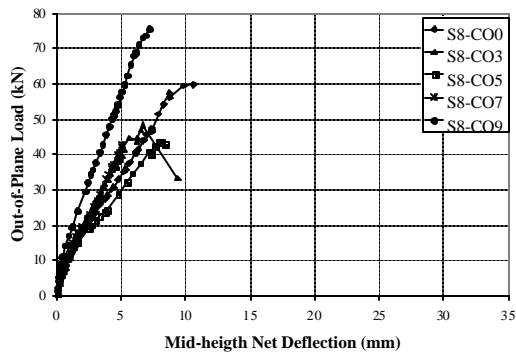


(e) Splitting of the Masonry Units (S8-CO3)

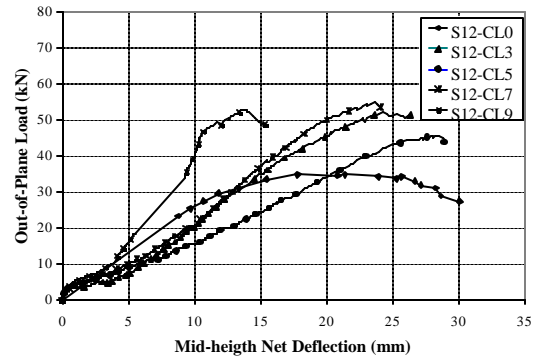


(f) Shear Failure (S12-CL9)

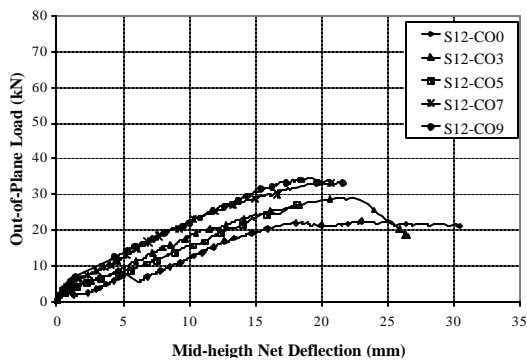
**Figure 5. Modes of Failure**



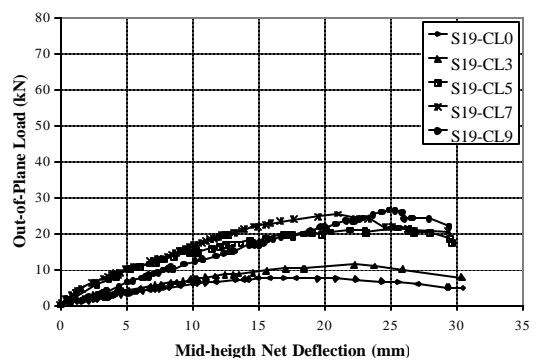
(a) Series S8



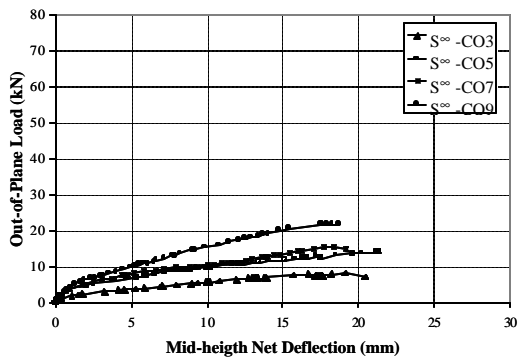
(b) Series S12 - CL



(c) Series S12 - CO

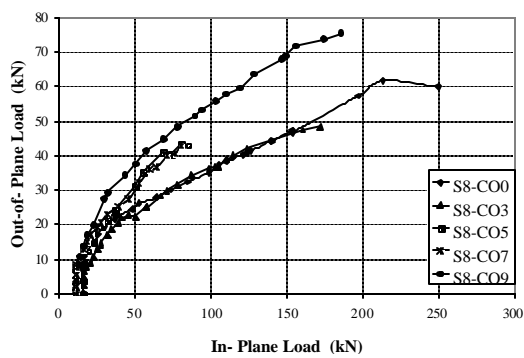


(d) Series S19

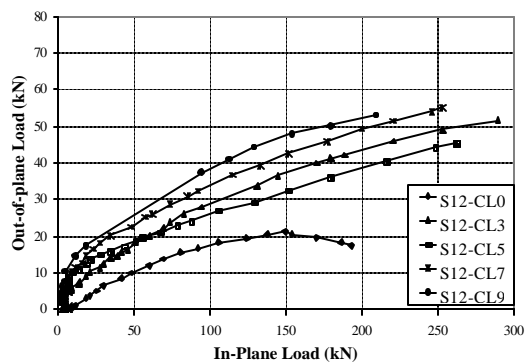


(e) Series S $\infty$

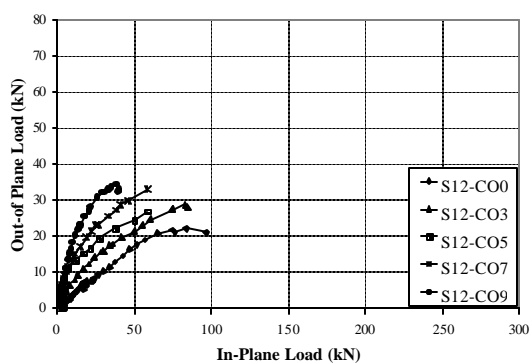
Figure 6. Load vs. Deflection of URM Walls Strengthened with FRP Laminates



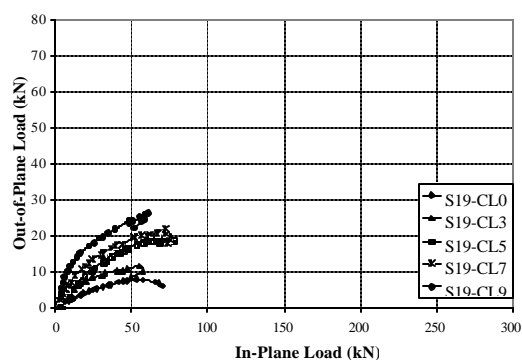
(a) Series S8



(b) Series S12 – CL

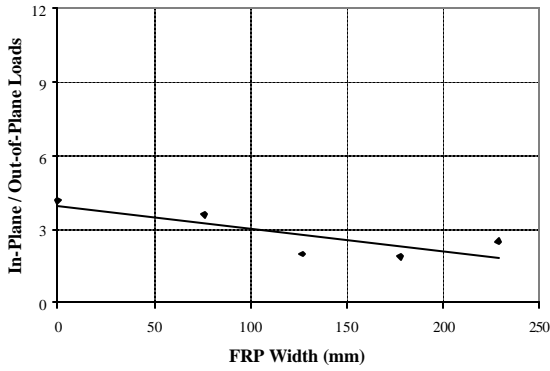


(c) Series S12 – CO

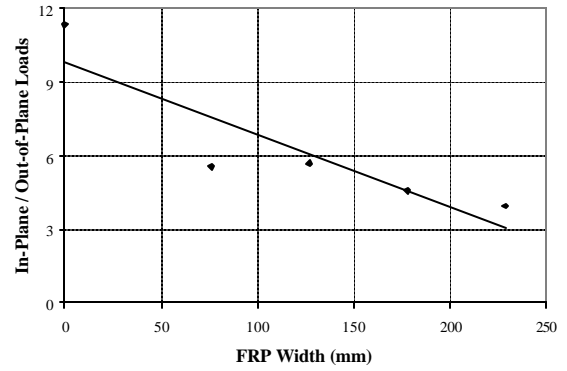


(d) Series S19

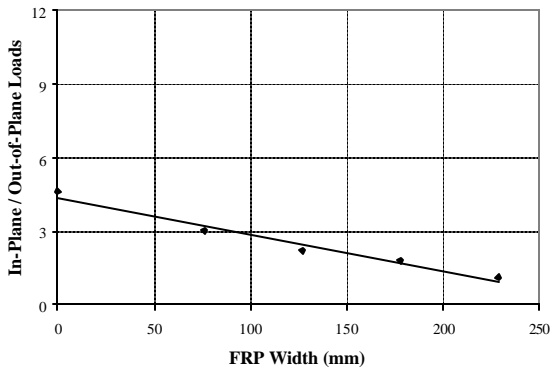
**Figure 7. Out-of-Plane Load versus In-Plane Load of URM Walls Strengthened with FRP Laminates**



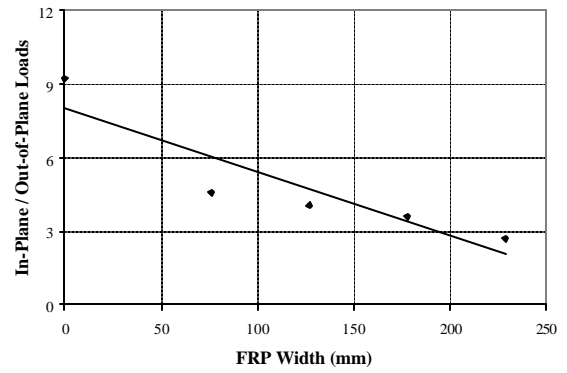
(a) Series S8



(b) Series S12 - CL



(c) Series S12 - CO



(d) Series S19

**Figure 8. In-Plane/Out-of-Plane Load Ratio as a Function of FRP Width**

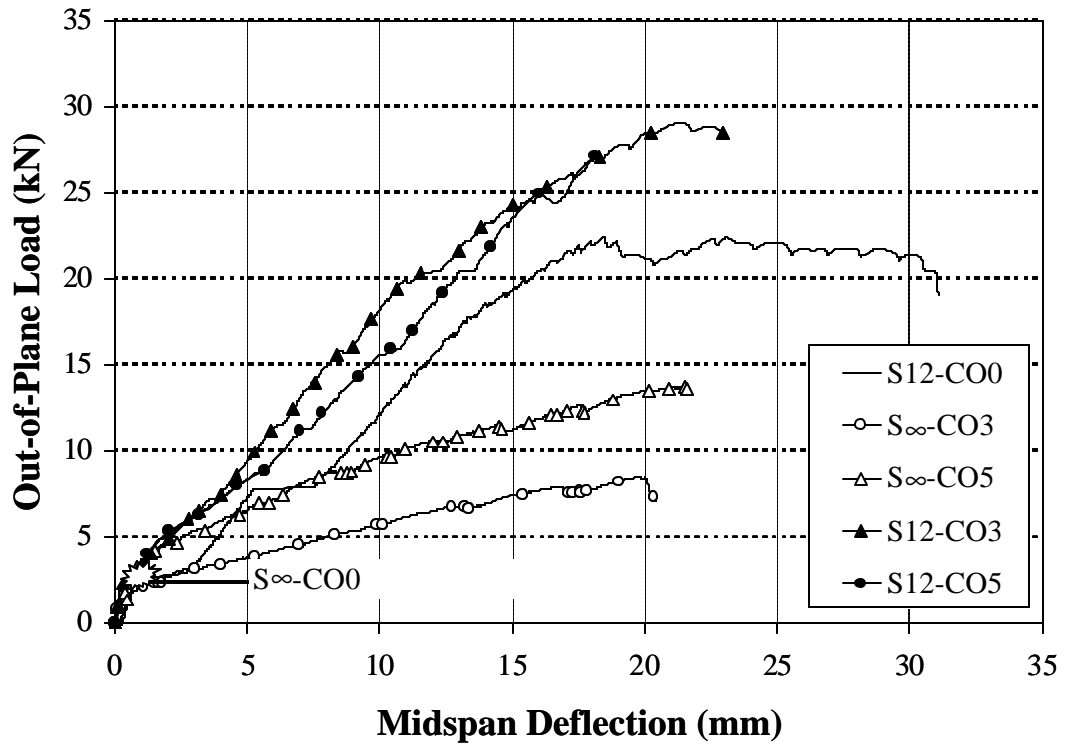
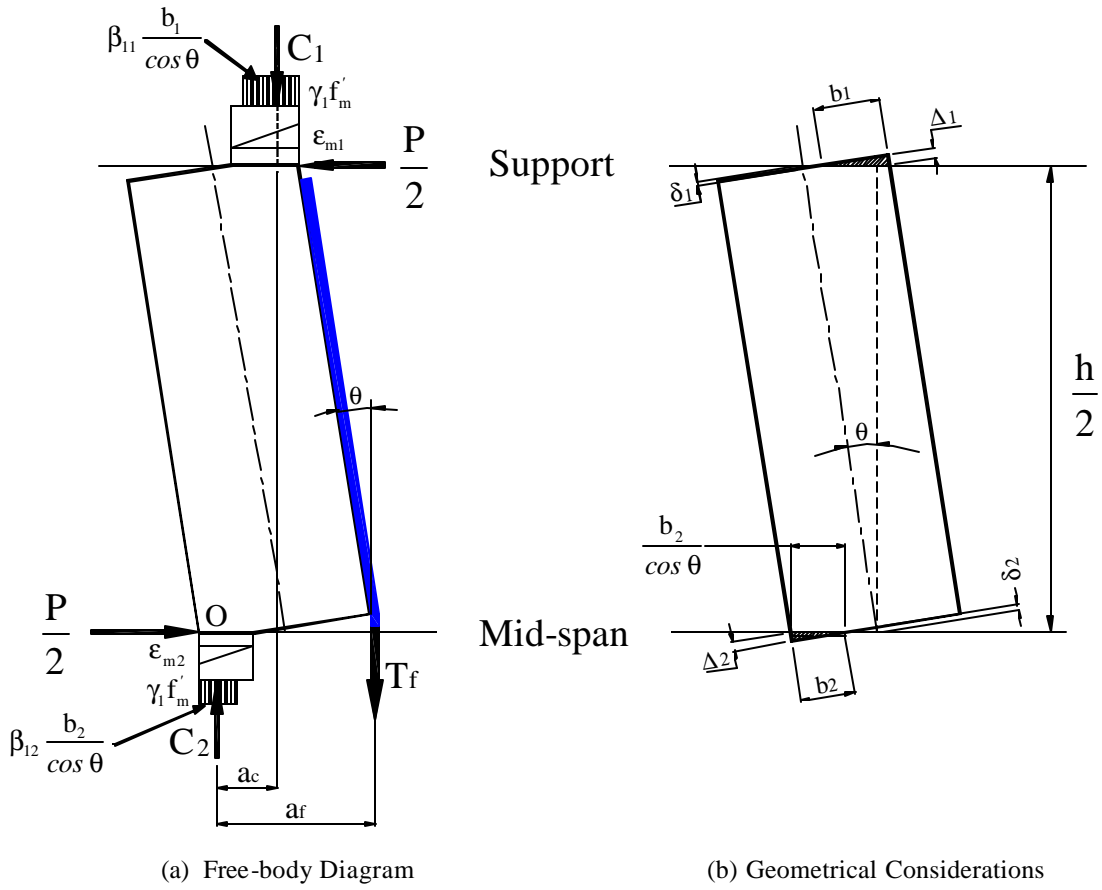


Figure 9. Comparison between Simply Supported and End-Restrained Walls



**Figure 10. Half Part of Analyzed Wall**

## CONCLUSIONS

The following general conclusions can be drawn from the presented work.

A mechanism of failure that is not commonly considered for the analysis of FRP strengthened walls was studied. End-restrained walls exhibited an arching mechanism where crushing at the supports controlled the wall behavior. This mechanism of failure must be considered in the quantification of upgraded wall capacities to avoid overestimating the wall response.

The test results allowed identifying four basic modes of failure. Two modes, shear failure and crushing of the masonry at the boundaries regions, were related to the parent material (i.e. masonry); and two were associated with the reinforcing material, debonding and flexural failure (i.e. rupture of FRP or crushing of the masonry). For large amounts of reinforcement, shear failure was observed to be the controlling mode. For other reinforcement ratios, either FRP rupture or debonding or crushing of the masonry at the supports was observed, being the latter the most common.

An analytical model to determine the peak load and deflection of both unreinforced and strengthened walls was developed. The analytical model shows good agreement with experimental results. The analytical model can be easily modified to take into account distributed loads acting on the wall, and incorporated in design provisions.

The used test setup reproduces only fixed-fixed boundary conditions with no gap between the supports and the wall. These boundary conditions cannot be easily found in real structures. Generally, the fixed-fixed condition is not satisfied because columns and beams have a stiffness that is not infinite. This reduces the degree of fixity of the supports

and therefore changes the overall behavior of the infill wall. Sometimes it is even difficult to avoid the presence of a gap between the top beam and the wall. If a gap is present, then the arching mechanism is delayed: it starts as soon as the top beam and masonry wall come in contact, due to the deflection under the out-of-plane loading.

Another limitation of the experimental program was the applied load. In particular, the load was applied in static conditions. In reality, during an earthquake, the supports are moving and therefore this loading condition cannot be applied to simulate seismic actions.

Another interesting observation can be made about the loading condition. Generally during an earthquake it is not possible to separate the in-plane action from the out-of-plane one. Therefore the reinforcement designed for out-of-plane loads will be acting even for the in-plane action. It is not possible to say if this reinforcement has a positive or detrimental effect on the overall behavior of the building. In fact, the behavior under in-plane loads is greatly influenced by the boundary conditions and particularly by the relative stiffness of the system frame - wall (i.e. the two extreme cases are weak frame - strong wall or stiff frame- weak wall). A change in the stiffness of the wall will affect the behavior even of the frame and therefore the overall behavior of the building.

The developed analytical model presents the same limitations. It assumes fixed-fixed boundary conditions and no gap between the top beam and masonry wall.

Future work will be on the analytical model to take into consideration the effect of the stiffness of columns and beams, and to include in the analytical model the presence of a gap between the top part of the wall and the top beam.

On the experimental side further research is needed. In particular, it is necessary to investigate the influence of the stiffness of the frame on the out-of-plane behavior. This research will be completed very soon at the Catholic University of Peru. At this University, full scale infill walls will be tested under seismic action through the use of a shaking table. This experimental program will allow to validate the analytical model and therefore to provide provisional design guidelines.

Also, the interaction between flexural and shear strengthening needs to be addressed from an experimental and from a theoretical point of view.

## **APPENDIX A**

### **TEST SETUP AND MODES OF FAILURE**

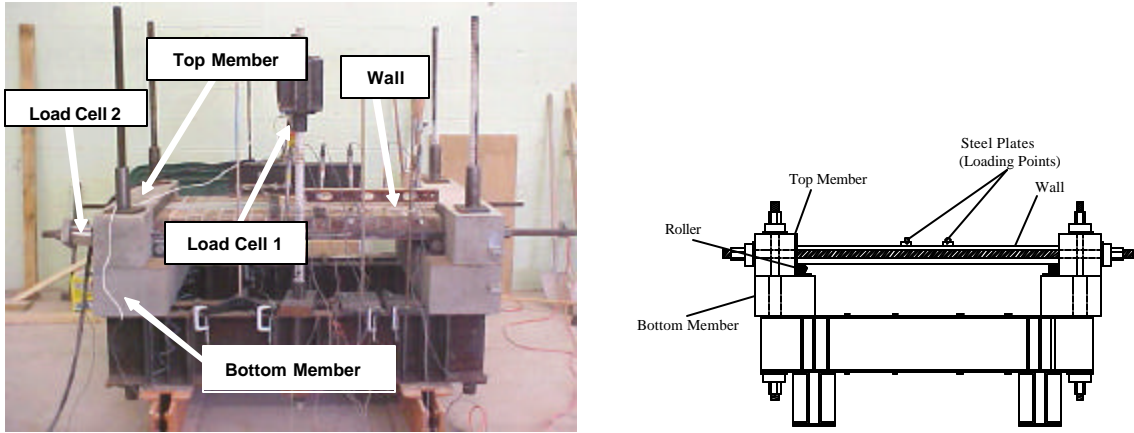


**Fig A.1 Test Setup Scheme**

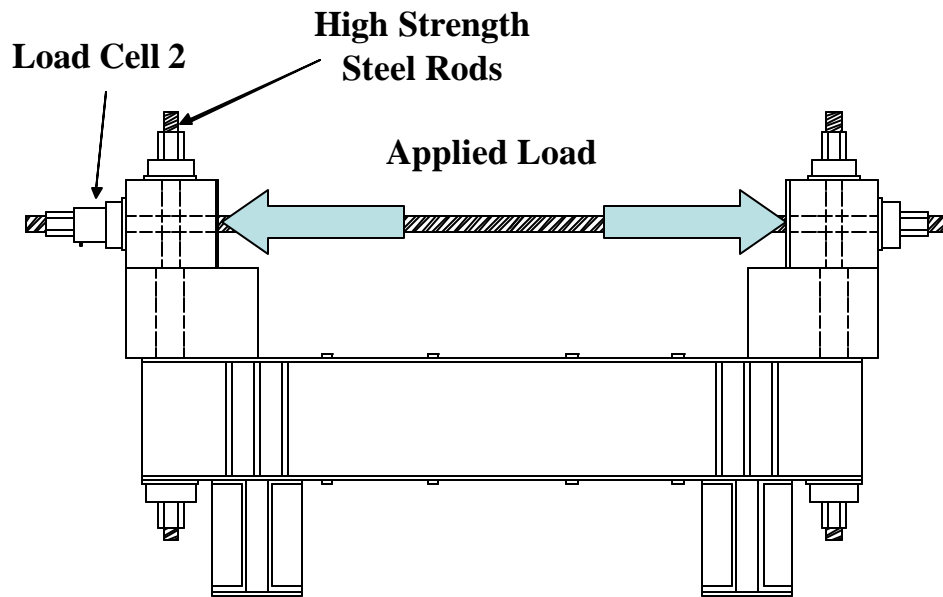


**Fig A.2 Calibration of the System (Scheme)**

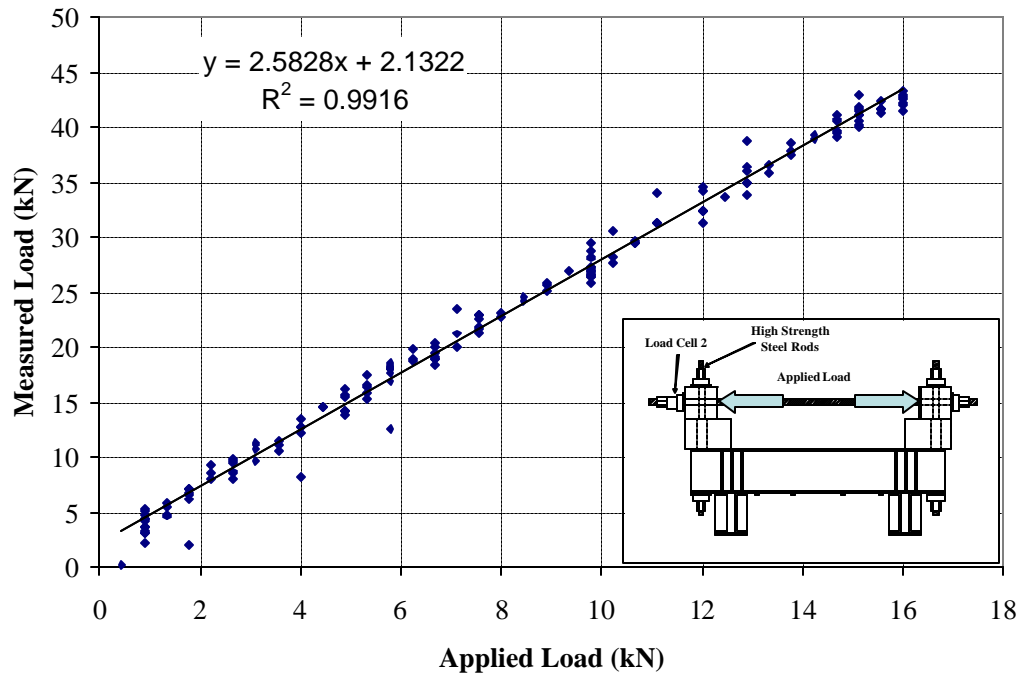


**Fig A.3 Calibration Curve of the System**

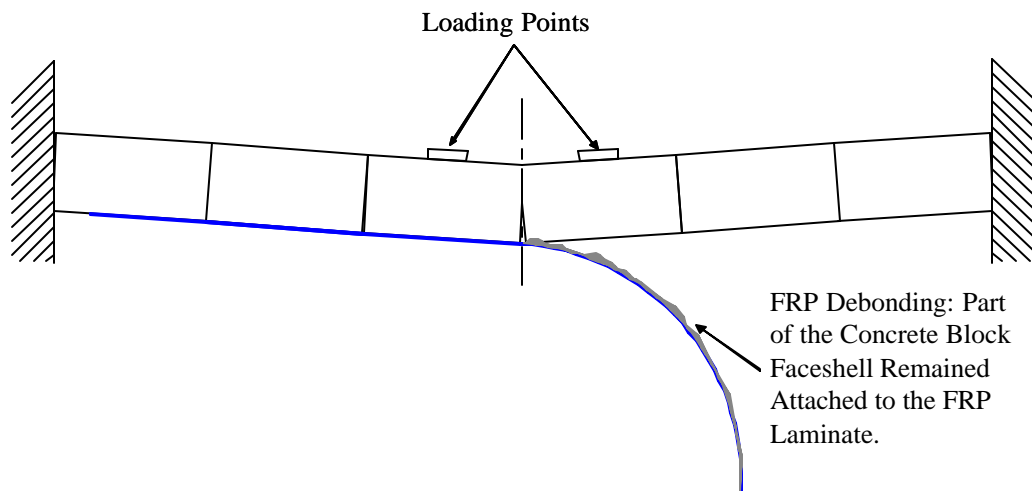


**Fig A.4 Flexural Failure: FRP Debonding**

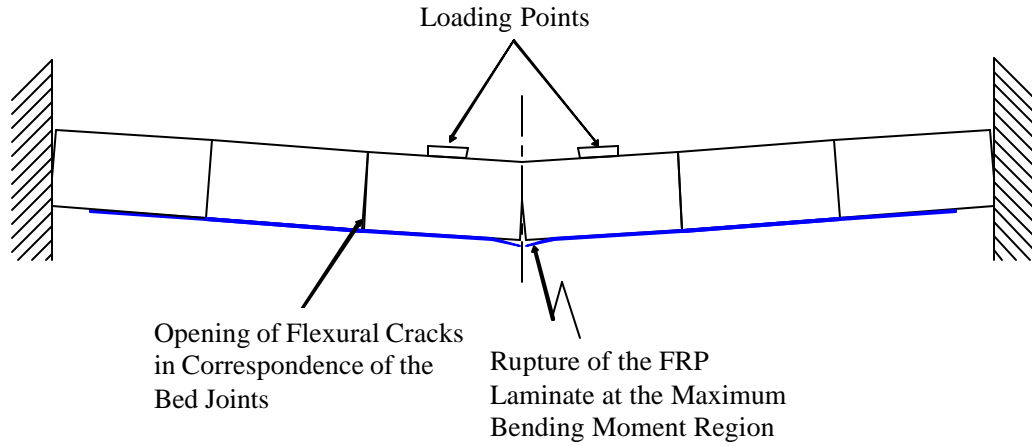


**Fig A.5 Flexural Failure: FRP Rupture**

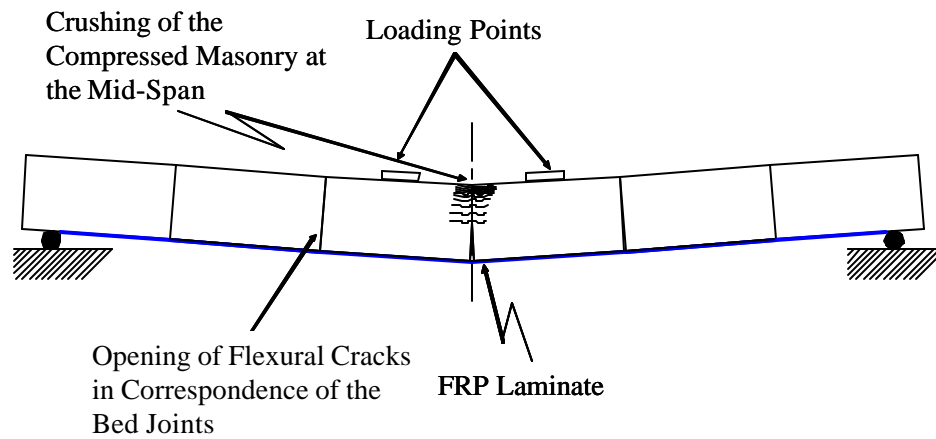


**Fig A.6 Crushing of the Compressed Masonry at the Mid-Span (Simply Supported Boundaries Conditions)**

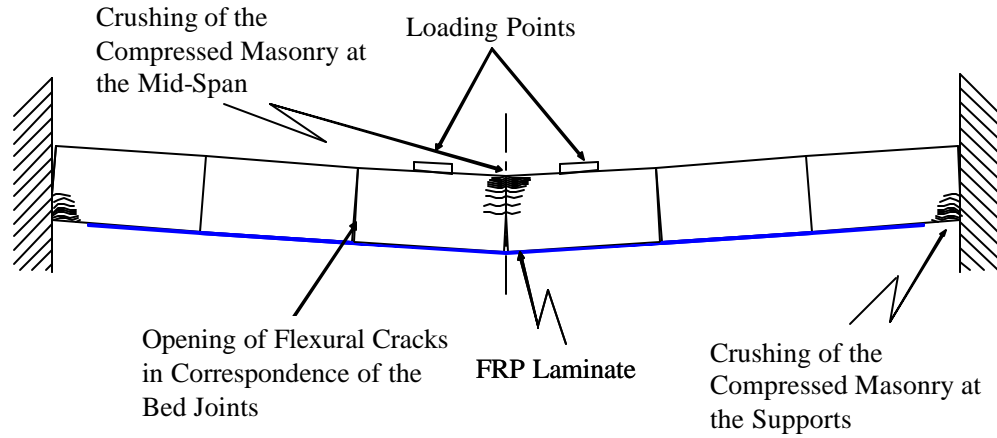


**Fig A.7 Crushing of the Masonry at the Supports or at the Mid-Span due to the Membrane Forces Generated by Arching Action**

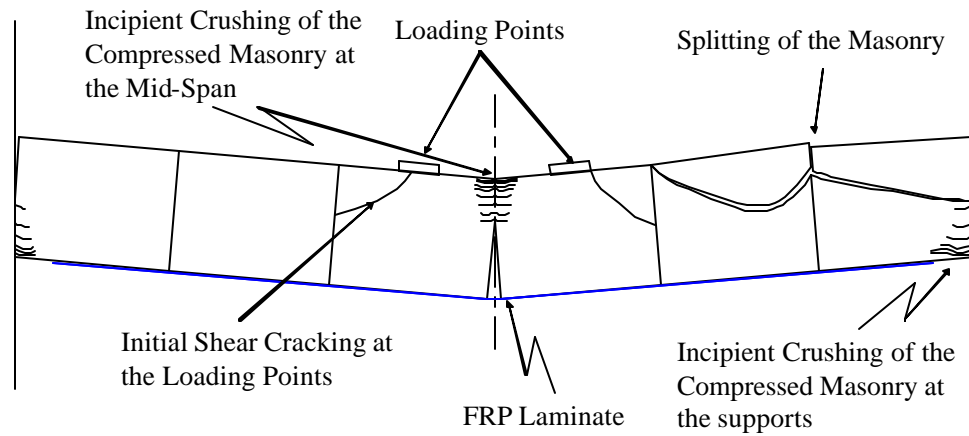


**Fig A.8 Splitting of the Masonry at the Supports due to the High Membrane Forces Generated by Arching Action**

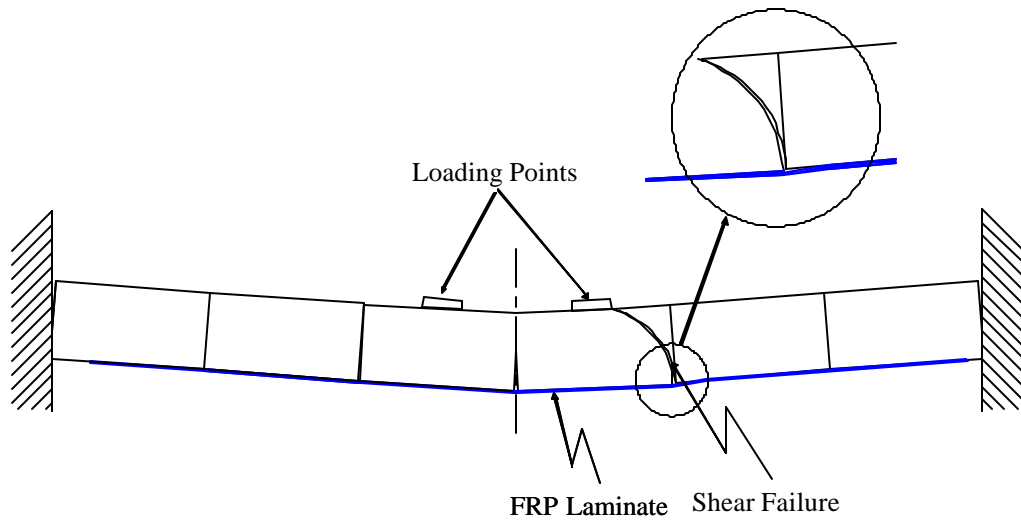


**Fig A.9 Shear Failure**



**Fig A.10 Flexural Failure: FRP Debonding (S12-CL5)**



**Fig A.11 Flexural Failure: FRP Debonding (S12-CL5)**



**Fig A.12 Flexural Failure : FRP Debonding (S19-CL5)**



**Fig A.13 Flexural Failure: FRP Rupture (S12-CL3)**



**Fig A.14 Flexural Failure: Crushing of the Masonry (S12-CO0)**



**Fig A.15 Flexural Failure: Crushing of the Masonry (S12-CO0)**



**Fig A.16 Crushing of the Masonry at the Supports (S12-CL0)**



**Fig A.17 Splitting of the Masonry at the Supports (S8-CO5)**



**Fig A.18 Shear Failure (S19-CL7)**



**Fig A.19 Shear Failure (S12-CL7)**

**APPENDIX B**  
**DIAGRAMS**

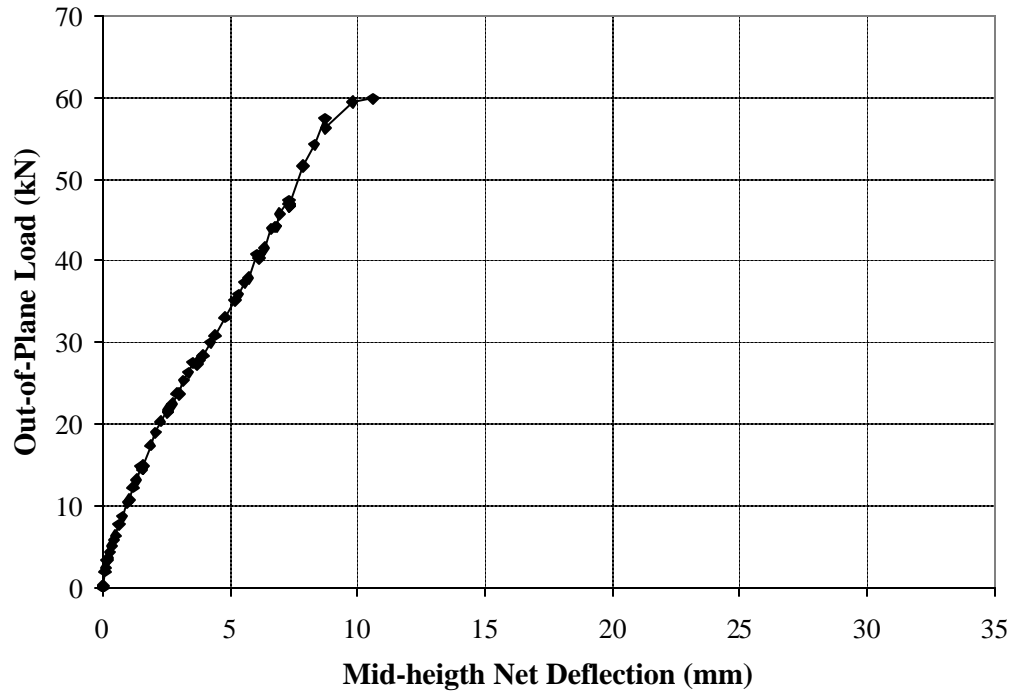


**Fig B.1 Load vs. Mid-height Deflection S8-CO0**

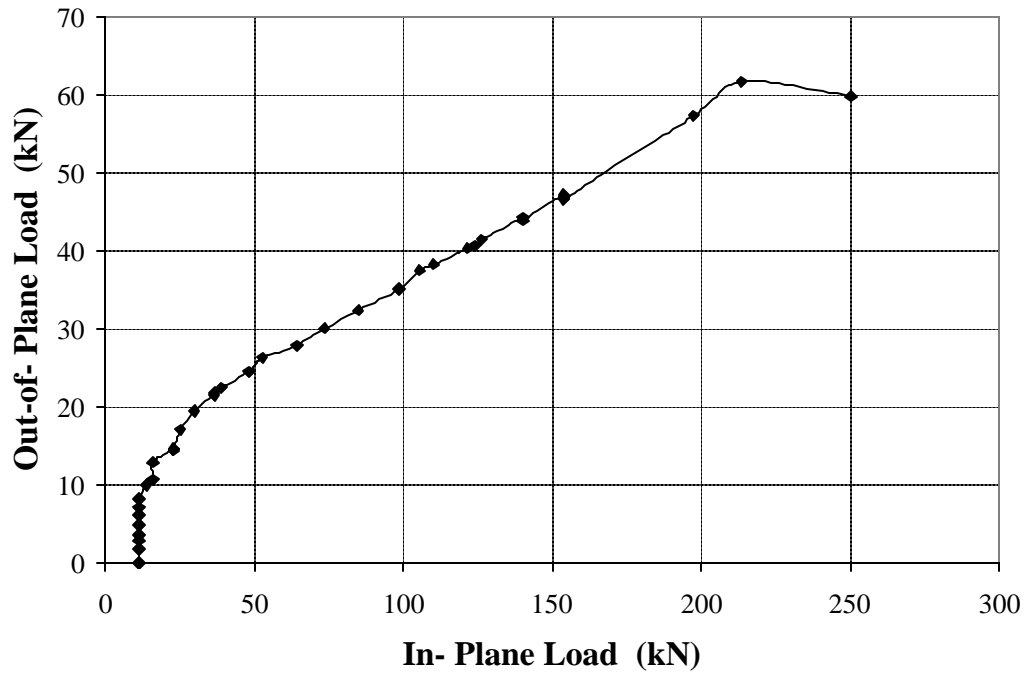


**Fig B.2 Out-of-Plane Load versus In-Plane Load S8-CO0**

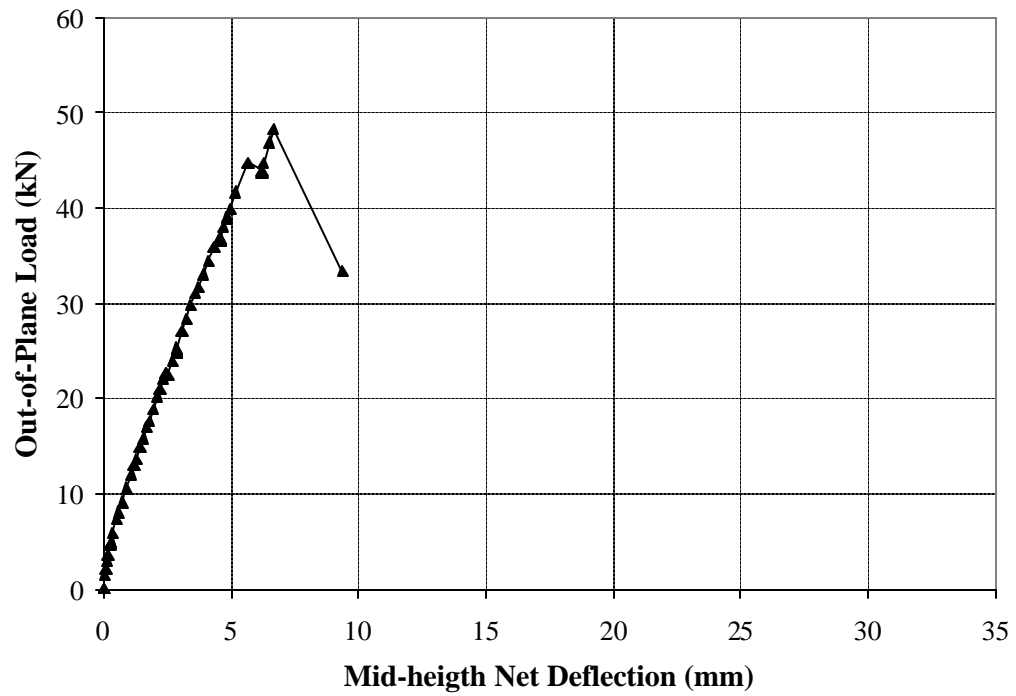


**Fig B.3 Load vs. Mid-height Deflection S8-CO3**

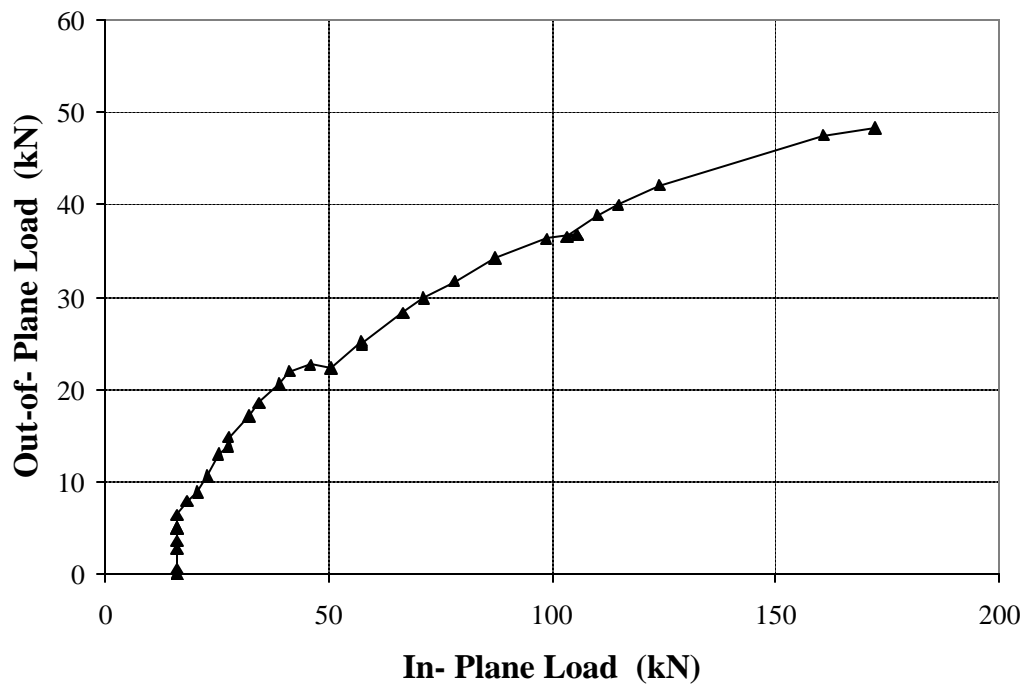


**Fig B.4 Out-of-Plane Load versus In-Plane Load S8-CO3**

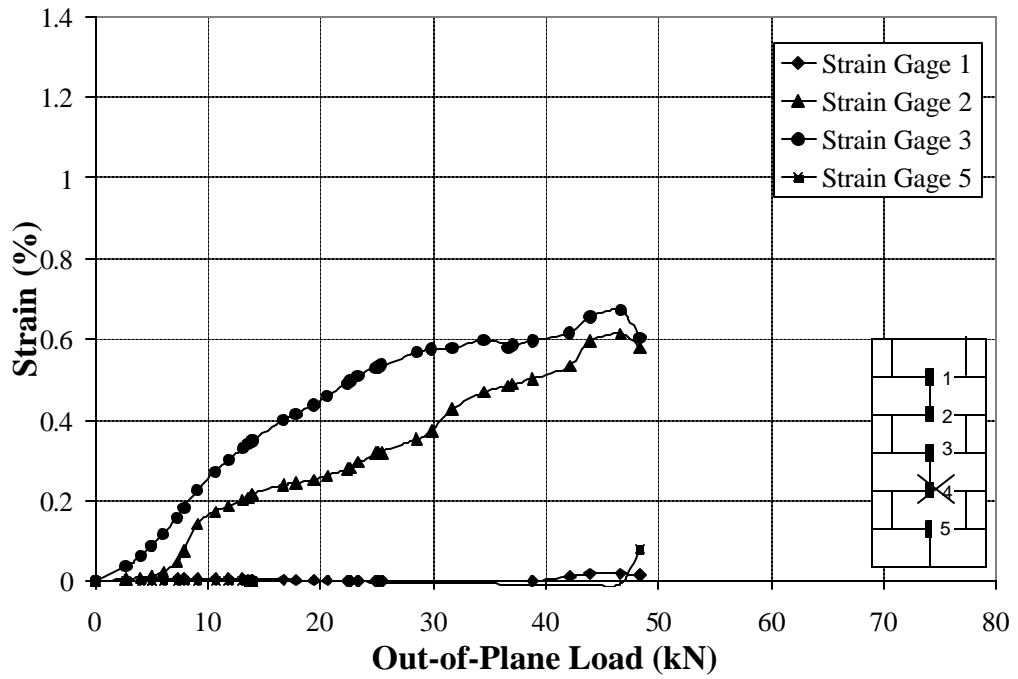


Fig B.5 Strain Distribution S8-CO3

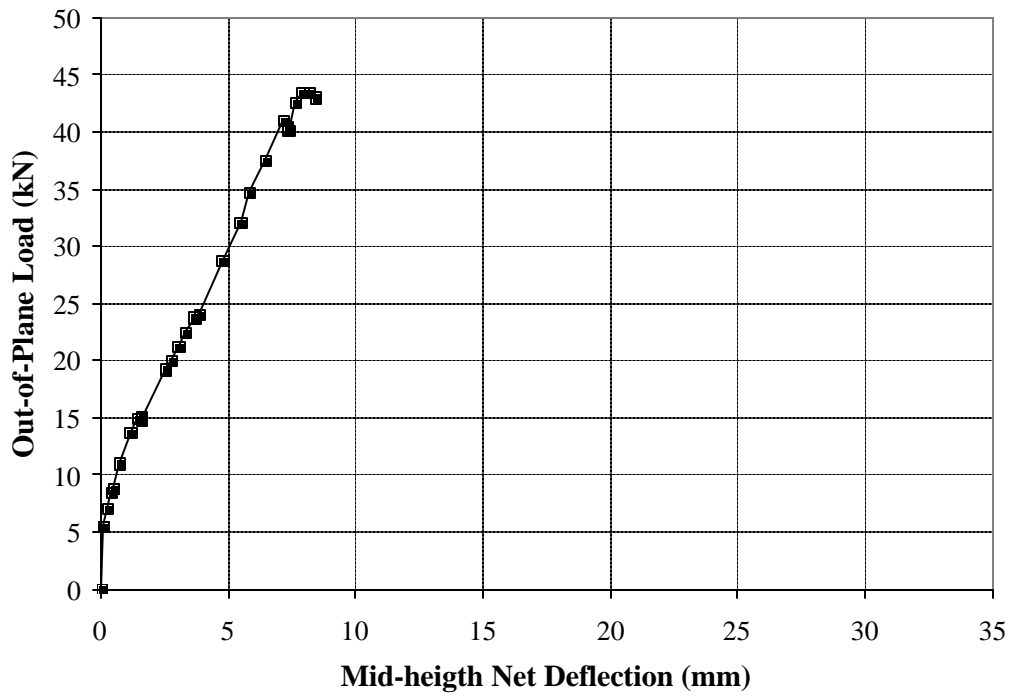
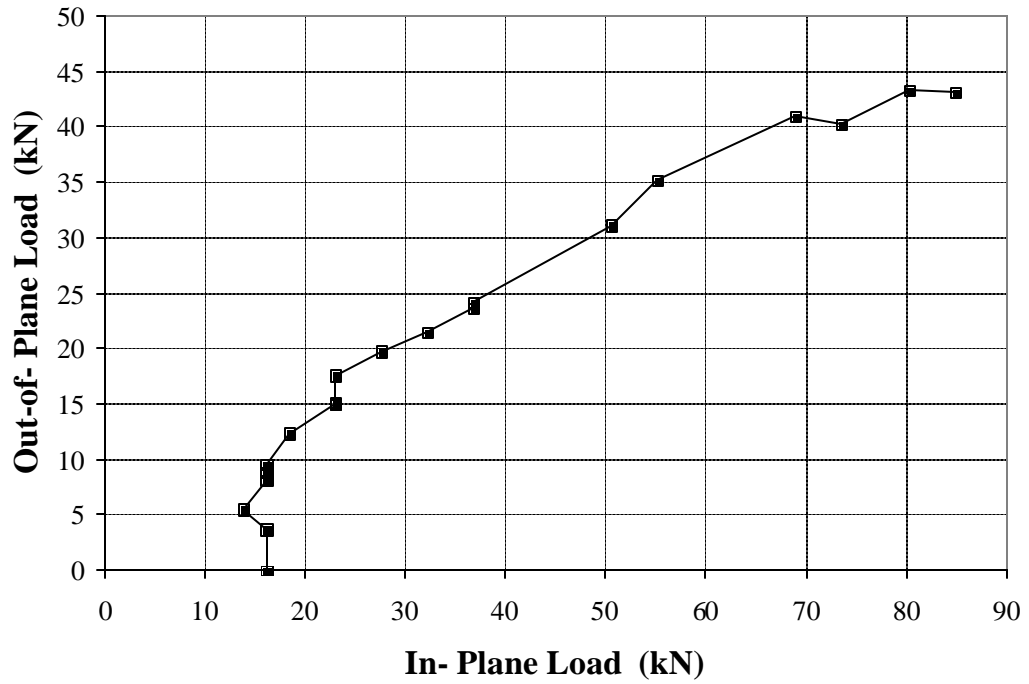
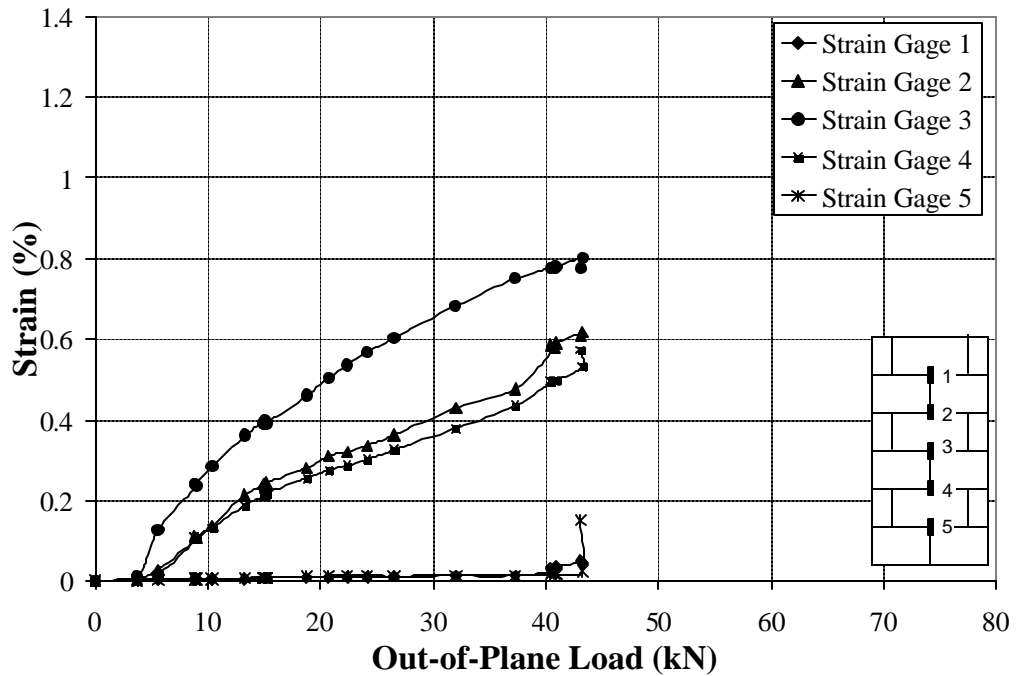


Fig B.6 Load vs. Mid-height Deflection S8-CO5



**Fig B.7 Out-of-Plane Load versus In-Plane Load S8-CO5**



**Fig B.8 Strain Distribution S8-CO5**

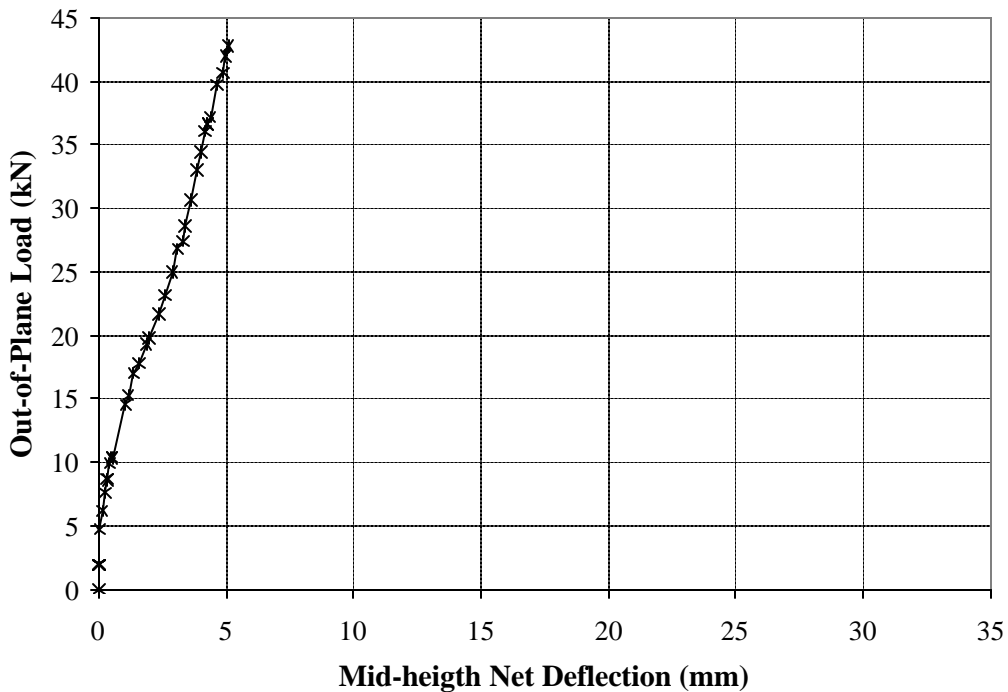


**Fig B.9 Load vs. Mid-height Deflection S8-CO7**

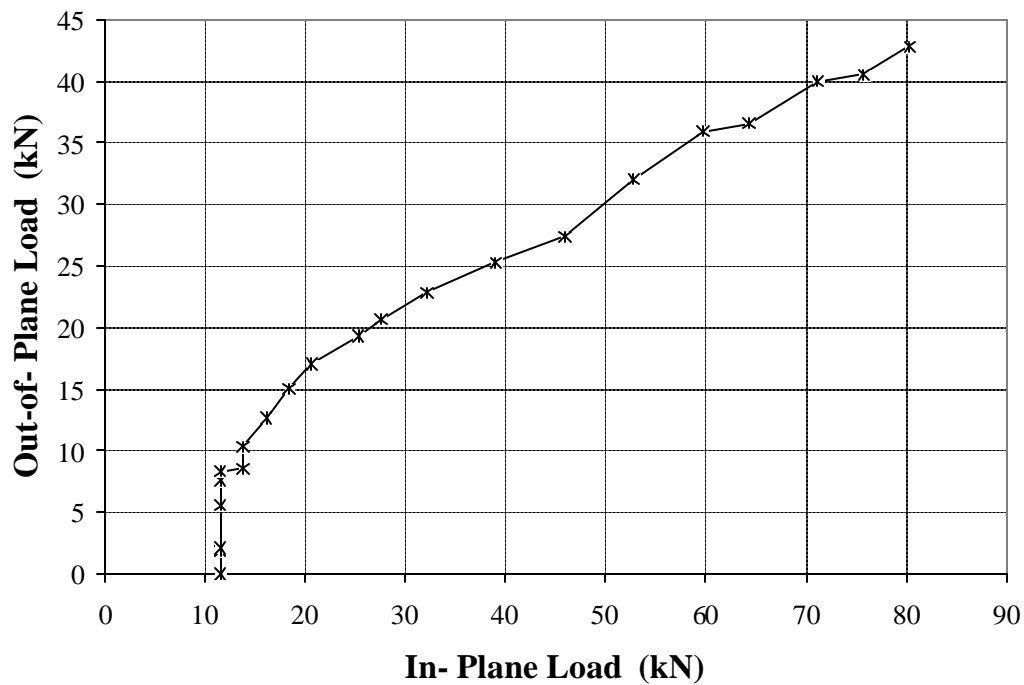


**Fig B.10 Out-of-Plane Load versus In-Plane Load S8-CO7**

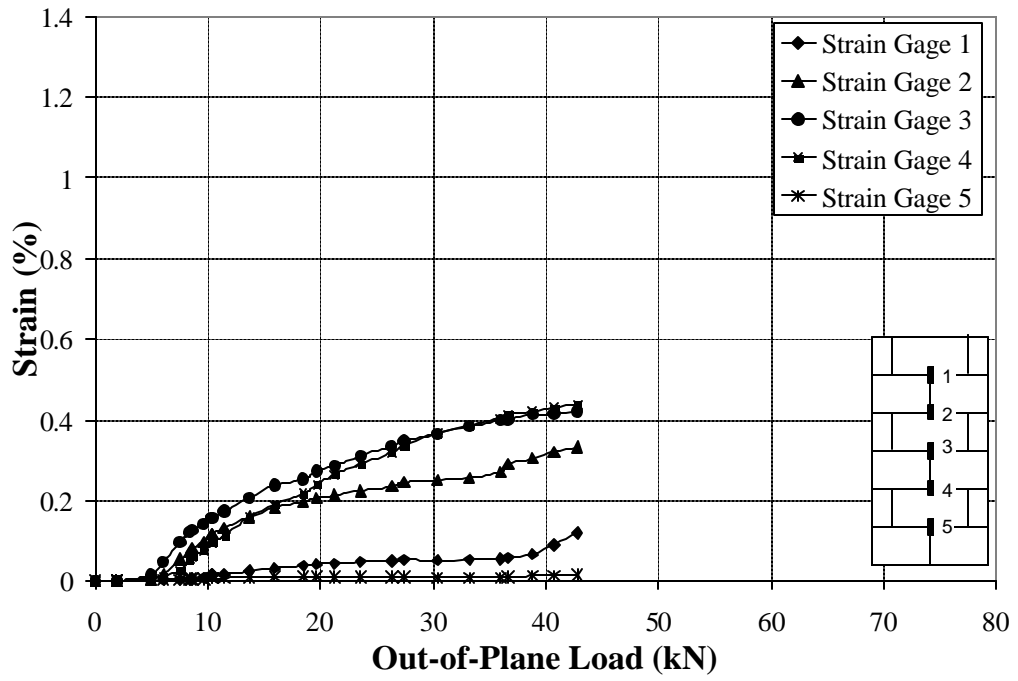


Fig B.11 Strain Distribution S8-CO7

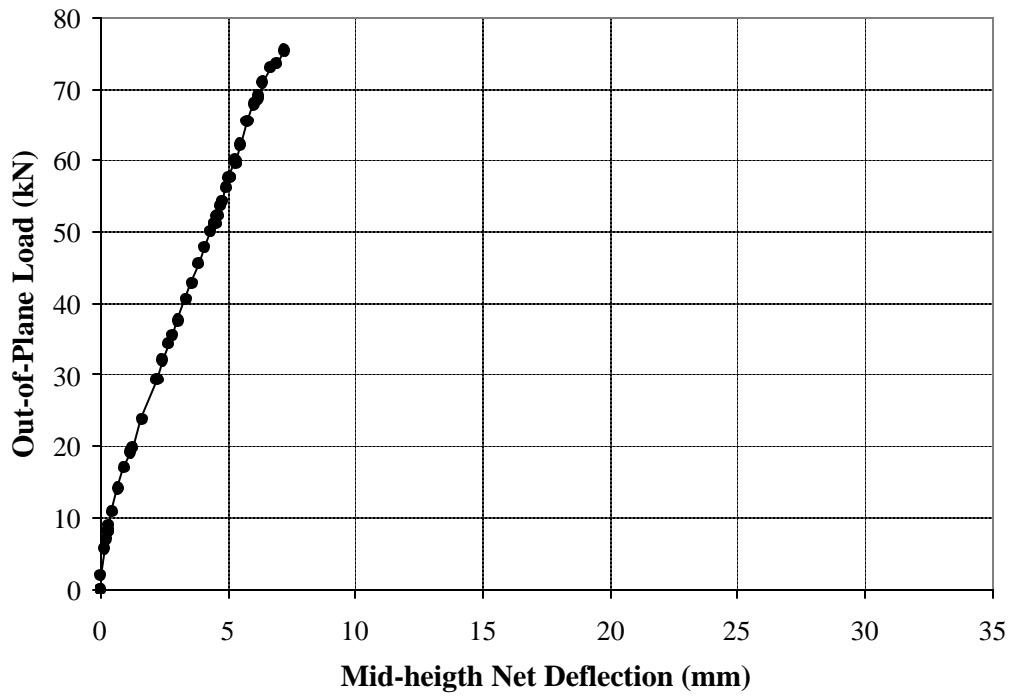


Fig B.12 Load vs. Mid-height Deflection S8-CO9

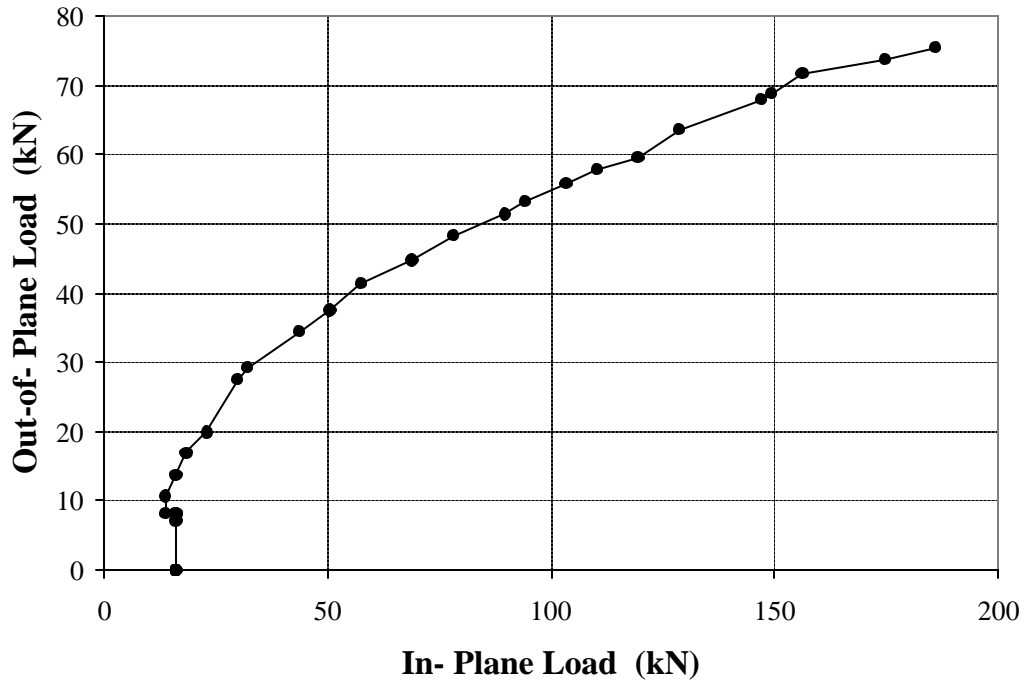


Fig B.13 Out-of-Plane Load versus In-Plane Load S8-CO9

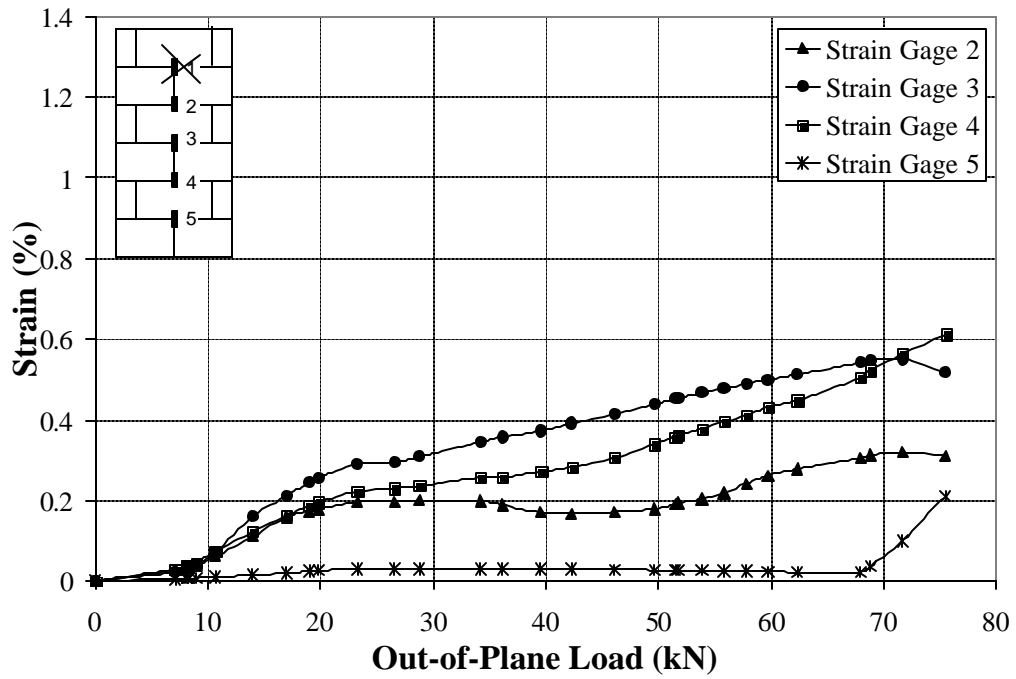
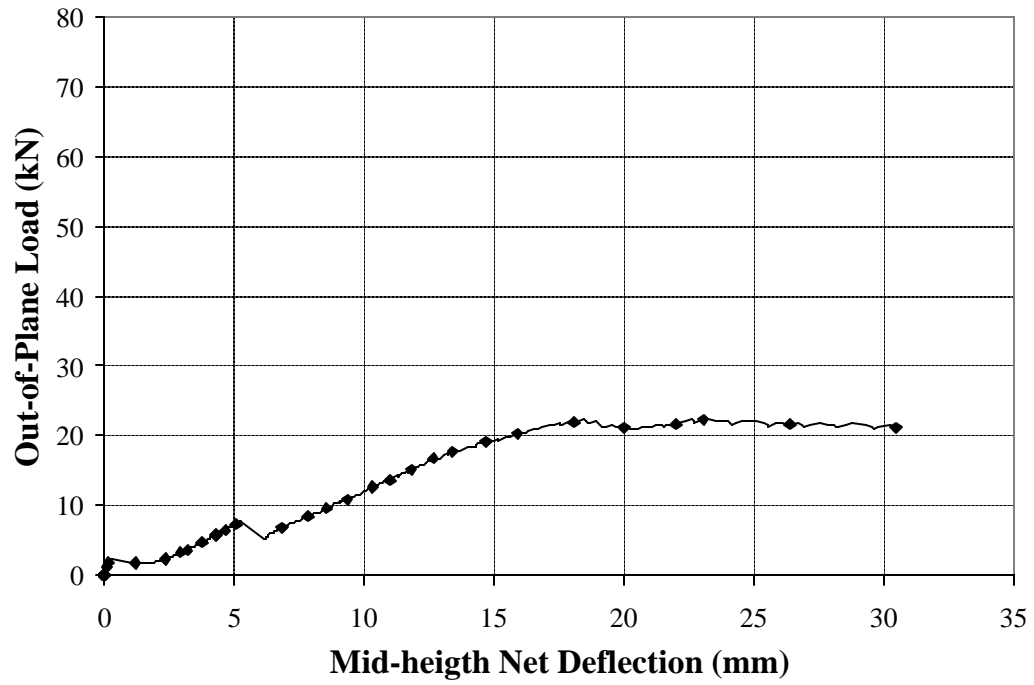
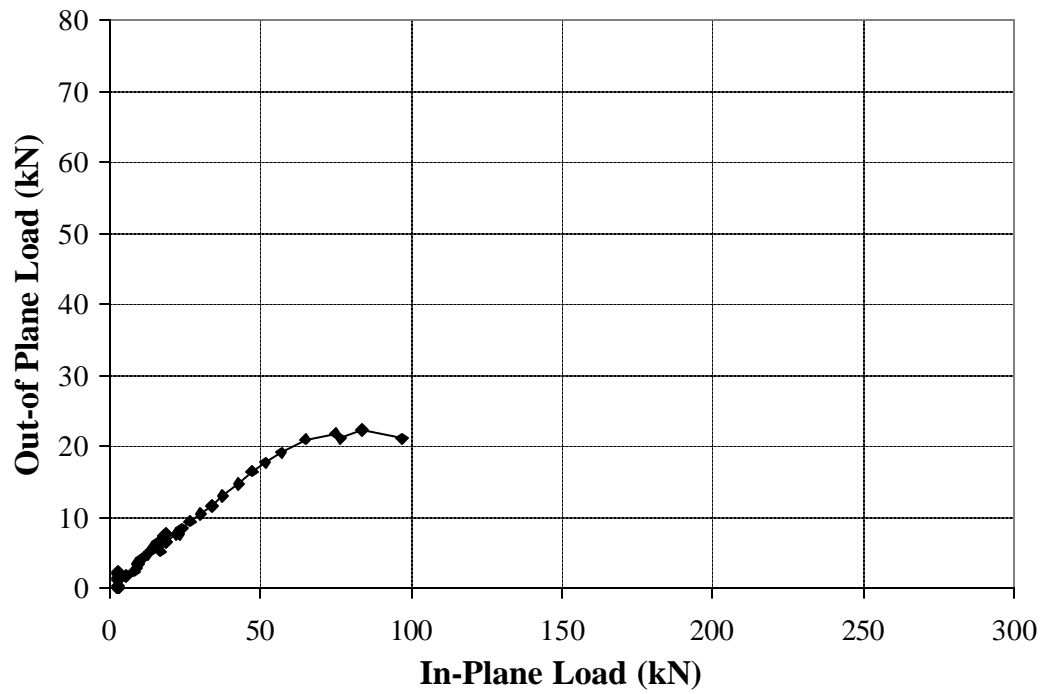


Fig B.14 Strain Distribution S8-CO9



**Fig B.15 Load vs. Mid-height Deflection S12-CO0**



**Fig B.16 Out-of-Plane Load versus In-Plane Load S12-CO0**

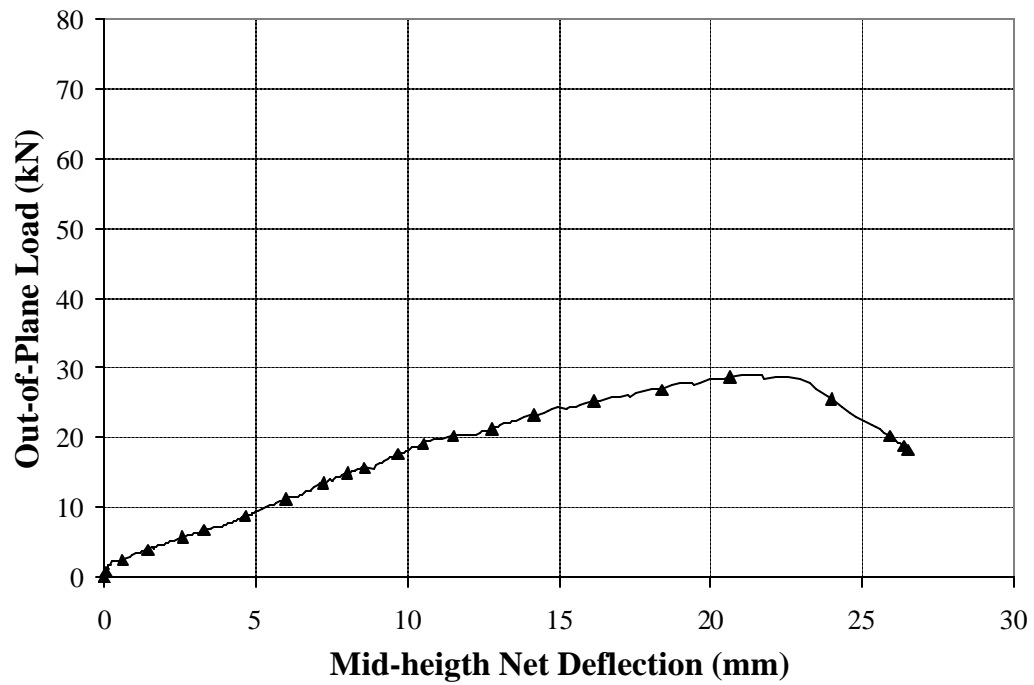


**Fig B.17 Load vs. Mid-height Deflection S12-CO3**

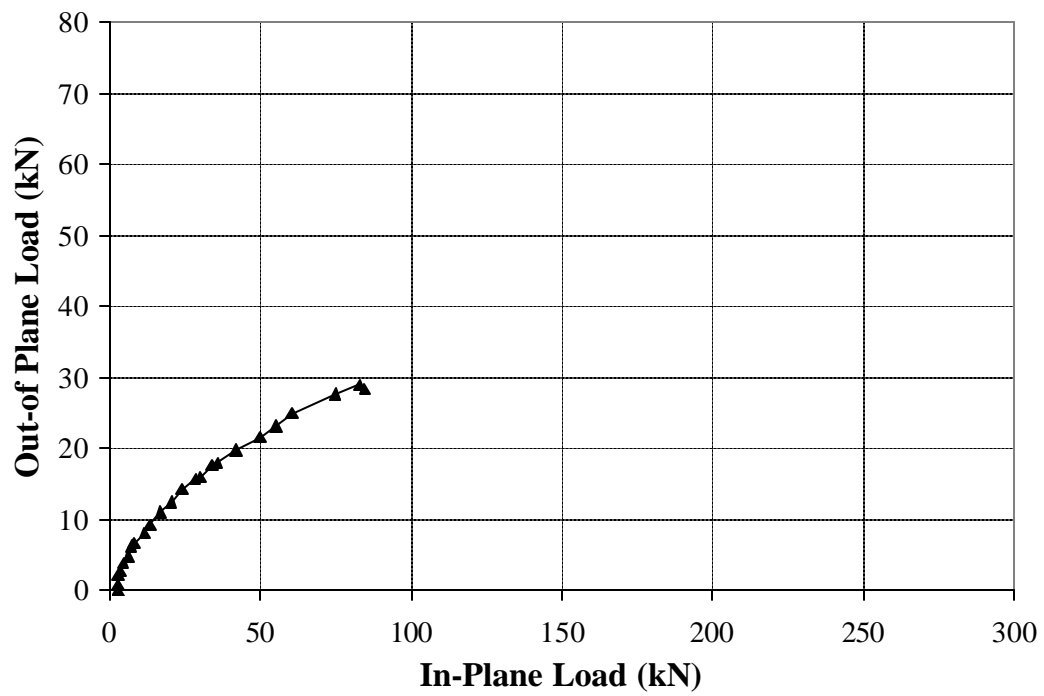


**Fig B.18 Out-of-Plane Load versus In-Plane Load S12-CO3**

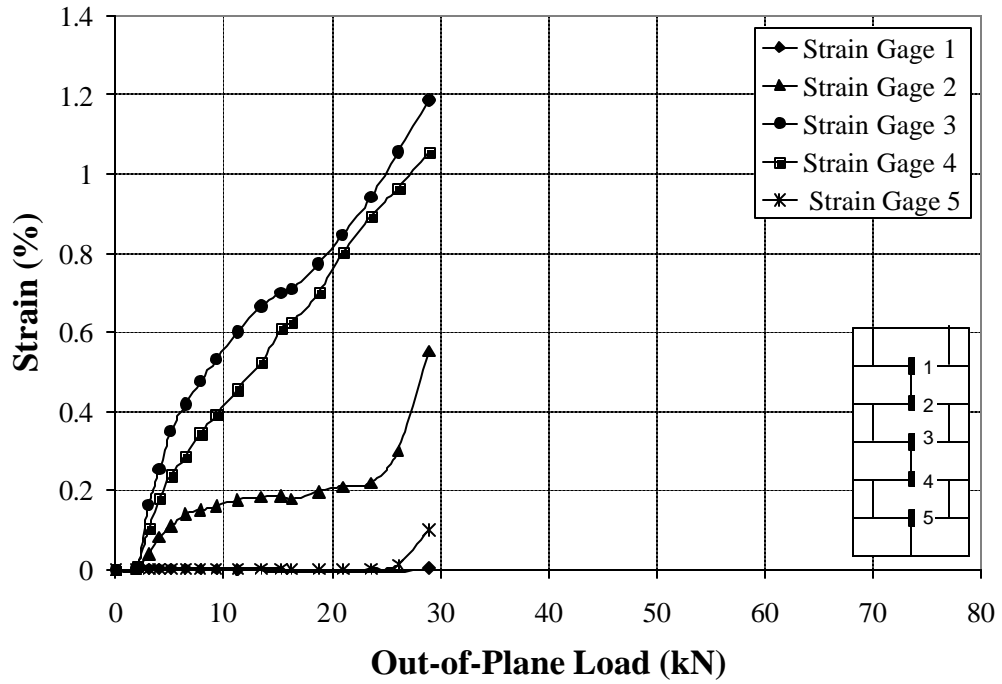


Fig B.19 Strain Distribution S12-CO3

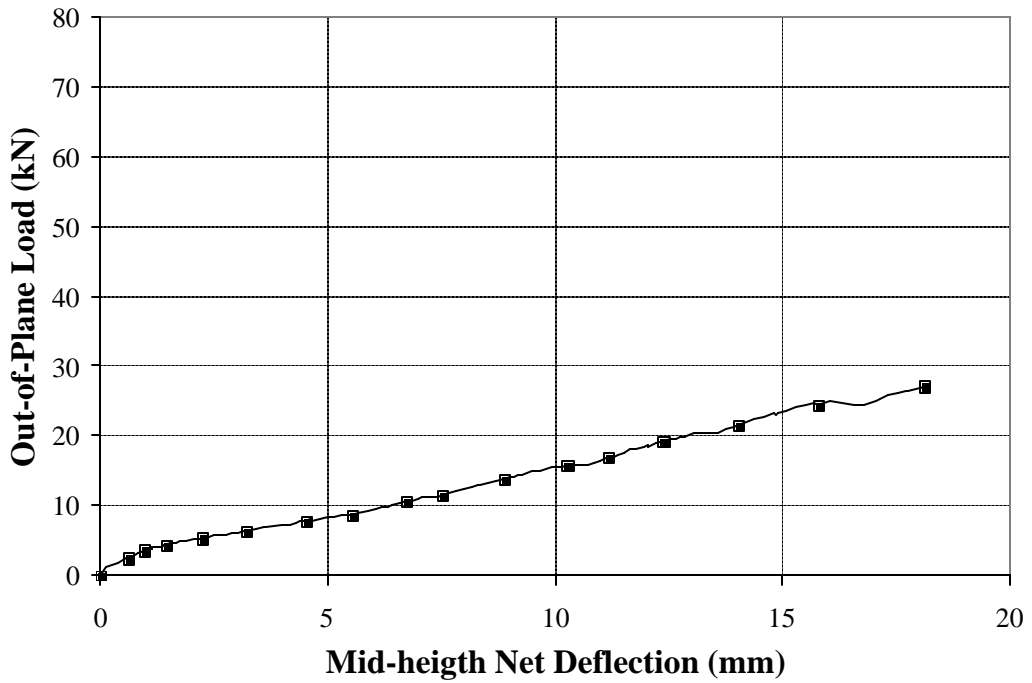
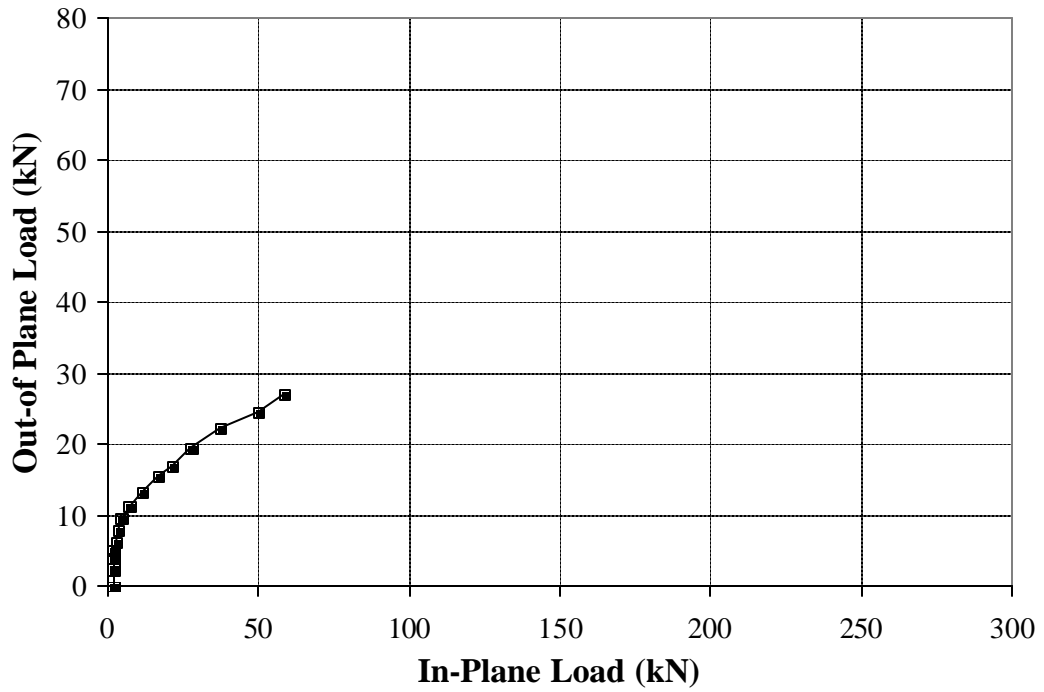
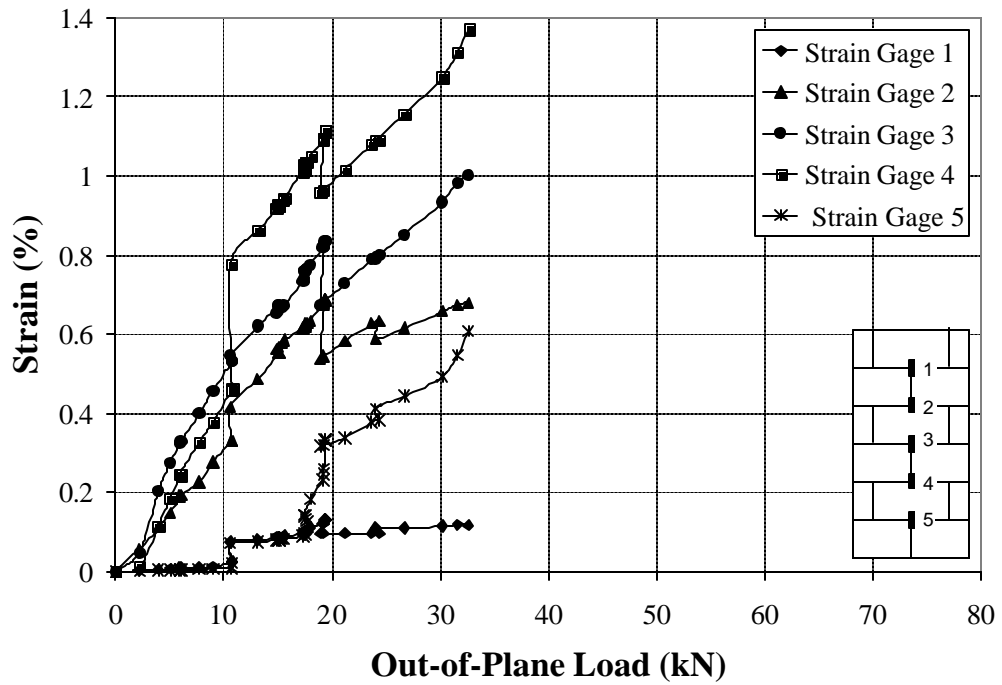


Fig B.20 Load vs. Mid-height Deflection S12-CO5



**Fig B.21 Out-of-Plane Load versus In-Plane Load S12-CO5**



**Fig B.22 Strain Distribution S12-CO5**

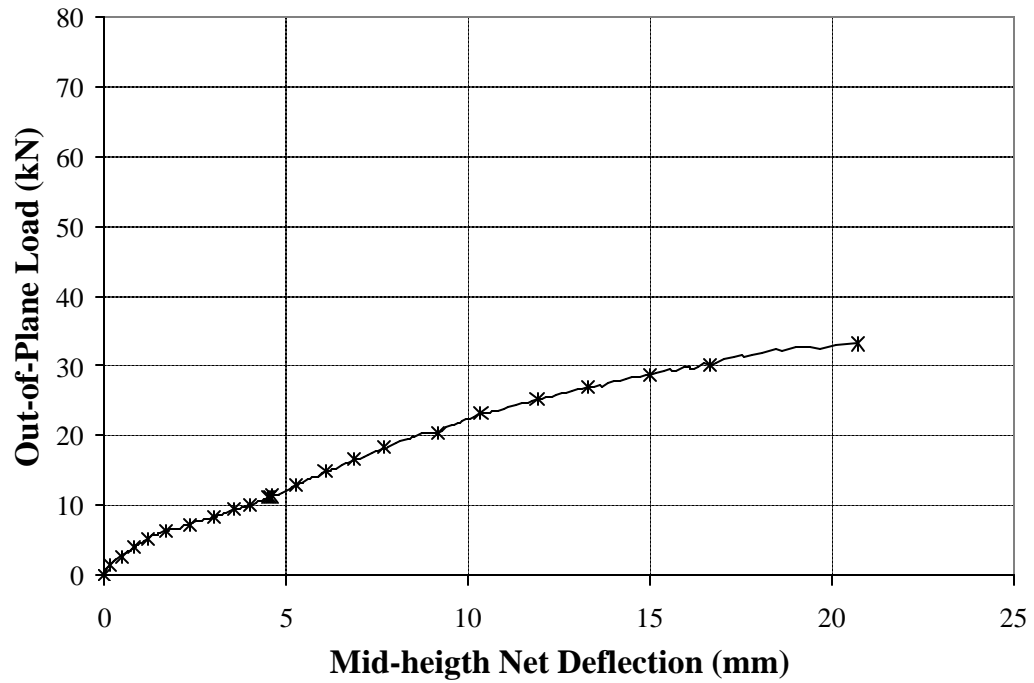


**Fig B.23 Load vs. Mid-height Deflection S12-CO7**

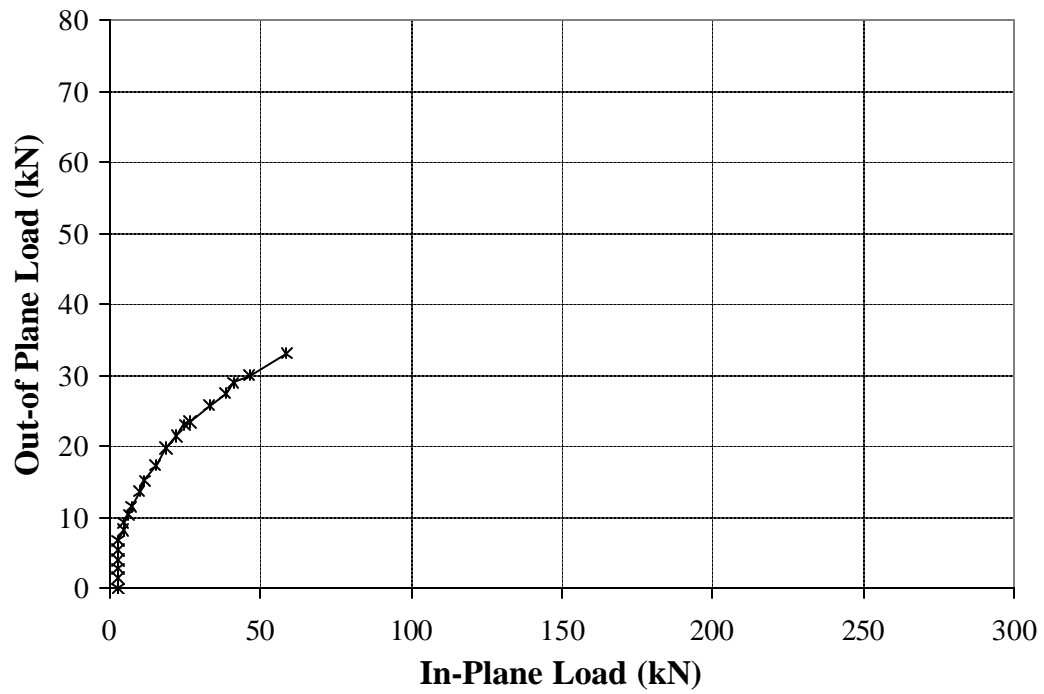


**Fig B.24 Out-of-Plane Load versus In-Plane Load S12-CO7**

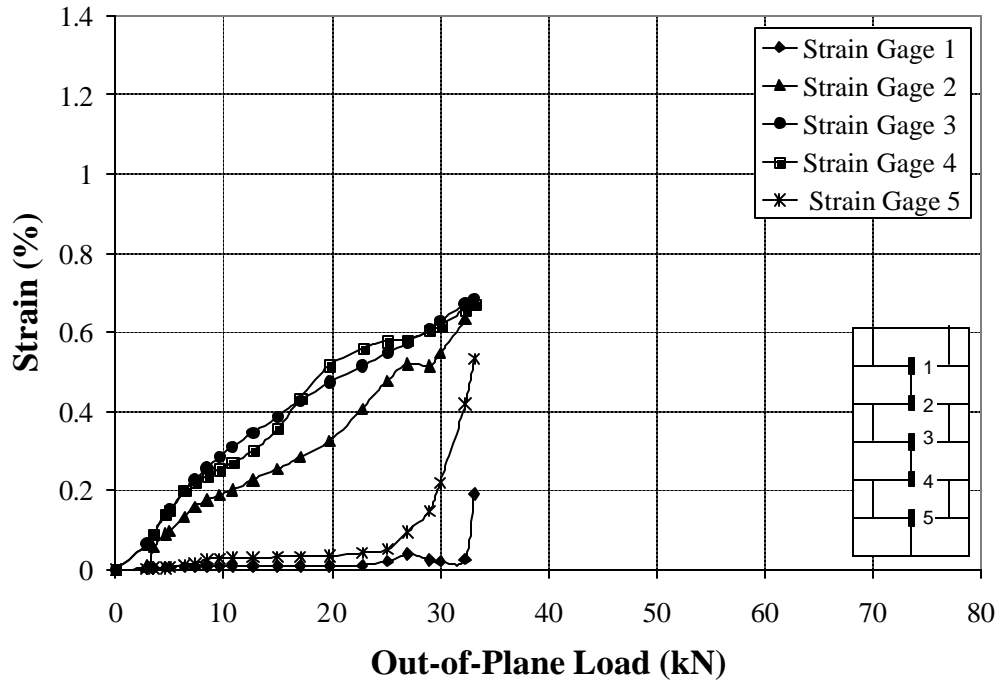


Fig B.25 Strain Distribution S12-CO7

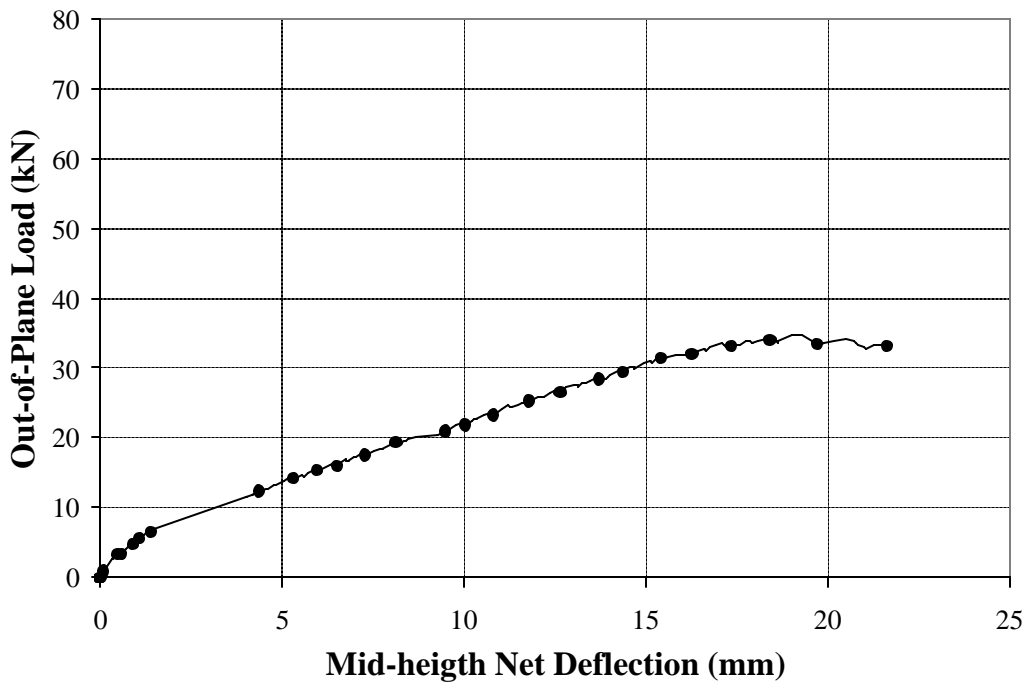


Fig B.26 Load vs. Mid-height Deflection S12-CO9

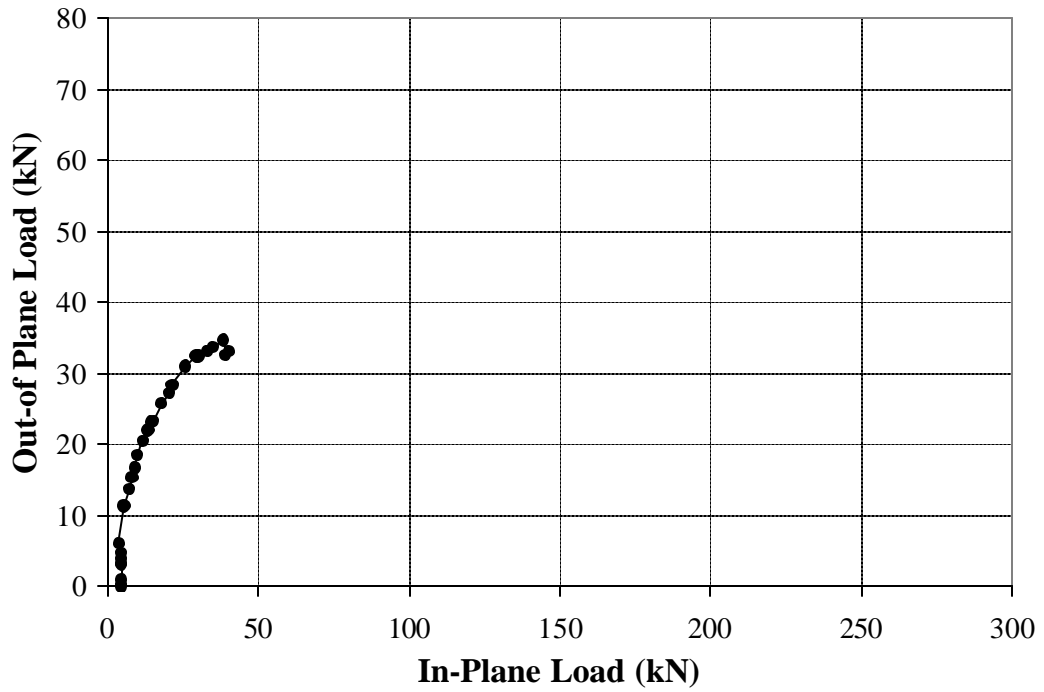


Fig B.27 Out-of-Plane Load versus In-Plane Load S12-CO9

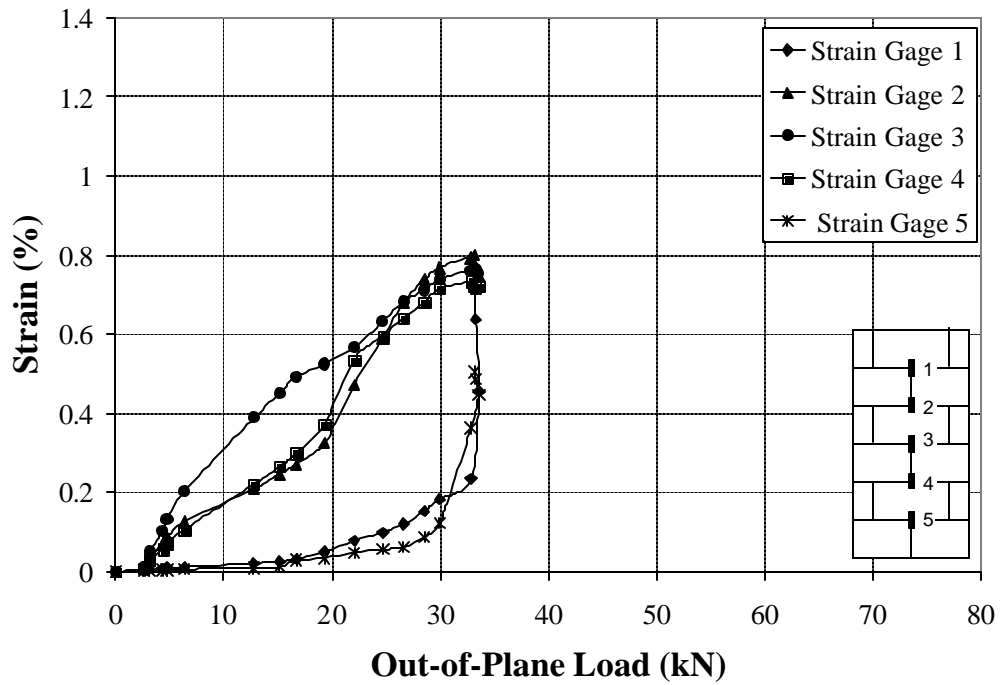
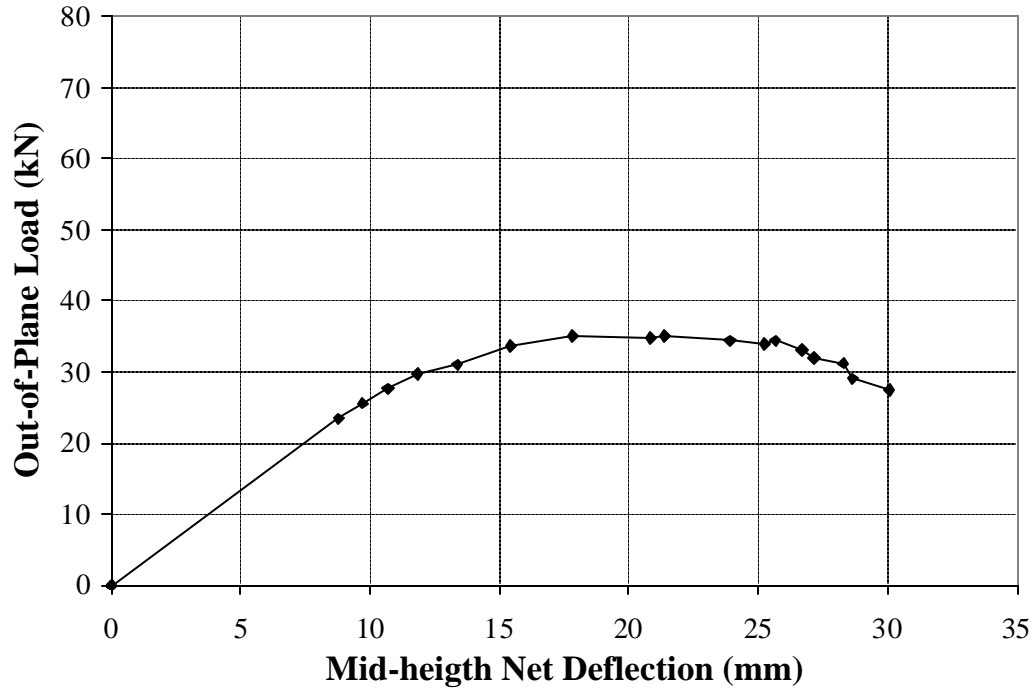
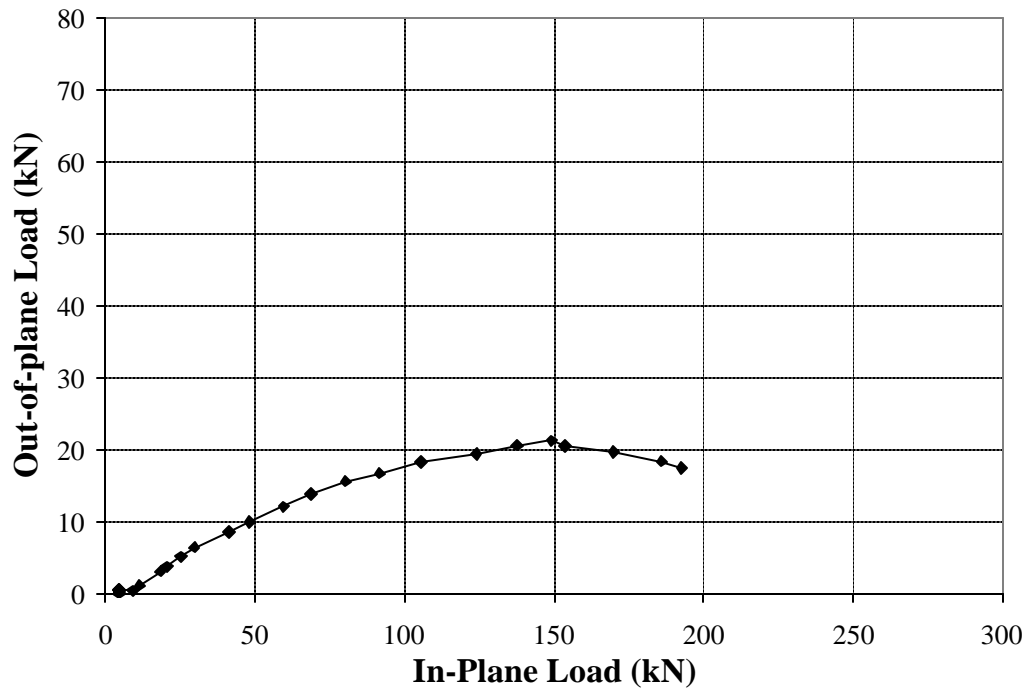


Fig B.28 Strain Distribution S12-CO9



**Fig B.29 Load vs. Mid-height Deflection S12-CL0**



**Fig B.30 Out-of-Plane Load versus In-Plane Load S12-CL0**

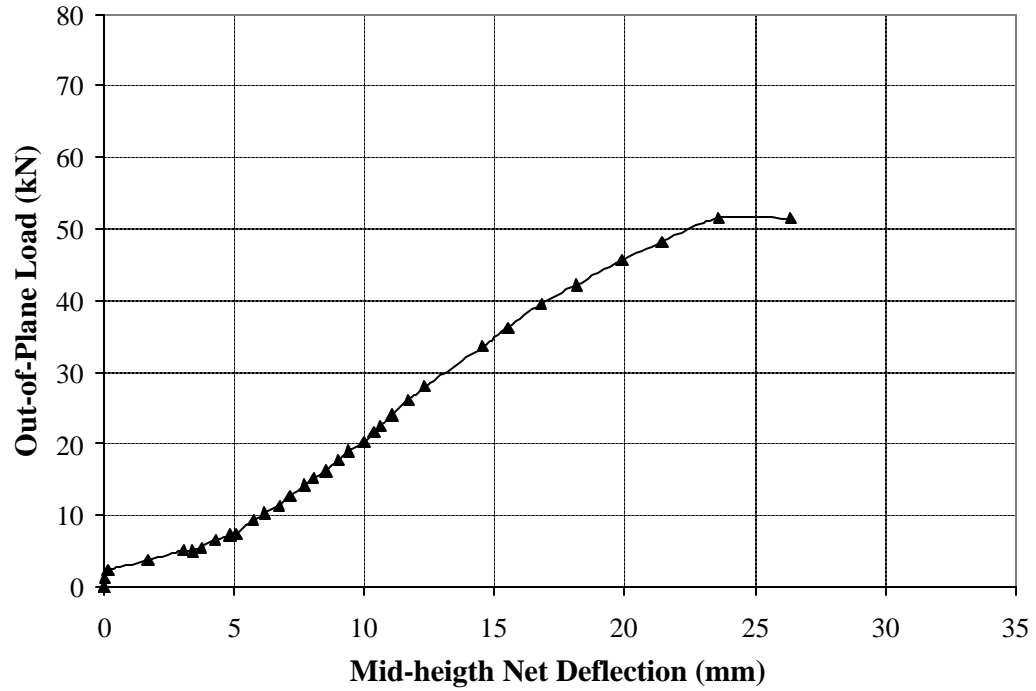


**Fig B.31 Load vs. Mid-height Deflection S12-CL3**

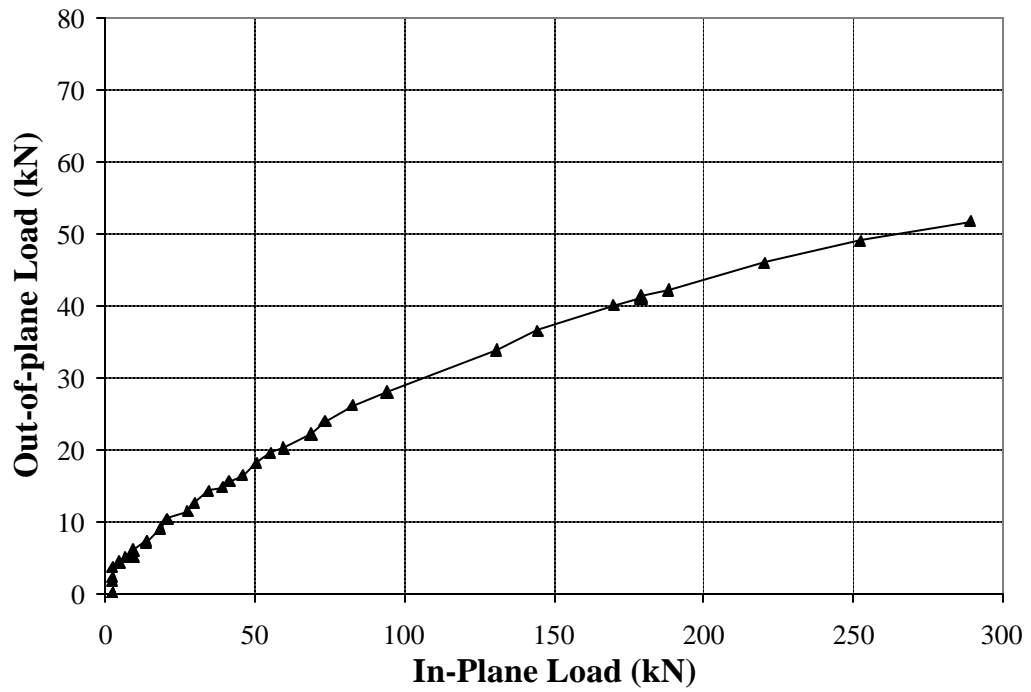


**Fig B.32 Out-of-Plane Load versus In-Plane Load S12-CL3**

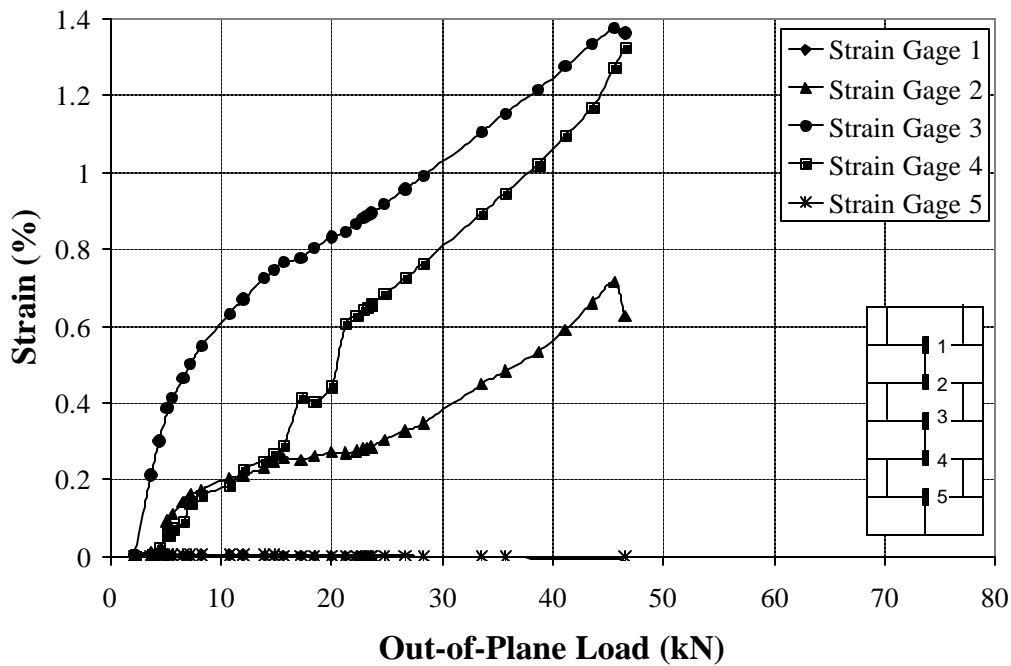


Fig B.33 Strain Distribution S12-CL3

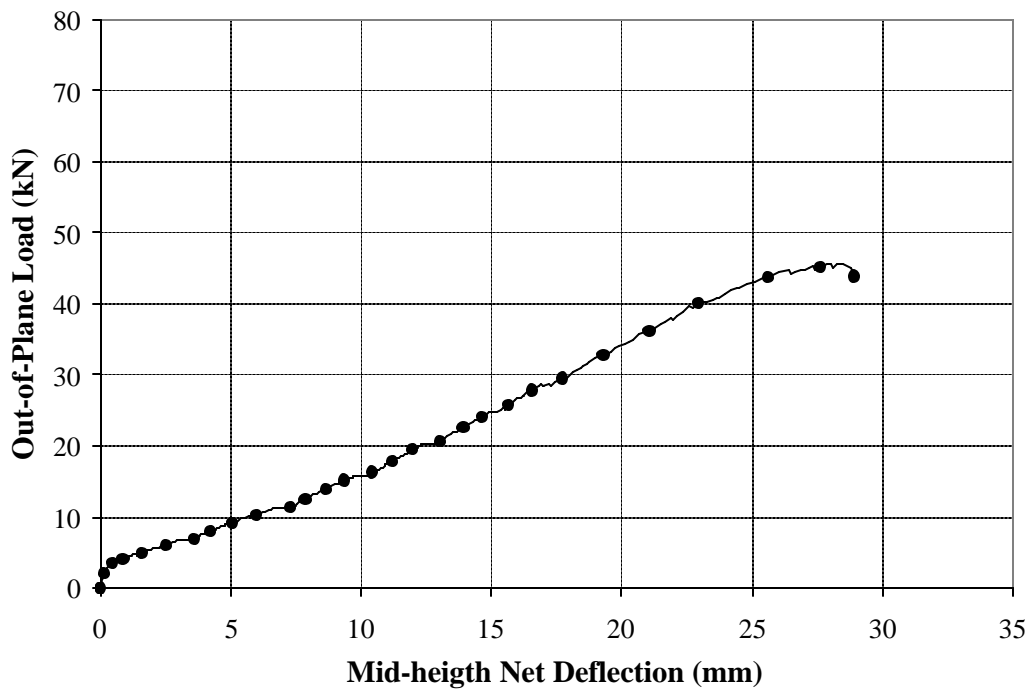
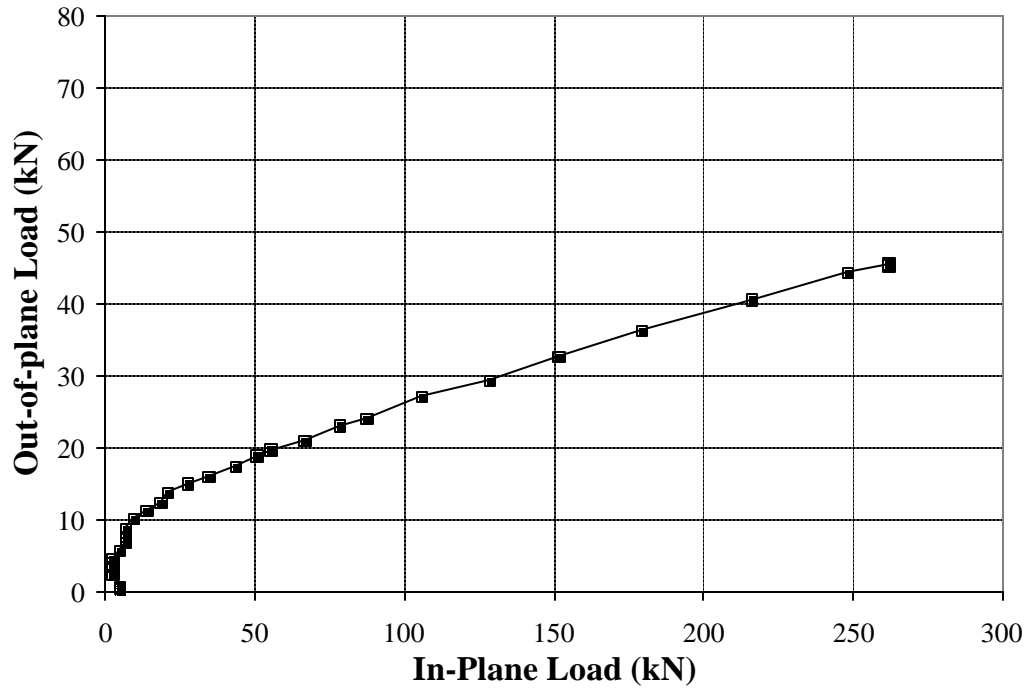
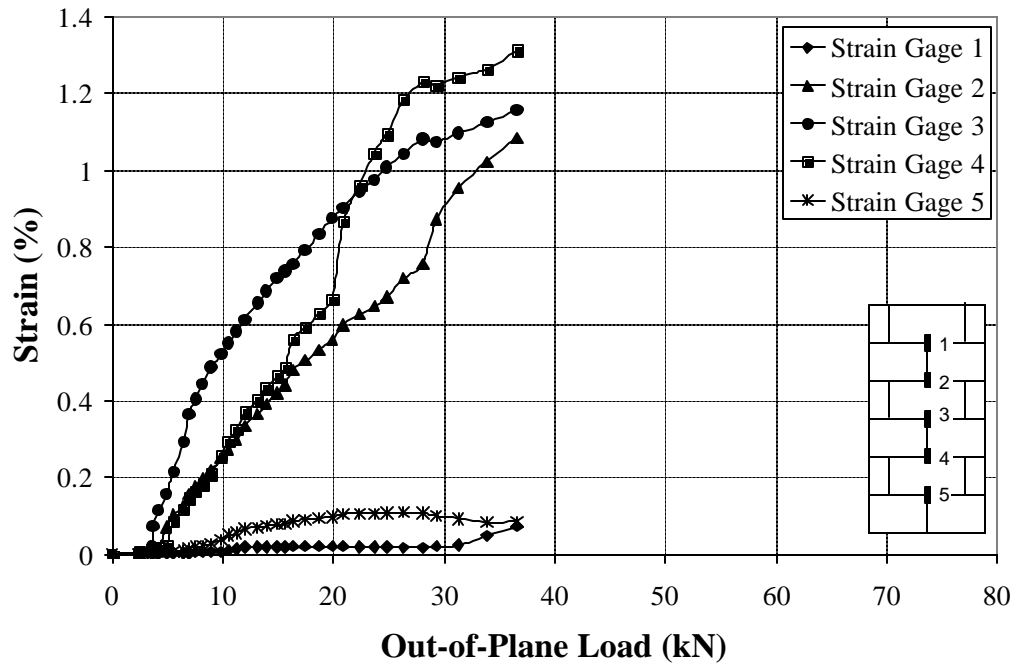


Fig B.34 Load vs. Mid-height Deflection S12-CL5



**Fig B.35 Out-of-Plane Load versus In-Plane Load S12-CL5**



**Fig B.36 Strain Distribution S12-CL5**

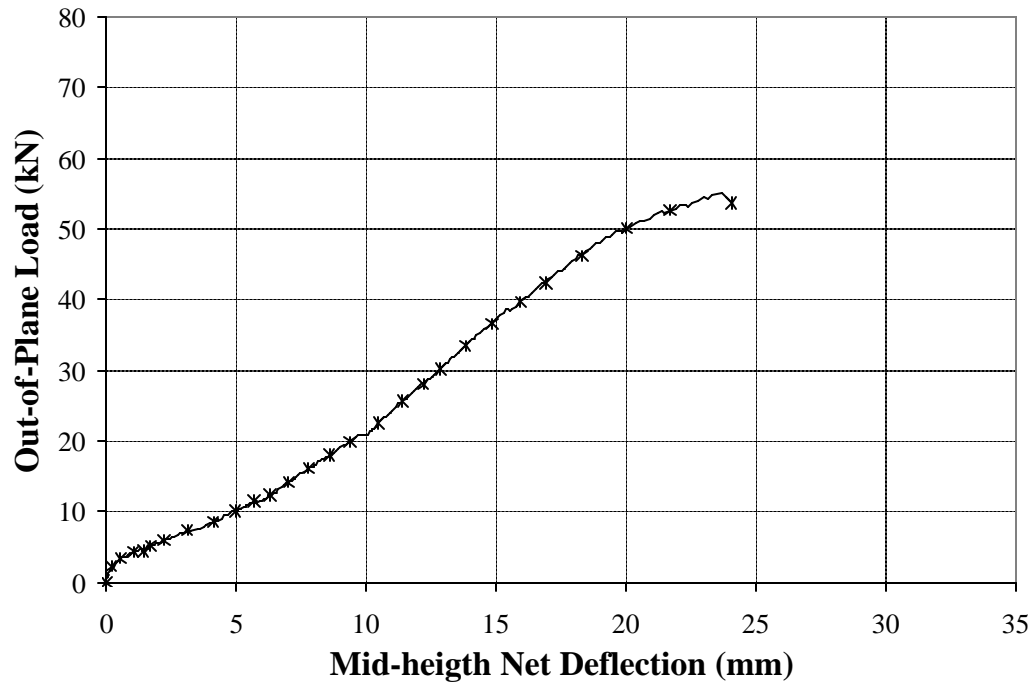


**Fig B.37 Load vs. Mid-height Deflection S12-CL7**

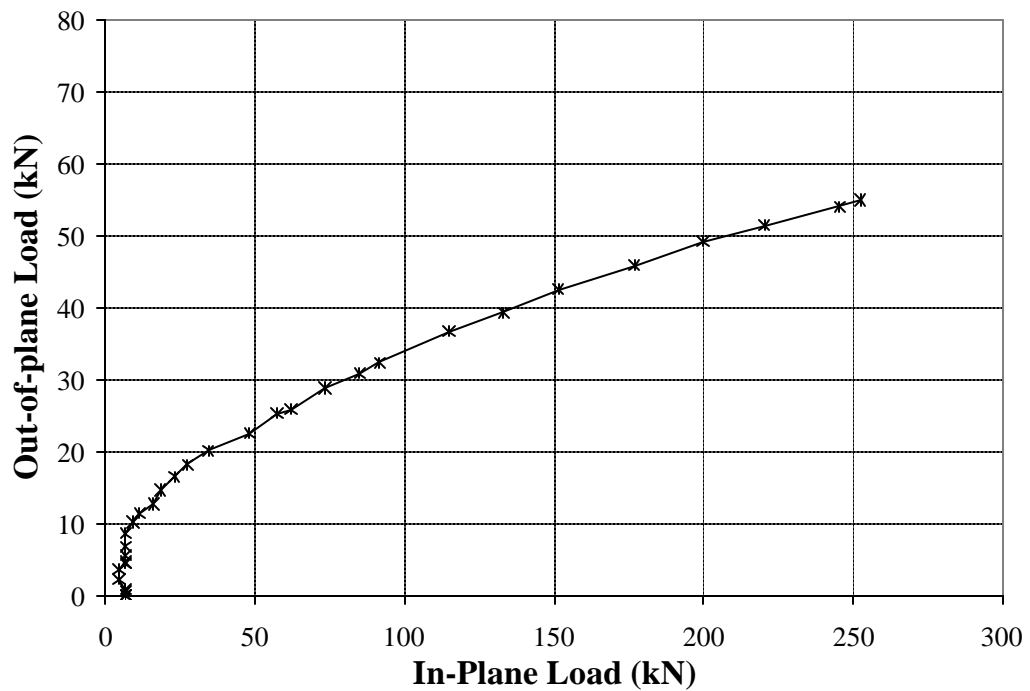


**Fig B.38 Out-of-Plane Load versus In-Plane Load S12-CL7**

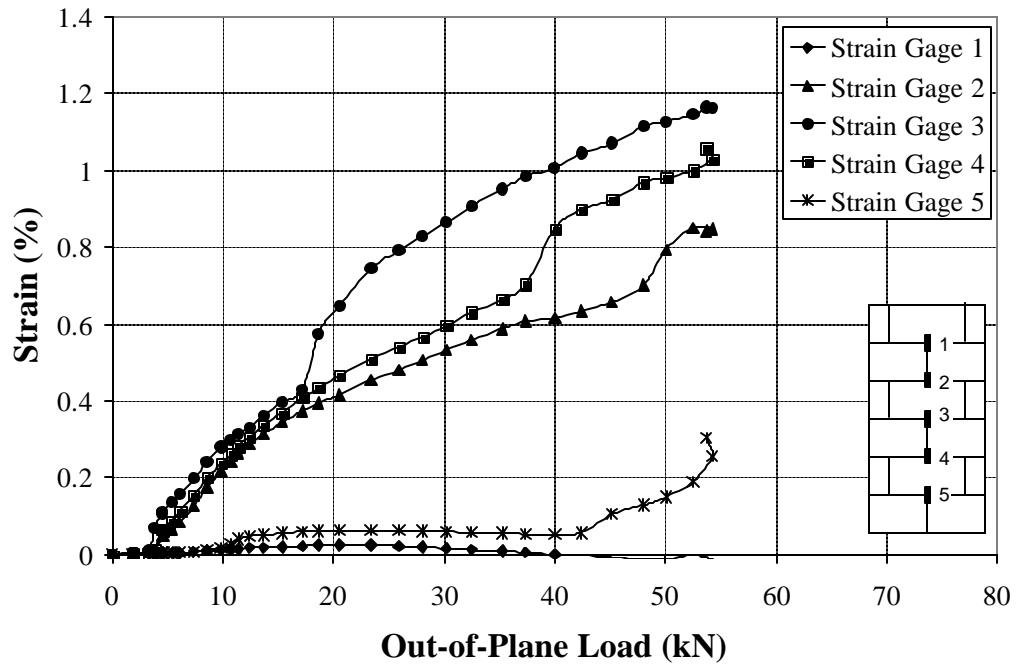


Fig B.39 Strain Distribution S12-CL7

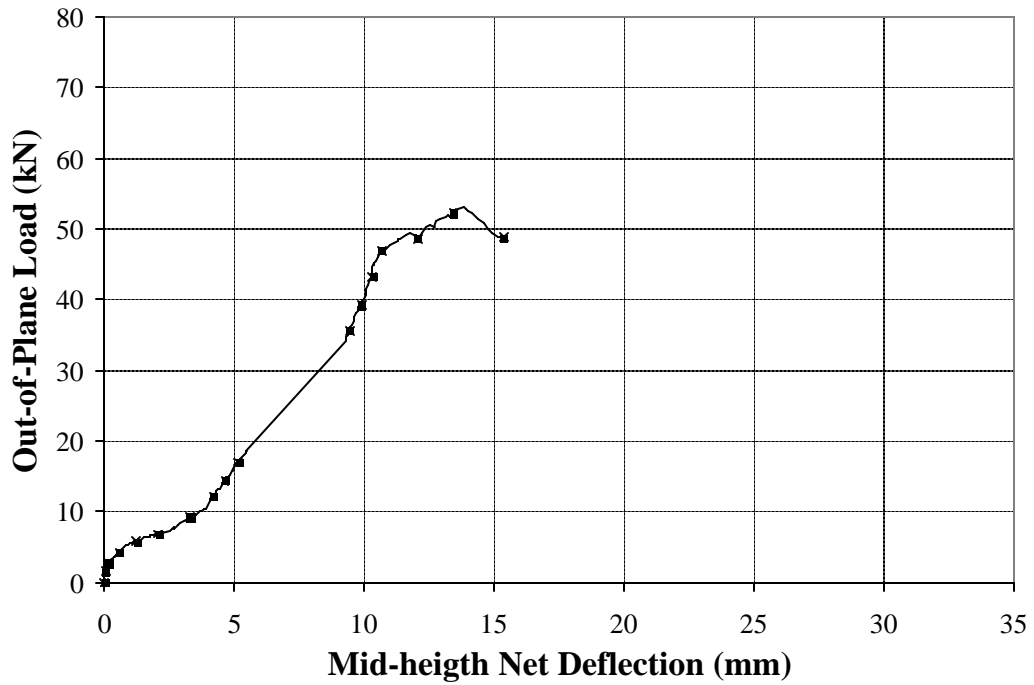
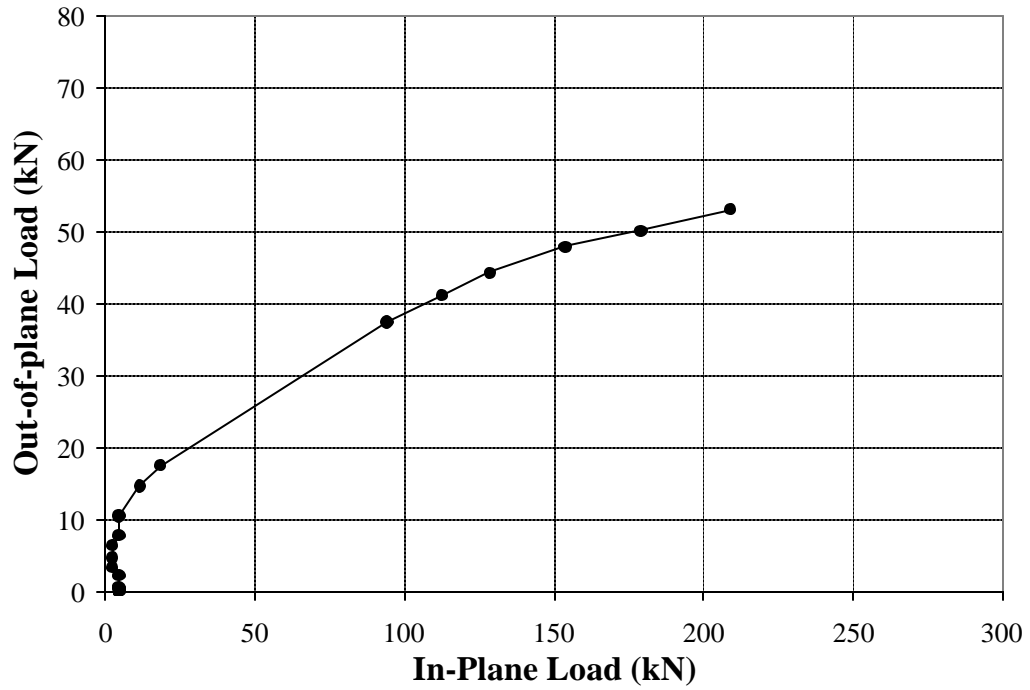
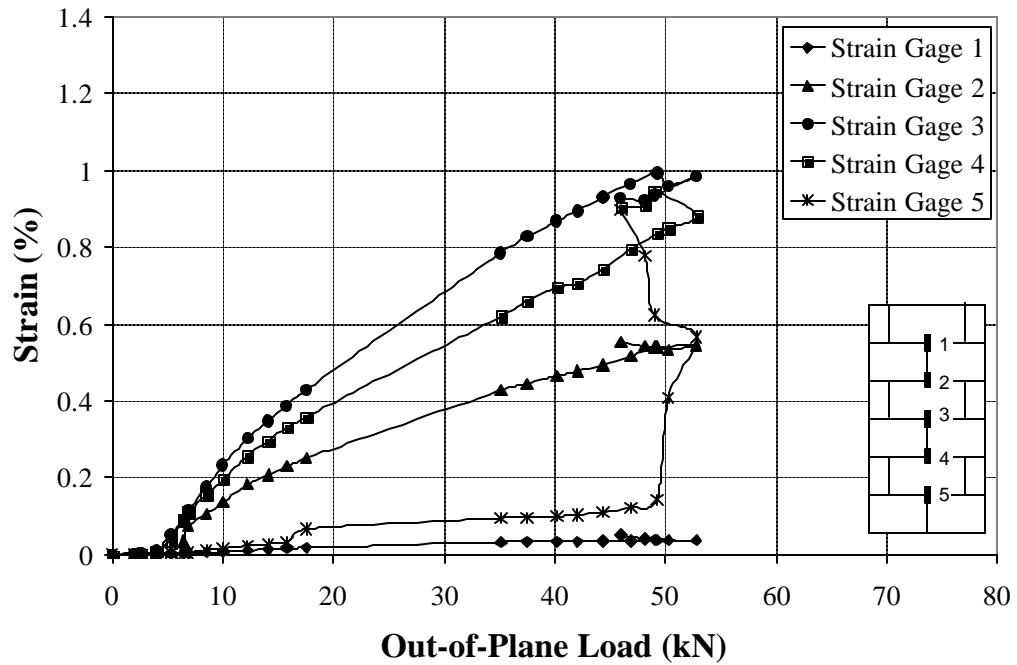


Fig B.40 Load vs. Mid-height Deflection S12-CL9



**Fig B.41 Out-of-Plane Load versus In-Plane Load S12-CL9**



**Fig B.42 Strain Distribution S12-CL9**

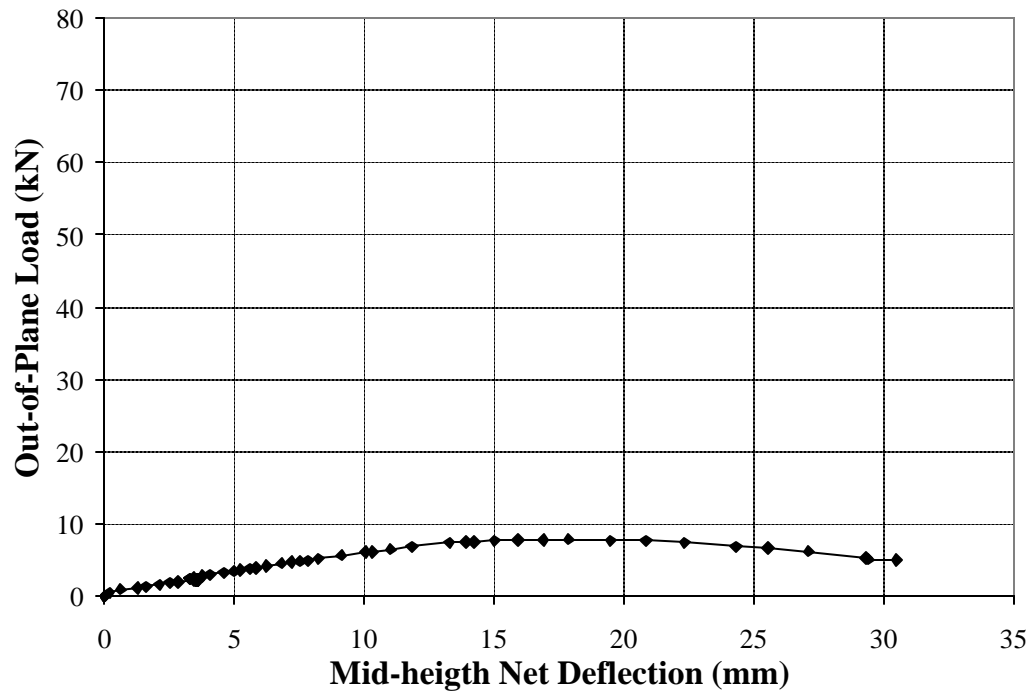


**Fig B.43 Load vs. Mid-height Deflection S19-CL0**

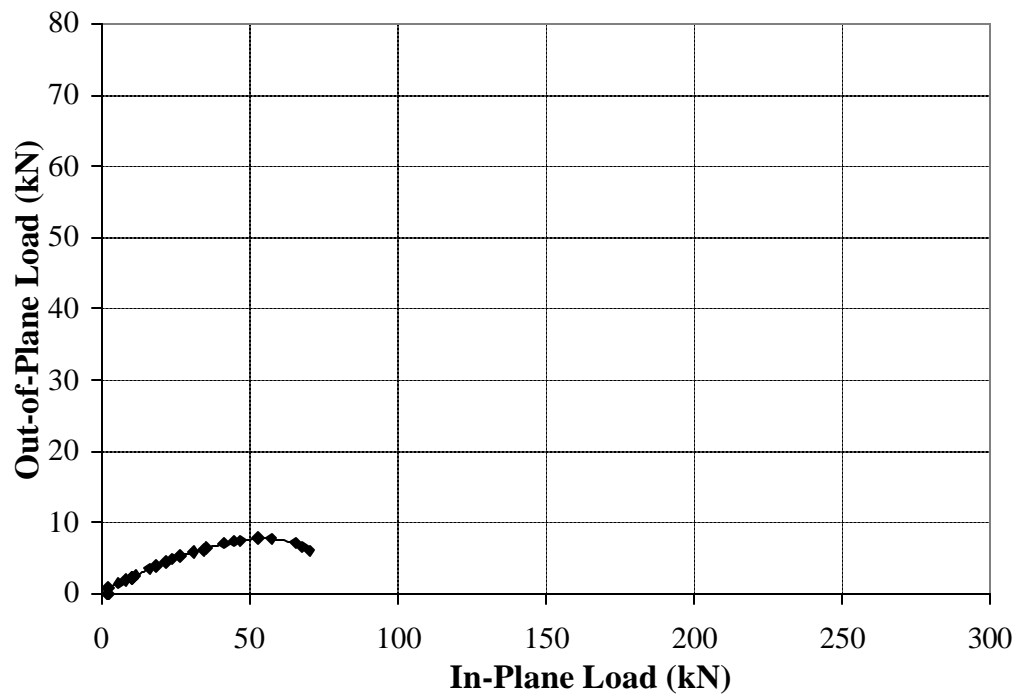


**Fig B.44 Out-of-Plane Load versus In-Plane Load S19-CL0**

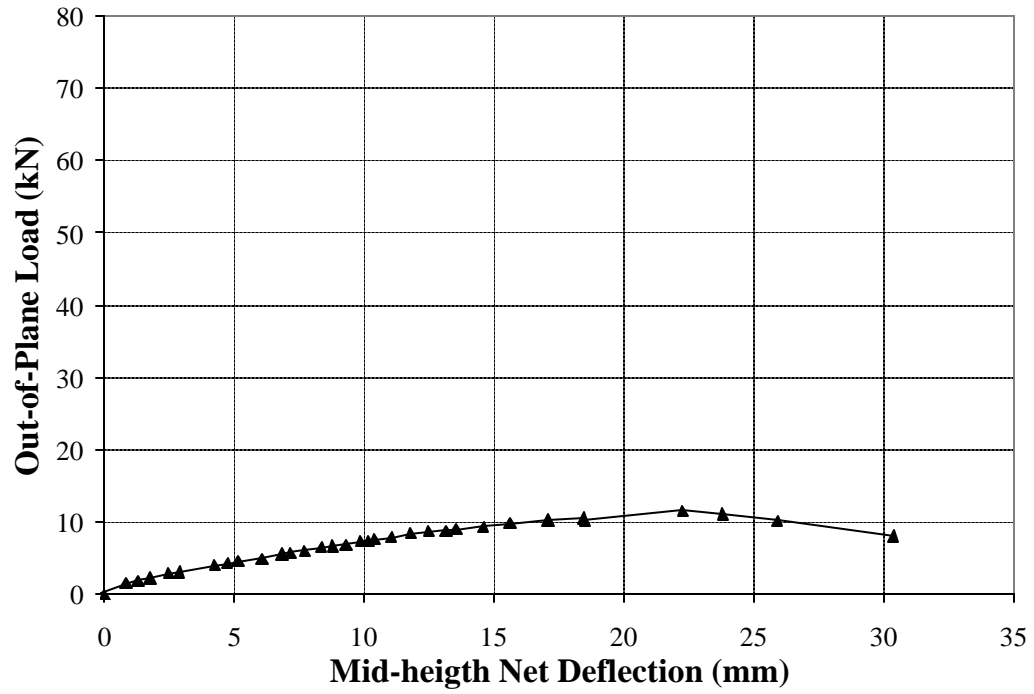


**Fig B.45 Load vs. Mid-height Deflection S19-CL3**

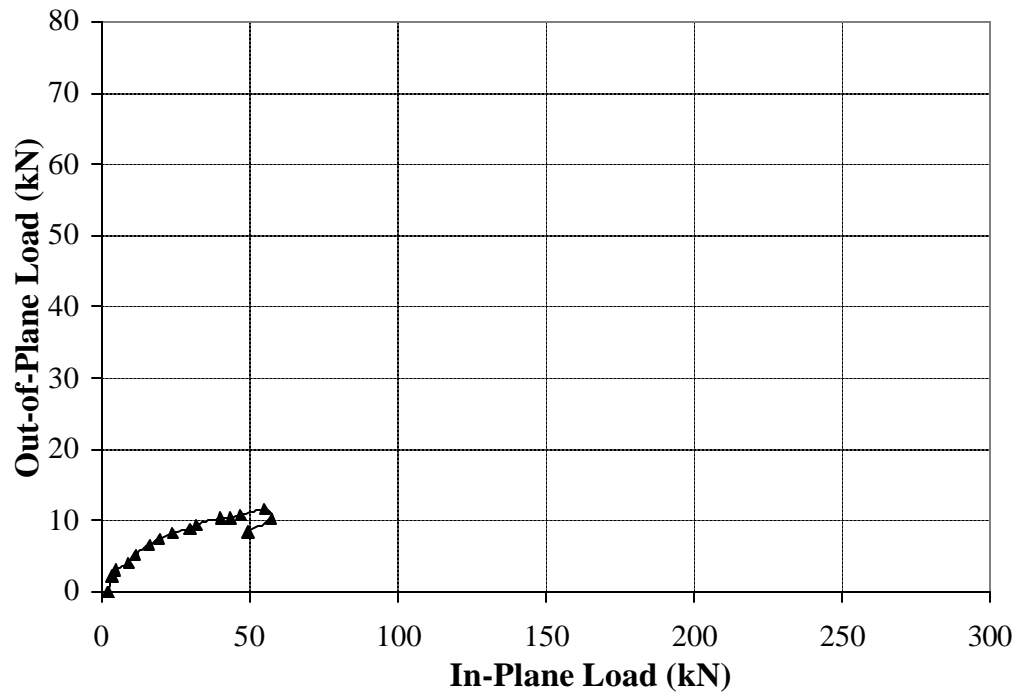


**Fig B.46 Out-of-Plane Load versus In-Plane Load S19-CL3**

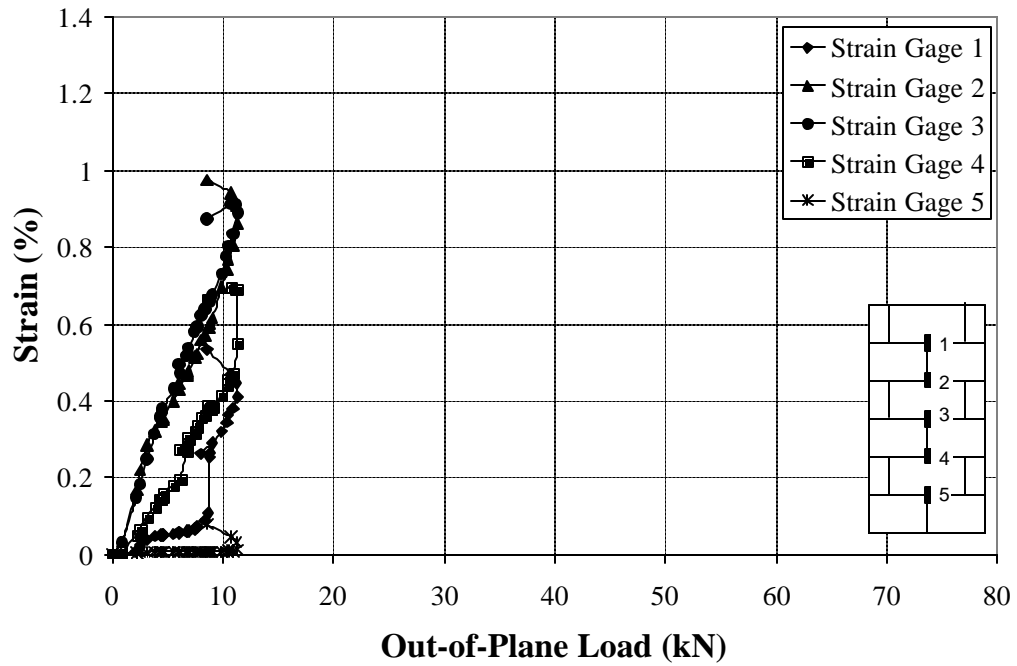


Fig B.47 Strain Distribution S19-CL3

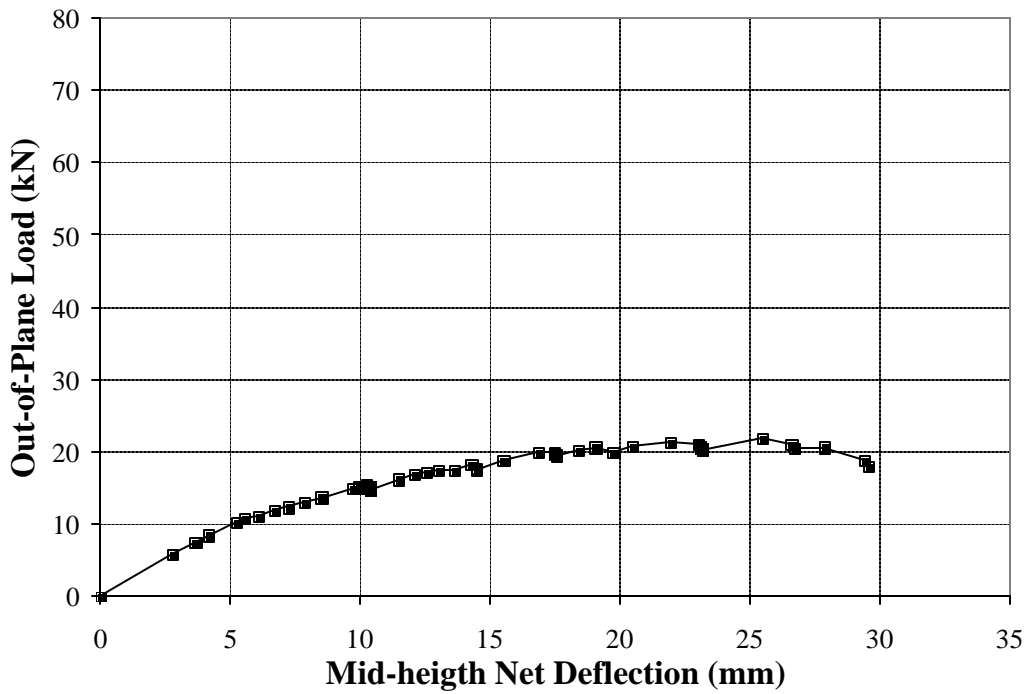
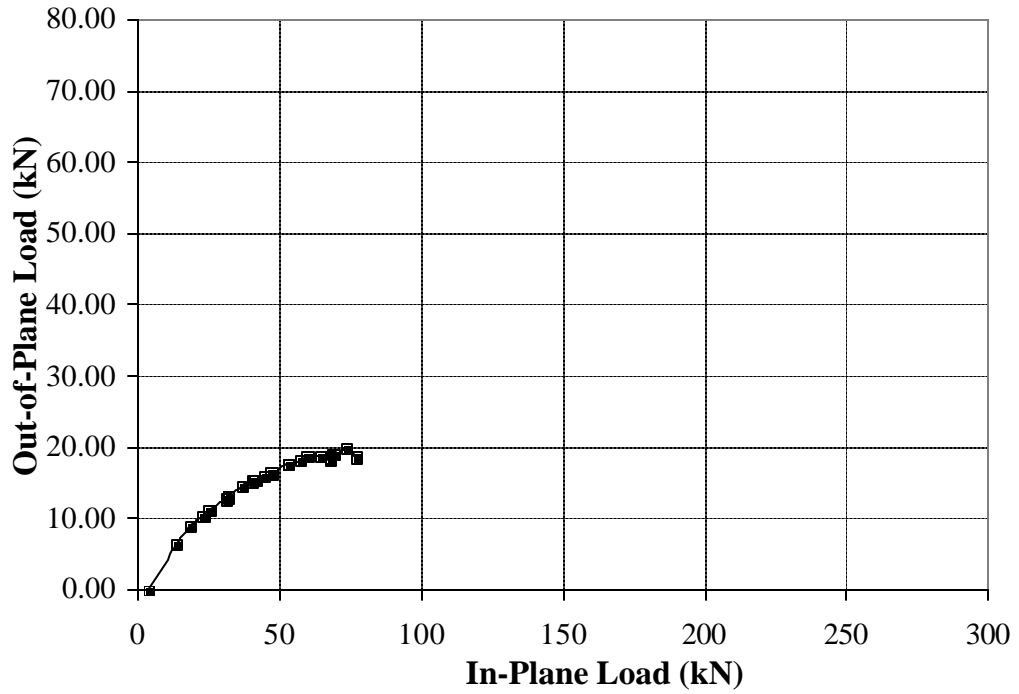
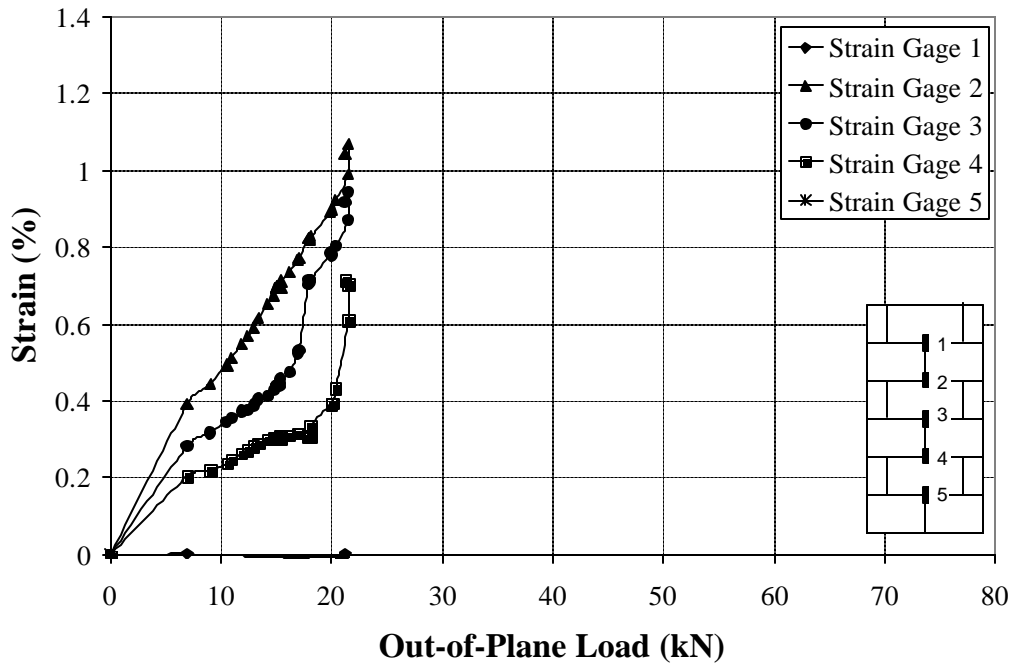


Fig B.48 Load vs. Mid-height Deflection S19-CL5



**Fig B.49 Out-of-Plane Load versus In-Plane Load S19-CL5**



**Fig B.50 Strain Distribution S19-CL5**

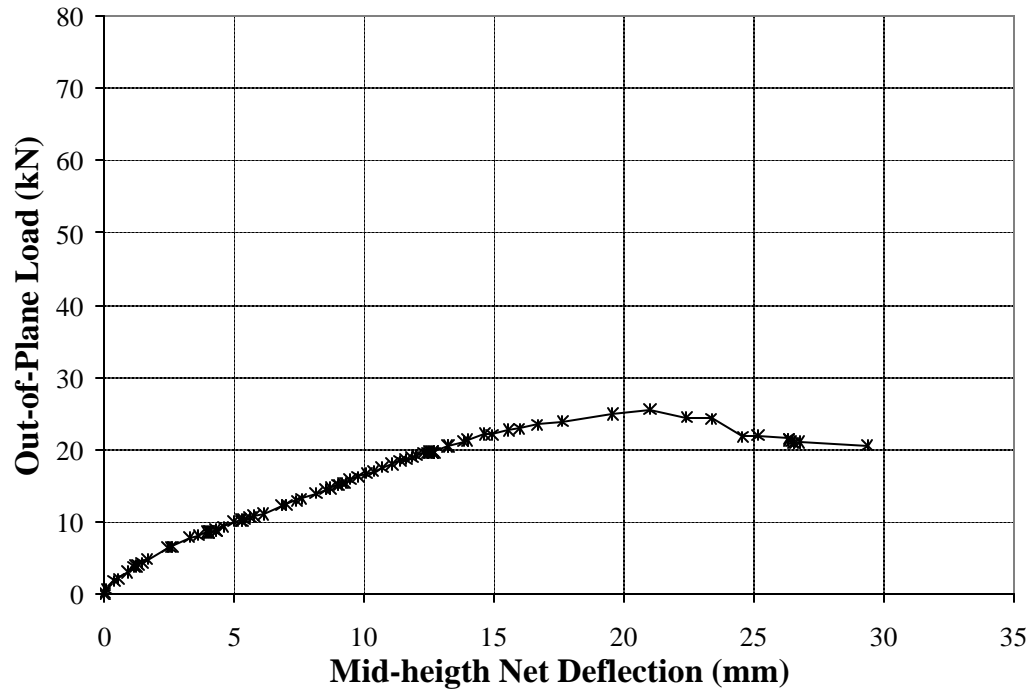


**Fig B.51 Load vs. Mid-height Deflection S19-CL7**

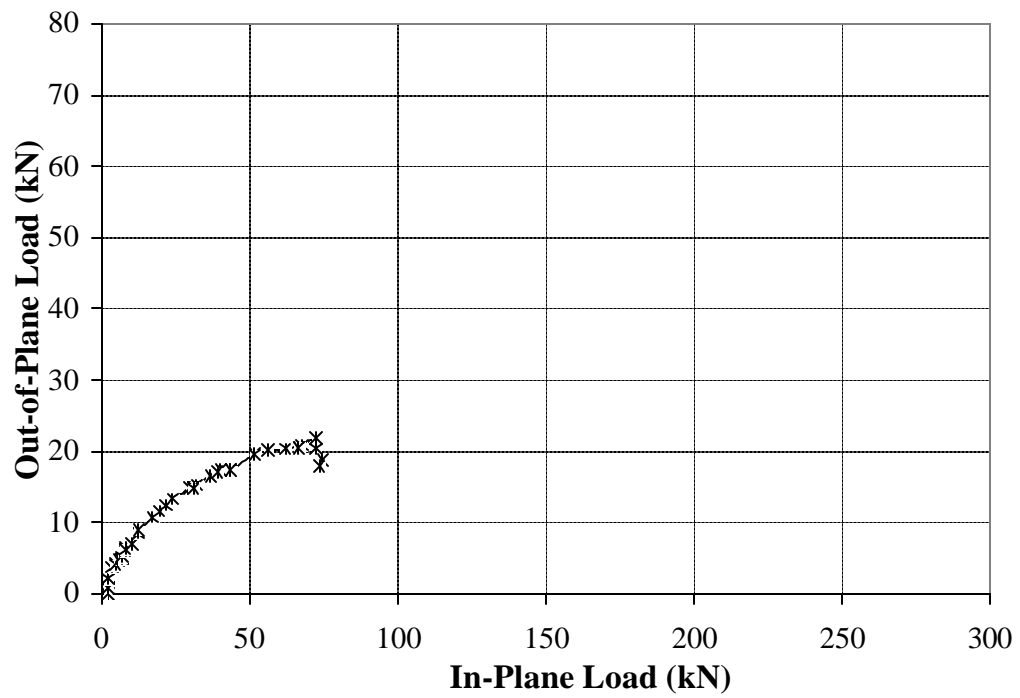


**Fig B.52 Out-of-Plane Load versus In-Plane Load S19-CL7**

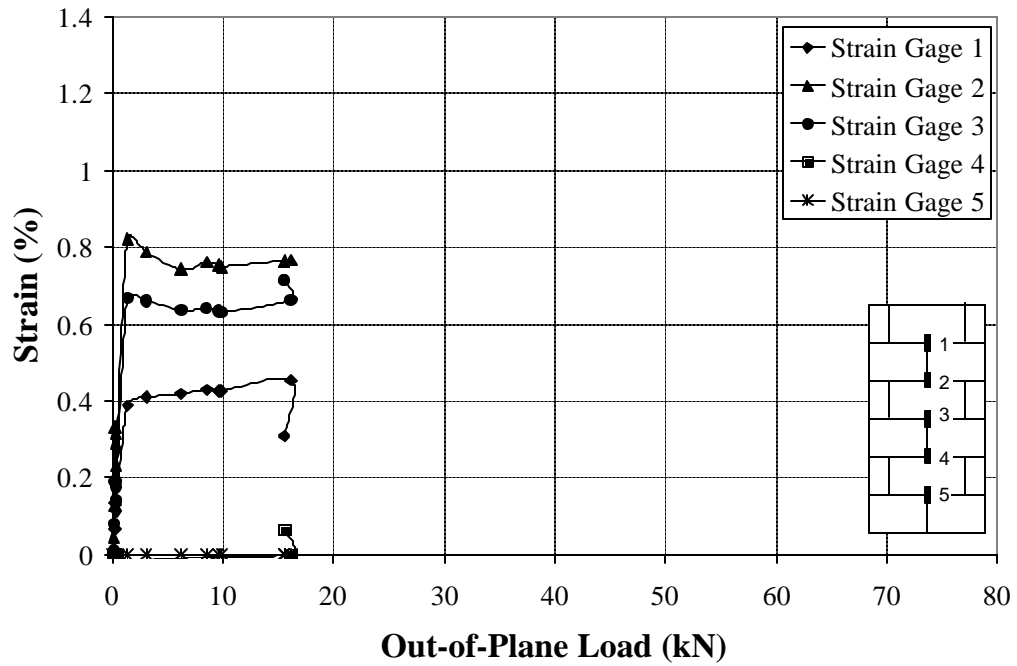


Fig B.53 Strain Distribution S19-CL7

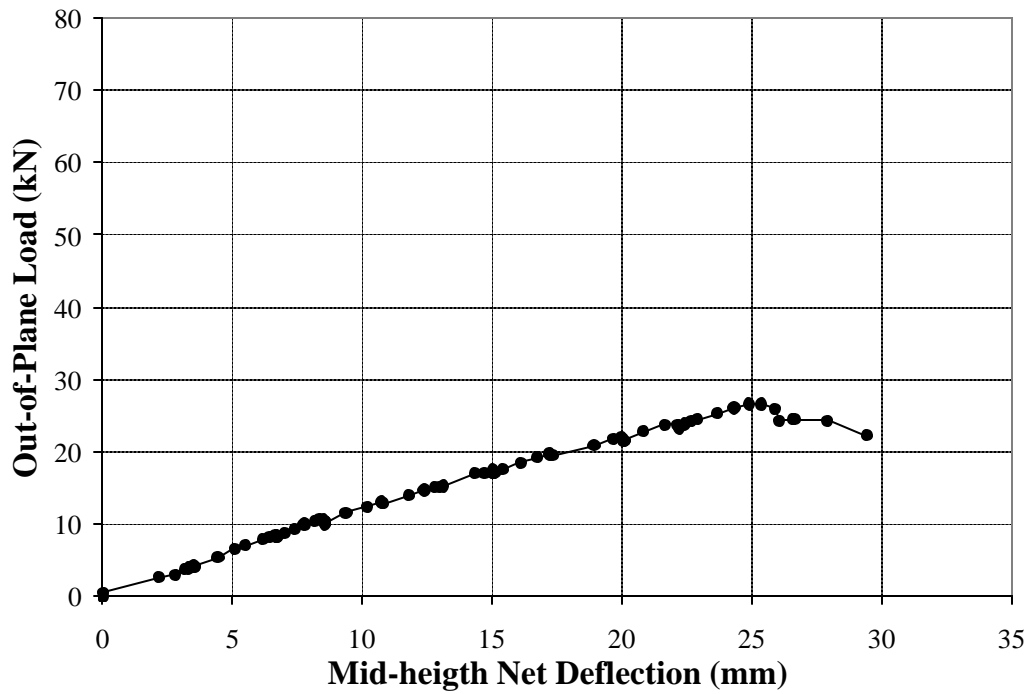
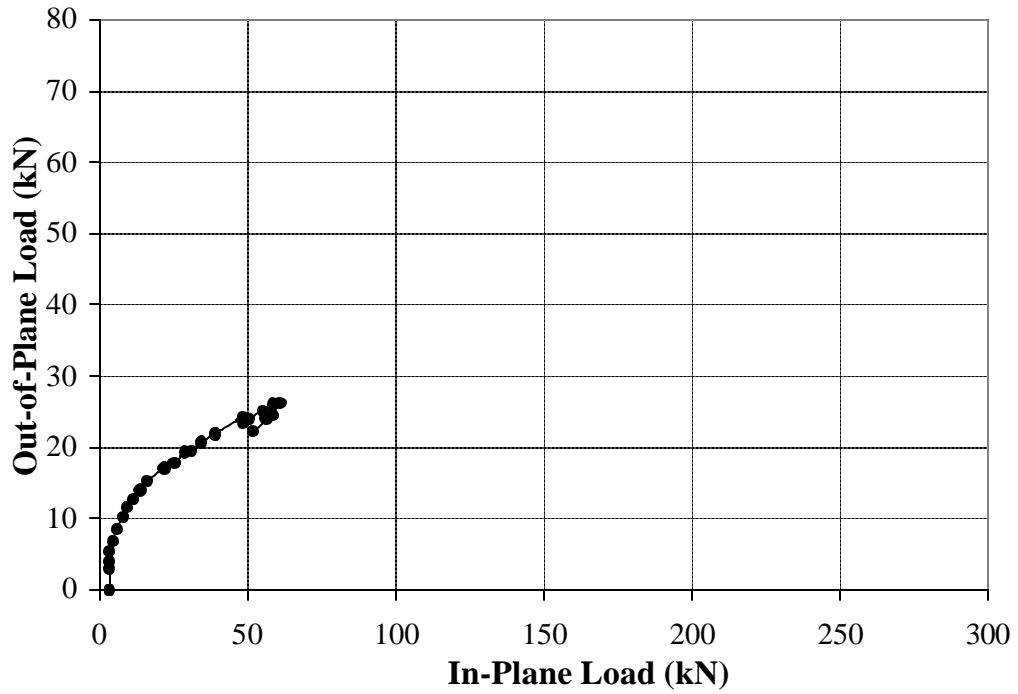
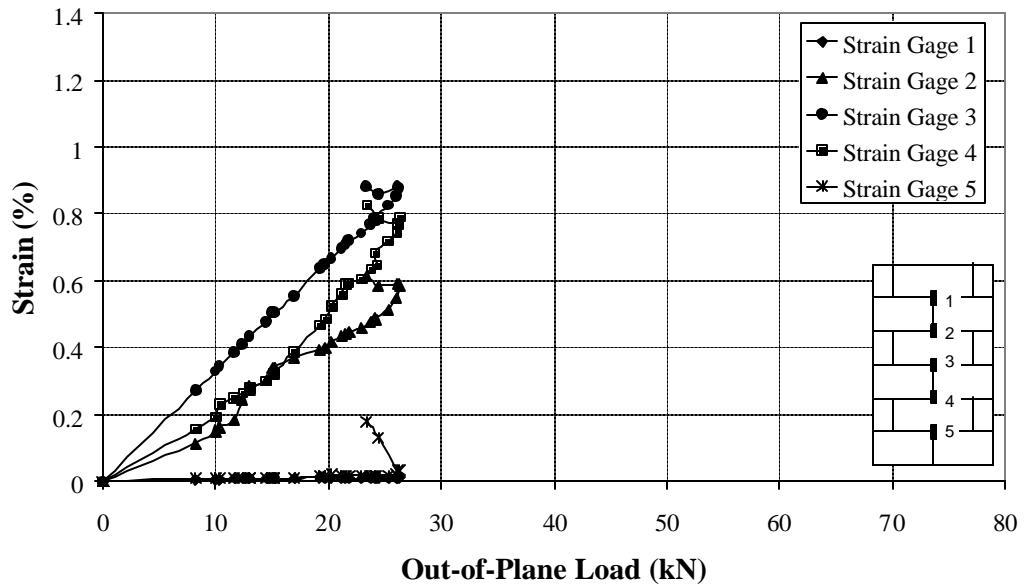


Fig B.54 Load vs. Mid-height Deflection S19-CL9



**Fig B.55 Out-of-Plane Load versus In-Plane Load S19-CL9**



**Fig B.56 Strain Distribution S19-CL9**

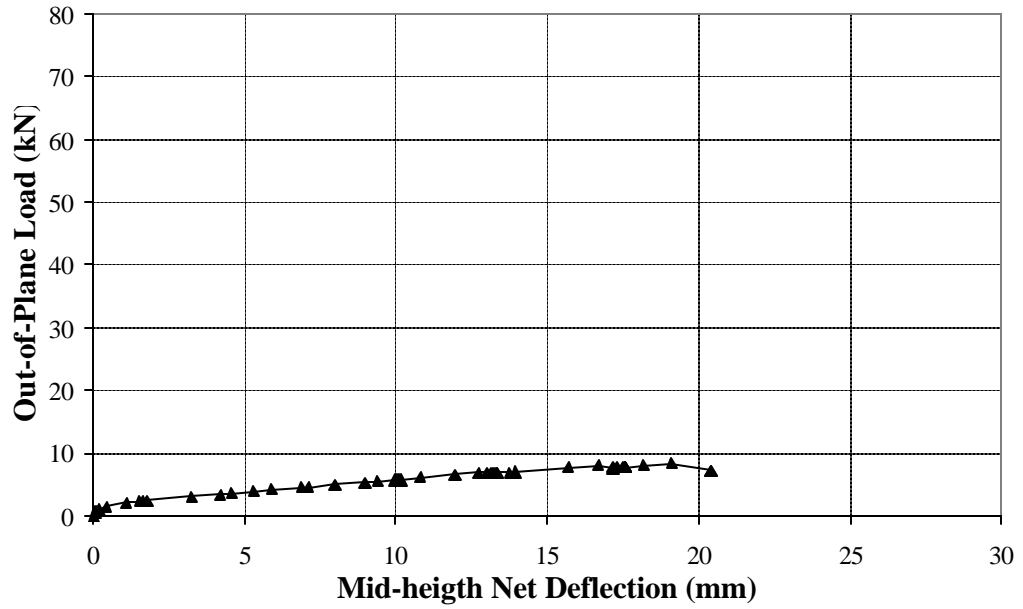


**Fig B.57 Load vs. Mid-height Deflection S8 -CO3**

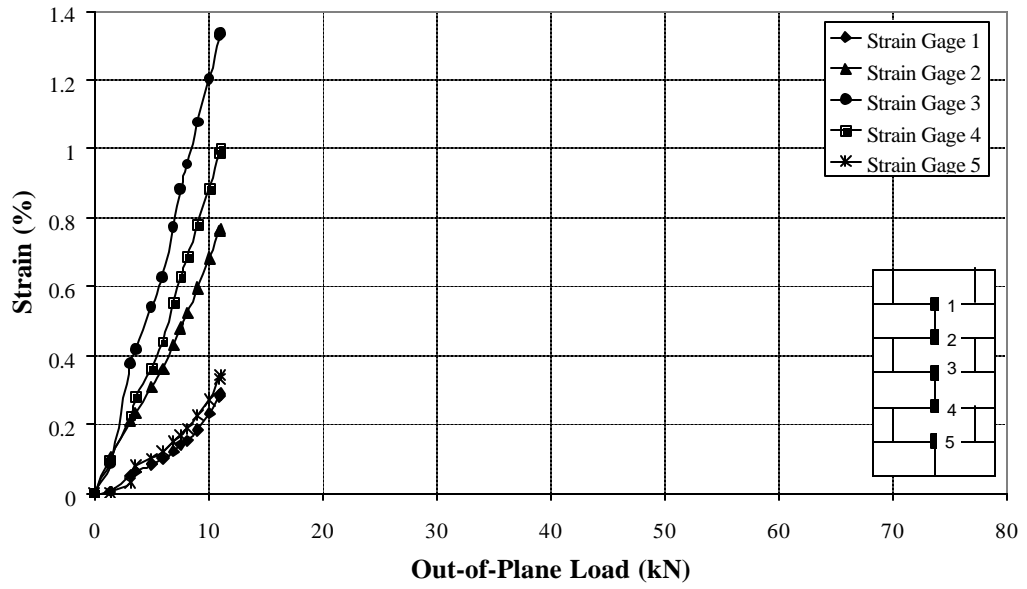


**Fig B.58 Strain Distribution S8 -CO3**

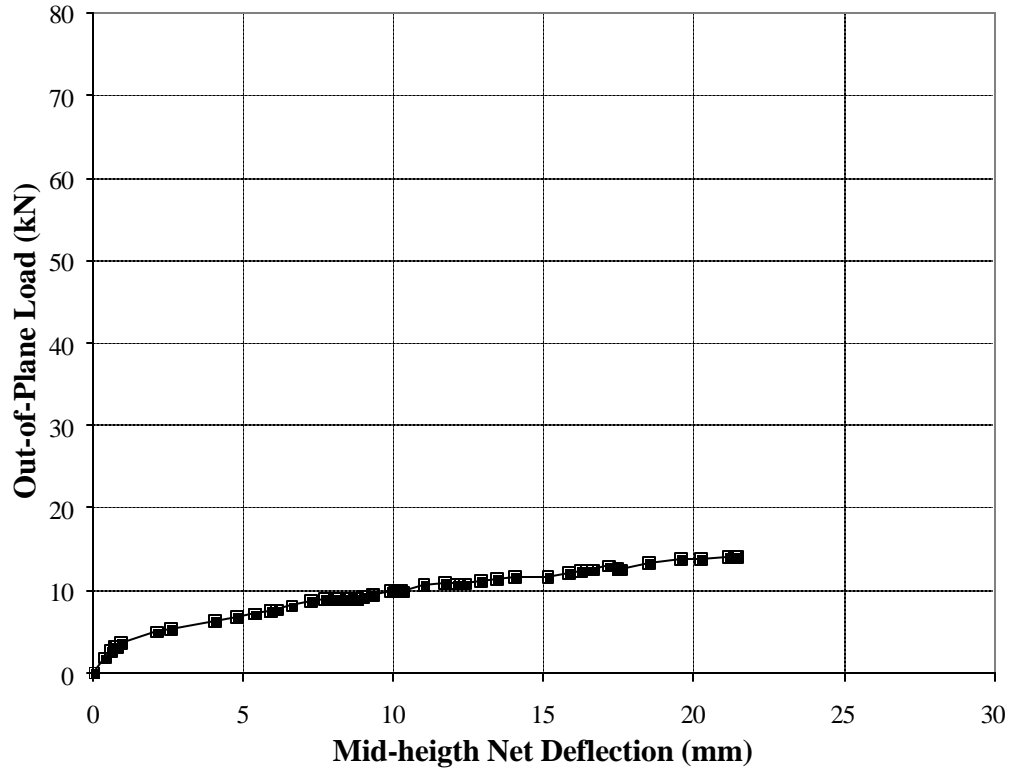


Fig B.59 Load vs. Mid-height Deflection S8 -CO5

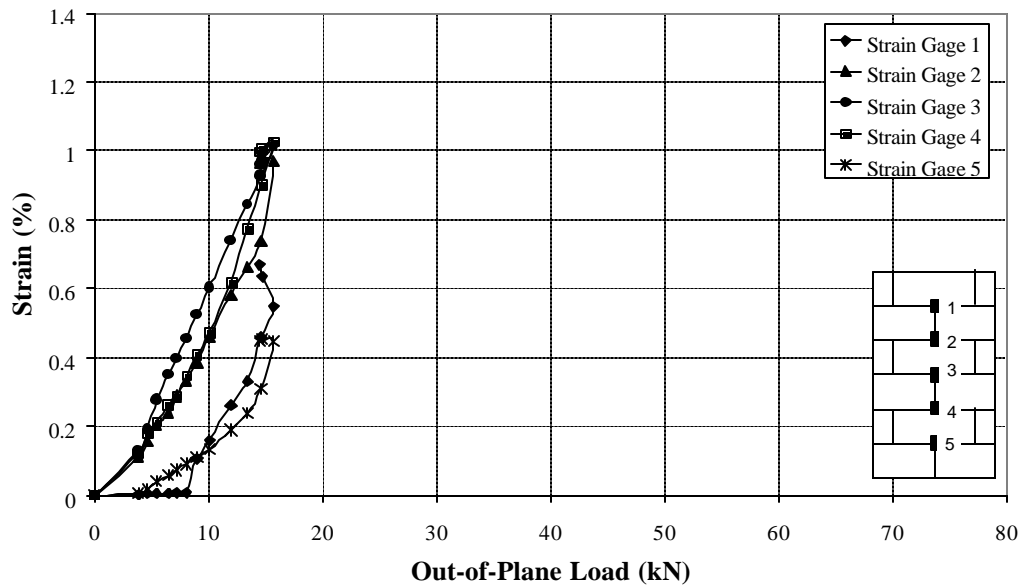
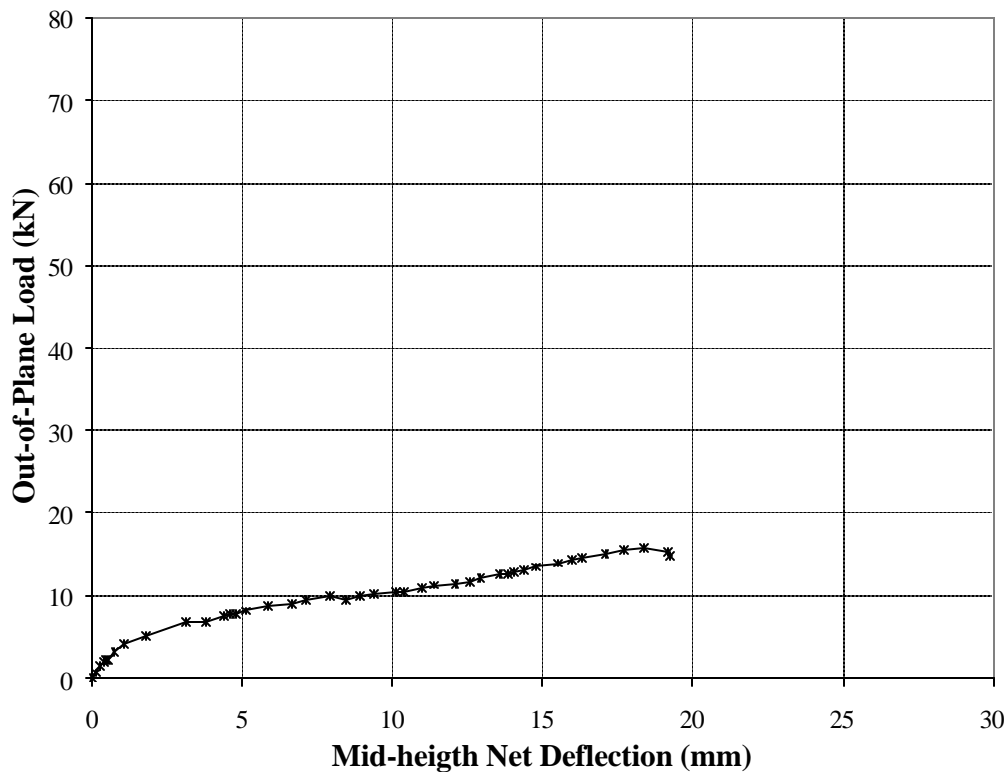
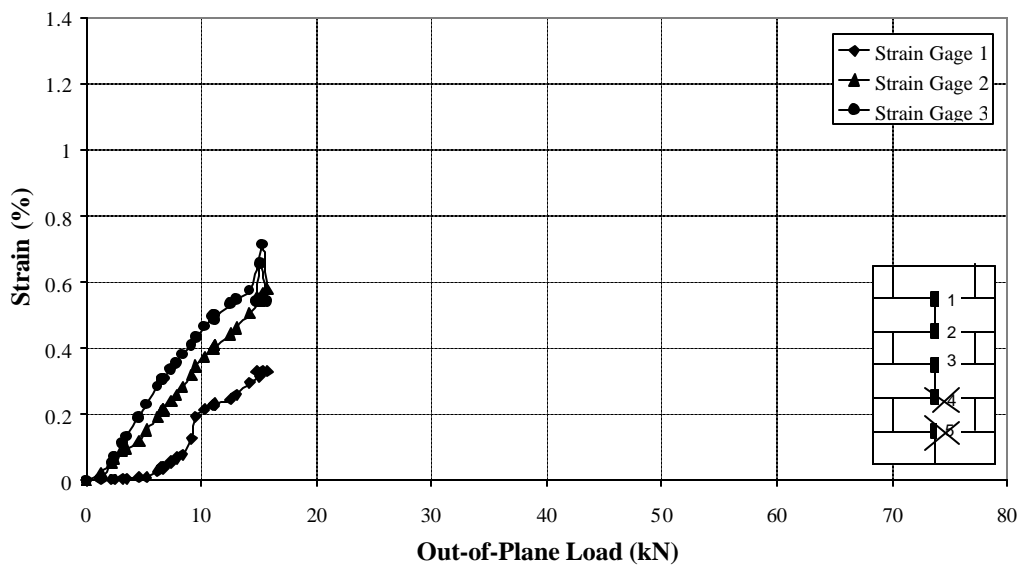


Fig B.60 Strain Distribution S8 -CO5



**Fig B.61 Load vs. Mid-height Deflection S8 -CO7**



**Fig B.62 Strain Distribution S8 -CO7**

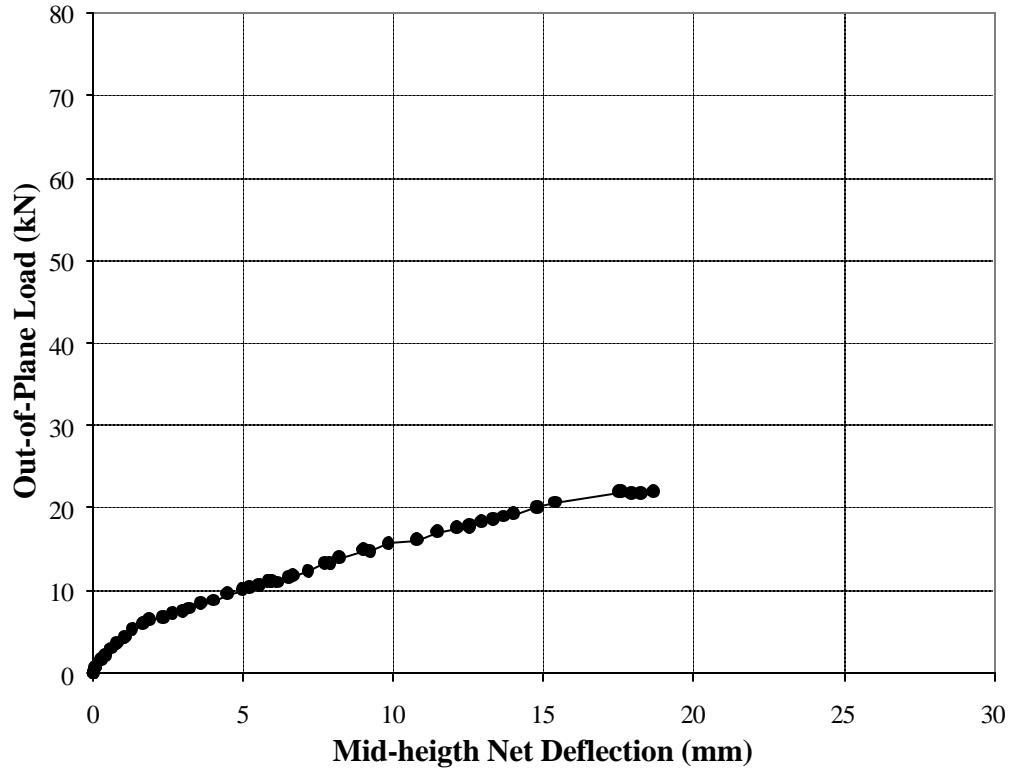


**Fig B.63 Load vs. Mid-height Deflection S8 -CO9**

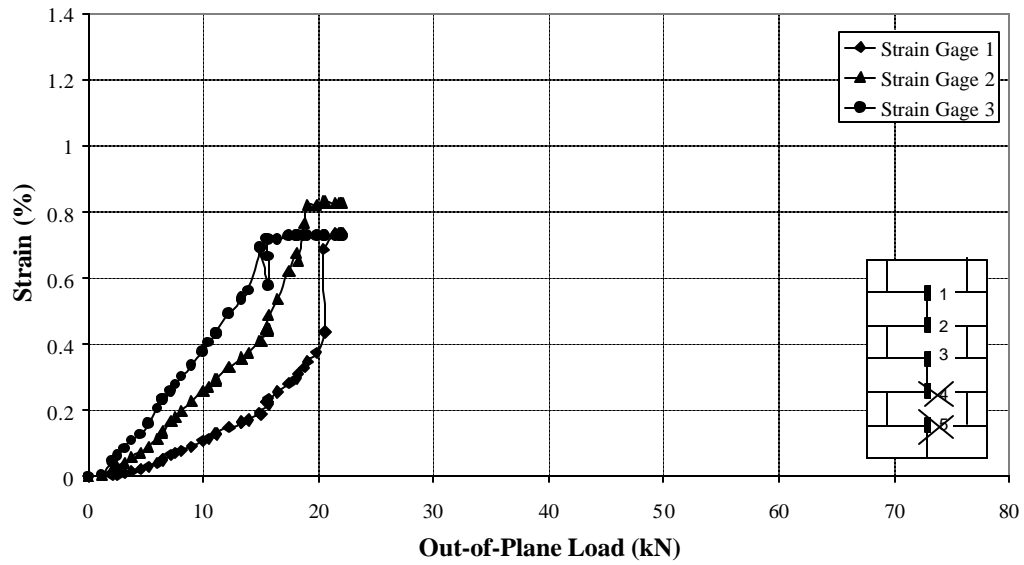


**Fig B.64 Strain Distribution S8 -CO9**

**APPENDIX C**

**OUT-OF-PLANE RELATED PAPERS**

## FRP Strengthening of URM Walls Subject to Out-of-Plane Loads

J. Gustavo Tumialan, Nestore Galati and Antonio Nanni

**Abstract:** Unreinforced masonry (URM) walls are prone to failure when subjected to out-of-plane loads caused by earthquakes or high wind pressure. This paper presents the results of an experimental program on the flexural behavior of URM walls strengthened with externally bonded Fiber Reinforced Polymer (FRP) laminates as well as on the influence of the putty filler on the bond strength. Based on the experimental evidence, the paper provides a design approach for the strengthening with FRP laminates of URM walls that are analyzed as simply supported members. The database includes URM walls strengthened with different amounts and types of externally bonded FRP reinforcement.

**Keywords:** FRP Laminates, Flexural Strengthening, Masonry Strengthening, Out-of-Plane Failure, Unreinforced Masonry (URM)

---

**J. Gustavo Tumialan** is a Research Engineer at the Center for Infrastructure Engineering Studies (CIES) at the University of Missouri-Rolla (UMR), where he received his M.Sc. and Ph.D. degrees in Civil Engineering. He received his B.Sc. from the Pontificia Universidad Catolica del Peru (PUCP). His research interests include rehabilitation of masonry and reinforced concrete structures.

**Nestore Galati** is a Graduate Research Assistant at CIES at UMR where he is pursuing a M.Sc. degree in Engineering Mechanics. He is also a doctoral student in Composite Materials for Civil Engineering at the University of Lecce, Italy, where he received his B.Sc. in Materials Engineering. His research interests include repair of masonry and reinforced concrete structures.

**Antonio Nanni**, FACI, is the V&M Jones Professor of Civil Engineering and Director of CIES at UMR. He is interested in construction materials, their structural performance, and field application. He is an active member of several ACI technical committees.

## **INTRODUCTION**

Structural weakness, overloading, dynamic vibrations, settlements, and in-plane and out-of-plane deformations can cause failure of unreinforced masonry (URM) structures. URM buildings have features that, in case of overstressing, can threaten human lives. Organizations such as The Masonry Society (TMS) and the Federal Emergency Management Agency (FEMA) have determined that failures of URM walls result in more material damage and loss of human life during earthquakes than any other type of structural element. Fiber reinforced polymer (FRP) composites may provide viable solutions for the strengthening of URM walls subjected to in-plane and out-of-plane loads caused by high wind pressures or earthquakes. As a reflection of retrofitting needs (e.g. approximately 96% of the URM buildings inventoried throughout California needed to be retrofitted<sup>1</sup>) and important advantages (i.e. material characteristics and ease of installation) interest in the use of FRP materials for the strengthening of masonry elements has increased in recent years. To respond to the interest of the engineering community, the American Concrete Institute (ACI) – Committee 440 along with the Existing Masonry Committee of TMS have formed a joint task group to develop design recommendations for the strengthening of masonry elements with FRP materials.

## **RESEARCH SIGNIFICANCE**

To observe improved performance and modes of failure, URM panels were strengthened with different amounts of externally bonded FRP laminates to be tested under out-of-plane loads. Two types of FRP fabrics were used for the strengthening. In addition, the influence of the putty filler on the bond strength was investigated. Based on

experimental evidence, a design methodology for the strengthening of URM walls when acting as simply supported members (i.e. arching mechanism is not present) is proposed.

## **EXPERIMENTAL PROGRAM**

### **Test Matrix**

Table 1 summarizes the characteristics of 25 masonry walls that were constructed for the experimental program<sup>2</sup>. Twelve walls were built with concrete blocks and the remaining 13 with clay bricks. Their nominal dimensions were 95×600×1200 mm (3.75×24×48 in.). The specimens were strengthened with glass FRP (GFRP) and aramid FRP (AFRP) laminates. Concrete and clay masonry units and two surface preparation methods (with or without putty filler) were used to take into account different compressive strengths and surfaces. Since clay brick wall surfaces exhibit more unevenness than those of concrete blocks, the surface preparation of the clay specimens required the use of putty. Similarly to the case of strengthening of reinforced concrete (RC) members, the putty is used to fill small surface voids and to provide a leveled surface to which the FRP can be adhered. All the masonry panels were strengthened with a single FRP strip placed along the longitudinal axis on the side in tension. The strip width ranged from 75 mm (3 in.) to 300 mm (12 in.). Table 2 provides an indication of the amount of FRP reinforcement ( $\rho_f = A_f / b_m t_m$ ), for specimens tested in this program and others. Four series of walls were tested: COC, COA, CLG, and CLA. The first two characters in the code represent the type of masonry used, “CO” for concrete masonry and “CL” for clay masonry. The third character represents the type of fiber, “G” for GFRP and “A” for AFRP. The last character indicates the width of the strip in inches. Thus, CLG5 represents a clay

masonry wall, strengthened with a GFRP laminate, having a width of 125 mm (5 in.) The character “R” indicates a test repetition. In every case, the length of the FRP strips was 1170 mm (46 in.). In this manner the laminate did not touch the roller supports used for testing. Unstrengthened specimens were not tested since their capacity in flexure when acting as simply supported members is relatively small. All the walls were tested under simply supported conditions. Details of the test procedure are shown elsewhere<sup>2</sup>.

### **Materials**

Tests were performed to characterize the engineering properties of the materials<sup>2</sup>. The average compressive strengths of concrete and clay masonry were 10.5 MPa (1520 psi) and 17.1 MPa (2480 psi), respectively. A Type N mortar cement was used for the construction of the specimens. Its average compressive strength at 28 days was 7.6 MPa (1100 psi).

Tensile tests were performed on FRP laminates. The results showed that the tensile strength of GFRP was equal to 1690 MPa (245 ksi) and the modulus of elasticity was 92.9 GPa (13460 ksi). In the case of AFRP, the tensile strength was 1876 MPa (272 ksi) and the modulus of elasticity was equal to 115.2 GPa (16700 ksi). These properties are related to the fiber content and not to composite area.

## **TEST RESULTS**

### **Modes of Failure**

URM walls strengthened with FRP laminates subjected to out-of-plane loads exhibited the following modes of failure: (1) debonding of the FRP laminate from the masonry

substrate, (2) flexural failure (i.e. rupture of the FRP laminate in tension or crushing of the masonry in compression), and (3) shear failure in the masonry near the support.

**FRP Debonding:** due to shear transfer mechanisms at the interface masonry/FRP laminate, debonding of the laminate from the masonry substrate may occur before flexural failure (see Figure 1a). Debonding started from flexural cracks at the maximum bending moment region and developed towards the supports. Since the tensile strength of masonry is lower than that of the epoxy resins, the failure line is in the masonry. In the case of concrete masonry walls, part of the concrete block faceshell remained attached to the FRP laminate.

**Flexural Failure:** after developing flexural cracks primarily located at the mortar joints, a wall failed by either rupture of the FRP laminate or masonry crushing. FRP rupture occurred at midspan (see Figure 1b). The compression failure was manifested by crushing of mortar joints.

**Shear Failure:** cracking started with the development of fine vertical cracks at the maximum bending region. Thereafter two kinds of shear failure were observed: flexural-shear and sliding shear (see Figure 1c and Figure 1d, respectively). The former was oriented at approximately  $45^\circ$ , and the latter occurred along a bed joint causing sliding of the wall at that location, typically, at the first mortar joint in walls heavily strengthened. In the flexural-shear mode, shear forces transmitted over the crack caused a differential displacement in the shear plane, which resulted in FRP debonding.

## Discussion of Results

Figure 2 illustrates the moment vs. deflection curves for concrete and clay masonry walls strengthened with FRP laminates<sup>2</sup>. It is observed that the strength and stiffness of the FRP strengthened walls increased dramatically when comparing them to a URM specimen. Following the recommendations of the Masonry Standards Joint Committee<sup>3</sup>, the nominal moment for the URM concrete specimens was estimated as 0.23 kN-m (0.17 ft-kips), whereas for the clay specimens this value was 0.48 kN-m (0.35 ft-kips)<sup>2</sup>. By comparing them to the experimental results of the FRP strengthened walls, it can be observed that depending on the amount of FRP, increments ranging from 5 to 25 times of the nominal masonry capacity were achieved. Since there is a significant amount of variability attributed to labor and materials in masonry construction, this range of values should be taken simply as a reference.

The test results showed a clear and consistent pattern. Up to cracking, the walls behaved almost in a linear fashion. Initial cracking occurred at the interface of mortar and masonry for concrete masonry and in the mortar joint itself for clay masonry. Initial cracking was delayed due to the presence of FRP reinforcement. Following this, cracking at the adjacent joint occurred until almost every joint in the high moment bending area was cracked. After cracking, the flexural stiffness is a function of the amount of FRP; thus, a degradation of stiffness that is larger in walls with a high amount of FRP reinforcement was observed. In this phase of the test, the cracks widen until the failure occurred.

Rupture of the FRP laminate was observed only in clay masonry specimens. This was attributed to improved bond characteristics provided by the putty. In addition, even

though FRP rupture is a desirable mode of failure because the material is fully used, there is no certainty that this can be achieved all the time. This was evident from the test results of specimens built with the same type of masonry and strengthened with the same amount of reinforcement (see CLG3 and CLG3R, and CLG5 and CLG5R in Table 2).

Shear failure was observed in specimens with large amounts of FRP reinforcement. Increments in out-of-plane capacity were also observed in walls failing in a flexure-shear mode. Some specimens failed due to sliding shear and due to the nature of this failure, the overall capacity was less than that registered in similar walls strengthened with a lower amount of reinforcement (see Figure 2c and Figure 2d).

Table 2 shows specimens built with clay and concrete masonry units and strengthened with AFRP, GFRP and carbon FRP (CFRP) laminates. Of the three modes of failure described, experimental results indicate that the controlling mode is mostly debonding of the FRP laminate<sup>2, 4, 5, 6, 7, 8</sup>. If a large amount of FRP is provided, shear failure may be observed. Debonding may have a direct relationship with the porosity of the masonry surface. It is understood that masonry surface also refers to surfaces prepared with putty.

## **BASIS FOR DESIGN APPROACH**

Table 2 presents the experimental and theoretical results used as a database for the developing of a design approach for the FRP strengthening of URM walls. The theoretical flexural capacity of an FRP strengthened masonry wall was determined based on strain compatibility, internal force equilibrium, and the controlling mode of failure. Thus, the theoretical flexural capacities were estimated based on the assumption that no premature failure was to be observed (i.e. either rupture of the laminate or crushing of

masonry would govern the wall behavior). For simplicity and similarly to the flexural analysis of RC members, a parabolic distribution was used for compressive stresses in the computation of the flexural capacity of the strengthened walls (see Figure 3). The stress block parameters associated with such parabolic distribution are given as:

$$\gamma\beta_1 = \left( \frac{\epsilon_m}{\epsilon'_m} \right) - \frac{1}{3} \left( \frac{\epsilon_m}{\epsilon'_m} \right)^2 \quad (1a)$$

$$\gamma\beta_1 \left( 1 - \frac{1}{2} \beta_1 \right) = \frac{2}{3} \left( \frac{\epsilon_m}{\epsilon'_m} \right) - \frac{1}{4} \left( \frac{\epsilon_m}{\epsilon'_m} \right)^2 \quad (1b)$$

According to MSJC, the maximum usable strain  $\epsilon_{mu}$  was considered to be 0.0035 mm/mm (in./in.) for clay masonry, and 0.0025 mm/mm (in./in.) for concrete masonry<sup>3</sup>. The tensile strength of masonry was neglected.

The theoretical shear capacity was estimated according MSJC recommendations<sup>3</sup> based on a shear strength of 386 kPa (56 psi) as recommended for URM in a running bond that is not grouted solid. The net cross section was used for the computation of the shear capacity.

The reinforcement index,  $\omega_f$ , expressed as  $\rho_f E_f / f'_m (h/t_m)$ , is an index that intends to capture the key parameters that influence the flexural capacity. These include the FRP flexural reinforcement ratio,  $\rho_f$ , the FRP tensile modulus of elasticity,  $E_f$ , the masonry compressive strength,  $f'_m$ , and the slenderness ratio  $h/t_m$ . This index is intended to represent the ratio of axial stiffness (cross sectional area  $\times$  modulus of elasticity) between FRP and masonry ( $A_f E_f / b_m t_m E_m$ ) but since the modulus of elasticity of masonry  $E_m$  is directly proportional to  $f'_m$ , the latter can replace  $E_m$ . The inclusion of the slenderness ratio  $h/t_m$  has been identified as influential in the out-of-plane behavior of masonry walls.

$h/t_m$  accounts for the ability of the masonry wall behavior to be controlled by flexural capacity rather than shear capacity.  $h/t_m$  and the required out-of-plane load to cause failure are inversely proportional; thus, as the slenderness ratio decreases, the out-of-plane load becomes larger.

Figure 4 shows the relationship between the experimental-theoretical flexural capacity ratio ( $M_{experimental} / M_{theoretical}$ ), and  $\omega_f$ , for all specimens included in Table 2. The ratio  $M_{experimental} / M_{theoretical}$  represents the effectiveness of the FRP reinforcement. In Figure 4a, data on concrete masonry specimens (without putty) is presented. Figure 4b shows data on clay masonry specimens where the surface was leveled with putty. The ratio  $M_{experimental} / M_{theoretical}$  for the specimens failing in shear was computed based on the bending moment associated with the shear capacity. Table 2 and Figure 4 indicate that, in general, the experimental and theoretical results for walls failing in flexure and shear showed a good agreement. Obviously, when debonding becomes the governing failure this is no longer true.

For design purposes, rather than attempting to predict bond failure, the strain in the FRP laminates can be limited. Similarly,  $\omega_f$  can be limited to a given threshold to rule out shear failure in the masonry. In this context, Figure 4 suggests that the lower limit ratio  $M_{experimental} / M_{theoretical}$  for non-puttied masonry surfaces can be taken as 0.45; whereas for puttied surfaces this value can be 0.65.  $\omega_f$  has an upper limit equal to 0.70 to prevent masonry shear failure. The effectiveness of the FRP reinforcement depends on the bond of the FRP laminate to the masonry substrate. Since the flexural capacity is dependant of the strain developed in the laminate, it is reasonable to express the effective strain in the laminate,  $e_{fe}$ , as the product  $\kappa_m \epsilon_{fu}$ , where  $\kappa_m$  is the bond dependent coefficient and  $\epsilon_{fu}$  is

the design rupture strain of FRP. Thus, for non-puttied surfaces  $\kappa_m$  can be assumed to be 0.45, and for puttied surfaces  $\kappa_m$  can be 0.65. These considerations can be taken into account for the implementation of a design methodology.

Figure 5 illustrates the normal distribution for  $\gamma$  and  $\beta_1$  values for the database. The  $\gamma$  and  $\beta_1$  values were computed for the experimental moment of each specimen in Table 2. For simplicity, both  $\gamma$  and  $\beta_1$  can be assumed to be 0.70. Figure 6 illustrates the relationship between the normalized experimental flexural strength and the reinforcement index for the walls tested in this investigation ( $h/t_m = 12$ ). The solid line curve indicates the normalized theoretical flexural capacity. The first portion is a parabola-shape curve obtained from equilibrium of internal forces in the cross section (see Figure 3); thus:

$$M_n = A_f f_f \left( t_m - \frac{\beta_1 c}{2} \right) \quad (2a)$$

$$(\gamma'_m)(\beta_1 c) b_m = A_f f_f \quad (2b)$$

If the product  $\kappa_m \varepsilon_{fu}$  represents the effective strain in the laminate, the stress in the FRP,  $f_f$ , can be written as:

$$f_f = \varepsilon_{fe} E_f = (\kappa_m \varepsilon_{fu}) E_f \quad (2c)$$

Replacing Eqs. 2b and 2c in 2a, and multiplying both terms by the factors  $b_m t_m f'_m$  and  $h/t_m$ , one obtains:

$$\frac{M_n}{b_m t_m^2 f'_m (h/t_m)} = \frac{\rho_f E_f}{f'_m (h/t_m)} (\kappa_m \varepsilon_{fu}) \left( 1 - \frac{\beta_1 c}{2} \right) \quad (2d)$$

Finally, making  $\omega_f$  explicit on the right end side of Eq. 2d one obtains:

$$\frac{M_n}{b_m t_m^2 f'_m (h/t_m)} = \omega_f (\kappa_m \varepsilon_{fu}) \left( 1 - \frac{\omega_f (\kappa_m \varepsilon_{fu}) (h/t_m)}{2 \gamma} \right) \quad (2e)$$

To plot Eq. 2e in Figure 6,  $\kappa_m$ , the bond dependent coefficient, was taken as 0.45 for concrete/non-puttied masonry and 0.65 for clay/puttied masonry.  $\varepsilon_{fu}$  of GFRP was used since it represented the lowest bound.  $h/t_m$  was equal to 12 and  $\gamma$  was assumed to be 0.70. The second portion (horizontal line) is the normalized strength associated with the theoretical shear capacity of the masonry. The shear capacity was estimated based on MSJC provisions<sup>3</sup>. The intersection of the two lines represents the limit between flexural and shear controlled failure. For clay masonry,  $\omega_f$  is about 0.75, while for concrete masonry,  $\omega_f$  is around 0.90. This observation reaffirms the assumption that the index  $\omega_f$  may be limited to 0.70 to prevent the occurrence of shear failure.

## PROPOSED DESIGN PROTOCOL

### Outline of Design Approach

The following design approach is applicable when the wall can be assumed to behave under simply supported conditions (i.e. arching mechanism is not present). The ultimate strength design criteria states that the design flexural capacity of a member must exceed the flexural demand:

$$M_u \leq \phi M_n \quad (3)$$

The following assumptions and limitations should be adopted:

- The strains in the reinforcement and masonry are directly proportional to the distance from the neutral axis.

- The maximum usable strain,  $\epsilon_{mu}$ , at the extreme compressive fiber is assumed to be 0.0035 mm/mm (in./in.) for clay masonry and 0.0025 mm/mm (in./in) for concrete masonry<sup>3</sup>.
- The maximum usable strain in the FRP reinforcement is considered to be  $\kappa_m \epsilon_{fu}$  (for non-puttied surfaces  $\kappa_m$  is 0.45, for puttied surfaces  $\kappa_m$  is 0.65).
- The tensile strength of masonry is neglected.
- The FRP reinforcement has a linear elastic stress-strain relationship up to failure.
- A masonry stress of  $0.70 f'_m$  is assumed uniformly distributed over an equivalent compression zone bounded by edges of the wall cross section and a straight line parallel to the neutral axis at a distance  $a = 0.70c$  from the fiber of maximum compressive strain (i.e.  $\gamma = 0.70$  and  $\beta_1 = 0.70$ ).
- The reinforcement index  $\omega_f$  is limited to 0.70 to avoid shear failure.

The design protocol can be outlined as follows:

1. The nominal flexural capacity is computed by considering a reduction factor  $\phi$  equal to 0.70.

The approach for the reduction factor is similar to that of the ACI-318<sup>10</sup>, where a section with low ductility must be compensated with a higher reserve of strength.

The higher reserve of strength is attained by applying a strength reduction factor of 0.70 to sections prone to have brittle or premature failures such as debonding of the FRP laminate.

2. To account for environmental attack  $\epsilon_{fu}$  is derived from the manufacturer's guaranteed strain,  $\epsilon_{fu}^*$ , as follows:

$$\varepsilon_{fu} = C_E \varepsilon_{fu}^* \quad (4)$$

where  $C_E$  is an environmental reduction factor. Table 3 shows different values for  $C_E$  based on the relative durability of each fiber type to different exposure conditions as recommended by the ACI-440<sup>10</sup>.

From the stress distribution in a masonry section, the equation to determine the flexural nominal capacity of a URM section strengthened with FRP is given as:

$$M_n = (\gamma f'_m) (\beta_1 c) b_m \left( t_m - \frac{\beta_1 c}{2} \right) \quad (5a)$$

In order to satisfy the internal force equilibrium:

$$(\gamma f'_m) (\beta_1 c) b_m = A_f f_f \quad (5b)$$

$$f_f = E_f \varepsilon_{fe} \quad (5c)$$

$\gamma$  and  $\beta_1$  are considered to be equal to 0.70.

The effective strain in the FRP laminate,  $\varepsilon_{fe}$ , is limited by the strain controlled by debonding:

$$\varepsilon_{fe} \leq \kappa_m \varepsilon_{fu} \quad (6a)$$

$$\text{If putty is used} \quad : \quad \kappa_m = 0.65 \quad (6b)$$

$$\text{If putty is not used:} \quad \kappa_m = 0.45 \quad (6c)$$

Typically, concrete masonry surfaces require putty only in the mortar joints if these are racked. Clay masonry surfaces need to be puttied because more unevenness due to poor construction, lack of uniformity in the units is present or mortar joints are racked. In the latter case due to the reduced height of the clay brick unit, it is more convenient to putty the entire surface for ease of construction.

$A_f$  and  $c$  can be determined from Eqs. 3 to 6. From the strain distribution in a masonry section, the strain level in masonry,  $\varepsilon_m$ , can be checked from:

$$\varepsilon_m = \varepsilon_{fe} \frac{c}{t_m - c} \leq \varepsilon_{mu} \quad (7)$$

For concrete masonry:  $\varepsilon_{mu} = 00025$  mm/mm (in./in.)

For clay masonry :  $\varepsilon_{mu} = 00035$  mm/mm (in./in.)

If  $\varepsilon_m$  exceeds  $\varepsilon_{mu}$ , a new strain in the FRP needs to be calculated using Eq. 7 and  $\varepsilon_m$  equal to  $\varepsilon_{mu}$ . Next, the amount of FRP reinforcement,  $A_f$ , can be estimated using Eqs. 3 to 5.

3. There is no scientific evidence for the recommendations on maximum clear spacing,  $s_f$ , of FRP laminate adhered to a wall surface.  $s_f$  could be set equal to two times the wall thickness based on stress distribution criteria along the wall thickness. Alternatively,  $s_f$  could be set equal to the length of the masonry unit, the rationale being to engage most of the masonry units and avoid loosening of units, which could cause the partial collapse of the wall. The maximum clear spacing between FRP strips could then defined as follows:

$$s_f = \min\{2t_m, L\} \quad (8)$$

For block units:  $L = l_b$

For brick units:  $L = 2l_b$

where  $t_m$  is the thickness of the wall being reinforced without including the wall veneer, if present, and  $l_b$  is the length of the masonry unit.

Figure 7 illustrates the validation of the proposed design protocol. In Figure 7a, the flexural capacity,  $M_n$ , is estimated considering the  $\phi$  and  $C_E$  factors equal to 1.0. By observing the ratio  $M_{experimental}/\phi M_n$ , it can be concluded that the proposed methodology provides appropriate and conservative values. The calculations were carried out under

the premise that debonding would govern the wall behavior (i.e. the flexural capacities were estimated based on the FRP strain limitations). For that reason the ratios  $M_{experimental}/\phi M_n$  are higher for specimens that failed due to FRP rupture in Figure 7a. Conversely, when debonding occurred, the  $M_{experimental}/\phi M_n$  ratios were closer to the unit. In Figure 7b, when the  $\phi$  factor is equal to 0.70 and the  $C_E$  factors are as shown in Table 2, the safety margin is at least 1.60.

### Design Example

The flexural capacity of a non-bearing URM concrete block wall needs to be increased to sustain a moment demand of 6.4 kN-m/m (1.5 ft-kips/ft). The nominal dimension of the concrete masonry units is 200x200x400 mm (8x8x16 in.). The wall is assumed to behave as a simply-supported element. A glass/epoxy FRP system has been selected to upgrade the flexural capacity.

Masonry Properties:  $f'_m = 10.3 \text{ MPa (1500 psi)}$   
 $\epsilon_{mu} = 0.0025 \text{ mm/mm (in./in.)}$

FRP Properties:  $f_{fu}^* = 1.52 \text{ GPa (220 ksi)}$   
 $E_f = 72.4 \text{ GPa (10500 ksi)}$   
 $\epsilon_{fu}^* = 0.021 \text{ mm/mm (in./in.)}$   
 $t_f = 0.35 \text{ mm (0.014 in.)}$

- Compute the nominal flexural capacity

The nominal flexural capacity is calculated from Eq. 3 as:

$$M_n = \frac{M_u}{\phi} = \frac{(6.4 \text{ kN-m/m})}{0.7} = 9.14 \text{ kN-m/m} = (2.14 \text{ ft-kips/ft})$$

- Compute the depth of the neutral axis

The depth of the neutral axis is computed from Eq. 5a:

$$M_n = (0.70c)(0.70f'_m)b_m \left( t_m - \frac{0.70}{2}c \right)$$

$$9.14 \text{ kN-m/m} = (0.70c)(0.70)(1.03\text{MPa})(1000)(1.0\text{m}) \left( (0.20\text{m}) - \frac{0.70}{2}c \right)$$

Solving this relationship:  $c = 9.2 \times 10^{-3} \text{ m} = 9.2 \text{ mm} (0.37 \text{ in.})$

- Compute strains in masonry and FRP

Considering an environmental factor  $C_E$  equal to 0.8 (see Table 3), the design rupture strain is:

$$\varepsilon_{fu} = C_E f_{fu}^* = 0.8(0.021 \text{ mm/mm}) = 0.0168 \text{ mm/mm (in./in.)}$$

Considering that debonding will control the wall behavior and that the concrete masonry surface will not require to be putted (i.e.  $\kappa_m = 0.45$ ):

$$\varepsilon_{fe} = \kappa_m \varepsilon_{fu} = 0.45(0.0168 \text{ mm/mm}) = 0.0075 \text{ mm/mm (in./in.)}$$

Check that crushing of masonry does not occur:

$$\varepsilon_m = \varepsilon_{fe} \frac{c}{t_m - c} = (0.0075 \text{ mm/mm}) \frac{(9.2 \text{ mm})}{((200 \text{ mm}) - (9.2 \text{ mm}))} = 0.0004 \text{ mm/mm} < 0.0025 \text{ mm/mm}$$

Thus the stress in the GFRP is:

$$f_f = \varepsilon_f E_f = (0.0075 \text{ mm/mm})(72.4 \text{ GPa}) = 0.54 \text{ GPa} (78.8 \text{ ksi})$$

- Compute the area of GFRP

The required area of FRP is calculated from the relationship shown in Eq. 5b:

$$A_f f_f = (0.70 f'_m)(0.70 c) b_m$$

$$A_f(0.54 \text{ GPa})(1000) = ((0.70)(10.3 \text{ MPa}))((0.70)(9.2 \times 10^{-3} \text{ m}))(1.0 \text{ m})$$

$$A_f = 86 \text{ mm}^2 / \text{m} (0.041 \text{ in}^2 / \text{ft})$$

Then, the width of GFRP per wall unit is:  $w_f = \frac{A_f}{t_f} = \frac{(86 \text{ mm}^2 / \text{m})}{(0.35 \text{ mm})} = 246 \text{ mm/m} (2.90$

*in/ft)*

*∴ Use 250 mm/m (3 in/ft) of GFRP laminates*

- Determine the maximum clear spacing  $s_f$

$t_m$  and  $l_b$  are equal to 200 mm and 400 mm, respectively.

Thus, in the Eq. 8 the clear spacing can be calculated as:

$$s_f = \min\{2(200 \text{ mm}), 400 \text{ mm}\} = 400 \text{ mm} (16 \text{ in.})$$

The strengthening layout is illustrated in Figure 8, which satisfies the maximum spacing requirement.

## **SUGGESTED DETAILING CONSIDERATIONS**

Proper FRP reinforcement detailing at wall boundaries is necessary to ensure proper strengthening and improve the wall behavior by avoiding or delaying premature failures such as debonding. This may be attained with anchorage systems that include the use of steel angles, steel bolts, and Near-Surface-Mounted (NSM) bars. Different systems offer their own advantages and disadvantages. Steel angles are easy to install but aesthetically problematic. As they may locally fracture the wall due to displacement and rotation restraint, the angles should not be in direct contact with the masonry surface. Steel bolts have shown high effectiveness but require a demanding installation effort<sup>11</sup>. NSM bars have been successfully used for anchoring FRP laminates in both RC joists strengthened

in shear<sup>12</sup> and URM walls<sup>13</sup>. The installation technique consists of grooving a slot in the upper and lower boundary members. The ply is wrapped around an FRP bar and placed in the slot. The bar is then bonded with a suitable epoxy-based paste (see Figure 9).

## SUMMARY AND CONCLUSIONS

The following conclusions can be drawn from this experimental program:

- Strength and pseudo-ductility of URM walls can be significantly increased by strengthening them with FRP laminates. This increase can be observed in walls that can behave as simply supported members, such as walls with high  $h/t_m$  ratios (i.e. larger than 20), or in any walls where the supports do not restrain the outward movement (i.e. arching mechanism is not observed).
- The test results allowed to identify three basic modes of failure. One, shear failure, related to the parent material (i.e. masonry); and two, associated with the reinforcing material, debonding and flexural failure (i.e. rupture of FRP or crushing of the masonry). For large amounts of reinforcement (i.e. reinforcement index,  $\omega_f$ , larger than 0.70), shear failure was observed to be the controlling mode. For other reinforcement ratios, either FRP rupture or debonding was observed, being the latter the most common.
- Finally, a design methodology for flexural strengthening of walls that can be idealized as simply supported is presented. Based on experimental data generated by the present investigation and others, it is recommended to consider the maximum usable strain is the FRP reinforcement as  $0.45\varepsilon_{fu}$  for non-puttied surfaces and  $0.65\varepsilon_{fu}$

for puttied surfaces. The reinforcement index  $\omega_f$  should not exceed 0.70 to avoid shear failure in the masonry.

- The proposed design method described in this paper offers a first rational attempt for consideration by engineers interested in out-of-plane upgrade of masonry walls with externally bonded FRP laminates.

### **ACKNOWLEDGEMENTS**

The authors would like to acknowledge the support of the National Science Foundation Industry/University Cooperative Research Center at the University of Missouri–Rolla.

## NOTATION

- $A_f$  = area of FRP reinforcement  
 $b_m$  = width of the masonry wall considered in the flexural analysis  
 $C_E$  = environmental reduction factor  
 $c$  = distance from extreme compression fiber to the neutral axis  
 $E_f$  = tensile modulus of elasticity of FRP  
 $E_m$  = modulus of elasticity of masonry  
 $f_f$  = stress level in the FRP reinforcement  
 $f_{fu}^*$  = ultimate tensile strength of the FRP material as reported by the manufacturer  
 $f_m'$  = compressive strength of masonry  
 $h/t_m$  = slenderness ratio (wall height-to-wall thickness)  
 $L$  = clear spacing based on length of masonry units  
 $l_b$  = length of masonry units  
 $M_n$  = nominal flexural capacity  
 $M_u$  = flexural demand based on factored loads  
 $s_f$  = maximum clear spacing between FRP strips  
 $t_f$  = nominal thickness of one ply of FRP reinforcement  
 $t_m$  = nominal thickness of masonry wall  
 $w_f$  = width of FRP reinforcing plies  
 $\beta_1$  = ratio of the depth of the equivalent rectangular stress block to the depth to the neutral axis  
 $\epsilon_m$  = compressive strain in masonry  
 $\epsilon_m'$  = compressive strain in masonry associated to peak  $f_m'$  in a parabolic distribution  
 $\epsilon_{mu}$  = ultimate compressive strain of masonry  
 $\epsilon_{fu}$  = design rupture strain of FRP reinforcement  
 $\epsilon_{fe}$  = effective strain in FRP reinforcement  
 $\epsilon_{fu}^*$  = ultimate rupture strain of FRP reinforcement  
 $\phi$  = strength reduction factor  
 $\gamma$  = multiplier on  $f_m'$  to determine the intensity of an equivalent block stress for

$\kappa_m$  = bond dependent coefficient

$\rho_f$  = ratio of FRP flexural reinforcement

$\omega_f$  = FRP reinforcement index

**REFERENCES**

1. California Seismic Safety Commission, “*Status of Unreinforced Masonry Building Law*,” SSC 2000-02, Sacramento California, 2000.
2. Tumialan J.G., Morbin A., Micelli F. and Nanni A., “*Flexural Strengthening of URM Walls with FRP Laminates*,” Third International Conference on Composites in Infrastructure (ICCI 2002), San Francisco, CA, June 10-12, 2002, 11 pp. CD ROM.
3. Masonry Standards Joint Committee, “*Building Code Requirements for Masonry Structures*,” ACI-530/ASCE 5/TMS 402, American Concrete Institute, American Society of Civil Engineers, and The Masonry Society, Detroit, New York, and Boulder, 2002.
4. Velazquez-Dimas J.I., “*Out-of-Plane Cyclic Behavior of URM Walls Retrofitted with Fiber Composites*,” Doctoral Dissertation, Department of Civil Engineering and Engineering Mechanics, The University of Arizona, Tucson, Arizona, 1998.
5. Roko K., Boothby T.E., and Bakis C.E., “*Failure Modes of Sheet Bonded Fiber Reinforced Polymer Applied to Brick Masonry*,” Fourth International Symposium on Fiber Reinforced Polymer (FRP) for Reinforced Concrete Structures, Baltimore, Maryland, November 1999, pp. 305-311.
6. Albert L.M., Elwi A.E., Cheng J.J., “*Strengthening of Unreinforced Masonry Walls Using FRPs*,” ASCE Journal of Composites for Construction, Vol.5, No.2, May 2001, pp. 76-84.
7. Hamilton H.R. III, and Dolan C.W., “*Flexural Capacity of Glass FRP Strengthened Concrete Masonry Walls*,” ASCE Journal of Composites for Construction, Vol.5, No.3, August 2001, pp. 170-178.

8. Tumialan J.G., “*Strengthening of Masonry Structures with FRP Composites,*” Doctoral Dissertation, Department of Civil Engineering, University of Missouri-Rolla, Rolla, Missouri, 2001, 186 pp.
9. American Concrete Institute (ACI), Committee 318, “*Building Code Requirements for Reinforced Concrete and Commentary,*” American Concrete Institute, Detroit, Michigan, 1999.
10. American Concrete Institute (ACI), Committee 440, “*Guide for the Design and Construction of Externally Bonded FRP Systems for Strengthening Concrete Structures,*” ACI 440.2R-02, July 2002 (in press).
11. Schwegler G. and Kelterborn P., “*Earthquake Resistance of Masonry Structures strengthened with Fiber Composites,*” Eleventh World Conference on Earthquake Engineering, Acapulco, Mexico, 1996, 6 pp. CD-ROM.
12. Annaiah H.R., “*Shear Performance of Reinforced Concrete Beams Strengthened in situ with Composites,*” Master’s Thesis, Department of Civil Engineering, University of Missouri-Rolla, 2000, 136 pp.
13. Morbin A., “*Strengthening of Masonry Elements with FRP Composites,*” Tesi di Laurea, Dipartimento di Ingegneria Edile, Università di Padova, Italy, December 2001, 190 pp.

**LIST OF TABLES**

Table 1. Test Matrix

Table 2. Experimental and Theoretical Results

Table 3.  $C_E$  Factor for Various Fibers and Exposure Conditions

**LIST OF FIGURES**

Figure 1. Modes of Failure (Ref. 2)

Figure 2. Moment vs. Deflection of URM Walls Strengthened with FRP Laminates (Ref. 2)

Figure 3. Strain and Stress Distributions

Figure 4. Influence of Amount of FRP Reinforcement

Figure 5. Normal Distributions for  $\gamma$  and  $\beta_1$

Figure 6. Normalized Experimental Flexural Capacity vs. Reinforcement Index

Figure 7. Validation of Design Approach

Figure 8. Strengthening Layout (Dimensions in mm)

Figure 9. Anchorage with NSM Bars

Table 1. Test Matrix (Ref. 2)

Masonry Type	Series	FRP Fiber	Strip Width, mm (in.)				
			75 (3)	125 (5)	175 (7)	225 (9)	300 (12)
Concrete	COG	GFRP	COG3 COG3R	COG5 COG5R	COG7	COG9	COG12
	COA	AFRP	COA3	COA5	COA7	COA9	COA12
Clay	CLG	GFRP	CLG3 CLG3R	CLG5 CLG5R	CLG7 CLG7R	CLG9	CLG12
	CLA	AFRP	CLA3	CLA5	CLA7	CLA9	CLA12

Table 2. Experimental and Theoretical Results (Ref. 2)

Source	Masonry		FRP		Flexure			Shear		Failure
	Type	$h/t_m$	System	$\rho_f$	$M_{exp}$ (kN-m)	$M_{the}$ (kN-m)	$\epsilon_{fexp}$ (%)	$V_{exp}$ (kN)	$V_{the}$ (kN)	
COG3	CO	12.	GFRP	0.000	2.05	4.18	NA	4.27	11.37	D
COG3	CO	12.	GFRP	0.000	3.22	4.18	1.49	5.52	11.37	D
COG5	CO	12.	GFRP	0.000	3.33	5.64	NA	6.89	11.37	D
COG5	CO	12.	GFRP	0.000	5.37	5.64	1.83	7.16	11.37	R
COG7	CO	12.	GFRP	0.001	3.74	6.51	NA	7.74	11.37	D
COG9	CO	12.	GFRP	0.001	5.23	7.23	NA	10.85	11.37	S <sup>(1)</sup>
COG1	CO	12.	GFRP	0.001	6.06	8.12	NA	12.59	11.37	S <sup>(1)</sup>
COA3	CO	12.	AFRP	0.000	2.54	3.66	NA	5.25	11.37	D
COA5	CO	12.	AFRP	0.000	3.57	5.57	NA	7.38	11.37	D
COA7	CO	12.	AFRP	0.000	4.66	6.44	NA	9.70	11.37	S <sup>(1)</sup>
COA9	CO	12.	AFRP	0.001	5.25	7.16	NA	10.90	11.37	S <sup>(1)</sup>
COA1	CO	12.	AFRP	0.001	6.33	8.05	NA	13.12	11.37	S <sup>(1)</sup>
CLG3	CL	12.	GFRP	0.000	3.23	4.23	NA	7.78	22.98	D
CLG3	CL	12.	GFRP	0.000	3.88	4.23	2.25	8.05	22.98	R
CLG5	CL	12.	GFRP	0.000	4.89	6.97	NA	10.14	22.98	D
CLG5	CL	12.	GFRP	0.000	5.37	6.97	1.97	11.56	22.98	R
CLG7	CL	12.	GFRP	0.001	6.58	9.57	NA	13.61	22.98	D
CLG7	CL	12.	GFRP	0.001	7.20	9.57	1.54	14.63	22.98	D
CLG9	CL	12.	GFRP	0.001	6.94	11.09	NA	14.37	14.81	S <sup>(2)</sup>
CLG1	CL	12.	GFRP	0.001	6.16	12.47	NA	12.77	14.81	S <sup>(2)</sup>
CLA3	CL	12.	AFRP	0.000	2.94	3.70	NA	6.09	22.98	D
CLA5	CL	12.	AFRP	0.000	5.23	6.10	NA	10.85	22.98	R
CLA7	CL	12.	AFRP	0.000	6.13	8.45	NA	12.72	22.98	D
CLA9	CL	12.	AFRP	0.001	8.45	10.66	NA	17.48	22.98	D
CLA1	CL	12.	AFRP	0.001	5.90	12.35	NA	12.23	14.81	S <sup>(2)</sup>
Albert	CO	19.	GFRP	0.000	21.14	35.52	0.69	18.01	36.93	D
Albert	CO	18.	CFRP	0.000	29.50	40.86	0.78	25.13	37.08	D
Albert	CO	18.	CFRP	0.000	24.48	40.86	0.73	20.86	50.17	D
Albert	CO	18.	CFRP	0.000	12.28	21.24	0.78	10.45	50.17	R
Hamilt	CO	8.6	GFRP	0.000	3.44	5.46	NA	7.92	25.86	D
Hamilt	CO	8.6	GFRP	0.000	4.23	5.46	NA	9.74	22.54	R
Hamilt	CO	8.6	GFRP	0.000	4.89	5.46	NA	11.30	25.86	R
Hamilt	CO	8.6	GFRP	0.000	5.45	5.46	NA	12.54	22.54	R
Hamilt	CO	22.	GFRP	0.000	15.60	21.14	NA	13.48	26.48	R
Hamilt	CO	22.	GFRP	0.000	19.35	21.38	NA	16.72	25.24	R
Tumial	CO	6.0	GFRP	0.000	11.33	20.86	0.72	25.66	24.06	S <sup>(1)</sup>
Tumial	CO	6.0	AFRP	0.000	10.10	22.51	0.82	22.91	24.06	S <sup>(1)</sup>

**Legend:** D: FRP Debonding    S: Masonry Shear <sup>(1)</sup> Flexural-Shear  
R: FRP Rupture <sup>(2)</sup> Sliding Shear

Table 3.  $C_E$  Factor for Various Fibers and Exposure Conditions (Ref. 10)

Exposure Condition	Fiber Type	$C_E$
Enclosed Conditioned Space	Carbon	1.00
	Glass	0.80
	Aramid	0.90
Unenclosed or Unconditioned Space	Carbon	0.90
	Glass	0.70
	Aramid	0.80

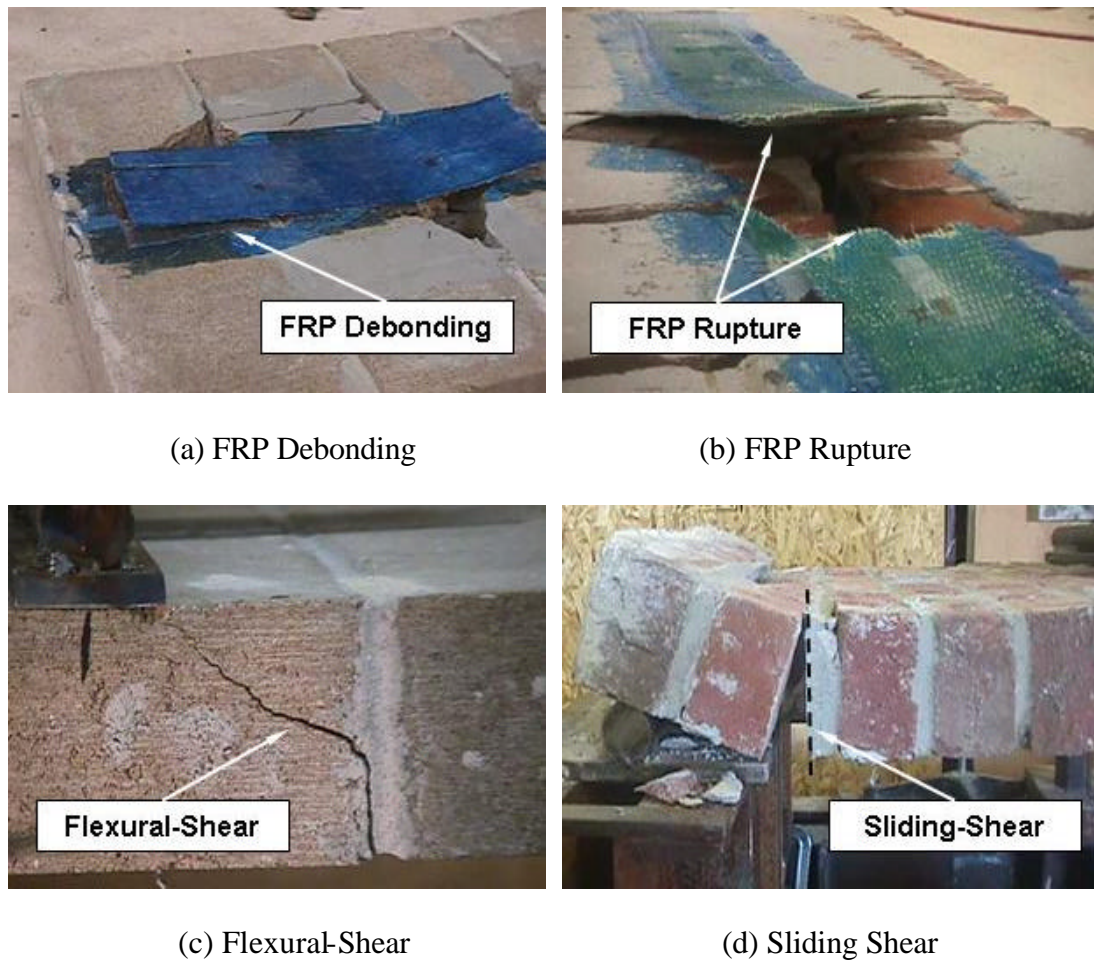
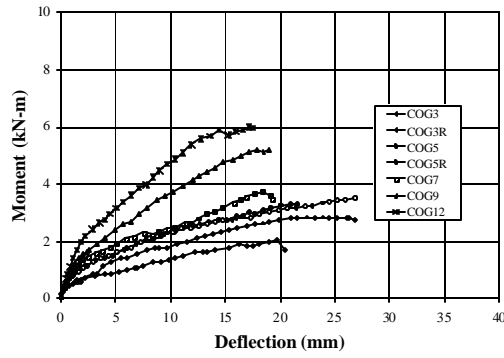
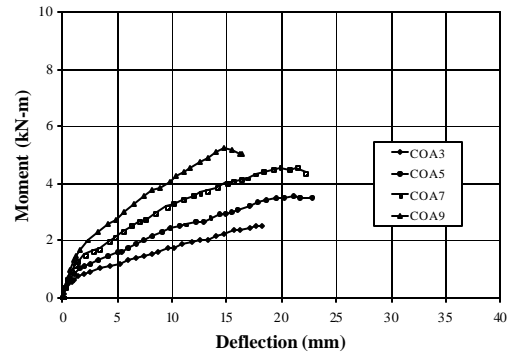


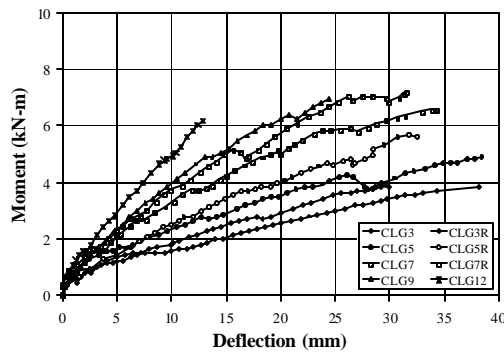
Figure 1. Modes of Failure (Ref. 2)



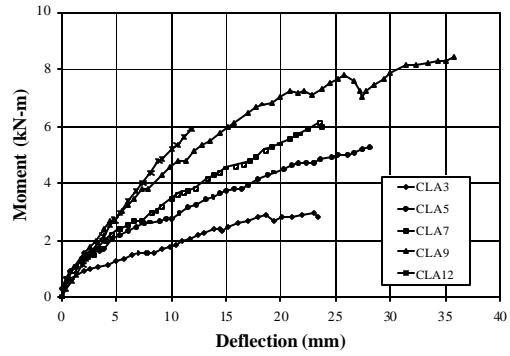
(a) Series COG



(b) Series COA



(c) Series CLG



(d) Series CLA

Figure 2. Moment vs. Deflection of URM Walls Strengthened with FRP Laminates (Ref. 2)

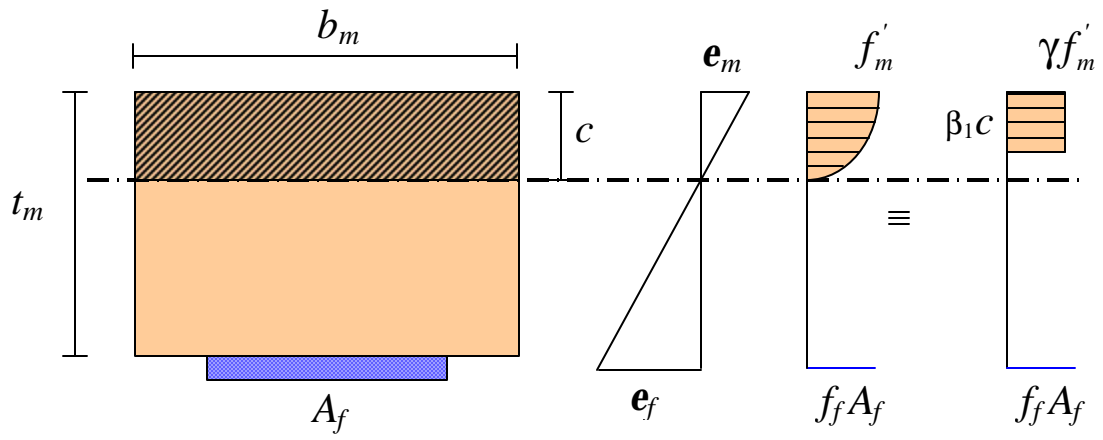


Figure 3. Strain and Stress Distributions

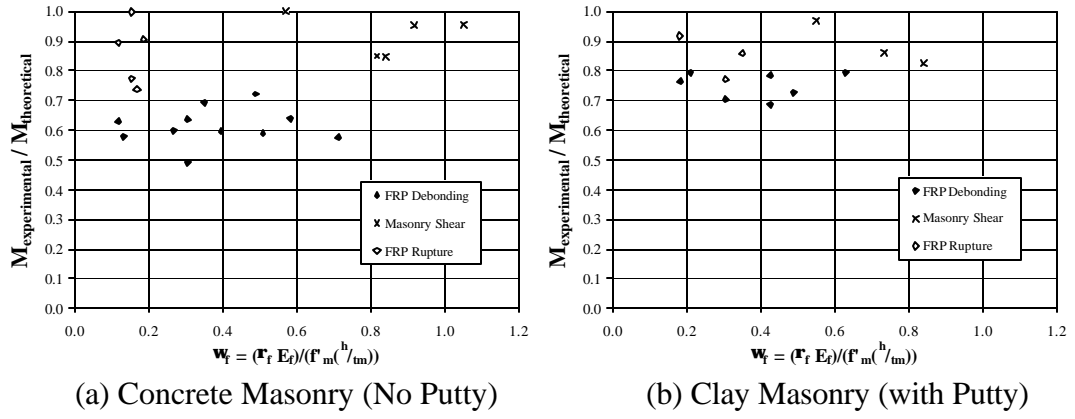


Figure 4. Influence of Amount of FRP Reinforcement

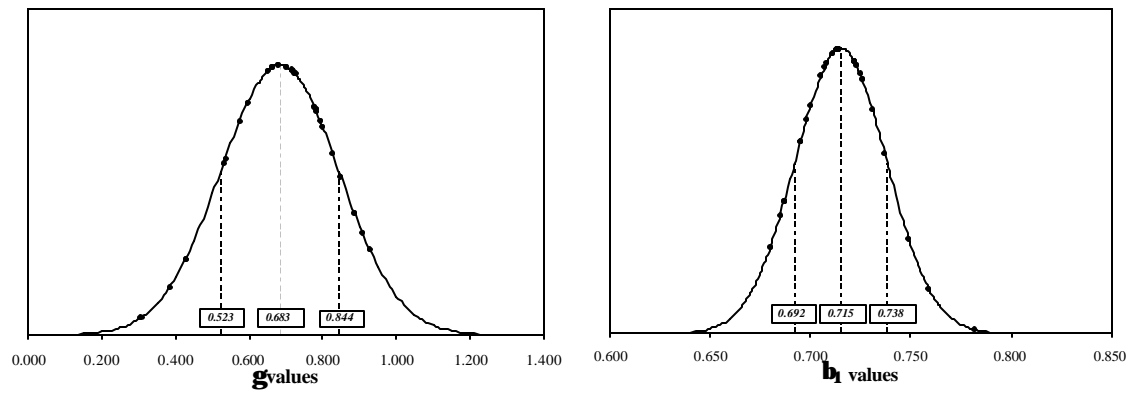


Figure 5. Normal Distributions for  $\gamma$  and  $\beta_1$

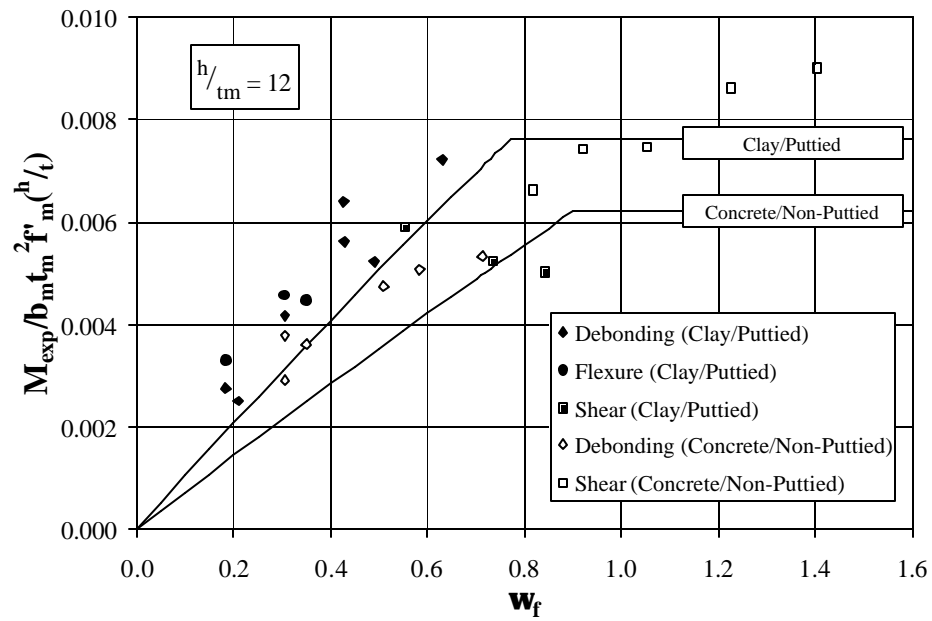


Figure 6. Normalized Experimental Flexural Capacity vs. Reinforcement Index

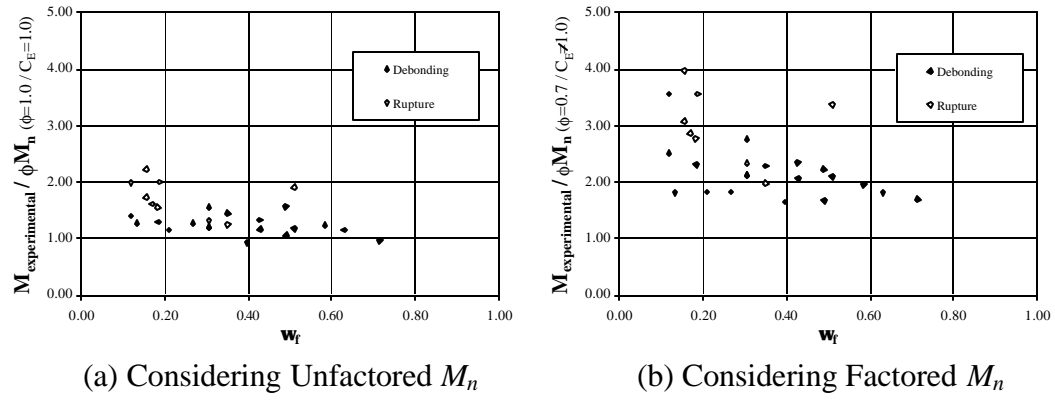


Figure 7. Validation of Design Approach

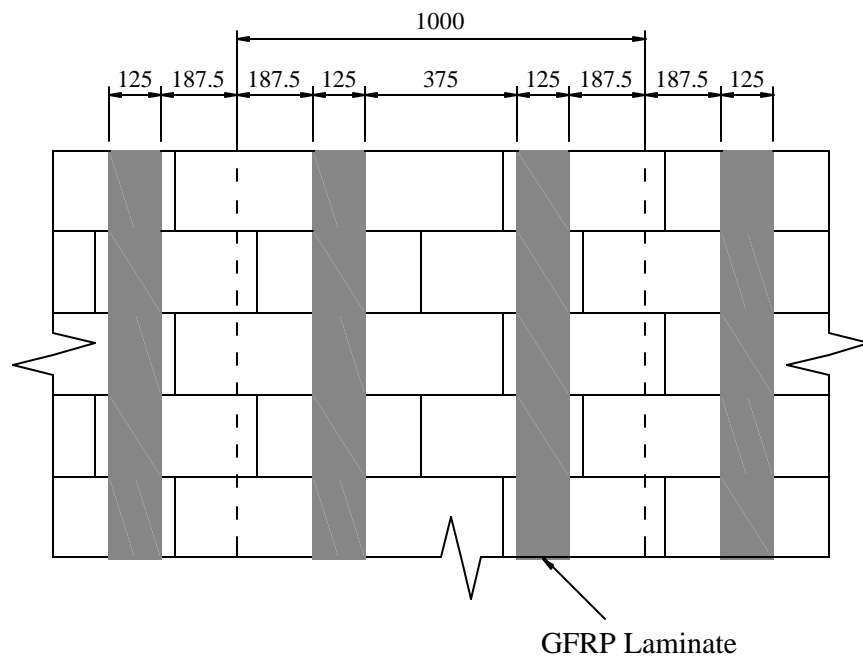


Figure 8. Strengthening Layout (Dimensions in mm)

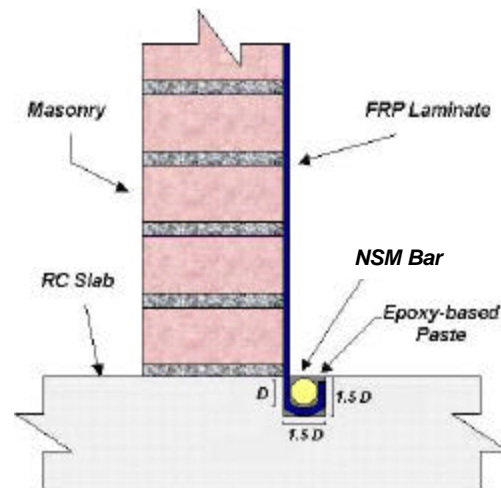


Figure 9. Anchorage with NSM Bars

## **STRENGTHENING OF MASONRY WITH NEAR SURFACE MOUNTED FRP BARS**

*J. Gustavo Tumialan, University of Missouri-Rolla, Rolla, MO*

*Nestore Galati, University of Missouri-Rolla, Rolla, MO*

*Sinaph M. Namboorimadathil, University of Missouri-Rolla, Rolla, MO*

*Antonio Nanni, University of Missouri-Rolla, Rolla, MO*

### **Abstract**

For the retrofitting of the civil infrastructure, an alternative to Fiber Reinforced Polymer (FRP) externally-bonded laminates is the use near surface mounted (NSM) FRP bars. This technique consists of placing a bar in a groove cut into the surface of the member being strengthened. The FRP bar may be embedded in an epoxy- or cementitious-based paste, which transfers stresses between the substrate and the bar. The successful use of NSM FRP bars in the strengthening of concrete members has been extended to unreinforced masonry (URM) walls, one of the building components most prone to failure during a seismic event. This paper describes three applications of FRP bars for the strengthening of URM and reports on the obtained experimental results. In the first application, FRP bars are applied vertically to resist out-of-plane forces acting on the masonry walls (i.e. flexural strengthening). In the second application, bars are inserted horizontally in the masonry joints to strengthen the wall when subjected to in-plane forces (i.e. shear strengthening). Finally, the third application deals with the retrofitting of masonry walls showing deficient anchorage to the base beam. In this application, FRP bars are placed in the toe region of the wall acting as anchors to increase flexural capacity. In each of these three applications, the strengthening was remarkably effective.

### **Introduction**

Unreinforced masonry (URM) walls are prone to failure when subjected to overstresses caused by out-of-plane and in-plane loads. Externally bonded FRP laminates have been successfully used to increase the flexural and/or the shear capacity of reinforced concrete (RC) and masonry members. The use of near-surface-mounted (NSM) FRP bars is an attractive method for increasing flexural and shear strength of deficient RC members (De Lorenzis et al., 2000) and masonry walls and, in certain cases, can be more convenient than using FRP laminates (i.e. anchoring requirements, aesthetics requirements). Application of NSM FRP bars does not require any surface preparation work and requires minimal installation time compared to FRP laminates. Another advantage is the feasibility of anchoring these bars into members adjacent to the one

being strengthened. For instance, in the case of the strengthening of a masonry infill with FRP bars, they can be easily anchored to columns and beams.

This paper presents three applications of FRP bars for the strengthening of URM walls. In the first application, NSM FRP bars are used as flexural reinforcement to strengthen URM walls to resist out-of-plane forces. In the second application, a retrofitting technique denominated FRP Structural Repointing is described. In this technique the FRP bars are placed into the bed masonry joints to act as shear reinforcement to resist in-plane loads. Finally, in the third application, masonry walls exhibiting deficient anchorage to the base beam are retrofitted by placing NSM FRP bars in the toe region of the wall which act as anchors to increase the flexural capacity of walls subject to in-plane loads.

## **Flexural Strengthening**

FRP bars can be used as reinforcement to provide flexural capacity to URM walls. A previous investigation has shown the effectiveness of FRP bars for increasing the flexural capacity of URM walls (Hamid, 1996). In that investigation, the FRP reinforcement was internally placed, this technique demanded the cutting of slots at the top course of the wall to place the bars, drilling of holes to pump grout, and grouting. The successful use of near-surface-mounted (NSM) bars for improving the flexural capacity of RC members led to extending their potential use for the strengthening of URM walls. The use of NSM FRP bars is attractive since their application does not require any surface preparation work and requires minimal installation time.

### **Strengthening Procedure**

The NSM technique consists of the installation of FRP reinforcing bars in slots grooved in the masonry surface. An advantageous aspect of this method is that it does not require sandblasting and puttying. The strengthening procedure can be summarized as: (1) grooving of slots having a width of approximately one and a half times the bar diameter and cleaning of surface, (2) application of embedding paste (epoxy-based or cementitious-based) (see Figure 1a), (3) encapsulation of the bars in the groove (see Figure 1b), and (4) finishing. If hollow masonry units are the base material, special care must be taken to avoid a groove depth exceeding the thickness of the masonry unit shell, and local fracture of the masonry. In addition, if an epoxy-based paste is used, strips of masking tape or other similar adhesive tape can be attached at each edge of the groove to avoid staining of the masonry (see Figure 1).

Depending on the kind of embedding paste, a mortar gun for tuckpointing or an epoxy gun may be used for its application. The guns can be hand, air or electric powered, being the latter two the most efficient.



(a) Application of Embedding Paste



(b) Encapsulation of FRP Bar

**Figure 1.** Installation of NSM FRP Bars

### Experimental Results

Four masonry specimens were constructed with concrete blocks using a Type N mortar. Their dimensions were 24 in. wide by 48 in. high. The wall thickness was about 3.75 in. The average compressive strength of masonry (ASTM C1314) was 1520 psi. The masonry specimens were strengthened with #3 GFRP bars having a tensile strength of 110 ksi and modulus of elasticity of 5900 ksi. An epoxy-based paste, having a compressive strength of 12.5 ksi and a tensile strength of 4000 psi, was used as embedding material. The strengthening layout intended to represent URM wall strips with GFRP bars at different spacing. Thus, Wall 1 was strengthened with one GFRP bar (spacing = 24 in.), Wall 2 with two GFRP bars (spacing = 12 in.), and Wall 3 with three GFRP bars (spacing = 8 in.). Conversely, Wall 1S was strengthened with externally bonded GFRP laminates applied by manual lay-up. The amount of reinforcement was equivalent to that of Wall 1 in terms of axial stiffness  $EA$  (Modulus of Elasticity  $\times$  FRP Gross Cross Sectional Area). Due to the brittle nature of URM it is meaningless to test an URM wall.

The walls were tested under simply supported conditions (see Figure 2). An out-of-plane load was applied along two load lines spaced 8 in. Linear Variable Differential Transducers (LVDTs) were placed at midspan and supports to register deflections and settlements. Also, strain gauges were placed on the GFRP bars to record strains at different levels of load.

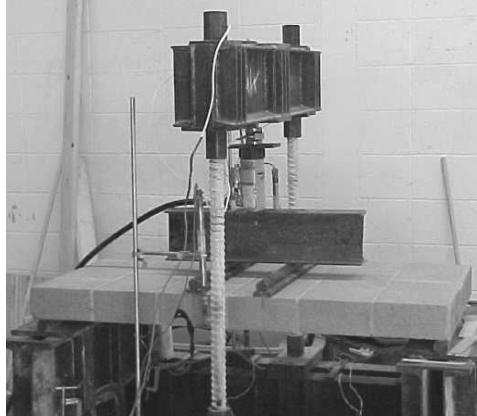
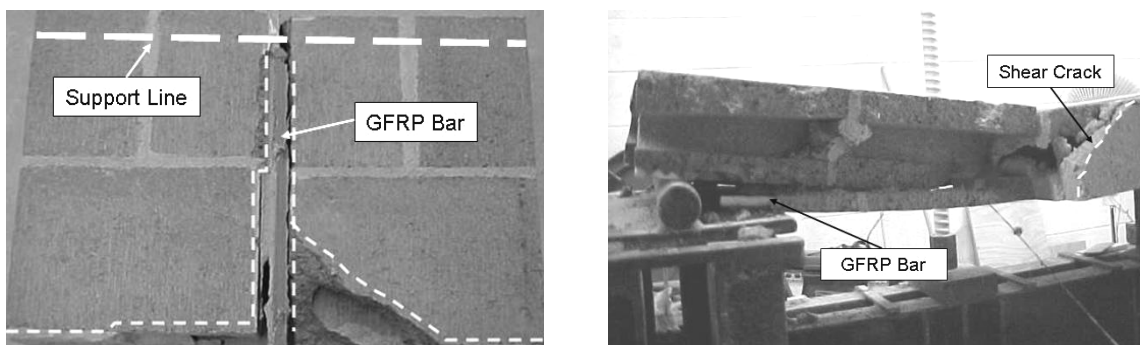


**Figure 2.** Test Setup

Wall 1 failed due to debonding of the embedding material from the masonry. Initial flexural cracks were primarily located at the mortar joints. A cracking noise during the test revealed a progressive cracking of the embedding paste. Since the tensile stresses at the mortar joints were being taken by the FRP reinforcement, a redistribution of stresses occurred. As a consequence, cracks developed in the masonry units oriented at  $45^\circ$  (see Figure 3a) or in the head mortar joints. Some of these cracks followed the epoxy paste and masonry interface causing debonding and subsequent wall failure.

Walls 2 and 3 failed due to shear (see Figure 3b). Similarly to Wall 1, cracking started in the mortar joints at the maximum bending region. At the final stage, some debonding of the FRP bars was observed, a consequence of differential displacement in the shear plane. In general, initial cracking was delayed and the crack widths were thinner as the amount of FRP reinforcement increased.



(a) Debonding Failure (Wall 1)

(b) Shear Failure (Wall 3)

**Figure 3.** Specimens after Failure

Figure 4 illustrates the moment vs. deflection curves for the four test specimens. The flexural strength and stiffness of the FRP strengthened walls increased as the amount of reinforcement increased. Following the Masonry Standards Joint Committee (MSJC, 1999), the nominal strength of an URM member can be computed as 0.33 ft-kips. Thus, increments of 4, 10 and 14 times the original masonry capacity were achieved for Walls 1, 2 and 3, respectively. These large increments should be taken as reference, since they

depend on the masonry variability (i.e. labor and materials) and boundary conditions (i.e. if the wall can be analyzed as simply supported). Wall 1S, which failed by debonding of the FRP laminate, exhibited a similar behavior to that observed in Wall 1.

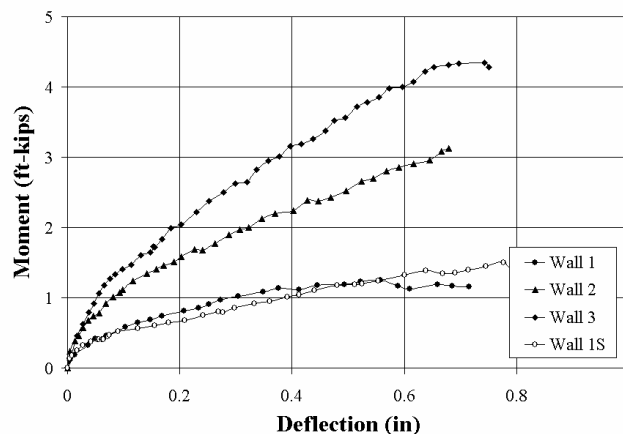


**Figure 4.** Moment vs. Deflection Curves

Figure 4 allows to observe that the flexural stiffness is a function of the amount of FRP, the levels of pseudo-ductility appear to be similar. Wall 2 exhibited a lower ultimate load than Wall 3, which can be attributed to the nature of the shear failure. In the case of Wall 2, sliding shear in the plane of a mortar joint was observed, whereas in Wall 3, the shear crack was diagonally oriented. The GFRP strain in Wall 1 at failure was 0.8%, which represented about 43% of the ultimate strain of a #3 GFRP bar. In Walls 2 and 3, the strain readings indicated 0.8% and 1.0%, respectively.

## Shear Strengthening

The technique denominated FRP structural repointing is basically a variant of the NSM technique, and consists of placing FRP bars in mortar bed joints (Tumialan et al., 2001). Repointing is a traditional retrofitting technique commonly used in the masonry industry for replacing missing mortar in the joints. The term “structural” is added because the proposed method allows for restoring the integrity and/or upgrading the shear and/or flexural capacity of walls.

### Strengthening Procedure

In FRP structural repointing, the aesthetics of masonry can be preserved. In this technique, the diameter size of the FRP bars is limited by the thickness of the mortar bed joint, which usually is not larger than  $\frac{3}{8}$  inches. The strengthening procedure consists of: (1) cutting out part of the mortar using a grinder, (2) filling the bed joints with a epoxy-based or cementitious-based paste (see Figure 5a), (3) embedding the bars in the joint (see Figure 5b), and (4) retooling.

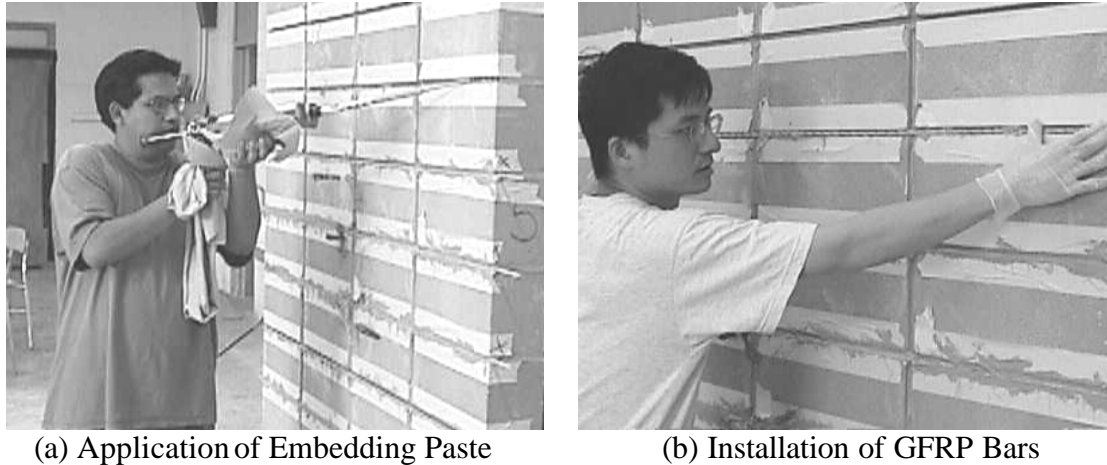


**Figure 5.** Strengthening by Structural Repointing

To ensure a proper bonding between the paste and masonry, dust must be removed from the grooves by means of an air blower prior to filling the bed joints. A masking tape or another suitable adhesive tape can be used to avoid staining if an epoxy-based paste is used. Stack bond masonry allows to install FRP bars in the vertical joints, if required (see Figure 5). In this case, the faceshell thickness of the masonry units does not limit the groove depth. In FRP structural repointing, grinding of the mortar joints is a simpler task than grooving the masonry units. For this reason, spacing of FRP bars is practically dictated by the height of the masonry unit.

### Experimental Results

The test results of four square masonry walls built with 6x8x16 in. concrete blocks are presented. The specimens had a nominal dimension of 64x64 in. and were built with a running bond pattern. The average compressive strength of masonry obtained from prisms (ASTM C1314) was 2490 psi. The walls were strengthened with #2 GFRP bars having a diameter of 0.25 in., a tensile strength of 120 ksi and modulus of elasticity of 5900 ksi.

Wall 1 was the control specimen. Wall 2 was strengthened with GFRP bars at every horizontal joint. Walls 2 and 3 had similar amounts of reinforcement. In the latter specimen, the reinforcement was distributed in the two faces, following an alternate pattern, to observe the influence of the reinforcement eccentricity. Wall 4 was strengthened with GFRP bars at every second horizontal joint to observe the behavior of a wall with half the amount of strengthening. Wall 2S was strengthened with externally bonded GFRP laminates; the amount of FRP was equivalent to that of Wall 2 in terms of axial stiffness. Thus, Wall 2S was strengthened with four horizontal 4 in. wide GFRP strips.

The specimens, tested in a close loop fashion, were loaded along one diagonal. LVDTs were placed along the wall diagonal to monitor deformations. The force was applied to the wall by steel shoes placed at the top corner, and transmitted to similar shoes at the bottom corner through high-strength steel bars. Figure 6 illustrates the test setup.



**Figure 6.** Test Setup

The tests results showed that in the control Wall 1 the failure was brittle, controlled by bonding between the masonry units and mortar. In the strengthened walls 2 and 3, when the tensile strength of masonry was overcome, the wall cracked along the diagonal, following the mortar joints (stepped crack vertical/horizontal). Wall failure occurred when the shear cracks widen and the GFRP bars were not able to carry tensile stresses due to debonding at the top and bottom paste/block interface (see Figure 7a). For the specimens strengthened with FRP, the maximum increment in shear capacity was about 80%, registered in Walls 2 and 3, strengthened with GFRP bars placed at every bed joint. Strengthened walls showed stability (i.e. no loose material was observed) after failure. This fact can reduce risk of injuries due to partial or total collapse of walls also subjected to out-of-plane loads. In addition, due to the reinforcement eccentricity, which caused the crack growth on the unstrengthened side to increase at a higher rate than the strengthened side, Wall 2 tilted towards the direction of the strengthened face (see Figure 7b). Data showing the crack opening is presented elsewhere (Tumialan et al., 2001). Failure in Walls 4 and 2S was due to sliding shear along an unstrengthened joint. This failure mechanism is also commonly known as knee brace or joint-slip. However, in the case of Wall 2S a larger increase in shear capacity was recorded due to the fact that the horizontal laminates engaged the masonry layers where the sliding occurred, and cracks running along the head joints were bridged. Due to its premature nature and negative effect to the boundary elements (i.e. columns in an infill wall), sliding shear failure should be avoided. A potential way to prevent is to place of vertical FRP reinforcement on the masonry infill, which would act as a dowel. A previous investigation has shown that placing vertical FRP reinforcement does not increase significantly the wall shear capacity (Tumialan et al., 2001).

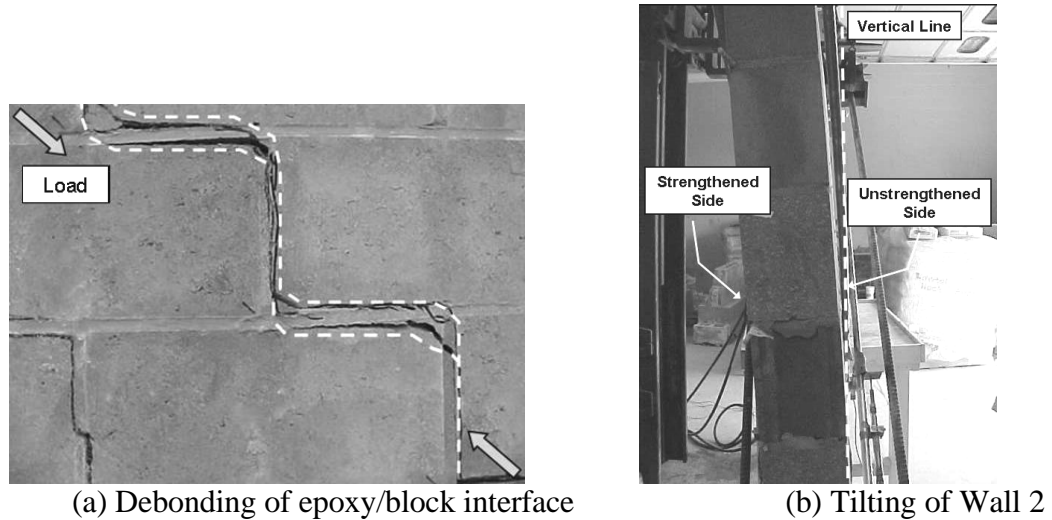


**Figure 7.** Specimens after Failure

The test setup configuration did not allow estimating pseudo-ductility,  $\mu$ , as conventionally defined ( $\mu = \delta_u / \delta_y$ ,  $\delta_u$  and  $\delta_y$  are the horizontal displacements at ultimate and “yielding” caused by an in-plane load). Instead, a criterion using the shear strain was adopted. Thus, the pseudo-ductility,  $\mu$ , was quantified as the ratio  $\gamma_u / \gamma_y$ ; where  $\gamma_u$  is the shear strain at ultimate and  $\gamma_y$  is the shear strain, corresponding to the point where the in-plane load vs. shear strain curve flattens out. Considering the normal strains generated by the diagonal in-plane load as principal strains, the maximum shear strain is expressed as:

$$\gamma = |\varepsilon_0| + |\varepsilon_{90}|$$

where  $\varepsilon_0$  and  $\varepsilon_{90}$  are the normal strains associated to the wall diagonals. The  $\gamma$  values at ultimate and yielding are presented in Figure 8.

Figure 8 illustrates the in-plane load vs. shear strain curves for the test walls. It can be observed that Wall 3 exhibited the largest pseudo-ductility value, which can be attributed to reinforcement staggering on the two wall sides. The pseudo-ductility values estimated for Wall 4 was the smallest of all the strengthened walls. As it was mentioned before, this is caused by the occurrence of sliding shear. It is observed that the walls strengthened with FRP bars (Wall 2) and FRP laminates (Wall 2S) had similar shear capacity; however, the pseudo-ductility was less in the Wall 2S, which was caused by the occurrence of the sliding shear failure.

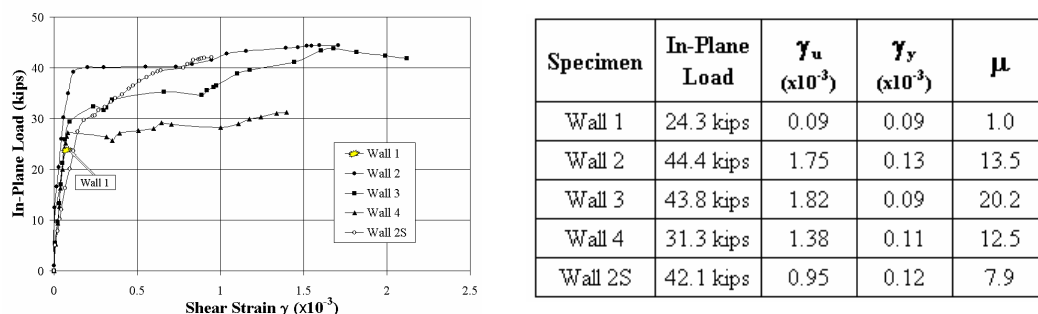


**Figure 8.** In-Plane Load vs. Shear Strain

## Anchorage Improvement

The following experimental program dealt with the retrofitting of masonry walls exhibiting anchorage deficiencies. To be effective, FRP shear strengthening depends on the development of the wall flexural capacity, which in turns relies on the anchorage of the existing steel reinforcement.

### Experimental Program

Three multiwythe steel reinforced masonry walls built using clay units were tested (see Figure 9a). These walls were parapets of a decommissioned building in St. Louis, Missouri. Their dimensions were 5x5 ft. The overall thickness of the walls was 12.5 in. The multiwythe walls were built with cored bricks having the following dimensions, 3.75 in. wide, 2.25 in. high and 8 in. long, with three cores of 1.5 in. diameter. The compressive strength in masonry was determined to be 1400 psi. Tests performed on the steel reinforcement showed that the yielding strength was 50 ksi.

According to the original drawings, the walls were horizontally and vertically reinforced with #3 steel bars, spaced at 6 in. on center, and placed in the joints between wythes. However, after inspection, it was observed that several steel bars were missing or irregularly placed as can be observed in Figure 9b. This fact made difficult to assess the actual capacity of the members.

Wall 1 was selected as a control specimen. The remaining two specimens were strengthened with externally bonded GFRP laminates and NSM FRP bars. Wall 2 was strengthened with three 10 in. wide GFRP strips (vertically oriented), and six #3 GFRP bars spaced at 10 inches (horizontally oriented). The strengthening scheme for Wall 3 was similar to that of Wall 2. In addition, ten #3 NSM GFRP bars having a length of 36 in., two per slot, were placed in the first 18 in. at each wall toe (see Figure 10). Prior to installing the GFRP bars, the holes in the RC slab and slots were filled with an epoxy-based paste. The additional anchors were placed with the purpose of increasing the flexural capacity of the wall. The rationale for their calculation was to provide enough flexural reinforcement to force the occurrence of shear failure (Tumialan, 2001) It would have been desirable to strengthen both sides of the walls, but since these walls were part of the parapets at the uppermost story only one side was easily accessible.

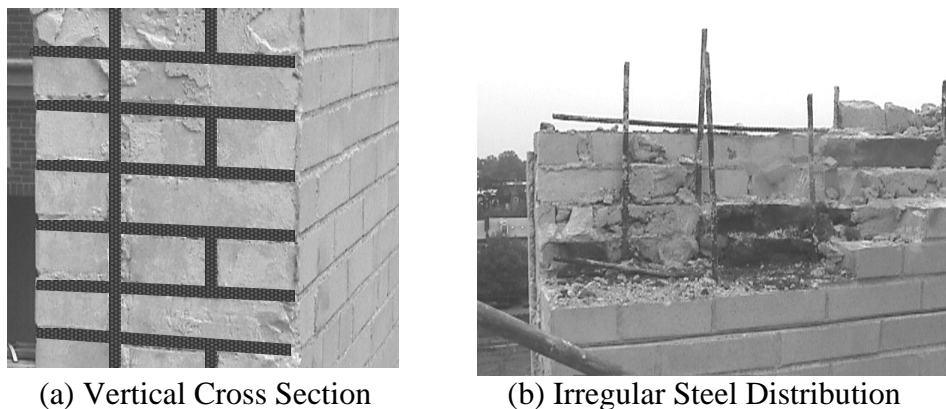


**Figure 9.** Details of Masonry Walls

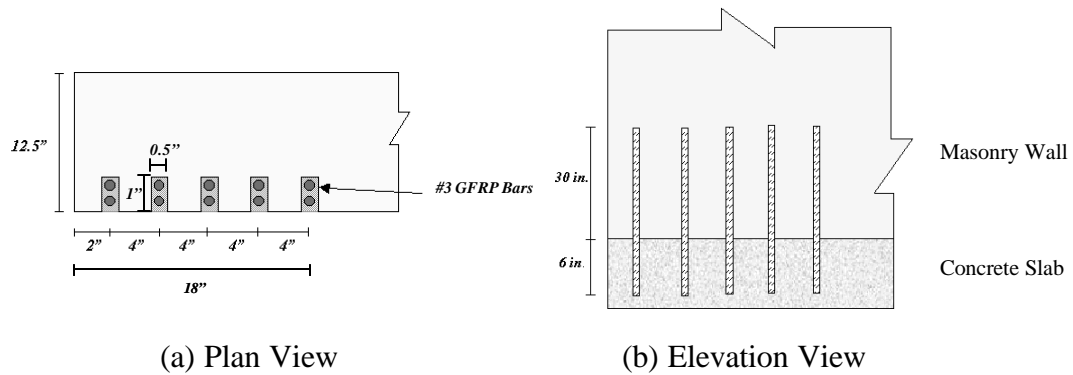


**Figure 10.** #3 GFRP Bars in one toe region of Wall 3

The masonry walls were in-plane loaded as cantilever walls, with free rotation and movement at the top and fixed at the base. The loads were generated by the alternate use of two hydraulic jacks. Thus, two walls could be tested in series at the same time (See Figure 11). LVDTs were placed at the top of the walls to register displacements. Details of the strengthening schemes and test procedure are presented elsewhere (Tumialan, 2001).

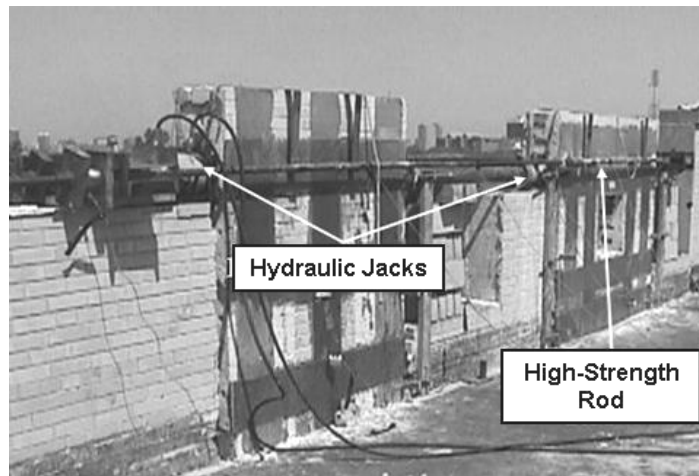


**Figure 11.** In-Plane Test Setup

Wall 1 was used as control specimen to assess the flexural capacity from in-plane loading prior to strengthening. A maximum force of 9.7 kips occurred for a displacement of about 0.03 in. The wall lost carrying capacity due to the crack growth caused by rocking. The crack length when the test was terminated covered approximately two-thirds of the base length (see Figure 12a). Base sliding was not observed at this final stage. Compared to calculations, the flexural capacity in Wall 1 was significantly low. This was attributed to the deficient anchorage of the existing vertical steel reinforcement, which pulled out from the wall. This reinforcement was placed in the space between the wythes, which was filled with the same mortar used to lay the masonry units.

Similarly to Wall 1, a flexural crack was observed at the base of the Wall 2 for a load of 3.5 kips. Flexural failure was observed at about 12 kips for a displacement of 0.04 in. This slight increment may be attributed to the bridging of some secondary cracks near the bottom by the FRP laminates. Similarly to Wall 1, the primary flexural crack causing the failure was observed at the bottom of the wall (see Figure 12b).

In Wall 3 a crack running along the base of the wall was visible at a load of 5 kips. A flexural failure was observed for a maximum load of 24 kips with a corresponding displacement of about 0.18 in. After reaching a displacement of about 0.3-in., significant load degradation was observed. The opening of the horizontal crack in the strengthened side was controlled by means of the GFRP bars. However, due to the eccentricity of the GFRP bars reinforcement, the wall tilted, preventing the development of the full flexural capacity.

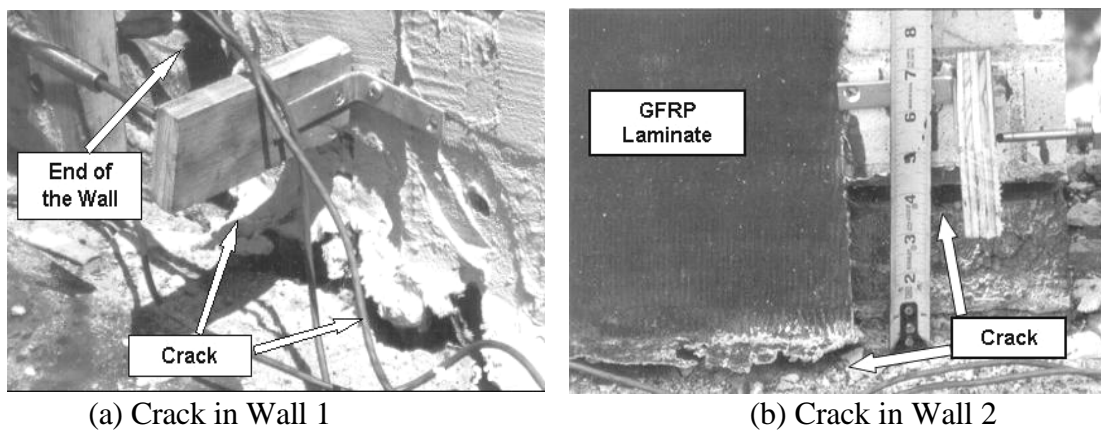


**Figure 12.** Flexural Cracks at the Bottom of Walls

An envelope of the load vs. top wall displacement curves is illustrated in **Figure 13**. By comparing Wall 3 to Wall 2, the increment in capacity was over 100%. Since the steel reinforcement was pulled out, the concept of ductility defined as the ratio between the deflection at the ultimate state of failure and the deflection at the yielding of steel can not be applied. In Wall 3, due to the contribution of the anchors, a notable increase in pseudo-ductility was attained.

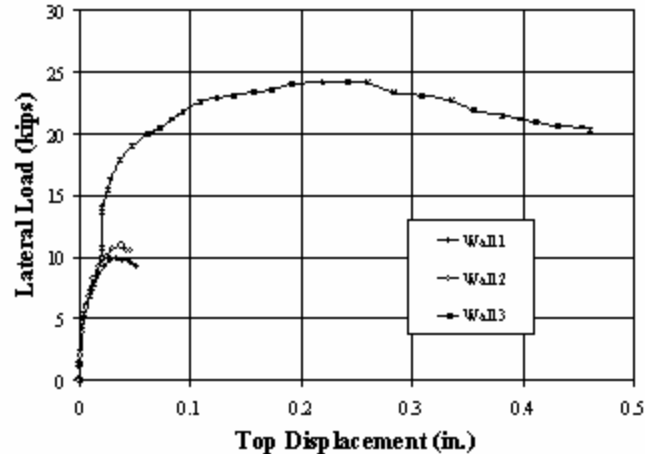


**Figure 13.** Lateral Load vs. Top Displacement

## Conclusions

Experimental results of three different applications of NSM FRP bars for the strengthening of masonry walls were presented. Each of them shows promising potential for the retrofitting of existing structures. In general, strength and pseudo-ductility can be substantially increased by strengthening masonry walls with NSM FRP bars:

- Masonry walls strengthened with NSM FRP bars exhibited similar performance to walls strengthened with FRP laminates
- For flexural strengthening, increments ranging between 4 and 14 times of the original masonry capacity may be achieved. These large increments should be taken as a reference only in walls that can be idealized as simply supported (i.e. when arching mechanism is not observed)
- Remarkable increases in shear capacity ranging between 30 and 80% may be achieved by FRP structural repointing. However, these increment levels should not be generalized for walls built with clay bricks, where different masonry characteristics (i.e. compressive strength) and wall geometries (i.e. number of wythes and number of layers) are observed.
- The use of FRP NSM bars for anchorage improvement may provide increases over 100% in in-plane flexural capacity.

## Acknowledgements

The support of the National Science Foundation Industry/University Cooperative Research Center at the University of Missouri–Rolla is greatly acknowledged. The authors would also like to acknowledge the support of the Rolla Technical Institute (RTI).

## References

1. De Lorenzis L., Nanni A., and La Tegola A., "Flexural and Shear Strengthening of Reinforced Concrete Structures with Near Surface Mounted FRP Rods," Proceedings of Third International Conference on Advanced Composite Materials in Bridges and Structures, Ottawa, Canada, pp. 521-528.
2. Hamid A.A., "Strengthening of Hollow Block Masonry Basement Walls with Plastic Reinforcing Bars," The Masonry Society Journal, August 1996, pp. 29-33.
3. Masonry Standards Joint Committee, "Building Code Requirements for Masonry Structures," ACI-530-99/ASCE 5-99/TMS 402-99, American Concrete Institute, American Society of Civil Engineers, and The Masonry Society, Detroit, New York, and Boulder, 1999.
4. Tumialan J.G., "Strengthening of Masonry Structures with FRP Composites," Doctoral Dissertation, Department of Civil Engineering, University of Missouri-Rolla, Rolla, Missouri, 2001.
5. Tumialan J.G., Morbin A., Nanni A., and Modena C., "Shear Strengthening of Masonry Walls with FRP Composites," COMPOSITES 2001 Convention and Trade Show, Composites Fabricators Association, Tampa, FL, October 3-6, 2001, 6 pp. CD-ROM.

*COMPOSITES 2002 Convention and Trade Show*  
*Composites Fabricators Association*  
*September 25-27, 2002*  
*Atlanta, Georgia USA*

## **Flexural Strengthening of Unreinforced Masonry with FRP Bars**

by

Gustavo Tumialan, Nestore Galati, and Antonio Nanni

### **Abstract**

Unreinforced masonry (URM) walls are prone to failure when subjected to out-of-plane and in-plane loads. Fiber reinforced polymer (FRP) materials offer viable solutions to solve the effects of overloading. This paper presents an experimental program dealing with flexural strengthening of URM walls with FRP bars to withstand out-of-plane loads. A field application where FRP bars were used for the strengthening of damaged URM walls is also presented.

### **Introduction**

Fiber reinforced polymer (FRP) composites in the form of laminates or bars can provide viable solutions for the strengthening of unreinforced masonry (URM) walls subjected to overstresses. In addition to their mechanical properties, advantages of FRP composites include lower installation costs, improved corrosion resistance, on-site flexibility of use, and minimum changes in the member size after repair. In addition, the disturbance of the occupants of the facility is minimized and there is minimal loss of usable space during strengthening.

For the retrofitting of the civil infrastructure, an alternative to FRP externally-bonded laminates is the use near surface mounted (NSM) FRP bars. This technique consists of placing a bar in a groove cut into the surface of the member being strengthened. The FRP bar is embedded in either an epoxy or cementitious-based paste, which transfers

stresses between the substrate and the bar. The successful use of NSM FRP bars in the strengthening of concrete members (De Lorenzis et al., 2000) has been extended to URM walls, one of the building components most prone to failure due to overstressing (see Fig. 1). FRP bars have been successfully used for increasing the in-plane capacity of URM walls (Tumialan et al., 2001).

This paper describes an experimental program on the upgrading of the out-of-plane capacity (i.e. flexural strengthening) of URM concrete panels with FRP bars. A field application where FRP bars were used for the strengthening of damaged URM walls is also presented.

### **Material Characterization**

Tests were performed to characterize the engineering properties of the materials used in this investigation. The average compressive strength of concrete masonry obtained from the testing of prisms (ASTM C1314) was 1520 psi. The walls were strengthened with #3 glass FRP (GFRP) bars having a diameter of 0.75-in., a tensile strength of 110 ksi and modulus of elasticity of 5900 ksi.

The GFRP bars are deformed by a helical wrap with a sand coating to affect the bond with the embedding paste (see Fig. 2). The bars are produced using a variation of the pultrusion process using 100% vinylester resin and e-glass fibers. The typical fiber content is 75% by weight.

The GFRP bars were embedded into an epoxy-based paste with the following mechanical properties: compressive strength of 12.5 ksi, tensile strength of 4 ksi, and modulus of elasticity of 450 ksi.

### **Strengthening Procedure**

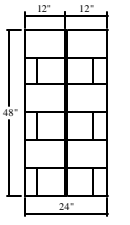
The NSM technique consists of the installation of FRP reinforcing bars in slots grooved in the masonry surface. The strengthening procedure consists of: (1) grooving of slots having a width and depth of approximately 1.5 times the bar diameter, and cleaning of the groove, (2) application of embedding paste (epoxy-based or cementitious-based), (3) insertion of the bar in the groove (see Fig. 3), and (4) finishing.

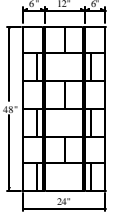
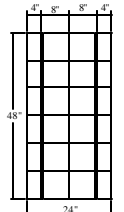
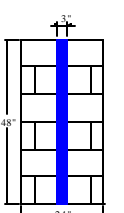
If hollow masonry units are the base material, the groove depth should not exceed the thickness of the masonry unit shell to avoid local fracture of the masonry. In addition, if an epoxy-based paste is used, strips of masking tape or other similar adhesive tape can be attached at each edge of the groove to avoid staining of the masonry (see Fig. 3). The NSM technique offers advantages compared to the use of FRP laminates; the method itself is simpler since the surface preparation is reduced (sandblasting and puttying) is not required.

### Test Specimens

Four masonry specimens were built using concrete masonry blocks using a Type N mortar. Their dimensions were 24 in. wide by 48 in. high. The wall thickness was about 3.75 in. The strengthening layout intended to represent URM wall strips with GFRP bars placed at different spacing. Wall B1 was strengthened with one GFRP bar, which represented a bar spacing equal to 24 in., Wall B2 with two GFRP bars (spacing = 12 in.), and Wall B3 with three GFRP bars (spacing = 8 in.). Conversely, Wall S1 was strengthened with a 3-in wide layer of externally bonded GFRP laminates, installed by manual lay-up, to compare the behavior of walls strengthened with laminates and bars. In Wall S1 the amount of reinforcement was equivalent to that of Wall B1 in terms of axial stiffness  $EA$  (Modulus of Elasticity  $FRP \times$  Gross Cross Sectional Area). Due to the brittle nature of URM it was meaningless to test an URM wall. Table 1 summarizes the test matrix

**Table 1. Test Matrix**

Specimen	Reinforcement	Front Side
Wall B1	1#3 GFRP Bar Spacing = 24"	

Wall B2	2#3 GFRP Bars Spacing = 12"	
Wall B3	3#3 GFRP Bars Spacing = 8"	
Wall S1	3-in wide GFRP Laminate Spacing = 24"	

### Test Setup

The walls were tested under simply supported conditions (see Fig. 4). An out-of-plane load, generated by a hydraulic jack, was applied along two load lines spaced 8 in. The data was acquired by a load cell and linear variable differential transducers (LVDTs), which were placed at midspan and supports to register deflections and settlements. Also, strain gauges were placed on the GFRP bars to record strains at different levels of load.

### Mechanisms of Failure

Wall B1 failed due to debonding of the embedding material from the masonry. Initial flexural cracks were primarily located at the mortar bed joints. A cracking noise during the test revealed a progressive cracking of the embedding paste. Since the tensile stresses at the mortar joints were being taken by the FRP reinforcement, a redistribution of stresses occurred. As a consequence, cracks developed in the masonry units oriented at  $45^\circ$  (see Fig. 5) or in the head mortar joints. Some of these cracks followed the epoxy paste and masonry interface causing debonding and subsequent wall failure.

Walls B2 and B3 failed by shear (see Fig. 6). Similarly to Wall B1, cracking started in the mortar joints at the maximum bending region. At the final stage, some debonding of the FRP bars was observed. This was attributable to a differential displacement in the shear plane. In general, initial cracking was delayed and the crack widths were thinner as the amount of FRP reinforcement increased.

## Test Results

Fig. 7 illustrates the moment vs. deflection curves for the four test specimens. The flexural strength and stiffness of the FRP strengthened walls increased as the amount of reinforcement increased. Following the recommendations provided by the Masonry Standards Joint Committee (MSJC, 2002), the theoretical strength of an URM wall was computed as 0.33 ft-kips. Thus, increments of 4, 10 and 14 times the original masonry capacity were achieved for Walls B1, B2 and B3, respectively. These large increments should be taken as reference, since they depend on the masonry variability (i.e. labor and materials) and boundary conditions (i.e. if the wall can be analyzed as simply supported). Wall S1, which failed by debonding of the FRP laminate, exhibited a similar behavior to that observed in Wall B1.

Fig. 7 also allows to observe that the flexural stiffness is a function of the amount of FRP, the levels of pseudo-ductility appear to be similar. Even though Wall B2 and Wall B3 failed in shear, the former exhibited a lower ultimate load than the latter. This can be attributed to the nature of the shear failure. In the case of Wall B2, sliding shear in the plane of a mortar joint was observed, whereas in Wall B3, the shear crack was diagonally oriented. The GFRP strain in Wall B1 at failure was 0.8%, which represented about 43% of the ultimate strain of a #3 GFRP bar. In Walls B2 and B3, the strain readings indicated 0.8% and 1.0%, respectively.

## Field Application

Two URM concrete walls at an educational facility in Missouri exhibited cracking in the bed joints at the mid-height region. The cracking was caused by an unstable foundation. FRP bars were used to reinstate the integrity of the cracked masonry walls. The design approach consisted of restoring the flexural capacity of the cracked

walls to that of an uncracked wall. The design protocol was in compliance with the recommendations provided by ACI 440.1R-01 (ACI 440, 2001), the Masonry Standards Joint Committee (MSJC, 2002).

The proposed strengthening strategy consisted of placing one #2 GFRP bar every 16 in. Since the masonry wall has a stack bonded pattern the GFRP bars were placed in the vertical mortar joints to ease the construction process and to preserve the wall aesthetics. Fig. 8 illustrates the application of the epoxy paste. Fig. 9 shows the insertion of the FRP bar into the groove.

## Conclusions

The following conclusions can be drawn from this experimental program:

- The use of FRP bars for retrofitting of masonry structures has a promising potential.
- Flexural strength and pseudo-ductility can be substantially increased by strengthening masonry walls with FRP bars.
- Increments ranging between 4 and 14 times of the original masonry capacity may be achieved. These large increments should be taken as a reference only in walls that can be idealized as simply supported (i.e. when arching mechanism is not observed)
- A masonry wall strengthened with NSM FRP bars exhibited similar performance to a wall strengthened with FRP laminates
- A field application where the NSM technique for the retrofitting of masonry has already been completed.

## References

- ACI Committee 440, "Guide for the Design and Construction of Concrete Reinforced with FRP Bars", American Concrete Institute, Farmington Hills, MI, 2001.
- De Lorenzis L., Nanni A., and La Tegola A., "Flexural and Shear Strengthening of Reinforced Concrete Structures with Near Surface Mounted FRP Rods," Proceedings of Third International Conference on Advanced Composite Materials in Bridges and Structures, Ottawa, Canada, August, 2000, pp. 521-528.
- Masonry Standards Joint Committee (MSJC), "Building Code Requirements for Masonry Structures," ACI-530-99/ASCE 5

99/TMS 402-99, American Concrete Institute, American Society of Civil Engineers, and The Masonry Society, Detroit, New York, and Boulder, 2002.

- Tumialan J.G., Morbin A., Nanni A., and Modena C., “Shear Strengthening of Masonry Walls with FRP Composites,” COMPOSITES 2001 Convention and Trade Show, Composites Fabricators Association, Tampa, FL, October 3-6, 2001, 6 pp. CD-ROM.

### Acknowledgements

This research study was sponsored by the National Science Foundation Industry/University Cooperative Research Center at the University of Missouri–Rolla (UMR). The authors would like to acknowledge the support of the Rolla Technical Institute (RTI).



**Figure – 1.** Out-of-Plane Failure – Turkey (1999)



**Figure – 2.** GFRP Bar



**Figure – 3.** NSM Technique



**Figure – 4.** Test Setup

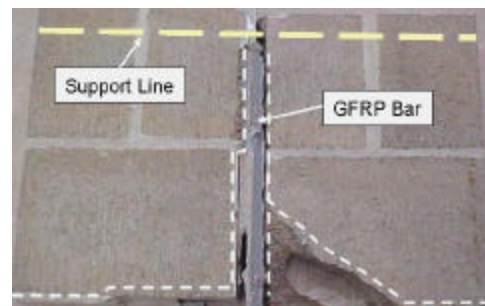


**Figure – 5.** Debonding Failure (Wall B1)



Figure – 6. Shear Failure (Wall B3)



Figure – 9. Installation of GFRP Bar

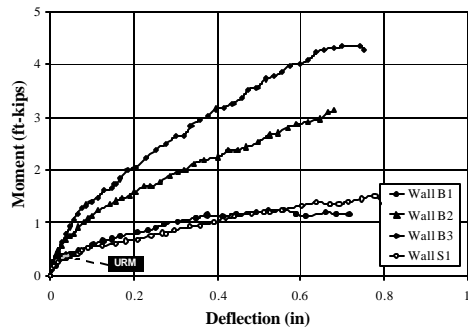


Figure – 7. Moment vs. Deflection Curves



Figure – 8. Application of Epoxy Paste

**Authors:**

Gustavo Tumialan is a Research Engineer at the Center for Infrastructure Engineering Studies (CIES)

of the University of Missouri-Rolla (UMR). Nestore Galati is a Graduate Research Assistant at the Department of Engineering Mechanics at UMR.

Antonio Nanni is the V&M Jones Professor of Civil Engineering at UMR and Director of CIES.